Characterisation and Correction of the F508del-CFTR defect

A thesis submitted to the University of Manchester for the degree of Doctor of Philosophy in the Faculty of Biology, Medicine and Health.

2020

Jack Clews

School of Biological Sciences

List of Contents

Word Count: 55,317

Declaration

I declare that no portion of the work referred to in the thesis has been submitted in support of an application for another degree or qualification of this or any other university or other institute of learning.

Copyright statement

Abstract

Cystic Fibrosis is an autosomal recessive disease that is characterised by conditions present throughout the body. The majority of cystic fibrosis cases are caused by the deletion of phenylalanine at position 508 in the Cystic Fibrosis Transmembrane Conductance Regulator (CFTR). A large amount of research, from across a number of fields, has gone into correcting the defect caused by the mutation. The work in this thesis continues this principle of research providing a multi-disciplinary approach to providing insight into the mechanism of disease and solving the issue of F508del-CFTR. There exists limited pharmacological options for cystic fibrosis patients who are homozygous for the F508del mutation, with current treatments currently exorbitantly expensive, providing limited rescue and still leaving patients with a greatly reduced quality of life; this thesis provides an assay by which to develop novel compounds, or investigate existing pre-clinical compounds, which would benefit patients in the future. The method is validated by determination of the stability impacts of a novel biosensor and novel pre-clinical corrector, as well as the testing of an FDA approved library of existing widely used drugs. Recently, the cystic fibrosis research field has been bolstered by the publication of several cryo-electron microscopy structures showing CFTR in its various states. Work in this thesis aims to provide insight into the differences of these states, via limited exposure to proteases, as well as provide further insight into the protein population that is recognised by cell quality control machinery and degraded.

Acknowledgements

First of all I would like to thank my supervisor and mentor Professor Robert Ford. Thank you for your guidance, supervision, patience and acceptance into the scientific community. Without any of this, this thesis could not have been written. The past 5 years have been a profound experience that has introduced me to the world of scientific research, changing and growing me for the better. I would like to thank my Postgraduate Advisor, Professor David Thornton, as well as my Postgraduate Tutor, Dr Minsung Kim. I am deeply grateful and indebted to the members of the F508del-SRC; Professor Frédéric Becq, Professor David Sheppard, Dr Paola Vergani and Professor Ineke Braakman, as well as their early career researchers, Arnaud Billet, Bartholomew Harvey, Stella Prins and Laura Tadé. I would like to thank my colleagues and lab mates, Talha Shafi, Iqra Younis, Nopnithi Thongin, Swathi Lingam, Ellie Martin, Vasileios Kargas, Joe Shakeri, and Becky Crawshaw. I will always be grateful to Dr Xin Meng for her help, friendship and collaboration for the work throughout this thesis. Finally, I would like to thank my friends and family who have helped me greatly along the way. My sincerest gratitude goes to the Lord Jesus Christ who has made all things in this thesis and my life possible.

Chapter 1.0 Introduction

1.1 F508del SRC

This PhD was funded by the cystic fibrosis trust (CF Trust UK), as part of the F508del Strategic Research Consortium (SRC). It exists as a collaborative effort between 5 labs that, through interdisciplinary partnership, would aim to correct the affect of the F508del mutation, leading to cystic fibrosis. The Manchester arm of the branch was utilised for its ability to purify the cystic fibrosis transmembrane conductance regulator (CFTR) to a reasonable amount and with a high grade of purity. The purified protein would then be tested using a medium-throughput compound testing process in order to identify compounds that would correct the F508del mutation. The insight for this PhD became present due to the inadequacy of current drugs for treatment of cystic fibrosis (CF). The F508del mutation requires both correction and potentiation in order to show clinical benefit. Vertex pharmaceuticals have developed drugs that are fit for that task, VX-809 (Lumacaftor) to correct and VX-770 (Ivacaftor) to potentiate. The combination therapy was shown to increase lung function and aid with disease stability in clinical trials [1], however further studies show that chronic administration of this combination therapy actually reduced correction, leading to abrogation of the disease [2] [3]. Therefore, new compounds were sought after for the sake of further treatment of the disease. The drugs wrought from Vertex pharmaceuticals had been the most successful to date prior to the start of this research, thus novel methods were sought in order to provide fresh insight into the correction process. Therefore, the Manchester arm of the SRC would be testing novel compounds developed by the French portion of the consortium. The aim was to develop an assay that can test novel compounds for their direct action against CFTR, seeing a pharmacological modulation effect where any positive changes seen in the stability of the protein are due to the effect of the drug on the protein rather than due to changes in the cellular machinery. Thus the pharmacological work in this thesis aims to distinguish between development of pharmacological chaperones from proteostasis regulators. The chaperones would be defined in the literal

sense of the word, something to bind to the protein and affect it in a positive way. Whereas regulators would be defined as a compound that would affect the cellular machinery in such a way that the regulation leads to increased trafficking of CFTR to the membrane either through a reduction in cellular degradation or through increased expression [4].

This thesis presents results from this aim as well as other research conducted into investigating the affects of cystic fibrosis causing mutations on the conformation, stability and structure of CFTR. These data have been published over a number of papers which are presented here as an alternative format theses.

1.2 The cystic fibrosis transmembrane conductance regulator (CFTR) and its stability (Chapter 3)

This paper involved written text looking at the general disease of cystic fibrosis and the background of research undertaken into developing a cure. Work was carried out in developing data for a time course, providing F508del expression data to accompany WT and G551D data already present. Samples were collected at relevant hourly points after induction. The samples were ran on an SDS-PAGE gel, the CFTR fluorescence was ratioed against an intrinsic fluorescent yeast protein and plotted logarithmically against the relevant time point taken. The WT and G551D data had already been provided from experiments carried out by another of the authors, Xin Meng. Time course data is provided in one of the other papers therefore this paper provides a basis from which the others can be deduced. This paper is important to the field, providing an introduction to the basis of the disease and the need for development of correction compounds to occur. It summarises the structure of the CFTR protein, describing the function and topology of the domains and how the function of the protein is formed from these. It argues that the basis of cystic fibrosis is rooted in the instability of the protein caused by the deletion of phenylalanine at position 508. Therefore this paper introduces the fundamental basis of the pharmacological aspect of this thesis. That to correct the F508del mutation, providing pharmacological relief to the patient, fundamental correction of the instability of the mutant protein must

occur. Indeed the paper introduces the thermal stability assay, which will be presented as the main method in chapter 8 of this thesis. In terms of writing, the majority of the introduction text was written by the candidate.

1.3 The structural basis of cystic fibrosis (Chapter 4)

This paper provides a general introduction to the Cystic Fibrosis Transmembrane Conductance Regulator (CFTR), its structural parameters and their relation to its function as an ABC transporter. The paper explores the effect of the mutation on the conformation of the protein, providing the scientific basis to provide pharmacological correction to the mutation, as well as elucidate more about the overall biogenesis of the mutated protein and how its structure and conformation is affected in a normal state. Similarly to the previous chapter, this paper introduces the field looking at aspects of the structure of the protein and how the mutation leads to the disease by affecting this structure. The candidate contributed text to this paper and is included in this thesis as a means to provide an introduction the field and provide a basis for the research chapters presented later in the thesis.

1.4 CFTR structure, stability, function and regulation (Chapter 5)

The main premise of the paper is that F508del has an effect on the overall stability of the protein, rather than affecting the wider conformation.
The studies in the paper test the effect of the F508del mutation on the structure, conformation and stability of the CFTR protein. The limited proteolysis experiments were carried out in as part of this PhD, comparing pure protein and microsomal membranes. All of the constructs used; F508del, WT and G551D possessed a GFP tag at the c-terminus, therefore as the samples were ran on SDS-PAGE gel, and subsequently scanned, the fluorescence given by the GFP tag could be visualised. Similarly, all of the constructs possessed an N-terminal SUMO-tag, this was visualised by immunoblotting, using a primary anti-SUMO antibody followed by a Li-Cor conjugated secondary antibody that would provide a signal following scanning. The degradation profile of each construct, in both its pure protein

and microsomal aspect was compared. The conclusions from these limited proteolysis studies identify the similarity between purified protein and microsomal membranes, arguing there is a retained conformation throughout purification, at least at the lower temperatures that the experiments were carried out at. The differences between F508del and WT in the degradation profiles seen here do show conformation differences but this can be summarised as an effect on the stability of the protein rather than the overall conformation. The candidate contributed to Figures 2 & 3 of this paper, as well as the main body of text.

Chapters 3, 4 and 5 are included in the thesis as an introduction to the basis of the PhD and introduce the background of CFTR and the disease to which the mutation causes. They also provide an introduction to the methods used in the primary research papers presented in this thesis, validating the premise of the research and the direction that was taken to answer the two objectives presented earlier on in this chapter. The CPM method is shown in chapter 3 of this thesis and the limited proteolysis method is identified in chapter 5 of this thesis.

The cystic fibrosis transmembrane conductance regulator (CFTR) CFTR has been widely studied for decades[5]. Particularly, studies have always tried to elucidate the similarities between structure and function and how this may relate to disease. Early studies utilised non-human CFTR analogues that were more stable and easier to express than the WT and mutant forms of the human protein. There have been many structural and expression studies using other orthologues of human CFTR. Their genetic similarity has allowed for postulation and planned experimentation on human CFTR, as the functional domains of the protein have been conserved in the orthologous structures [6, 7]. Particularly interesting is the fact that the functional domains of CFTR, the nucleotide binding domains and the transmembrane domains are highly conserved across the orthologous mammalian system. These orthologous structures have been expressed using a variety of expression systems that allow the protein to be studied by structural studies such as cryo-electron microscopy or X-ray crystallography.

The CFTR construct used in this paper has been expressed in a *Saccharomyces cerevisiae* strain, FGY217. Using a plasmid provided from David Drew's lab [8] .The plasmid contains a *pep4* deletion corresponding to the removal of lysosomal endopeptidase Pep4p [9]. Previous work carried out with this genetic modification has shown improved expression, in regards to limiting degradation of membrane proteins in yeast, particularly *S. cerevisiae* [10]. The CFTR construct has been placed downstream of a galactose promoter (GAL1) [8] indicating induction of cellular manufacture of the protein when the log phase of growth yeast cells are exposed to galactose. It has been shown that overexpression of recombinant proteins can be toxic to the yeast cell, indeed the overexpression of a large, unstable, membrane bound protein would prove taxing and energy depleting of the cell. Therefore, the expression of CFTR is beneficial to the host expression system if placed downstream of a tightly regulated promoter rather than a promoter that may exhibit sporadic or delayed expression. The phase of growth, and abundance of glucose can be monitored by optical density and colorimetric tests respectively. This allows rather exact induction of the expression system and also allows accurate monitoring of the effect of the expressed CFTR protein on the yeast expression system. During the log phase, the cellular cycle of the yeast organism has achieved a status that is able to efficiently produce the protein. Similarly the cellular density is high enough that enough of the recombinant protein is expressed for experimental purposes. Yeast has been chosen and is continued to be used for membrane protein expression due to its robustness its ability to be grown to a large scale and it's genetic manipulability [11]. It allows for post-translational modifications on proteins that are generated allowing for mammalian membrane proteins to be in their nascent state. It has limitations for human membrane proteins but strains of varying genetic use can be used to enhance their expression.

1.5 CFTR structure and the effects of disease-causing mutations probed by limited proteolysis (Chapter 6)

This paper provides insight into the effect of proteolytic enzymes on purified CFTR and CFTR containing microsomal membranes. Due to CFTR's nature as an ABC transporter, it is heavily influenced by phosphorylation. Work has been shown that indicates its activity is regulated by phosphorylation and that its structure changes upon phosphorylation. [6, 7, 12-15] Work has already been carried out showing the efficacy of limited proteolysis in determining conformational differences between protein structures [16, 17]. Therefore, using the strength of the purified protein, we have carried out work identifying differences between the phosphorylated and dephosphorylated forms of the protein. This adds weight to the current cystic fibrosis field as the recent cryo-EM structures have variable conclusions ascertaining to what the conformation of the protein is at. A paper in this thesis [18] has already put forward the hypothesis that CFTR, in the presence or absence of substrate, actually exists as a number of states, outward or inward. The work in this paper investigates the differences between phosphorylated and dephosphorylated protein in terms of its susceptibility to proteases. All of the limited proteolysis work presented was carried out by the candidate and is being presented as one of two main chapters for examination. The candidate carried out preparation of samples. In this chapter, other authors, namely in Figure 7 and 4, carried out work involving cryo-EM and fluorescence microscopy respectively. The data is included in here for the sake of the publication. The author's names are present and credited duly.

1.6 Exploitation of a novel biosensor on the full-length human F508del-CFTR with computational studies, biochemical and biological assays for the characterization of a new Lumacaftor/Tezacaftor analogue (Chapter 7)

This paper was a means by which to validate and use a novel biosensor for identification of a novel corrector that could be used against the F508del-CFTR mutation. Computational modelling in combination with surface

plasmon resonance (SPR) and thermal stability studies aimed to identify a useful biosensor in the development of novel correctors.

This paper identifies the importance of using full length F508del-CFTR as means to test the effect of new pharmacological compounds. It argues that in recent cystic fibrosis history drug development has been hindered by the complexity of the CFTR protein in general but also by the extreme limitations of expression, stability and function caused by the F508del mutation. This has led to poor generation of the full-length protein leading to insensitive novel compound testing and an inhibited treatment pipeline. The paper aims to illustrate the use of surface plasmon resonance (SPR) as a means to test the interaction of a novel pharmacological compound with detergent purified CFTR as well as setting up a useful model that can be used for future development.
The PhD work involved proof of principle of the CPM assay, using purified protein from the lab in Manchester in combination with CPM dye to test the viability of the assay. The candidate tested the novel compounds and biosensor in the CPM assay.

This paper shows use of the isothermal CPM assay as a means to test the effects of certain variables on CFTR stability. It also argues the point of using purified full-length CFTR as a means of developing new compounds for cystic fibrosis treatment. The effect of the mutation leads to a global effect on the whole protein so any testing of correction is useful in terms of affecting the full-length protein rather than an isolated domain.

Novel compounds sent from Italy were used in combination with WT-hCFTR purified in LPG-14. The protein was diluted in various buffers that were used for SPR and ran via the thermal stability assay. Overall, the candidate contributed to Figure 2; with panel C. Figure 2C provides comparison of the various buffers that would be used for the SPR, comparing the control of PBS-DMSO with a synthetic phospholipid blend as well as the HBS-EP. This figure provides further validation of the assay, allowing it to test the effect of various buffer conditions, detergent profiles, reagent conditions, etc. on the stability of a protein. The CPM dye is greatly

beneficial for the use of stability testing for membrane proteins due to the nature of their structure and the likely presence of buried cysteine residues. This paper demonstrates a marked difference between the stability of certain buffers, showing the assay's sensitivity to differences in stability caused by the different reaction conditions.

The candidate's work also contributed to Figure 8, panel A, in which a novel compound, EN503a was tested using the assay and compared with an existing compound, Tezacaftor, one of Vertex's compounds[19]. EN503a was tested following its use with SPR. The method by which it was tested should set the precedent for the testing of the other compounds later in this thesis, in chapter 8. It provides a proof of principle to the development of novel compounds. Both EN503a and Tezacaftor (VX-661) are shown to have some correction ability when used in this regard.

1.7 Assessment of fluorescent assays for F508del CFTR stability and the screening of FDA-approved and natural product compound libraries (Chapter 8)

This paper identifies testing of compounds to find novel correctors and potentiators. The main body of work presented by the candidate here involves testing of an FDA approved drug library. This presents two main benefits for the wider field. The principle of drug repurposing is a means by which existing drugs are investigated for different uses[20]. These drugs are already clinically used for alternative ailments to cystic fibrosis, having passed the stages of clinical trials necessary to be administered by a patient at various chronic concentrations. This presents a major benefit for the British cystic fibrosis field. It is in the interests of the NHS and the Cystic Fibrosis Trust UK charity to minimise the costs of new treatments, but also to provide competition to the current treatments that are available for the patient. Bypassing the costly, both in time and financially, clinical trials that come with traditional drug development will reap rewards for the patient if a new treatment is found. The second benefit of testing an FDA approved drug library is providing solutions to problems that may not currently exist. Due to the nature of the cystic fibrosis disease, patients suffer and require

treatment from birth until they die. Improvements in the treatment, the drugs available, as well as the clinics has increased the life expectancy of cystic fibrosis patients narrowing the gap in the quality of life between CF sufferers and healthy individuals. This of course leads to cystic fibrosis patients living a longer life than ever before increasing the likelihood of occurrence of other diseases and ailments that may affect the patient. The drugs contained in an FDA-approved drug library would more than likely be taken by CF patients, perhaps over an extended period of time. Data from an assay shown in this paper allows us to look at the potential effects of common drugs on CFTR, allowing clinicians to make informed decisions to patients about the negative, or indeed positive outcomes of different treatments. Indeed, similar work has already been seen in the effect of a Vertex potentiator, VX-770, on the ABC transporter P-glycoprotein[21].

The paper outlines the methods of the assay used, the compounds that were tested and how effective the method is for finding new compounds to be used for correction. The candidate presents this paper as joint first author. The majority of the work presented in this paper is present in the form of two assays, a 48-well assay and a 96-well assay. The candidate was the main proprietor of the 48-well assay whereas the other joint first author, Xin Meng was the main proprietor of the 96-well assay. The manuscript presented in this thesis was mainly written and compiled by the candidate – Xin Meng contributed to analysis and generation of figures. Purification of protein and preparation of samples was jointly shared by the candidate and the other first author.

Overall all this work contributes to the idea that there is still pharmacological progress to be made in the field of rescuing CFTR. It presents the idea that a different approach is needed in the future for effective drug discovery due to the slow progress of current treatments.

1.8 Objectives

The aim of this PhD was to promote the identification and development of novel compounds to treat the most common form of cystic fibrosis, F508del.

The finer objectives of this aim were as follows:

- to provide novel insight into new corrector compounds as well as provide a means to which novel correctors can be identified.
- To provide insight into the when and where the F508del mutation affects CFTR during biogenesis. The work presented in this thesis adds to the foundational experimental procedure of what can be used to elucidate this conundrum. Through evidence provided from the time course and addition to the limited proteolysis procedures a foundation for future work is provided to solve this mystery.

Chapter 2.0 Materials & Methods

2.1 Materials

- 30% acrylamide/Bis solution 29:1 (*Bio-Rad, 161-0156*)
- Adenosine 5'-triphosphaate magnesium salt (Mg-ATP) (*Sigma-Aldrich, A9187*)
- Agar (*Formedium, AGA03*)
- Aminoethylbenzenesulfonyl fluoride (AEBSF) *(Sigma-Aldrich, A8456*)
- Ammonium persulphate (APS) (*Fischer Scientific, BPE179-100*)
- Benzamidine hydrochloride (*Sigma-Aldrich, 434760*)
- Bestatin (*Sigma-Aldrich, B838*)
- Bradford reagent concentrate (*Bio-Rad, 500-0006*)
- Chymostatin (*Sigma-Aldrich, C7268*)
- Chymotrypsin (*Sigma-Aldrich*, *C4129*)
- Coumarin meleimide (CPM) (*Life Technologies, D-346*)
- D-galactose (*Fischer Scientific, G/0500/48*)
- D-glucose (*Fischer Scientific, G/0500/53*)
- Dimethylsulfoxide (DMSO) (*Sigma-Aldrich, D8418*)
- Dithiothreitol (DTT) (*Sigma-Aldrich, 43817*)
- Dodecyl-maltoside (DDM) (*Affymetrix, 69227-93-6*)
- Ethanol (*Fischer Scientific, E/0056DF/P17*)
- Epoxysuccinyl-leucylamido-butane (E-64) (*Sigma-Aldrich, E3132*)
- Glass beads, acid washed, 425-600µm diameter (*Sigma, G8722*)
- Glycerol (*Fischer Scientific, G/0650/17*)
- Glycine (*Fischer Scientific, BPE318*)
- Hydrocloric acid (HCl) (*Fischer Scientific, A466-2*)
- Imidazole (*Sigma-Aldrich, 1553)*
- Instant Blue Coomassie (*Novexin, 15BIL*)
- Leupeptin hydrochloride (*Sigma-Aldrich, L9783*)
- Lyso-phosphatidylglycerol 14 (LPG) (*Avanti, 185092*)
- mqH_2O (*lab supplied through a Millipore Q 0.22µM filter system*)
- PageRuler plus pre-stained protein ladder (*Fermentas, SM1811*)
- Pepstatin A (*Sigma-Aldrich, P4625)*

- Phenylmethanesulfonylfluoride (PMSF) (*Sigma-Aldrich, P7626*)
- Proteinase K (*Roche, RPROTKSOL-RO*)
- Pro-Q Diamond Phosphoprotein Gel Stain (*ThermoFisher Scientific, P33300*)
- Sodium adenosine triphosphate (Na_2ATP) (*Sigma-Aldrich, A2383*)
- Sodium Chloride (NaCl) (*Fischer Scientific, S/2920/53)*
- Sodium dodecyl-sulphate (SDS) (*Fischer Scientific, BPE166*)
- Sucrose (*Fischer Scientific, S/7400/53*)
- Tetramethylethylenediamine (TEMED) (*Bio-Rad, 161-0800*)
- Thermolysin (*Promega, V400A)*
- Tris Base *(Fischer Scientific, T/P631/48)*
- Trypsin (*Sigma-Aldrich, T8642*)
- Tween-20 (*Sigma-Aldrich, P1379*)
- Uracil Drop Out - Complete Supplement Mixture (CSM) (*Formedium, DCS0169*)
- VX-809 *(Selleckchem/S1565*)
- Yeast Nitrogen base (YNB) (*Formedium, CYN0410*)

2.2 Equipment

- Toledo pH Meter (*Mettler Toledo, 51302910)*
- Semi-dry Transfer Machine (*Bio-Rad, 1703940*)
- AKTA Purifier (*GE Healthcare, 29010831*)
- Optima XE-90 (*Beckman Coulter, A94471*)
- Optima Max-XP (*Beckman Coulter, 393315*)
- Avanti J20-XP (*Beckman Coulter, J320XP-IM-5*)
- Biospec Beadbeater (*Biospec, 11079100-105*)
- Chemidoc XRS+ (*Bio-Rad, 1708265)*
- UNcle (*Unchained Labs*)

2.3 Media and Buffers

YNB Broth 6.9g/L of YNB media, 0.77g/L of CSM drop out media and 2% glucose.

YNB Agar 6.9g/L of YNB media, 0.77g/L of CSM drop out media, 2% glucose and 20g/L of agarose.

mPIB Buffer 0.3M Tris (pH8), 0.3M Sucrose. Buffer was supplemented with 2mM DTT and 1x Protease Inhibitors depending on use.

CFTR Buffer 50mM Tris (pH8), 20% glycerol and 1M NaCl. Buffer was supplemented with 1mM DTT and 1x Protease Inhibitors depending on use.

Solubilisation Buffer 50mM Tris (pH8), 1M Salt (varies depending on experiment), 20% glycerol and 4% detergent (varies depending on experiment)

Purification Buffer A: 50mM Tris (pH8), 1M Salt (varies depending on experiment), 20% glycerol and 0.04% detergent (varies depending on experiment).

Purification Buffer B: 50mM Tris (pH8), 1M Salt (varies depending on experiment), 20% glycerol and 0.04% detergent (varies depending on experiment) and 1M imidazole.

Low Tris Limited Proteolysis Buffer – 50mM, 50mM NaCl, 10% Glycerol. s

2.4 Large Scale Fermenter Culture

Glycerol stocks of FGY217 containing the F508del-hCFTR plasmid were streaked out on YNB-Agar plates and grown for three days. A full plate of colonies was then picked and grown overnight in two baffled flasks containing 750ml of YNB broth and 2% glucose. The culture was then diluted into 14 litres of YNB broth. Glucose concentrated was monitored

using standard glucose testing strips and 0.1% glucose was supplemented if the glucose concentration of the media was depleted. The fermenter culture was left to grow at 30°C until an OD600 of 0.8-1.2 was reached or the glucose concentration was depleted.
Cultures were then induced with 2% galactose and 8% glycerol and left to grow for 16-18 hours at 20°C. Following this, cells were centrifuged at 3000 x g for 10 minutes at 4°C. The supernatant was discarded and the pellets were re-suspended in mPIB buffer and subsequently snap frozen for further use.

2.5 Large Scale Time Course Growth

For time course samples, a fermenter was prepared as usual. The glucose concentration and optimum density were monitored closely until the glucose concentration had expired. The fermenter was then induced with the galactose induction media; this was taken as time point 0. Time was monitored from this and subsequent samples were taken out of the fermenter at their respective time points and harvested with usual methods.

To maintain sample consistency, the time course samples corresponding to each batch were broken with the same weight of beads which were from the same batch from the supplier and were therefore of consistent durability.

2.6 Microsome Preparation

Cells from a large-scale fermenter culture were thawed on ice and added to 160/180g of glass beads 400-600µm. mPIB buffer was added to fill the line of the canister. The cells were broken using a BioSpec Beadbeater for 15 minutes total. For every minute of breakage, the cells were left to cool for two minutes to ensure that the cells would not heat up too much.
200µl was taken every two minutes to assess the efficiency of cell breakage via OD380. A 1 in 50 dilution was made of the 200µl sample with CFTR buffer and then recorded in a spectrometer. If, over time, the OD380 increased linearly it was deemed that efficient cell breakage had occurred.

Following this, the solution was centrifuged at 11,000rpm for 10 minutes at 4°C to pellet unbroken cells and any in-solution glass beads. The supernatant was then centrifuged at 200,000 x g for 90 minutes to pellet mitochondria and unwanted cell contents. The subsequent supernatant was centrifuged at 100,000 x g for 60 minutes to pellet the microsomal membranes. The pellet was re-suspended in CFTR buffer and the stock of microsomes subsequently snap-frozen for further use.

2.7 Solubilisation of microsomal membranes

Transfer of the protein from the microsomal membranes to detergent micelles required solubilisation of the protein with a detergent-containing buffer. DDM and LPG detergent were used at a final concentration of 2% as routine, but this can adjusted depending on the experimental procedure. The microsomal material was incubated for 2 hours at 4°C and centrifuged for 45 minutes at 100,000 x g to separate the soluble and insoluble fractions.
The soluble fraction was collected and the insoluble pellet was gently re-suspended in CFTR buffer.

2.8 SDS-PAGE

Samples of cells, microsomes and protein were ran on custom made 8% or 10% acrylamide gels. The samples were diluted with loading dye, usually at a 2:1 ratio but this could be adjusted depending on the protein concentration of the sample. Once added with loading dye, the sample was left at room temperature for 15 minutes and than span at 1500x g for 30 seconds in order to pellet any aggregates that may have formed. Following this the samples were added to the wells of the gel ran at 110 volts for 20 minutes to allow travel through the stacking portion of the gel followed by 130 volts for another 70 minutes to allow travel through the resolving part of the gel.
The gels were subsequently scanned for GFP signal using a Chemidoc MP scanner, using a blue light with a 530nm emission filter to scan for the GFP signal and a green and red light to visualise the PageRuler protein marker. The software available collated these three scans with the Chemidoc MP

scanner to provide a Multichannel image for analysis, which appears in this thesis alongside each corresponding 530nm scan representing the GFP signal.

2.9 Nickel-Affinity Chromatography Purification

Routine purification was carried out according to the protocol outlined in (Pollock et al., 2014). A HisTrap column was connected in parallel with an ÄKTA Purifier system (GE Healthcare). The column was equilibrated with 5 column volumes (CV) of MQ water followed by 5 column volumes of purification buffer. The solubilised material was supplemented with 5mM of imidazole and ran over the column at a flow rate of 0.5ml/min in order for the His-tagged CFTR protein to bind to the nickel resin. The flow through was collected. The column was then washed with varying ratios of imidazole containing purification buffer depending on the wash carried out at a rate of 0.5ml/min.

2.10 Concentration of Purified Sample

Purified protein stocks were concentrated using a 100kDa filter, Sartorius VIVASPIN TURBO 4. The solutions were centrifuged with the filter for 100,000 x g for 15 minutes at 4°C. The resultant purified protein was re-suspended from the filter with 500ul-1ml of purification buffer depending on the volume of pre-concentrated sample.

2.11 GFP Purification

The material for purification was incubated overnight with the GFP resin. The solution was span down at 2500 x g for two minutes. The supernatant, representing the unbound fraction of the protein, was collected. The resin was then washed with a sample volume of purification buffer. This was then span down at 2500 x g for two minutes and the wash fraction collected. TEV protease was added at 0.2ul/ug of protein, this was then incubated overnight at 4°C with 1 sample volume of purification buffer. One final spin at 2500 x g for two minutes provided the elution fraction containing the protein.

2.12 CPM Assay

Depending on the reaction carried out, the concentration of the protein was varied from 200-1000ng. The CPM dye was diluted from a 4mg/ml stock down to 0.05µg per reaction. The experiments were run using a UNcle system. The reactions were run in tandem using a 16 well cassette and the reactions were subjected to a thermal ramp from 15-90°C and excited with a UV spectrum laser. The resulting spectra were transferred from the connecting software for analysis.

2.13 Immunoblotting – Semi-dry Method

Following SDS-PAGE analysis, the acrylamide gel was transferred by semi-dry method onto nitrocellulose membrane paper using a prepared 'sandwich' of three pieces of 9 by 6 inch blotting paper soaked in cation buffer 1 followed by three pieces of blotting paper soaked in cation buffer 2 followed by the nitrocellulose membrane soaked in cation buffer 2 followed by the acrylamide gel followed by three pieces of blotting paper soaked in anion buffer. The transfer was ran for an hour at 15 minutes and transfer was confirmed via Ponceau stain.

2.14 Immunoblotting – Blocking and incubation with antibodies.

Following confirmation of transfer, the membrane was blocked with a 2% BSA solution. The BSA was dissolved into 1xTBST buffer and added to the membrane with gentle shaking for 1 hour at room temperature.
The primary antibody was then diluted in 1xTBST blocking buffer to the required concentration and added to the membrane for overnight incubation at 4°C. The next morning, the membrane was taken and washed for 5 minutes 5 times with 1xTBST buffer. Following washing, the secondary antibody was diluted in 1xTBST blocking buffer and added to the membrane and the membrane was subsequently left to incubate for 1 hour at room temperature. Following this the membrane was washed with 1xTBST buffer for 5 minutes 5 times. The membrane was then ready for visualisation, using the LiCor Odyssey machine.

2.15 Limited Proteolysis

Thermolysin

Limited Proteolysis reactions were carried out at 4 degrees in a 20ul reaction. Protein and microsomes previously prepared according to 2.9 and 2.6 respectively were incubated with enzyme for 15 minutes and then the reaction was halted with 12mM of EDTA. Pure protein amount was kept at a constant of 0.5µg and microsome concentration was kept at a constant of 1ug while thermolysin enzyme was maintained at 12.5µg/ml and 50µg/ml for pure protein reactions, and 25µg/ml and 250µg/ml for microsome reactions. The enzyme was diluted in a calcium-containing Thermolysin buffer to provide the co-factor for the enzyme reaction. The chelating buffer stopped the reaction after addition. 2x Sample Buffer was then added to the reaction 1:1 and left at room temperature for 30 minutes before being run on a 12% polyacrylamide gel. SDS-PAGE was conducted for 90 minutes at a constant of 130 volts.

Trypsin

Trypsin reactions were carried out in 20ul reactions on ice. The experiments were conducted by ratio of mass. 75:1, 150:1 and 300:1 – the trypsin quantity would vary depending on the amount of microsomal or pure protein being used. The reactions were carried out in a low Tris limited proteolysis buffer, which was usually used to make up the reaction to the full reaction volume. The proteolysis reaction was stopped with protease inhibitors from the PI cocktail which was diluted to a 1x stock. 2x loading dye was added at 1:1 ratio with the reaction volume of the sample and this was then run onto a SDS-PAGE gel.

Proteinase K

Proteinase K limited proteolysis reactions were carried out similar to trypsin reactions. They were conducted using mass ratios between the enzyme and the protein. The enzyme quantity was diluted in respect of the amount of microsomal or pure protein being used and the ratio for which the reaction was conducted. The reaction was stopped with protease inhibitors from the PI cocktail which was diluted to a 1x stock. 2x loading dye was added at a 1:1 ratio with the reaction volume of the sample and this was onto a SDS-PAGE gel.

2.16 Visualisation of anti-SUMO degradation profile

For Anti-Sumo identification, the gel was transferred using the semi-dry method using Anode and Cathode Transfer buffers. Following transfer, the membrane was incubated in a BSA blocking buffer for 1 hour at room temperature. The membrane was then incubated with an anti-Sumo primary antibody (Ms mAB to PAN SUMO *abcam ab176485*) overnight at 4°C. Following incubation the membrane was washed with TBST buffer 5 times for 5 minutes. The membrane was then incubated with a secondary antibody (Dnk pAb to Ms IgG (IRD® 800cw *abcam ab216774*) for an hour at room temperature. Followed by 3 washes with TBST buffer for 5 minutes. The membrane was then viewed on a LiCor Odyssey machine.

2.17 Q staining method

The method for Q staining was carried out per manufacturer's instructions. An SDS-PAGE acrylamide gel was ran as normal and explained as above in this chapter. All steps involve enough volume of the solution to submerge the gel in a sufficiently sized container. Following SDS-PAGE, the acrylamide gel was fixed with a 50% methanol, 10% acetic acid solution for 30 minutes and then overnight with fresh solution. The gel was then washed with mqH_2O water for 10 minutes for 3 times. The gel was then stained with the Pro-Q Diamond stain for between 60-90 minutes. The gel was then destained using a 20% acetonitrile solution for 30 minutes and 3 times. The gel was then washed for 5 minutes twice in mqH_2O. Following this the gel could then be scanned using a Chemidoc MP

Chapter 3.0

The cystic fibrosis transmembrane conductance regulator (CFTR) and its stability

Abstract

The cystic fibrosis transmembrane conductance regulator (CFTR) is responsible for the disease cystic fibrosis (CF). It is a membrane protein belonging to the ABC transporter family functioning as a chloride/anion channel in epithelial cells around the body. There are over 1500 mutations that have been characterised as CF-causing; the most common of these, accounting for ~70 % of CF cases, is the deletion of a phenylalanine at position 508. This leads to instability of the nascent protein and the modified structure is recognised and then degraded by the ER quality control mechanism. However, even pharmacologically 'rescued' F508del CFTR displays instability at the cell's surface, losing its channel function rapidly and it is rapidly removed from the plasma membrane for lysosomal degradation. This review will, therefore, explore the link between stability and structure/function relationships of membrane proteins and CFTR in particular and how approaches to study CFTR structure depend on its stability. We will also review the application of a fluorescence labelling method for the assessment of the thermostability and the tertiary structure of CFTR.

Introduction

Cystic fibrosis transmembrane conductance regulator (CFTR) is unique among ABC transporters as it is the only member of this family of membrane proteins to act as an ion channel (although two ABC proteins (SUR1 and SUR2) regulate a potassium channel rather than act as transporters [1, 2]). As expected, the cystic fibrosis transmembrane conductance regulator (CFTR) follows the same domain structure as other ABC transporters (Fig. 1): it has two nucleotide-binding domains (NBDs) in tandem with two transmembrane domains (TMDs). What differentiates it from the other transporters (apart from its channel activity) is

its regulatory domain or 'R' region (the word 'region' is suggested by Forman-Kay and co-workers as this 200-amino acid-long region is largely unstructured when analysed in isolation by NMR [3]). The R-region lies between the first TMD and the second NBD, within the cytoplasm. There is no significant sequence homology between the R-region and any other proteins in nature; hence, its origins are obscure. Within the ABC family, only ABCA1 in higher plants has a connecting region of similar length, and this is enriched in charged residues, like the CFTR R-region. The R-region contains a number of Protein Kinase A (PKA) phosphorylation sites which have been shown to be highly conserved across species [4] PKA is a cAMP-activated kinase and as cellular levels of cAMP increase, PKA phosphorylates CFTR. In a readily understood model, the R-region is proposed to block the NBDs from associating together which subsequently keeps the channel in a closed conformation. Phosphorylation causes a structural change that removes the R-region from its steric-interfering position and allows NBD dimerisation to occur, triggering a much larger conformational change (Fig. 1). It is then the binding of ATP that is thought to initiate channel opening whilst channel closure is associated with ATP hydrolysis and release of ADP and inorganic phosphate [5, 6]. Forman-Kay and co-workers have proposed a more complex model involving the C-terminal region [7], which also displays a sequence unique to CFTR. In this model, phosphorylation of the R-region causes a switch from it interacting with the NBDs to it interacting with the C-terminal region. In this scenario the R-region acts as a global regulator of CFTR via its alternative interacting partners [7].

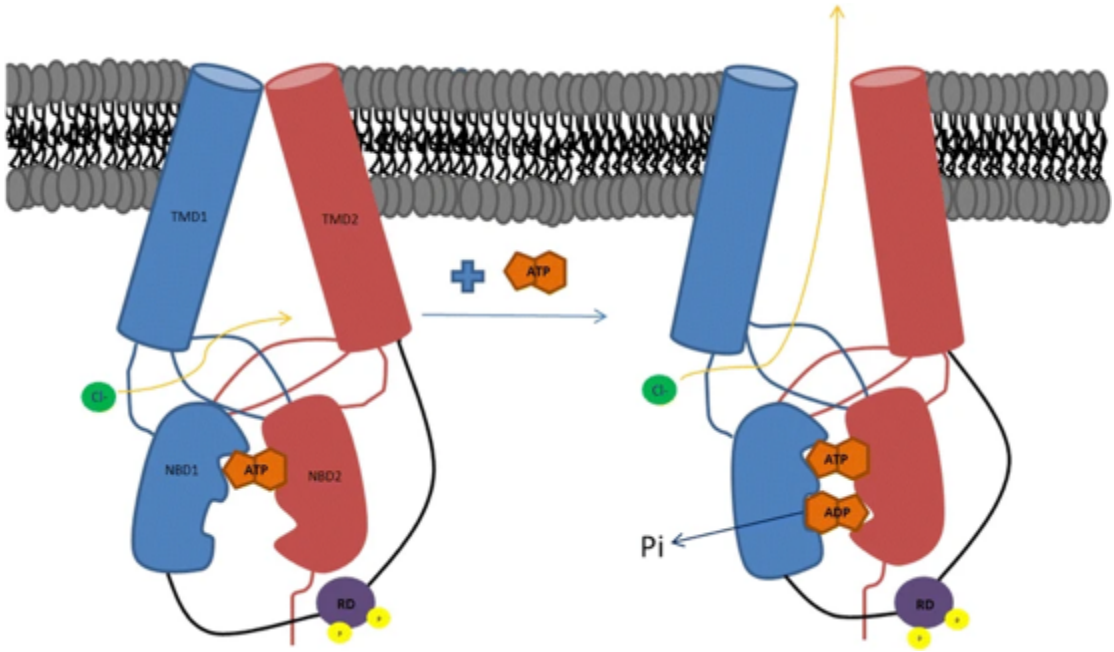

Figure 1: Cartoon illustrating how ATP binding and subsequent hydrolysis could lead to channel opening and flux of chloride ions (based on the model proposed by Wang et al. [3])

The effects on stability of F508 deletion

Cystic fibrosis is caused by mutation in the CFTR protein. There are estimated to be over 1800 different mutations that can lead to cystic fibrosis (http://www.genet.sickkids.on.ca). Of these, the deletion of phenylalanine at position 508 is by far the most common and 95 % of CF patients possess at least one allele with this mutation. Homozygous F508del patients account for 65–70 % of cystic fibrosis cases in some groupings [8] and they have almost complete loss of the protein at the apical membrane. These patients have the most severe form of the disease. Heterozygous individuals (carriers), with one WT gene and one F508del mutated gene, have no symptoms and there may have been some selective advantage in the past for such individuals—such as reduced water loss in diarrhea. This has led to a theory that the prevalence of this mutation in certain populations is due to the increased resistance to dehydration-causing diseases such as cholera and typhoid fever which were previously major causes of morbidity, especially in infancy [9].

The F508del mutation and its effect on the stability and function of the protein have been studied extensively [10–14]. The deletion of phenylalanine at position 508 is crucial due to the position of this residue in the tertiary structure of the protein. It probably lies at the connecting position between the helical sub-domain of NBD1 and the second cytoplasmic loop of TMD2, a conclusion based on homology modelling [15] as well as cross-linking studies [8, 16, 17]. As a result of the mutation, there is thought to be a less stable conformation between TMD2 and NBD1, resulting in a protein that is recognisable by ER chaperones and which is then degraded by the ER quality control system via ubiquitinylation and proteasome-mediated degradation [18–20].

Cui et al. also considered the defect of F508del in terms of a different set of domain interactions [21]. They proposed that F508 deletion has an effect early in the folding of the protein and that the interaction between NBD1 and TMD1 is stabilised by this residue. These conclusions were based on the observation of a defined TMD1-NBD1 unit that was resistant to exogenously added protease in the WT protein, but not in the F508del version. This early unit in the CFTR

folding pathway was proposed to be sufficient to escape endoplasmic reticulum quality control. If the F508del CFTR protein arrives at the apical membrane of the epithelial cell, it exhibits a reduced functionality as a chloride channel [22] and is susceptible to degradation. Two problems are thus associated with the mutated protein, a reduced migration to the apical membrane of the cell and the limited amount of protein that is found at the membrane has a highly reduced gating functionality. Treatments aimed at combating both of these defects have been considered [14].

Treatments affecting the stability defect

The first indication of a potential therapeutic method was reported by Denning et al. [23]. Their results showed, with cells from two different expression systems, that the induction of expression of F508del CFTR at lower growth temperatures gave a much greater amount of fully glycosylated protein (the so-called 'Band C', migrating with a roughly 25 kDa higher relative mass on SDS-PAGE gels is extensively glycosylated). They suggested that some of the mutated protein had escaped the usual endoplasmic reticulum quality control step and had been correctly glycosylated and had proceeded to the plasma membrane. Perhaps for the first time these results highlighted the role of thermal stability in the correct processing of full-length CFTR. Shortly after this, work by Sato et al. [24] showed that F508del-CFTR-expressing cells, when exposed to 10 % glycerol, increase their expression of the mutant protein. These results included immunoblotting of the mature, fully glycosylated protein after pulse chase and patch clamp recordings of the cells which identified an increase in chloride conductance. This discovery, alongside that of Denning and co-workers [23], illustrated that the instability/misfolding of F508del-CFTR can be reversibly corrected by either lowered thermal energetics of the protein, or by the inclusion of a molecular chaperone such as glycerol. Although glycerol treatment cannot be translated therapeutically, the work highlighted that development of small-molecule correctors of the instability/folding defect might achieve pharmacological practicality. It is now 20 years after these studies, and there has been the discovery of a number of pharmacological correctors aimed at treatment of the F508del mutation [25]. For example, compounds have been produced that affect the F508del-CFTR interactome including the proteasome

complex that leads to degradation of the protein and chaperones that specifically bind to the F508del-CFTR peptide [13, 26, 27].

One of the earliest pharmacological groups of compounds to be discovered was that of the tricyclic benzo[c]quinoliziniums or MPB compounds [28]. These were originally deduced as activators of the CFTR channel. A further study of these compounds carried out by Dormer et al. [29] revealed that application of a derivative of the original compounds, MPB-07, resulted in increased delivery of CFTR to the apical membrane, similar to the amount seen in wild-type cells. This was shown to be as a result of the prevention of normal degradation of the mutated protein, allowing for increased, yet unstable CFTR to make its way to the apical membrane.

Some of the first pharmacological chaperones discovered through high-throughput drug screening were reported by Pedemonte et al. [30]. Four classes of molecules were found by this group of workers, each showing some efficacy in helping to re-fold CFTR. Out of the four classes of molecules, two showed significant efficacy in promoting an increased amount of F508del-CFTR to the plasma membrane. Those of the bisaminomethylbithiazoles, class 4, were found to be the most effective. Two particular molecules, corr-4a and corr-4c, when incubated with CFTR-expressing Fischer Rat Thyroid (FRT) cells, showed an increased efficiency of CFTR folding as well as stabilisation of the protein. Classes 2 and 4 are both thought to be proteostasis regulators [31], due to their effect on either the endoplasmic reticulum quality control (class 4) or the lysosome-mediated degradation quality control system (class 2). Only class 4 molecules showed efficacy in primary bronchial epithelial cells which would be the primary target cell in the diseased lungs.

Pedemonte and co-workers went on to explore the class 2 molecules identified in the original screening; this led to identification of a particular group of compounds called aminoariathiozoles (AATs). These compounds showed enhanced channel trafficking and improved gating; this was seen as a promising result due to the fact that a potentiator would no longer be required in addition to a corrector. However, a further study involving these compounds failed to produce a statistically significant result in primary bronchial epithelial cells [32].

A number of studies have similarly fallen short in finding molecules that are effective in vivo.

Van Goor et al. [33] described a corrector compound with efficacy in human bronchial epithelial cells, a quinazolinone derivative, VRT-325. From their study, they showed that the drug also aided the expression of other mutant forms of CFTR. Further optimisation from this screen led to one of the most successful correctors to be developed [34]. When tested in cultured primary human bronchial epithelial cells, VX-809 increased chloride transport to that of 14 % of non-CF (HBE). Most importantly, this was enough to produce an increase in the thickness of the airway surface liquid (ASL) which shows a high clinical importance [35].

VX-809 did show some efficacy in Phase IIa clinical trials carried out by Clancy et al. [36]. These studies show a reduced sweat chloride concentration indicating that VX-809 is active in that particular organ. However, reduced sweat chloride is only a biomarker; it does not improve quality of life. A desired clinical outcome in CF patients would be improved lung function. This particular study proved that VX-809 has an acceptable safety profile and provided a foundation for an increase of the study on the particular drug.

Farinha, CM et al. [37] have shown that out of the three correctors currently developed: VRT-325, VX-809 and C4, VX-809 has been shown to be the most effective in increasing protein accumulation to the plasma membrane. Compared to VRT-325 and C4 in primary HBE cells, a higher production of F508del-CFTR was found with the use of VX-809. However, despite the promising results gained from VX-809, the rescuing effect was not high enough to restore CFTR function to wild-type levels. Cystic fibrosis symptoms may be prevented with as little as 25 % delivery of CFTR to epithelial cells, and certainly heterozygous individuals with presumably 50 % CFTR levels are unaffected. Synergistic trials were undertaken to try to increase the rescuing effect of VX-809 by applying another drug in the presence of VX-809. VX-770 is an FDA authorised potentiator drug, used to correct the gating defect present in the CFTR G551D mutation. This restores the channel into an open state which allows chloride conduction across the membrane where previously the G551D mutation resulted in a constitutively

closed formation. Two recent studies have explored the use of VX-770 in combination with VX-809 to potentially increase the efficacy of VX-809's rescue of F508del-CFTR to the plasma membrane.

Sampson et al. [38] showed development of a pharmacological chaperone corrector; that is, a compound that binds to the CFTR protein itself and stabilises the interaction between NBD1 and the TMD1. Despite no further work being carried out on the compound to date, Sampson and co-workers' study provides somewhat of a scaffold for future pharmacological chaperone development. In particular, they identify a terminal phenyl ring which they postulate to be necessary for interaction with the nucleotide-binding domain.

VX-661 is another promising pharmacological chaperone, an improved version of VX-809, which has shown improved lung function among homozygous F508del-CFTR patients in a phase II trial. Vertex Pharmaceuticals has announced the compound to be used in triple combination trials with newly developed correctors, VX-440 and VX-152, both of which are thought to have a positive effect on the processing and trafficking of the CFTR protein leading to a higher yield at the cell surface.

Despite the positive data achieved from Vertex's compounds, VX-770 has been shown to reduce the therapeutic effect of established CFTR chaperones. Two studies by Veit et al. [39] and Cholon et al. [40] have shown evidence which would suggest that VX-770 biochemically destabilises F508del-CFTR, thus reversing the effect of current correctors, VX-809 and VX-661. Although these are both in vitro studies and do not contradict the slight alleviation of CF symptoms by VX-809-derived treatments, discovery of new pharmacological correctors is probably required to ensure more effective treatment of the F508del mutation. A revised strategy to ensure effective drug discovery is also required, involving methods which increase the stability of the nascent protein, allowing it to progress to the plasma membrane. A compound of this nature will then suitably work in combination with VX-770 or another potentiator to maintain an effective amount of CFTR-F508del at the plasma membrane.

As renewed efforts are made towards the development of pharmacological compounds, assays of protein stability will be important to determine the

efficacy of corrector compounds. One could argue that the more stable the protein, the less likely it will be to unfold and the more likely it will be that it will escape the ER quality control steps. On the other hand, the global thermodynamic stability of the mutated protein may be irrelevant if the primary defect is at the early stages of protein folding. Although data on low-temperature rescue of F508del CFTR and its subsequent residence time at the plasma membrane point to the likelihood of a global thermodynamic defect, there remains the possibility that a specific step in the folding pathway is disrupted. To address this, studies on the stability and structure of purified CFTR are desirable, and this will be addressed in the next section.

Membrane proteins and the importance of stability for expression, purification and structural studies

Membrane proteins compose a significant fraction of the number of different proteins in the cell, and represent a disproportionately large fraction of the molecular targets of current drugs used to treat human disease. However, membrane proteins are vastly under-represented in the databases of protein structures [41]. This deficit in information is due to difficulties in membrane protein expression, purification and structure determination.

Membrane protein expression is fundamentally limited by available membrane area in the cell and by the capacity of the co-translational membrane insertion machinery. As a result, overproduction of membrane proteins like CFTR where membrane capacity is exceeded can lead to the production of aggregates in the cell that are highly resistant to detergent solubilisation and purification [42–44].

Purification is limited by the requirement for solubilisation of the membranes with detergent and then the need for detergent to be present throughout the subsequent fractionation processes [45]. The detergent may only partially solubilise the protein (if a 'mild' detergent is used) or may solubilise effectively but at the same time denature the protein (if a 'harsh' detergent is used [46, 47].

If a non-denatured protein can be purified, structural studies are still limited by the need for long-term stability of the tertiary and/or quaternary structure in the detergent, especially for NMR studies where the experiment will be performed well above 4 °C to increase the tumbling rate [48]. Moreover, the presence of the

detergent belt surrounding the protein can interfere with the structure determination. For NMR studies the micelle belt increases the size of the protein/detergent complex and reduces tumbling speed, with consequently broadened signals [48]. This has led to a bias in the range of detergents that have been used for NMR structures of membrane proteins (http://www.drorlist.com/nmr/MPNMR.html) with those forming small micelles being favoured. For X-ray crystallographic studies, the micelle must be accommodated within the crystal lattice without interfering with lattice contacts, hence must also be small and perhaps deformable. It is probably for this reason that membrane protein crystals are biased towards relatively high solvent contents—that is they have an open lattice that can accommodate the presence of the detergent micelle [49]. For single particle cryo-electron microscopy (cryo-EM) studies, the detergent micelle can be visualised as a weaker/diffuse band of density around the protein [50]. It is not yet clear whether this reduces the effectiveness of the cryo-EM approach, but the background presence of free detergent micelles can reduce contrast and the efficiency of single particle alignment steps in the 3D reconstruction procedure. For small-angle X-ray scattering studies (SAXS), the micelle's scattering needs to be divorced from the protein scattering to generate reasonable models which require a series of painstaking experiments with different solvent compositions so that either the protein or the detergent scattering component can be contrast-matched to remove its contribution to the scattering curve [51]. Similar approaches are employed for neutron scattering studies, but here the contrast is adjusted by varying the D_2O to H_2O ratio [52].

Stability - Many of these difficulties for membrane protein structure determination can be influenced by the stability of the protein. For example, a relatively unstable membrane protein such as CFTR may be recognised as such by the host cell's quality control machinery and degraded [14]. Similarly, an unstable protein is likely to have any instability accentuated by the presence of a detergent micelle; indeed the detergent may affect the membrane protein's soluble domains as well as the transmembrane domains [53]. Locally unstable regions of the protein in domains normally exposed to the aqueous milieu may give poor water solubility during purification because hydrophobic residues that are normally buried in the tertiary fold will become exposed with a concomitant

chance of forming polydisperse aggregates, especially at high protein concentrations [45, 54, 55]. Monodispersity is a strict requirement for structure generation from NMR and SAXS experiments, and is usually a pre-requisite for obtaining 3D crystals that diffract X-rays to high resolution [45, 56]. For single particle cryo-EM, monodispersity is also desirable, but is less strictly required for structure determination, especially if polydisperse aggregates can be readily distinguished from the non-aggregated monomeric or oligomeric particle [57]. Single particle cryo-EM and, to a similar extent, SAXS do not require high protein solubility for structure determination as they are compatible with protein concentrations below 1 mg/mL. However, NMR and X-ray crystallography usually require the concentration of the protein to be greater than 5 mg/mL.

Thus, the effects of the stability of a protein on its water solubility as well as its monodispersity properties are crucial for most structural biology techniques, with the possible exception of cryo-EM which is more tolerant of some polydispersity and does not require high water solubility of the protein. However, cryo-EM and SAXS-derived structures have typically been at much lower resolution than those obtained by X-ray crystallography and NMR. This is likely to change in the next few years for the cryo-EM technique with the introduction of new detection devices and software [58, 59]. Finally, it is possible that a membrane protein may adopt a non-native state that may still crystallise and generate a structure [60]. Thus, detergents and stability may be a factor even where structures are present in the protein data bank.

Measures of protein stability

For many membrane proteins, stability can be measured simply by detecting the activity of the protein as a function of time, temperature or denaturant concentration. For example, crystallisation of G protein-coupled receptor family members has been achieved by finding stabilising mutations, with stability assessed by measuring radioactive ligand binding as a function of temperature [61]. For proteins without an obvious activity read-out, or where activity measurements require excessive amounts of purified protein, alternative biophysical measures of stability are available. Biophysical methods such as small-angle X-ray scattering, differential scanning calorimetry and circular dichroism have been well described and are generally easily interpretable, but

have the drawback of consuming significant amounts of purified protein. Fluorescence methods are particularly useful for membrane proteins because of sensitivity, avoiding the consumption of large amounts of protein. Intrinsic fluorescence, where the differential properties of buried versus water-exposed tryptophan residues can be exploited, has been employed with membrane proteins, but the approach is hampered by the presence of detergent micelles or liposomes (where the protein has been reconstituted) [62]. Adding fluorescent probes has also been employed to measure membrane protein stability, although again, the presence of detergents or lipid complicates the interpretation of the data. The efficacy of three of the most commonly employed fluorescent reporters with two different purified membrane proteins was recently compared [63], and this provides a useful assessment of the methodology as applied to membrane proteins. Of note was that the cysteine (Cys)-reactive reporter 7-diethylamino-3-(4′-maleimidylphenyl)-4-methylcoumarin (CPM) was capable of distinguishing the unfolding of separate subunits of cytochrome c oxidase. We review the use of this reporter for CFTR stability measurement later.

Expression and purification of CFTR and the effects of stability

The expression and purification of CFTR has been reported previously [54, 64–67]. Challenges in its purification are manifold and it illustrates many of the problems described in the previous section. For CFTR, a comparison of constructs with different degrees of stability is informative and shows how this factor affects expression and purification. As discussed above, F508del CFTR is less stable than the WT protein, whilst the G551D CFTR mutation locks the channel in a closed state, and this mutant form of the protein appears to be more stable than the WT protein. Comparison of expression levels for these constructs can be made by monitoring a GFP tag on the C terminus of the CFTR protein. The degree of GFP fluorescence can be compared with fluorescence from an intrinsic fluorescent protein (e.g. yeast mitochondrial succinate dehydrogenase) to allow the CFTR expression level to be adjusted for cell density and to allow for variability in the harvesting and breakage of cells and for any and gel loading errors.

An illustration of such data for the CFTR expression is shown in Fig. 2. As predicted there is a correlation between the stability of the construct and levels of protein detected in the same expression system. G551D CFTR had a much higher yield than WT or F508del CFTR. It is known that the potentiator VX-770 is able to restore channel activity to the G551D CFTR channel and to stimulate channel activity of WT and F508del CFTR; there is predicted to be a loss of some stability as a result [40]. A comparison of expression levels of G551D CFTR in cells treated with and without the potentiator VX-770 is shown in Fig. 2b. Cells treated chronically with VX-770 after induction did not show a reversal to the expression levels of WT CFTR.

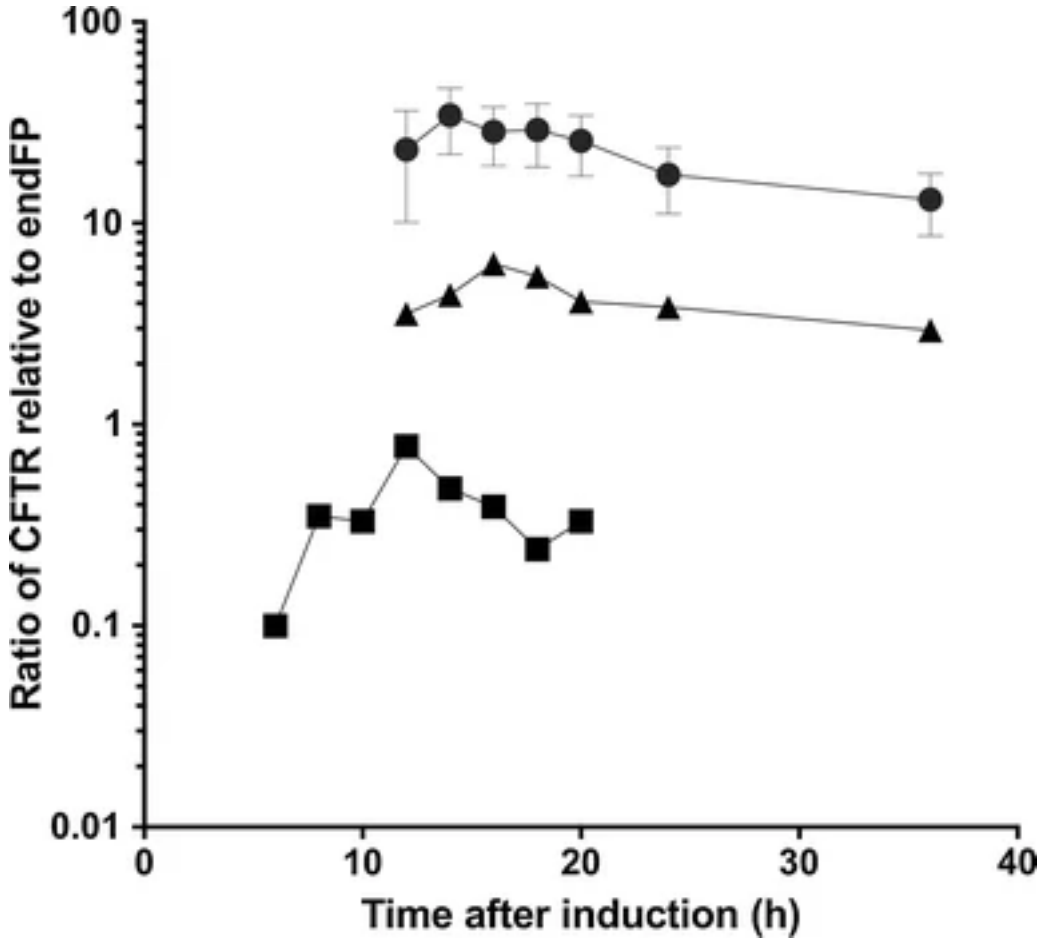

Figure 2: Expression levels are broadly related to stability for CFTR in S. cerevisiae. Comparison of WT (triangles), G551D (circles) and F508del (squares) CFTR expression as a function of time after induction. The fluorescence from the GFP tag attached to CFTR is compared to that from an endogenous fluorescent protein (endFP, succinate dehydrogenase) to correct for variability in cell breakage, microsome preparation and gel loading

Purification of CFTR

CFTR is also an example for how stability can influence the ability to purify a protein, and detergents used to solubilise and purify CFTR can be compared. For example, we can examine the purification of the protein in a mild detergent and in a harsher anionic detergent:

Purification of CFTR in an anionic lyso-lipid surfactant: lyso-phosphatidyl glycerol-14 (LPG14)

The anionic detergent, LPG is thought to be less mild in terms of its surface activity compared to non-ionic detergents [68]. In agreement with this, it was more efficient in solubilisation and purification. However, functional CFTR was successfully purified using this detergent [69, 70]. Figure 3 shows a Coomassie-stained SDS-PAGE gel of G551D CFTR purified using nickel-NTA affinity chromatography in 0.1 % LPG. Nearly 90 % of total CFTR in the microsomes can be solubilised in LPG and its binding efficiency to the nickel-NTA column can reach 90 % [67]. As a maximum, 20 mg of purified G551D protein can be obtained from a single 18-L fermenter run, compared to about 2 mg for WT CFTR [67]. These estimates of efficiency were estimated based on the GFP fluorescence of the fractions using a fluorometer. This tenfold increase in final yield of purified G551D protein compared to wild type [67] is in broad agreement with the cellular expression levels indicated in Fig. 2. The purity immediately after nickel-NTA affinity purification has been reported to reach 95 %, as judged by Coomassie-stained SDS-PAGE gels, but CFTR protein can then be injected onto a size-exclusion chromatography (SEC) column. This also allows monodispersity of the CFTR to be estimated as well as providing a polishing step for the purification. A fluorescence detector connected to the outlet from the SEC column allows the detection of either GFP fluorescence or tryptophan fluorescence. An illustration of a purification run is shown in Fig. 3.

Interestingly, the more stable G551D CFTR construct also seems to be more homogeneous than WT CFTR, as judged by the relative fluorescence of the larger aggregates versus monomer peak (Fig. 4). For both G551D and WT CFTR

proteins it is possible to concentrate them using a 100 kDa MWCO membrane concentrator up to 30 mg/mL in the LPG detergent. In general, the yield of LPG-purified G551D CFTR is high compared to other eukaryotic membrane proteins with the same GFP tag and yeast expression system [71]. The homogeneity of the protein and high yield makes it possible to employ biophysical characterisation methods that demand large amounts of protein and also to attempt high-resolution structural studies. For example, both WT and F508del CFTR protein purified in LPG have been used in small-angle X-ray scattering studies and for Cryo-EM [51].

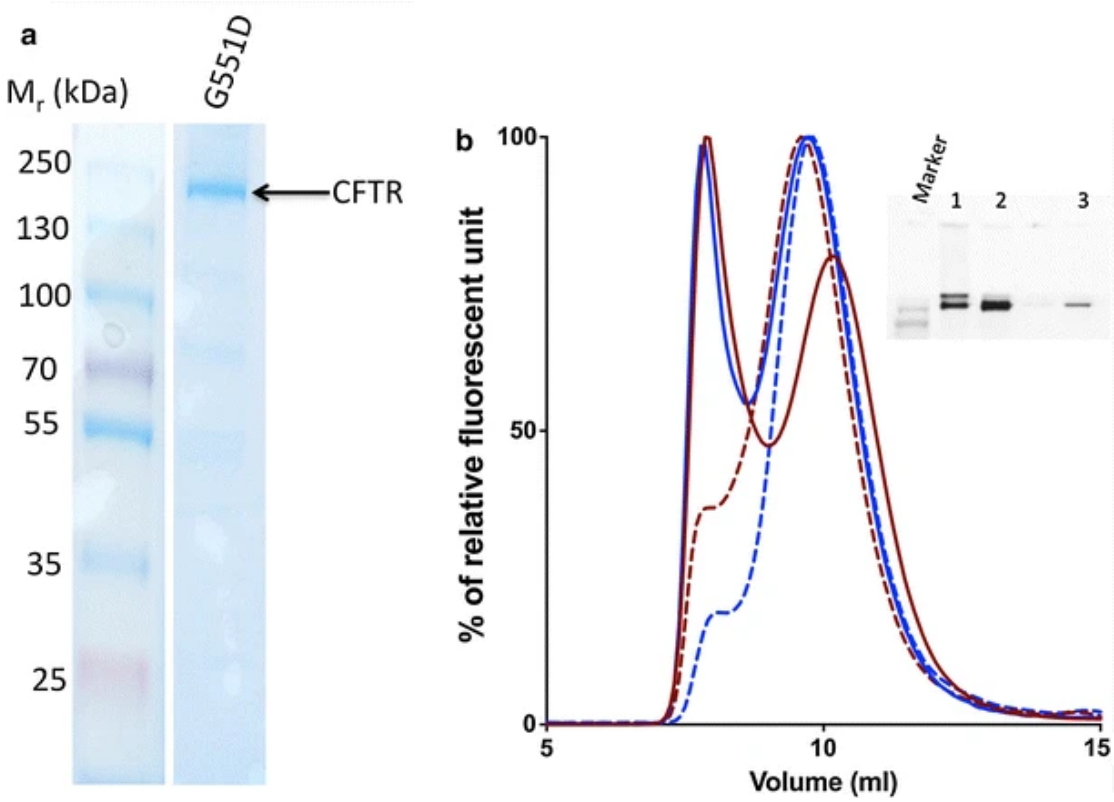

Figure 3: ***a*** *Coomassie-stained SDS-PAGE gel of G551D CFTR eluted from the main peak from the nickel-NTA purification step for protein extracted and purified with LPG.* ***b*** *SEC purification of WT (red line) and G551D (blue line) CFTR in LPG. The second peak fractions (solid lines) were re-injected onto the Sucrose 6 column and the curves are shown on the same graph, WT (red dashed line) and G551D (blue dashed line). The inset is an example gel of the purification procedure. Lanes 1 and 2 are the first and second fluorescence peak elution fractions. Lane 3 was the re-injected fluorescence peak elution for G551D CFTR. The intervening track contains the tail of the first elution peak (monomeric CFTR in small amounts)*

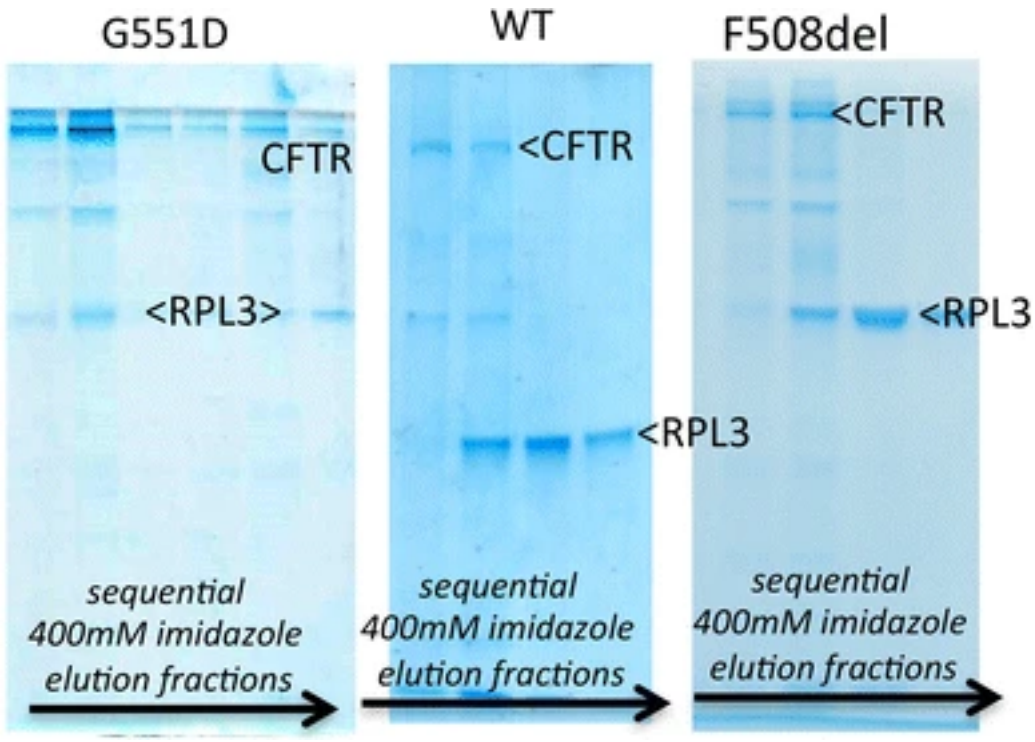

Figure 4: Coomassie-stained SDS-PAGE gels of (left to right) G551D, WT and F508del CFTR eluted in the 400 mM imidazole elution step from the nickel-NTA column for protein extracted and purified with DDM. The CFTR band (220 kDa) and the main contaminating protein in each case (RPL3: 44 kDa) are indicated. The intermediate contaminating band is an abundant yeast membrane protein (plasma membrane H^+-ATPase:100 kDa)

Purification of CFTR in a non-ionic detergent: dodecyl maltoside

DDM is the most commonly used detergent to purify membrane proteins and it has been the most successful for crystallisation [72]. Purification methods in both DDM and LPG are similar, as described in [67]. Figure 4 shows a comparison of Coomassie-stained SDS-PAGE gels of CFTR eluted after nickel-NTA affinity purification in 0.1 % DDM. Example gels of G551D, WT and F508del CFTR (left to right) are given. The main contaminating protein in the CFTR purification is yeast ribosomal protein L3 (RPL3, as confirmed by mass spectrometry), which clearly binds strongly to the Ni–NTA resin, eluting later than CFTR in a 400 mM imidazole elution step. Compared to WT CFTR purification, the G551D purification again appears to be more efficient, with equivalent levels of RPL3 present, but considerably higher levels of the full-length CFTR. WT and F508del CFTR show similar levels of purity after Ni-NTA affinity purification. Yields of G551D CFTR after the nickel-NTA affinity purification with DDM were reported to be about 3–4 mg from an 18-L fermenter while the yield was typically lower (2–3 mg) for WT CFTR [67]. The differences between G551D and WT protein can also be noted at the early stages of purification, with more solubilisation of the initial microsomal G551D CFTR by DDM. G551D can be solubilised to about 50 % yield with DDM (occasionally above 80 % can be observed) whereas typically 30 % solubilisation efficiency can be gained for WT CFTR. Concentrating DDM-purified CFTR proteins after affinity purification is a problem. The highest concentration that has been reported in this detergent is about 0.5 mg/mL, and beyond this precipitates can be observed. This behaviour can be monitored with SEC [67]. For DDM-purified material, SEC purification was not suitable for completely removing the contaminating proteins [67], but a second affinity purification step can be applied such as FLAG affinity chromatography. However, the yield of FLAG affinity steps is variable and for CFTR it remains about 20–30 % because of low binding affinity. The compromise between yield and purity is commonly encountered in protein purification and is particularly difficult for membrane proteins.

Thus, CFTR behaved very differently depending on which detergent was used in the purification and which version of the protein was expressed—even though the purification methods were broadly similar. In the DDM purification buffer, 1 M salt and 20 % glycerol are used to maintain the quality of the protein [73, 74] but the solubility and monodispersity are still not sufficient for some experimental methods such as Cryo-EM and X-ray crystallography. High salt and glycerol are also problems for Cryo-EM [75] where the presence of these solutes greatly reduces the contrast between the protein particles and the background. DDM-purified CFTR also forms a range of oligomeric but non-identical complexes of up to 30 nm diameter. These appear to be in a dynamic equilibrium with monomeric particles because ultrafiltration with a 1 MDa cutoff device did not remove these larger complexes. Even when these larger aggregates were removed by SEC, they reappeared upon concentration and re-passaging down the SEC column. In conclusion, LPG gives a better solubility efficiency and prevents aggregation of purified full-length CFTR [67, 70, 76].

Activity of purified CFTR and stability

The protein purified in LPG is highly mono-disperse as shown above, but has been reported to have less ATPase activity compared to the DDM-purified CFTR [67]. Isolated CFTR NBD1 loses its thermal unfolding transition detected by differential scanning calorimetry in the presence of LPG above a concentration of 0.05 % w/v [77]. Although this applies to the isolated domain, it does offer a plausible explanation for the loss of ATPase activity after LPG14 purification. However, from the thermal unfolding data, full-length CFTR purified in LPG shows a greater stability probably because the cytoplasmic NBDs are much more stable when associated with the other CFTR domains and where hydrophobic interfacial regions are buried (Cant, N. University of Manchester, PhD Thesis, 2013). Thus, it could be argued that stability measurements on isolated domains could be used to indicate trends in sensitivity to detergents and the effects of mutations on stability, but that studies on full-length membrane proteins which include the transmembrane domains are still essential.

CFTR and G551D CFTR ATPase activity can be compared after purification. The CFTR potentiator VX-770 can also applied in these studies because of its potentiation of CFTR G551D channel activity [78–82]. ATPase activity in CFTR

preparations is inevitably susceptible to contaminating yeast membrane proteins having ATPase activity, especially the highly expressed plasma membrane H^+-ATPase [83]. An ATPase activity inhibitor cocktail that includes Sch28080, sodium thiocyanate (SCN) and oligomycin inhibits F-, V- and P-type ATPases, but not CFTR channel gating [84]; hence, this cocktail can be employed to suppress the activity of the major yeast ATPases.

As shown in Fig. 5, VX-770 does not have any effect on the ATPase activity of the purified and reconstituted G551D protein, which is consistent with the hypothesis that VX-770 may exert its effect through prolonging channel opening (which is associated with ATP binding rather than ATP hydrolysis) [6]. However, Eckford and co-workers [82] found PKA-phosphorylated G551D CFTR ATPase activity was stimulated by VX-770. They proposed that VX-770 potentiates defective channel gating in a phosphorylation-dependent manner whereas PKA phosphorylation did not seem to affect ATPase activity of purified chicken CFTR (Dr. Natasha Cant Ph.D thesis, University of Manchester 2013). Reconstitution has been shown to stimulate purified CFTR's ATPase activity [67, 82]. Purified WT CFTR has much higher ATPase activity than G551D CFTR, as expected. These data are interesting and may be informative for considering the effects of detergent purification on activity; however, because the intrinsic ATPase activity of CFTR is relatively low ([85]—e.g. turnover of 0.1/s) the presence of even small amounts of highly active contaminating ATPases could be misleading and this urges caution in interpreting these data.

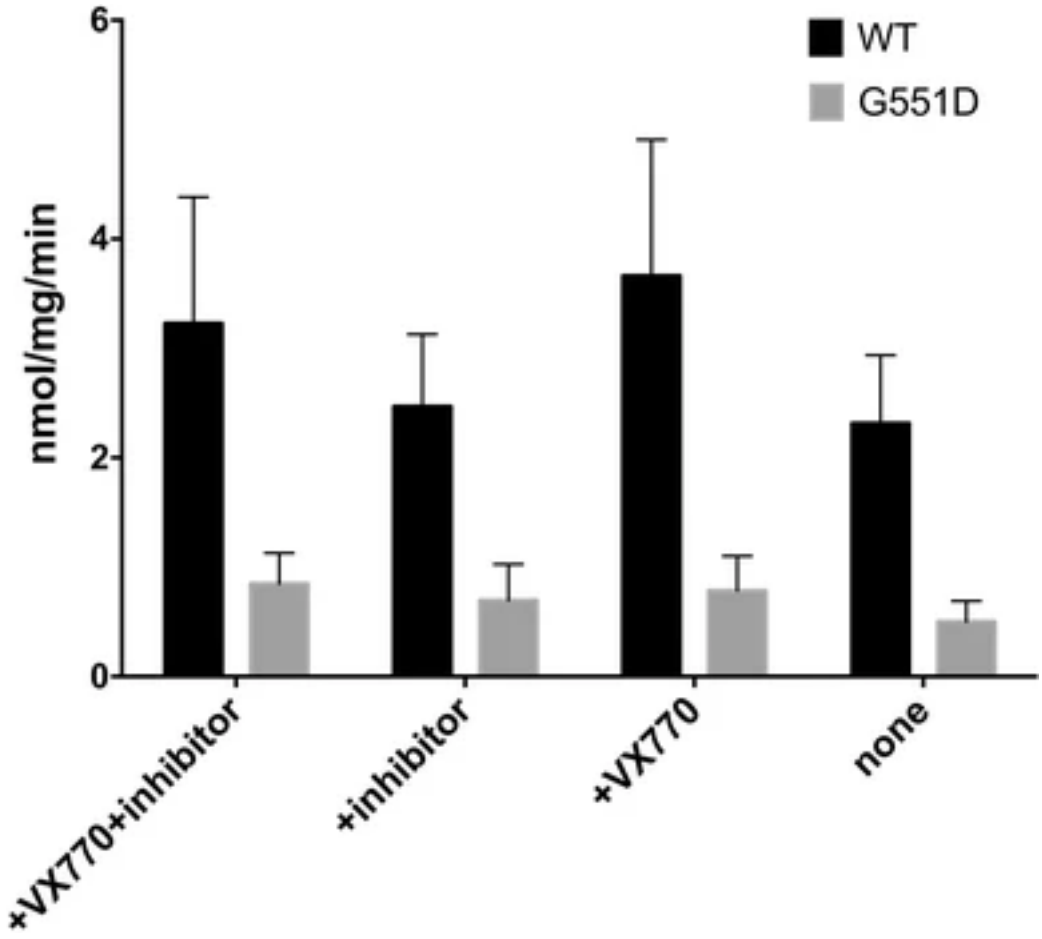

Figure 5: Comparison of the ATPase activity of WT and G551D CFTR with and without VX-770. Purified CFTR was reconstituted with lipids and its ATPase activity was measured using the Chifflet assay. The rate was measured at 25 °C at a concentration of 2 mM ATP. These experiments were repeated >3 times and error bars show the standard error of the mean. An inhibitor cocktail (+inhibitor) was also employed to check for contaminating ATPases of the V-, H- and P-type, as described earlier

Stability of CFTR as measured by the CPM assay

As discussed above, the CPM assay has been used for assessing the thermal stability of membrane proteins [63, 86–88]. The CPM (*N*-[4-(7-diethylamino-4-methyl-3-coumarinyl)phenyl]maleimide) dye is a thiol-specific fluorophore and it will fluoresce strongly in its thiol-linked state [89]. When incubated with protein, it will form a covalent bond with exposed cysteine residues [88]. Upon thermal denaturation, more cysteine residues will become surface exposed, resulting in the fluorescence yield increasing significantly. Only a small amount of protein is used in the CPM assay because the fluorescence read-out from the dye is very sensitive. Other advantages are that it is compatible with several detergents and exhibits a high signal-to-noise ratio [86–88]. The assay does require the presence of several Cys residues in a protein and (for measurement of thermal stability) that some of these Cys residues are secluded from the dye when the protein is in the folded state. Hence, it is less applicable to small proteins with few Cys residues. Nevertheless, it can, for example, be applied to measure the high-temperature unfolding of GFP which is a small protein, but one that fortuitously has 2 Cys residues—one buried and one surface exposed.

CPM, like many fluorescent dyes employed in biochemistry, is hydrophobic and photo-sensitive and, therefore, needs careful handling. It is recommended when making up CPM stock solutions in DMSO to store these solutions in glass vials at −20 °C and in the dark and then to dilute to the required experimental concentration just before use. Whenever possible, it is also advisable to use glass microsyringes for transfer and dilution of CPM stocks rather than the plastic tips employed routinely in biochemistry. The binding of CPM to proteins is affected by thiol-containing reducing agents such as DTT, so these must be removed from the protein and buffer samples before undertaking the assay. Reducing agent is normally present where protein aggregates are a problem, especially with higher protein concentrations (>1 mg/mL). However, the sensitivity of the CPM assay means that purified protein will not normally need to be concentrated, thus removal of DTT or reducing agent removal can be done just prior to assay. The concentration of membrane proteins used for the assay will typically be below 0.1 mg/mL at this stage. It is important to include a buffer control for all CPM-based assays. This is particularly important for membrane proteins where

buffers will contain detergent in a micellar form. Although CPM is almost non-fluorescent in water, it does have a significant fluorescence when it is associated with detergent micelles.

Application of the CPM assay to CFTR

There are a total of 18 Cys residues in the full-length WT human CFTR, 6 predicted to be in the TMDs, 11 in the NBDs and 1 in the R-region [90]. Examination of CFTR homology models [90] implies that 5 Cys are exposed in the outward-facing conformation and 7–8 Cys are exposed in the inward-facing state—see Fig. 6 [91]. In either conformation, there are still predicted to be a majority of Cys residues buried. At the beginning of the CPM assay, surface-exposed Cys will react with the CPM dye at the initial incubation temperature (in this case 10 °C to favour the native state). The buried Cys residues will probably only be exposed when the protein becomes unfolded. These predictions are based on models that are static snapshots of the CFTR structure, and CFTR may have more flexibility than expected due to the presence of the detergent. Nevertheless, it is possible to predict that CFTR will have at least 12 Cys that are partly buried and 6 surface-exposed Cys.

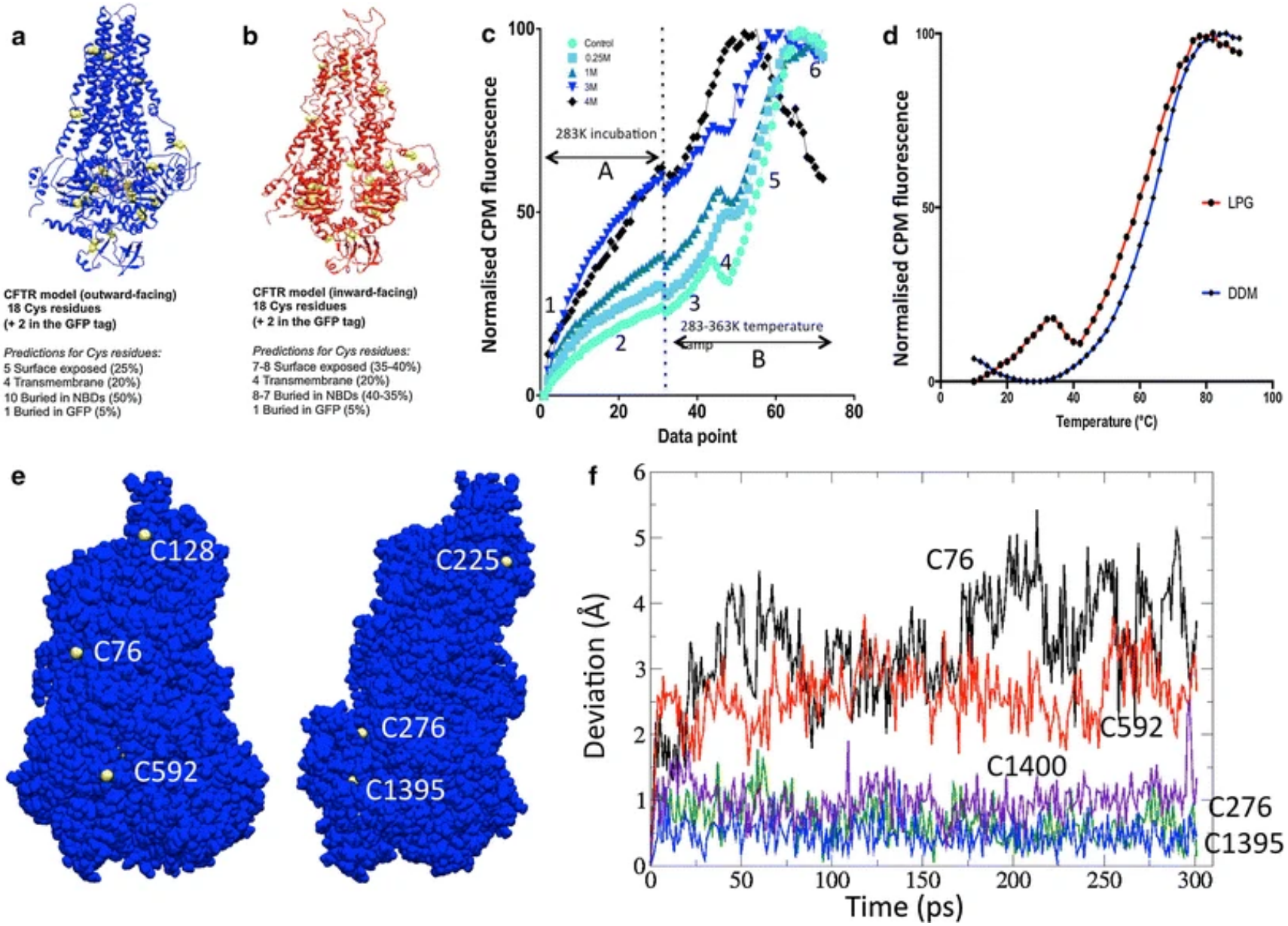
a
CFTR model (outward-facing)
18 Cys residues
(+ 2 in the GFP tag)
Predictions for Cys residues:
5 Surface exposed (25%)
4 Transmembrane (20%)
10 Buried in NBDs (50%)
1 Buried in GFP (5%)
b
CFTR model (inward-facing)
18 Cys residues
(+ 2 in the GFP tag)
Predictions for Cys residues:
7-8 Surface exposed (35-40%)
4 Transmembrane (20%)
8-7 Buried in NBDs (40-35%)
1 Buried in GFP (5%)
c
Control
0.25M
1M
3M
4M
283K incubation
A
B
283-363K temperature ramp
1
2
3
4
5
6
Normalised CPM fluorescence
Data point
d
Normalised CPM fluorescence
Temperature (°C)
LPG
DDM
e
C128
C76
C592
C225
C276
C1395
f
Deviation (Å)
Time (ps)
C76
C592
C1400
C276
C1395

***Figure 6 a**, **b** Homology models for CFTR in the **a** outward-facing state (blue ribbons) and **b** inward-facing state (red ribbons). The locations of the Cys residues in each model are indicated by the yellow space-filling atoms, and predictions about their exposure to solvent are listed below each model. **c** The unfolding of CFTR by thermal or chemical denaturation as detected by CPM fluorescence changes. The light green line shows purified G551D CFTR in an LPG-containing buffer. Other lines show the same protein but in the presence of 0.25–4 M Guanidium HCl as indicated by the key, top left. The experiment is initiated by the injection of CPM dye into a protein-containing cuvette at 10 °C which is then monitored for 30 min (phase A). The sample is then heated to 90 °C (phase B). Various changes in the CPM fluorescence are indicated: 1 immediate fluorescence from CPM in buffer (unbound to protein). 2 Kinetics of CPM binding to solvent-exposed Cys residues. For protein chemically denatured (black line), nearly all Cys residues are initially exposed. 3 Rise in CPM fluorescence as thermal motion exposes more Cys residues to solvent and CPM. 4 Thermal quenching of CPM fluorescence as the sample is heated (protein is still predominantly folded for the green line). 5 Cooperative thermal unfolding of the entire protein. 6 Continued thermal quenching of CPM fluorescence after complete unfolding of the protein. Data point scale represents time (1 min/point—phase A) and then temperature (phase B—heating rate = 2 °C/min with 1 min/point). **d** The thermal denaturation phase for G551D CFTR purified in a non-ionic detergent (DDM, blue line) and an anionic lyso-lipid (LPG, red line). **e** Two views of the surface of a CFTR homology model based on the outward-facing Sav1866 structure, with the sulphur atoms of Cys residues coloured yellow whilst all other atoms are blue. The TMDs and NBDs are towards the top and bottom, respectively. C128 and C225 are in membrane-spanning portions and will probably be buried by surrounding lipid or detergent. **b** Deviations of the Cys sulphur atoms for five selected residues over the time course of a molecular dynamics simulation. The highly surface-exposed residues C76 (black line) and C592 (red line) show much greater mobility than the mostly buried residues C1395 (blue) and C276 (green). Hence, the former two residues are likely to be labelled by CPM before thermal denaturation. The completely buried residue C1400 (indigo) shows similar dynamics to C1395 and C276.*

Figure 6 shows typical data for CFTR unfolding as measured using the CPM assay. In aqueous buffers, CPM fluorescence is low, but greatly increases upon formation of the covalent adduct with Cys residues in a protein. As shown in Fig. 6c, there is an increase in CPM fluorescence when CPM is added to purified CFTR protein due to adduct formation with the surface-exposed Cys residues (phase 2—Fig. 6c). The very fast initial increase in CPM fluorescence indicated by the number 1 is probably due to intrinsic CPM fluorescence in the buffer. Although the CPM fluorescence in aqueous buffers is normally extremely low, when detergent micelles are present, CPM can partition into the micelle and shows some significant fluorescence, as stated above. When CFTR is completely denatured by Guanidium HCl, the CPM fluorescence increases in phase '2' to about 60 % of the total signal over a period of about 30 min at 10 °C (Fig. 6c, black line) with a half-time for the Cys adduct formation of about 10 min at this temperature. Presumably the increase does not reach 100 % because the membrane-spanning portions of the protein are relatively resistant to this water-soluble chaotrope. Subsequent heating of the Guanidium-denatured protein gives a further increase in CPM fluorescence—probably due to the exposure of Cys residues that are in the membrane-spanning portions of the protein. The final phase (phase 6) of the heating of the protein is characterised by a loss of the fluorescence yield due to thermal quenching. In contrast, folded CFTR (green line) gives only a small increase in CPM fluorescence at 10 °C (solid line, Fig. 6), equivalent to about 20 % of the total signal. This probably represents the small number of surface-exposed Cys residues in the folded CFTR protein—i.e. about 5 of the 20 available residues in the CFTR-GFP construct (Fig. 6a, b). A large increase in fluorescence is observed upon heating and thermal denaturation of the protein in the absence of Guanidium HCl as in this case, about 80 % of the Cys residues are buried. Hence, the CPM-derived fluorescence data are broadly consistent with the available homology models for CFTR and interestingly are more consistent with the outward-facing state rather than the inward-facing conformation. After complete thermal unfolding of the protein at approximately 78 °C, a decrease in CPM fluorescence yield is again observed due to thermal quenching. These experiments were performed using an Avacta Optim Fluorescence Spectrometer coupled to a Peltier element for

heating, but a simple bench-top fluorescence spectrophotometer with an attached water bath for heating can also be employed.

As the CPM fluorescence at any given temperature is a convolution of the accessibility/dynamics of available Cys residues, the kinetics of protein unfolding and CPM–Cys bond formation (temperature dependent) and the heating rate, this assay will give differing mid-point temperatures for protein unfolding depending on these various parameters. Hence, mid-point temperatures estimated for proteins will be somewhat unreliable and, because of hysteresis, will likely overestimate the stability of the protein at high heating rates. Conversely, slow heating rates will tend to underestimate the mid-point unfolding temperature because the time dependence of stability at a given moderate temperature will have a stronger influence. Hence, the assay can be used for comparative purposes as shown in Figs. 6 and 7, where the experimental parameters such as heating rate are the same. These data provide evidence that CFTR material purified in the anionic lyso-lipid LPG and in the non-ionic detergent DDM have a folded, cooperative tertiary structure. There are, however, differences in the unfolding profiles of LPG-purified and DDM-purified CFTR. Whilst DDM-purified CFTR unfolds in a single cooperative transition, LPG-purified CFTR shows a two-phase unfolding profile (Fig. 6d). The latter is characterised by an initial increase in CPM fluorescence between 10 and 35 °C, followed by a brief thermal quenching between 35 and 41 °C. This low-temperature and low-amplitude transition may be due to a localised unfolding of a sub-domain of CFTR in LPG, or may be due to increased dynamics of partly buried Cys residues. The main unfolding transitions for CFTR purified in either detergent are very similar, with mid-point temperatures of about 60–65 °C (Fig. 6d).

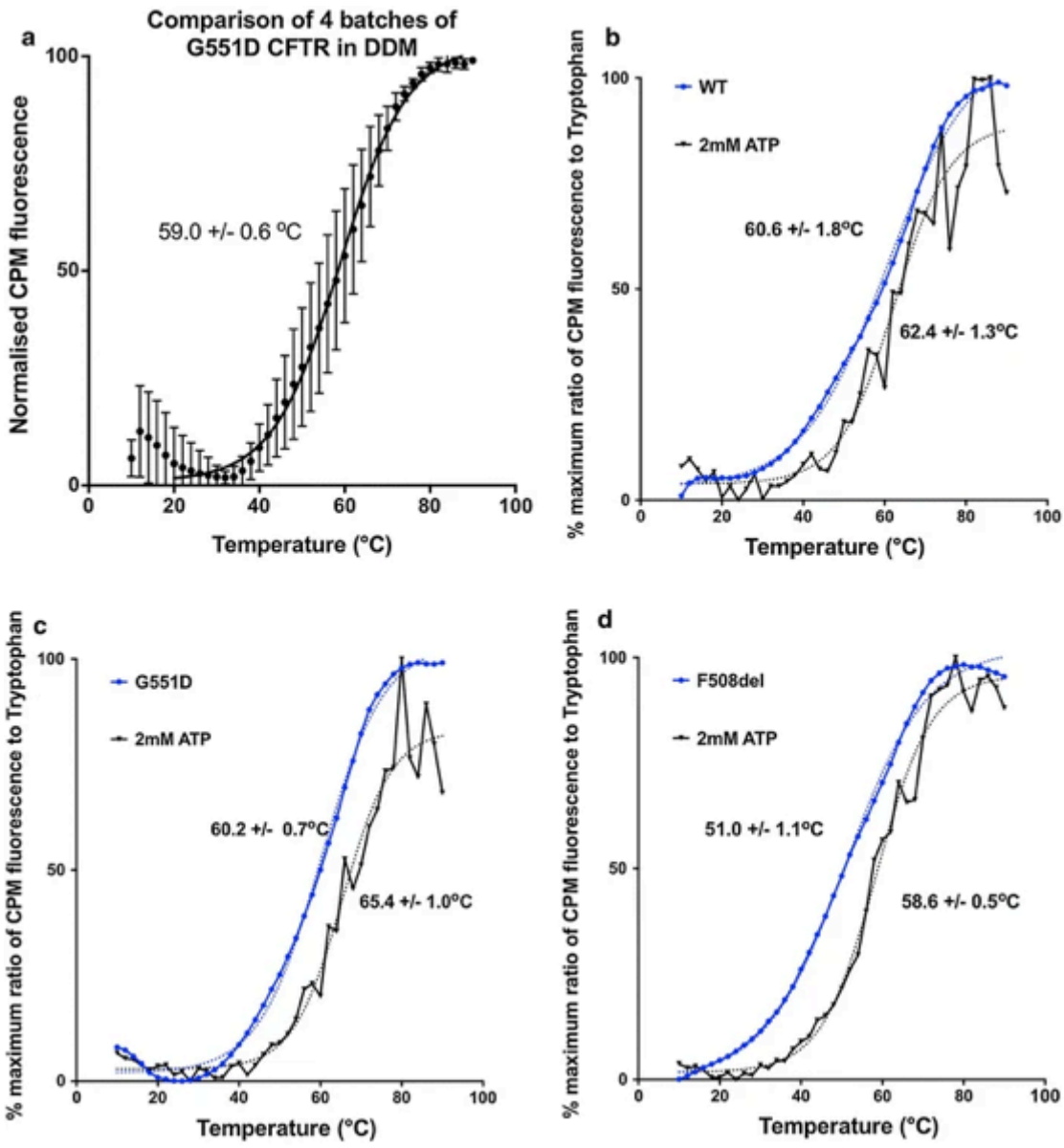

Figure 7: a *Batch-to-batch variability in the thermal denaturation phase of four batches of DDM-purified G551D CFTR, as detected by CPM fluorescence changes (each batch was measured three times). Samples were heated at 2 °C/min.* ***b****–****d*** *Effects of ATP on the thermal unfolding transition of WT (****b****), G551D (****c****) and F508del CFTR purified in DDM. The presence of ATP stabilises all three constructs. The increased noise in the data recorded in the presence of ATP is due to the absorption of excitation light by ATP. F508del CFTR is globally destabilised versus WT and G551D CFTR by about 8 °C. The midpoint temperatures for the thermal unfolding transition are shown for each curve and the error for its estimation by the curve fitting is indicated*

Molecular dynamics and modelling of Cys residues in CFTR

Of the 18 Cys residues in CFTR, and the 2 Cys residues in the GFP construct, some are clearly surface exposed in both inward- and outward-facing conformational models (Fig. 6a, b). In particular, Cys 832 (R-region) and Cys 1458 (C-term) are likely to be in disordered regions of the protein whilst Cys 48 in the GFP is likely to be surface exposed. Of the remaining Cys residues, Cys 78 and 647 are very close to regions of the CFTR structure that are known to be folded, hence may be at least partially buried. Residues 128, 225, 343, 866 are all in the membrane-spanning portions of the protein, and hence are likely to be secluded from CPM by detergent or lipid until the transmembrane domains are denatured. Most of the remaining Cys residues in CFTR are buried within the NBDs, although three display some exposure to the aqueous milieu in the outward-facing model (Fig. 6e). These are Cys residues at positions 276, 592 and 1395, with C592 and C1395 more buried than C276. Molecular dynamics of these Cys residues in a homology model for CFTR support the visual impression that C592 and C1395 are buried compared to C276 (Fig. 6f). These residues display dynamics that are similar to the completely buried C1400, whereas C276 shows much greater dynamics, similar to that modelled for C78. Hence, molecular dynamics simulation predicts that at least 4 Cys residues will be sufficiently surface-exposed to be labelled by CPM in the compact outward-facing configuration, viz., C276, C832, C1458 and C48 in the GFP tag. In addition, C78 and C647 may be labelled, but these residues are in regions of the CFTR structure for which little current structural data are available. Labelling of 4 of the 20 Cys residues in the purified CFTR-GFP construct with CPM is consistent with the fluorescence measurements shown in Fig. 6c.

Comparison of CFTR mutations

Thermal unfolding transitions for various purified CFTR constructs as detected with the CPM assay are shown in Fig. 7. F508del CFTR has a broader thermal unfolding transition, whilst G551D CFTR shows a more cooperative unfolding that was similar to WT CFTR. G551D may be more stable at the beginning of the thermal denaturation transition, i.e. in the temperature range that is relevant physiologically. This may relate to the fact that the G551D mutation fixes the CFTR channel in a closed state, which may correlate with a more stable

structural state for the whole protein. A re-scan of the CPM fluorescence for the thermally denatured protein is routinely monitored and should give a featureless profile with a negative slope, due to the thermal quenching of the CPM fluorescence. This also confirms that thermal unfolding is an irreversible process.

Batch-to-batch variability and studies of stability in the presence of small molecules

The effects of the purification procedure may also have a major influence on the measured stability of a given membrane protein. Clearly, variability in purification conditions can result in a protein batch that contains significant amounts of already unfolded protein. An assessment of batch-to-batch variability in the measured stability is, therefore, important, particularly if results on the effects of mutations or small molecules on stability are desired. Figure 7 a illustrates the variability in the unfolding data across 4 different batches of G551D CFTR protein purified in the presence of DDM. The error bars indicate that there will be significant batch-to-batch variability, even for this well-behaved version of the protein. Hence, studies on the effects of small molecules on stability should be performed on the same batch of protein, and comparisons of the stability of CFTR mutants should be carried out on several batches of the protein before conclusions are drawn. Figure 7b–d shows the effects of ATP addition which gives a significant thermostabilisation of the purified full-length proteins, as might have been predicted given similar conclusions for the isolated nucleotide-binding domains [92]. In this latter study [92], the isolated WT and F508del NBD1 were both thermostabilised by about 10–15 °C by the presence of millimolar levels of ATP. For the full-length protein, the thermostabilisation of the protein is less, as shown in Fig. 7. For F508del CFTR, ATP-induced stabilisation is greatest, by about 8–10 °C in the midpoint transition, though at lower temperatures, the difference in the CPM-detected thermal unfolding is more noticeable. This may be taken as evidence that NBD unfolding may occur at lower temperatures. For WT and G551D CFTR, the degree of ATP-mediated themostabilisation is smaller, perhaps indicating that there is an upper limit for stabilisation via ATP binding to the NBDs.

Summary

CFTR is a typical membrane protein that is somewhat difficult to express and purify. Stability is a major factor in the purification and structural analysis of membrane proteins, and CFTR is a good example of how increased stability can correlate with improved yield, purity and monodispersity. However, mutations that stabilise a given membrane protein may not always be associated with better activity. For example, the G551D mutation in CFTR improves its properties for structural studies, but by locking the protein into a channel closed conformation, it blocks its activity. Hence, it must be acknowledged that for some, perhaps the majority, of membrane proteins an inherent instability or flexibility may be crucial for the function of the protein. Structures of hyper-stabilised versions of membrane proteins must, therefore, be treated with some caution as they may bear less relevance for physiology. Indeed, for CFTR, even though the F508del version of the protein is by far the least stable, it is also probably the most relevant in terms of the disease, since loss of stability of F508del CFTR may be a major factor in its inability to reach the plasma membrane of the cell.

References

1. Mikhailov MV, Campbell JD, de Wet H, et al. 3-D structural and functional characterization of the purified KATP channel complex Kir6.2-SUR1. EMBO J. 2005;24:4166–4175. doi: 10.1038/sj.emboj.7600877. - DOI - PMC - PubMed
2. Bryan J, Aguilar-Bryan L. Sulfonylurea receptors: ABC transporters that regulate ATP-sensitive K(+) channels. Biochim Biophys Acta. 1999;1461:285–303. doi: 10.1016/S0005-2736(99)00164-9. - DOI - PubMed
3. Bozoky Z, Krzeminski M, Muhandiram R, et al. Regulatory R region of the CFTR chloride channel is a dynamic integrator of phospho-dependent intra- and intermolecular interactions. Proc Natl Acad Sci USA. 2013;110:E4427–E4436. doi: 10.1073/pnas.1315104110. - DOI - PMC - PubMed
4. Ostedgaard LS, Baldursson O, Welsh MJ. Regulation of the cystic fibrosis transmembrane conductance regulator Cl-channel by its R domain. J Biol Chem. 2001;276:7689–7692. doi: 10.1074/jbc.R100001200. - DOI - PubMed
5. Wang Y, Wrennal J, Cai Z, et al. Understanding how cystic fibrosis mutations disrupt CFTR function: from single molecules to animal models. Int J Biochem Cell Biol. 2014;52:47–57. doi: 10.1016/j.biocel.2014.04.001. - DOI - PubMed
6. Vergani P, Lockless SW, Nairn AC, et al. CFTR channel opening by ATP-driven tight dimerization of its nucleotide-binding domains. Nature. 2005;433:876–880. doi: 10.1038/nature03313. - DOI - PMC - PubMed
7. Bozoky Z, Krzeminski M, Muhandiram R, et al. Regulatory R region of the CFTR chloride channel is a dynamic integrator of phospho-dependent intra- and intermolecular interactions. Proc Natl Acad Sci USA. 2013;110:E4427–E4436. doi: 10.1073/pnas.1315104110. - DOI - PMC - PubMed
8. Ratjen F, Döring G. Cystic fibrosis. Lancet. 2003;361:681–689. doi: 10.1016/S0140-6736(03)12567-6. - DOI - PubMed

9. Goodman B, Percy W. CFTR in cystic fibrosis and cholera: from membrane transport to clinical practice. AJP Adv Physiol Educ. 2005;29:75–82. doi: 10.1152/advan.00035.2004. - DOI - PubMed
10. Van Goor F, Hadida S, Grootenhuis PDJ, et al. Correction of the F508del-CFTR protein processing defect in vitro by the investigational drug VX-809. Proc Natl Acad Sci USA. 2011;108:18843–18848. doi: 10.1073/pnas.1105787108. - DOI - PMC - PubMed
11. Molinski S, Eckford PD, Pasyk S, et al. Functional rescue of F508del-CFTR using small molecule correctors. Front Pharmacol. 2012;3:160. doi: 10.3389/fphar.2012.00160. - DOI - PMC - PubMed
12. He LH, Aleksandrov AA, An JL, et al. Restoration of NBD1 thermal stability is necessary and sufficient to correct delta F508 CFTR folding and assembly. J Mol Biol. 2015;427:106–120. doi: 10.1016/j.jmb.2014.07.026. - DOI - PMC - PubMed
13. Farinha CM, Matos P. Repairing the basic defect in cystic fibrosis—one approach is not enough. FEBS J. 2016;283:246–264. doi: 10.1111/febs.13531. - DOI - PubMed
14. Riordan JR. CFTR function and prospects for therapy. Annu Rev Biochem. 2008;77:701–726. doi: 10.1146/annurev.biochem.75.103004.142532. - DOI - PubMed
15. Serohijos AW, Hegedus T, Aleksandrov AA, et al. Phenylalanine-508 mediates a cytoplasmic-membrane domain contact in the CFTR 3D structure crucial to assembly and channel function. Proc Natl Acad Sci USA. 2008;105:3256–3261. doi: 10.1073/pnas.0800254105. - DOI - PMC - PubMed
16. He L, Kota P, Aleksandrov AA, et al. Correctors of DeltaF508 CFTR restore global conformational maturation without thermally stabilizing the mutant protein. FASEB J Off Publ Fed Am Soc Exp Biol. 2013;27:536–545. - PMC - PubMed
17. He L, Aleksandrov AA, Serohijos AW, et al. Multiple membrane-cytoplasmic domain contacts in the cystic fibrosis transmembrane conductance regulator (CFTR) mediate regulation of channel gating. J Biol Chem. 2008;283:26383–26390. doi: 10.1074/jbc.M803894200. - DOI - PMC - PubMed

18. Ward CL, Omura S, Kopito RR. Degradation of CFTR by the ubiquitin-proteasome pathway. Cell. 1995;83:121–127. doi: 10.1016/0092-8674(95)90240-6. - DOI - PubMed
19. Kopito RR. Biosynthesis and degradation of CFTR. Physiol Rev. 1999;79:S167–S173. - PubMed
20. Grove DE, Rosser MFN, Watkins RL, et al. Analysis of CFTR folding and degradation in transiently transfected cells. Cys Fibros Diagn Protoc Vol I Approaches Study Correct CFTR Defects. 2011;741:219–232. - PMC - PubMed
21. Cui L, Aleksandrov L, Chang XB, et al. Domain interdependence in the biosynthetic assembly of CFTR. J Mol Biol. 2007;365:981–994. doi: 10.1016/j.jmb.2006.10.086. - DOI - PubMed
22. Dalemans W, Barbry P, Champigny G, et al. Altered chloride ion channel kinetics associated with the delta F508 cystic fibrosis mutation. Nature. 1991;354:526–528. doi: 10.1038/354526a0. - DOI - PubMed
23. Denning GM, Anderson MP, Amara JF, et al. Processing of mutant cystic fibrosis transmembrane conductance regulator is temperature-sensitive. Nature. 1992;358:761–764. doi: 10.1038/358761a0. - DOI - PubMed
24. Sato S, Ward CL, Krouse ME, et al. Glycerol reverses the misfolding phenotype of the most common cystic fibrosis mutation. J Biol Chem. 1996;271:635–638. doi: 10.1074/jbc.271.2.635. - DOI - PubMed
25. Pedemonte N, Galietta LJ. Pharmacological correctors of mutant CFTR mistrafficking. Front Pharmacol. 2012;3:175. doi: 10.3389/fphar.2012.00175. - DOI - PMC - PubMed
26. Eckford PD, Bear CE. Targeting the regulation of CFTR channels. Biochem J. 2011;435:e1–e4. doi: 10.1042/BJ20110461. - DOI - PubMed
27. Meacham GC, Patterson C, Zhang WY, et al. The Hsc70 co-chaperone CHIP targets immature CFTR for proteasomal degradation. Nat Cell Biol. 2001;3:100–105. doi: 10.1038/35050509. - DOI - PubMed
28. Becq F, Mettey Y, Gray MA, et al. Development of substituted benzo[c]quinolizinium compounds as novel activators of the cystic fibrosis chloride channel. J Biol Chem. 1999;274:27415–27425. doi: 10.1074/jbc.274.39.27415. - DOI - PubMed
29. Dormer RL, Dérand R, McNeilly CM, et al. Correction of delF508-CFTR activity with benzo(c)quinolizinium compounds through facilitation of its

processing in cystic fibrosis airway cells. J Cell Sci. 2001;114:4073–4081. - PubMed

30. Pedemonte N, Lukacs GL, Du K, et al. Small-molecule correctors of defective deltaF508-CFTR cellular processing identified by high-throughput screening. J Clin Investig. 2005;115:2564–2571. doi: 10.1172/JCI24898. - DOI - PMC - PubMed
31. Hutt DM, Herman D, Rodrigues AP, et al. Reduced histone deacetylase 7 activity restores function to misfolded CFTR in cystic fibrosis. Nat Chem Biol. 2009;6:25–33. doi: 10.1038/nchembio.275. - DOI - PMC - PubMed
32. Pedemonte N, Tomati V, Sondo E, et al. Dual activity of aminoarylthiazoles on the trafficking and gating defects of the cystic fibrosis transmembrane conductance regulator chloride channel caused by cystic fibrosis mutations. J Biol Chem. 2011;286:15215–15226. doi: 10.1074/jbc.M110.184267. - DOI - PMC - PubMed
33. Van Goor F, Straley KS, Cao D, et al. Rescue of deltaF508-CFTR trafficking and gating in human cystic fibrosis airway primary cultures by small molecules. Am J Physiol Lung Cell Mol Physiol. 2006;290:L1117–L1130. doi: 10.1152/ajplung.00169.2005. - DOI - PubMed
34. Van Goor F, Hadida S, Grootenhuis PD, et al. Correction of the F508del-CFTR protein processing defect in vitro by the investigational drug VX-809. Proc Natl Acad Sci USA. 2011;108:18843–18848. doi: 10.1073/pnas.1105787108. - DOI - PMC - PubMed
35. Haq IJ, Gray MA, Garnett JP, et al. Airway surface liquid homeostasis in cystic fibrosis: pathophysiology and therapeutic targets. Thorax. 2015;71:284–287. doi: 10.1136/thoraxjnl-2015-207588. - DOI - PubMed
36. Clancy JP, Rowe SM, Accurso FJ, et al. Results of a phase IIa study of VX-809, an investigational CFTR corrector compound, in subjects with cystic fibrosis homozygous for the F508del-CFTR mutation. Thorax. 2012;67:12–18. doi: 10.1136/thoraxjnl-2011-200393. - DOI - PMC - PubMed
37. Farinha CM, Sousa M, Canato S, et al. Increased efficacy of VX-809 in different cellular systems results from an early stabilization effect of F508del-CFTR. Pharmacol Res Perspect. 2015;3:e00152. doi: 10.1002/prp2.152. - DOI - PMC - PubMed

38. Sampson HM, Robert R, Liao J, et al. Identification of a NBD1-binding pharmacological chaperone that corrects the trafficking defect of F508del-CFTR. Chem Biol. 2011;18:231–242. doi: 10.1016/j.chembiol.2010.11.016. - DOI - PubMed
39. Veit G, Avramescu RG, Perdomo D, et al. Some gating potentiators, including VX-770, diminish deltaF508-CFTR functional expression. Sci Transl Med. 2014;6:246ra297. doi: 10.1126/scitranslmed.3008889. - DOI - PMC - PubMed
40. Cholon DM, Quinney NL, Fulcher ML, et al. Potentiator ivacaftor abrogates pharmacological correction of deltaF508 CFTR in cystic fibrosis. Sci Transl Med. 2014;6:246ra296. doi: 10.1126/scitranslmed.3008680. - DOI - PMC - PubMed
41. Osmanbeyoglu HU, Wehner JA, Carbonell JG, et al. Active machine learning for transmembrane helix prediction. BMC Bioinform. 2010;11(Suppl 1):S58. doi: 10.1186/1471-2105-11-S1-S58. - DOI - PMC - PubMed
42. Zhang Z, Kuipers G, Niemiec L, et al. High-level production of membrane proteins in E. coli BL21(DE3) by omitting the inducer IPTG. Microb Cell Factories. 2015;14:142. doi: 10.1186/s12934-015-0328-z. - DOI - PMC - PubMed
43. Whittaker MM, Whittaker JW. Expression and purification of recombinant Saccharomyces cerevisiae mitochondrial carrier protein YGR257Cp (Mtm1p) Protein Expr Purif. 2014;93:77–86. doi: 10.1016/j.pep.2013.10.014. - DOI - PMC - PubMed
44. Lundstrom K, Wagner R, Reinhart C, et al. Structural genomics on membrane proteins: comparison of more than 100 GPCRs in 3 expression systems. J Struct Funct Genomics. 2006;7:77–91. doi: 10.1007/s10969-006-9011-2. - DOI - PubMed
45. Garavito RM, Picot D, Loll PJ. Strategies for crystallizing membrane proteins. J Bioenerg Biomembr. 1996;28:13–27. doi: 10.1007/BF02150674. - DOI - PubMed
46. Seddon AM, Curnow P, Booth PJ. Membrane proteins, lipids and detergents: not just a soap opera. Biochim Biophys Acta. 2004;1666:105–117. doi: 10.1016/j.bbamem.2004.04.011. - DOI - PubMed
47. Linke D. Detergents: an overview. Methods Enzymol. 2009;463:603–617. doi: 10.1016/S0076-6879(09)63034-2. - DOI - PubMed

48. Krueger-Koplin RD, Sorgen PL, Krueger-Koplin ST, et al. An evaluation of detergents for NMR structural studies of membrane proteins. J Biomol NMR. 2004;28:43–57. doi: 10.1023/B:JNMR.0000012875.80898.8f. - DOI - PubMed
49. Fethiere J. Three-dimensional crystallization of membrane proteins. Methods Mol Biol. 2007;363:191–223. doi: 10.1007/978-1-59745-209-0_10. - DOI - PubMed
50. Kim JM, Wu SP, Tomasiak TM, et al. Subnanometre-resolution electron cryomicroscopy structure of a heterodimeric ABC exporter. Nature. 2015;517:U396–U598. doi: 10.1038/nature13872. - DOI - PMC - PubMed
51. Pollock NL, Satriano L, Zegarra-Moran O, et al. Structure of wild type and mutant F508del CFTR. A small-angle X-ray scattering study of the protein-detergent complexes. J Struct Biol. 2016;194:102–111. doi: 10.1016/j.jsb.2016.02.004. - DOI - PubMed
52. Le Brun AP, Clifton LA, Holt SA, et al. Deuterium labeling strategies for creating contrast in structure-function studies of model bacterial outer membranes using neutron reflectometry. Methods Enzymol. 2016;566:231–252. doi: 10.1016/bs.mie.2015.05.020. - DOI - PubMed
53. Yang ZR, Wang C, Zhou QX, et al. Membrane protein stability can be compromised by detergent interactions with the extramembranous soluble domains. Protein Sci. 2014;23:769–789. doi: 10.1002/pro.2460. - DOI - PMC - PubMed
54. Aleksandrov LA, Jensen TJ, Cui LY, et al. Thermal stability of purified and reconstituted CFTR in a locked open channel conformation. Protein Expr Purif. 2015;116:159–166. doi: 10.1016/j.pep.2015.09.018. - DOI - PMC - PubMed
55. Geertsma ER, Groeneveld M, Slotboom DJ, et al. Quality control of overexpressed membrane proteins. Proc Natl Acad Sci USA. 2008;105:5722–5727. doi: 10.1073/pnas.0802190105. - DOI - PMC - PubMed
56. Hattori M, Hibbs RE, Gouaux E. A fluorescence-detection size-exclusion chromatography-based thermostability assay for membrane protein precrystallization screening. Structure. 2012;20:1293–1299. doi: 10.1016/j.str.2012.06.009. - DOI - PMC - PubMed

57. Oldham ML, Hite RK, Steffen AM, et al. A mechanism of viral immune evasion revealed by cryo-EM analysis of the TAP transporter. Nature. 2016;529:537–540. doi: 10.1038/nature16506. - DOI - PMC - PubMed
58. Bai XC, Yan CY, Yang GH, et al. An atomic structure of human gamma-secretase. Nature. 2015;525:212–217. doi: 10.1038/nature14892. - DOI - PMC - PubMed
59. Nogales E, Scheres SHW. Cryo-EM: a unique tool for the visualization of macromolecular complexity. Mol Cell. 2015;58:677–689. doi: 10.1016/j.molcel.2015.02.019. - DOI - PMC - PubMed
60. Zhou HX, Cross TA. Influences of membrane mimetic environments on membrane protein structures. Annu Rev Biophys. 2013;42:361–392. doi: 10.1146/annurev-biophys-083012-130326. - DOI - PMC - PubMed
61. Tate CG. A crystal clear solution for determining G-protein-coupled receptor structures. Trends Biochem Sci. 2012;37:343–352. doi: 10.1016/j.tibs.2012.06.003. - DOI - PubMed
62. Moon CP, Fleming KG. Using tryptophan fluorescence to measure the stability of membrane proteins folded in liposomes. Methods Enzymol. 2011;492:189–211. doi: 10.1016/B978-0-12-381268-1.00018-5. - DOI - PMC - PubMed
63. Kohlstaedt M, von der Hocht I, Hilbers F, et al. Development of a Thermofluor assay for stability determination of membrane proteins using the Na(+)/H(+) antiporter NhaA and cytochrome c oxidase. Acta Crystallogr D Biol Crystallogr. 2015;71:1112–1122. doi: 10.1107/S1399004715004058. - DOI - PubMed
64. Huang P, Liu Q, Scarborough GA. Lysophosphatidylglycerol: a novel effective detergent for solubilizing and purifying the cystic fibrosis transmembrane conductance regulator. Anal Biochem. 1998;259:89–97. doi: 10.1006/abio.1998.2633. - DOI - PubMed
65. Huang P, Stroffekova K, Cuppoletti J, et al. Functional expression of the cystic fibrosis transmembrane conductance regulator in yeast. Biochim Biophys Acta. 1996;1281:80–90. doi: 10.1016/0005-2736(96)00032-6. - DOI - PubMed
66. O'ryan L, Rimington T, Cant N et al (2012) Expression and purification of the cystic fibrosis transmembrane conductance regulator protein in Saccharomyces cerevisiae. Jove J Vis Exp 61:e3860 - PMC - PubMed

67. Pollock N, Cant N, Rimington T et al (2014) Purification of the cystic fibrosis transmembrane conductance regulator protein expressed in Saccharomyces cerevisiae. J Vis Exp (87):51447. doi:10.3791/51447 - PMC - PubMed
68. Yang Z, Wang C, Zhou Q, et al. Membrane protein stability can be compromised by detergent interactions with the extramembranous soluble domains. Protein Sci Publ Protein Soc. 2014;23:769–789. doi: 10.1002/pro.2460. - DOI - PMC - PubMed
69. Zhang L, Aleksandrov LA, Zhao Z, et al. Architecture of the cystic fibrosis transmembrane conductance regulator protein and structural changes associated with phosphorylation and nucleotide binding. J Struct Biol. 2009;167:242–251. doi: 10.1016/j.jsb.2009.06.004. - DOI - PubMed
70. Huang P, Liu Q, Scarborough GA. Lysophosphatidylglycerol: a novel effective detergent for solubilizing and purifying the cystic fibrosis transmembrane conductance regulator. Anal Biochem. 1998;259:89–97. doi: 10.1006/abio.1998.2633. - DOI - PubMed
71. Newstead S, Kim H, von Heijne G, et al. High-throughput fluorescent-based optimization of eukaryotic membrane protein overexpression and purification in Saccharomyces cerevisiae. Proc Natl Acad Sci USA. 2007;104:13936–13941. doi: 10.1073/pnas.0704546104. - DOI - PMC - PubMed
72. Newstead S, Ferrandon S, Iwata S. Rationalizing alpha-helical membrane protein crystallization. Protein Sci. 2008;17:466–472. doi: 10.1110/ps.073263108. - DOI - PMC - PubMed
73. Vogel R, Fan GB, Sheves M, et al. Salt dependence of the formation and stability of the signaling state in G protein-coupled receptors: evidence for the involvement of the Hofmeister effect. Biochemistry. 2001;40:483–493. doi: 10.1021/bi001855r. - DOI - PubMed
74. Gekko K, Timasheff SN. Thermodynamic and kinetic examination of protein stabilization by glycerol. Biochemistry. 1981;20:4677–4686. doi: 10.1021/bi00519a024. - DOI - PubMed
75. Rubinstein JL. Structural analysis of membrane protein complexes by single particle electron microscopy. Methods. 2007;41:409–416. doi: 10.1016/j.ymeth.2006.07.019. - DOI - PubMed

76. Ramjeesingh M, Li C, Garami E, et al. A novel procedure for the efficient purification of the cystic fibrosis transmembrane conductance regulator (CFTR) Biochem J. 1997;327(Pt 1):17–21. doi: 10.1042/bj3270017. - DOI - PMC - PubMed
77. Yang Z, Wang C, Zhou Q, et al. Membrane protein stability can be compromised by detergent interactions with the extramembranous soluble domains. Protein Sci. 2014;23:769–789. doi: 10.1002/pro.2460. - DOI - PMC - PubMed
78. Accurso FJ, Rowe SM, Clancy JP, et al. Effect of VX-770 in persons with cystic fibrosis and the G551D-CFTR mutation. N Engl J Med. 2010;363:1991–2003. doi: 10.1056/NEJMoa0909825. - DOI - PMC - PubMed
79. Ramsey BW, Davies J, McElvaney NG, et al. A CFTR potentiator in patients with cystic fibrosis and the G551D mutation. N Engl J Med. 2011;365:1663–1672. doi: 10.1056/NEJMoa1105185. - DOI - PMC - PubMed
80. Van Goor F, Hadida S, Grootenhuis PD, et al. Rescue of CF airway epithelial cell function in vitro by a CFTR potentiator, VX-770. Proc Natl Acad Sci USA. 2009;106:18825–18830. doi: 10.1073/pnas.0904709106. - DOI - PMC - PubMed
81. Yu H, Burton B, Huang CJ, et al. Ivacaftor potentiation of multiple CFTR channels with gating mutations. J Cyst Fibros. 2012;11:237–245. doi: 10.1016/j.jcf.2011.12.005. - DOI - PubMed
82. Eckford PD, Li C, Ramjeesingh M, et al. Cystic fibrosis transmembrane conductance regulator (CFTR) potentiator VX-770 (ivacaftor) opens the defective channel gate of mutant CFTR in a phosphorylation-dependent but ATP-independent manner. J Biol Chem. 2012;287:36639–36649. doi: 10.1074/jbc.M112.393637. - DOI - PMC - PubMed
83. Carmelo V, Bogaerts P, Sa-Correia I. Activity of plasma membrane H+-ATPase and expression of PMA1 and PMA2 genes in Saccharomyces cerevisiae cells grown at optimal and low pH. Arch Microbiol. 1996;166:315–320. doi: 10.1007/s002030050389. - DOI - PubMed
84. Schultz BD, Bridges RJ, Frizzell RA. Lack of conventional ATPase properties in CFTR chloride channel gating. J Membr Biol. 1996;151:63–75. doi: 10.1007/s002329900058. - DOI - PubMed

85. Al-Zahrani A, Cant N, Kargas V, Rimington T, Aleksandrov L, Riordan JR, Ford RC. Structure of the cystic fibrosis transmembrane conductance regulator in the inward-facing conformation revealed by single particle electron microscopy. AIMS Biophys. 2015;2:131–152. doi: 10.3934/biophy.2015.2.131. - DOI
86. Lee SC, Bennett BC, Hong WX, et al. Steroid-based facial amphiphiles for stabilization and crystallization of membrane proteins. Proc Natl Acad Sci USA. 2013;110:E1203–E1211. doi: 10.1073/pnas.1221442110. - DOI - PMC - PubMed
87. Sonoda Y, Newstead S, Hu NJ, et al. Benchmarking membrane protein detergent stability for improving throughput of high-resolution X-ray structures. Structure. 2011;19:17–25. doi: 10.1016/j.str.2010.12.001. - DOI - PMC - PubMed
88. Alexandrov AI, Mileni M, Chien EY, et al. Microscale fluorescent thermal stability assay for membrane proteins. Structure. 2008;16:351–359. doi: 10.1016/j.str.2008.02.004. - DOI - PubMed
89. Ayers FC, Warner GL, Smith KL, et al. Fluorometric quantitation of cellular and nonprotein thiols. Anal Biochem. 1986;154:186–193. doi: 10.1016/0003-2697(86)90513-0. - DOI - PubMed
90. Mornon JP, Lehn P, Callebaut I. Atomic model of human cystic fibrosis transmembrane conductance regulator: membrane-spanning domains and coupling interfaces. Cell Mol Life Sci. 2008;65:2594–2612. doi: 10.1007/s00018-008-8249-1. - DOI - PubMed
91. Mornon JP, Lehn P, Callebaut I. Molecular models of the open and closed states of the whole human CFTR protein. Cell Mol Life Sci CMLS. 2009;66:3469–3486. doi: 10.1007/s00018-009-0133-0. - DOI - PubMed
92. Protasevich I, Yang Z, Wang C, et al. Thermal unfolding studies show the disease causing F508del mutation in CFTR thermodynamically destabilizes nucleotide-binding domain 1. Protein Sci Publ Protein Soc. 2010;19:1917–1931. doi: 10.1002/pro.479. - DOI - PMC - PubMed

Chapter 4.0

The Structural Basis of Cystic Fibrosis.

Xin Meng, Jack Clews, Eleanor R. Martin, Anca D. Ciuta and Robert C. Ford[1].

Michael Smith Building, School of Biology, Faculty of Biology Medicine and Health, Universuty of Manchester, Manchester M13 9PL, UK.

1. To whom correspondence should be addressed:

robert.ford@manchester.ac.uk

Keywords: CFTR, cystic fibrosis, membrane protein, protein structure, ion channel.

Abstract: CFTR (ABCC7) is a phospho-regulated chloride channel that is found in the apical membranes of epithelial cells, is gated by ATP, and the activity of the protein is crucial in the homeostasis of the extracellular liquid layer in many organs (1,2). Mutations in CFTR cause the inherited disease cystic fibrosis (CF), the most common inherited condition in humans of European descent (2,3). The structural basis of cystic fibrosis will be discussed in this article.

Introduction:

CFTR is a member of the ATP-binding cassette (ABC) family of proteins. As such, CFTR has the standard four-domain structure consisting of two transmembrane domains and two soluble nucleotide-binding domains (4). The ABC family are predominantly active transporters. In accord with the Jardetzky model for transporter action (5), the ATP is employed to drive the transition of the transmembrane domains from an inward-facing to an outward-facing conformation (or vice-versa for ABC importers). However for CFTR it is thought that ATP drives a conformational change that opens a channel in the transmembrane domains, through which chloride ions can diffuse passively(6).

CFTR is the only member of the ABC family that has this channel-type functionality, although some members do act as regulatory switches for other channels (7,8).

Initial CFTR structural data.

Initial structural studies were carried out over a decade ago on the soluble CFTR domains studied in isolation from the transmembrane portions (9,10). In these early studies, the first soluble ATP-binding domain (nucleotide- binding domain 1, NBD1) containing the most common CF-causing mutation (F508 deletion) was crystallised in the presence and absence of this phenylalanine residue. The F508 deletion was found to have almost no effect on the structure of the isolated domain apart from some local rearrangements around the F508 position. This was unexpected: prior studies of the mutation in various cells had been interpreted in terms of its protein folding, with the F508del mutation discussed as a mis-folding mutation that led to its recognition by the endoplasmic reticulum quality control machinery (11-14). However crystallisation of the domain, as well as the second NBD (NBD2), required an exhaustive search for mutations that promoted solubility and stability. In the case of NBD1, these same mutations were later demonstrated to partially rescue the defect caused by F508 deletion (15). Isolated domains were also studied by NMR although as above, mutations that increased the protein solubility were needed to meet the criteria for these biophysical approaches (16-18).

NMR was also employed to study the interactions of the third soluble 'domain' in CFTR, the 200 residue-long Regulatory-domain or R-domain (19). These interactions were studied with several potential partner proteins, including the two soluble NBDs. Whether this region was intrinsically disordered (as suggested by the NMR data and predictions based on its amino acid sequence), or a structured domain, remained a moot point until recently. When cryo-EM data for single CFTR particles emerged(20-23), the data implied that the R-domain existed in an intermediate state in the absence of phosphorylation – i.e. it displayed weak, but localized, Coulomb-scattering density in the cryo-EM maps. This weak density was observed between the two NBDs and in one map it protruded into the aqueous compartment generated by the two transmembrane

domains in their inward-facing configuration (23, see Figure 1). Upon phosphorylation, the weak density for the R-region could no longer be observed (21,23), implying that the addition of about 7-9 negative charges to Serine and Threonine residues in this region caused its dissociation from the CFTR core domains and resulted in disorder throughout this portion of the protein. Such a phosphorylation-dependence on R-region/NBD association was predicted by the NMR interaction studies using the isolated domains(19).

Disease-causing mutations.

The multiple cryo-EM derived structures for CFTR at medium resolution (3-9 Angstrom resolution) represent structures equivalent to the wild-type protein, or structures of CFTR with mutations that were incorporated to stabilise the protein(20-23). The structural effects of mutations that are cystic fibrosis-causing in a significant number of patients (such as F508del) still remain to be studied using cryo-EM, although small-angle X-ray scattering has been employed to study this most prevalent disease-causing mutation(24). The structural data so far imply that F508 deletion causes significant changes in the overall structure of the purified full-length protein as detected by SAXS. This is in accord with the biochemical data that show that F508 deletion has a major effect on the stability of the protein(25,26). F508 sits in a buried position in NBD1 at its interface with the 2nd intracellular loop of transmembrane domain 2 (Figure 1). This loop links transmembrane helices 10 and 11 which cross over from the opposite side of the molecule in a domain-swap type arrangement. Hinge-like movements of these transmembrane helices are closely associated with the transition from inward- to outward-facing conformations and this may explain why F508del CFTR has poor channel activity. However the position of F508 at a crucial and exquisitely-conserved domain-domain interface may explain why it has a large effect on the overall stability of the structure of the protein (Figure 1A).

The second most common missense mutation that causes CF is G551D, which results in a predominantly closed channel. The open probability of fully-phosphorylated G551D CFTR channels in the presence of milliMolar ATP concentrations is ten-fold lower (P_O=0.04) compared to the WT channel (P_O=0.40)(26). G551 is part of the 'signature' sequence of NBD1 which jointly binds ATP in association with the Walker A and Walker B residues from NBD2

(Figure 1B). The signature sequence is a characteristic of all ABC proteins (27-29). The incorporation of an additional negative charge at this position as well as the $-CH_2-COO^-$ side-chain of aspartate is likely to impede ATP binding and make the formation of the NBD1-NBD2 sandwich dimer much less likely. Not only are the negatively-charged phosphate groups of the ATP in close proximity to G551, but also the E1391 and D1390 residues in the Walker B region of NBD2. A drug to treat G551D patients was developed over the last decade (ivacaftor(30,31)) and this therapeutic compound greatly increases the open probability of the channel to close to WT levels(30). Ivacaftor has been shown to be effective at increasing the channel function of many, but not all CF-causing mutations studied in vitro (32), and these mutations are distributed throughout the 3D structure of the protein. Of note is that many of the mutations that ivacaftor can work on involve a change in the charge of the mutated residue, akin to G551D. Hence elucidation of the mode of action of the drug is challenging but we can infer that Coulombic charge effects appear to be implicated. Examination of the distribution of charged residues across the water-exposed surface of CFTR allows the calculation of the Coulombic surface potential, which is displayed using colour-coding in Figure 1C. This shows that the inner surfaces of the intracytoplasmic loops are strongly positively charged, a feature of significance for the above discussion since these surfaces must be pressed together in order to reach the outward-facing state and hence open the channel.

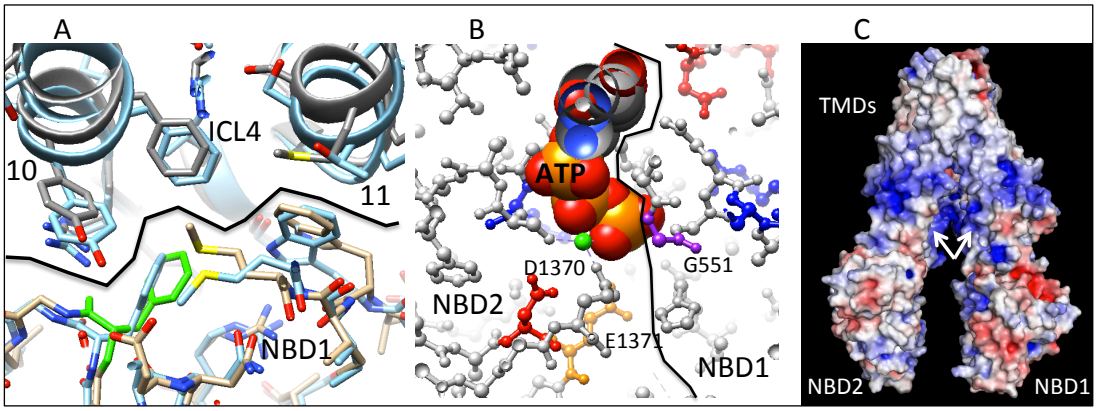

Figure 1. (A) Zebrafish CFTR in the outward-facing state shows F508 (highlighted green) which is present in NBD1 (taupe backbone) and is at the interface (solid line) with ICL4 of TMD2 (grey). The ribbon trace shows the paths of the long cytoplasmic extensions of transmembrane helices 10 and 11. The human CFTR structure (sky blue) in the inward-facing state is shown superimposed after alignment. There is strict conservation of the interface across species and it is retained despite the global conformational changes involved in the transit from inward- to outward-facing states. (B) Position of G551 in the signature sequence of NBD1 (right) and at the NBD1/NBD2 interface (black line). Nearby charged residues in NBD2 and the phosphate groups of ATP (yellow/red space-fill atoms) imply that mutation of G to D will disfavour NBD dimersation and hence channel opening. The zebrafish CFTR in the outward- facing state is shown. (C) Surface charge distribution in the inward-facing human CFTR structure with no nucleotide and unassigned R-region residues removed. Blue and red shades represent varying positive or negative charge and white, no charge. Positively charged patches on the inner surface (arrows) must be brought together for formation of the outward-facing state.

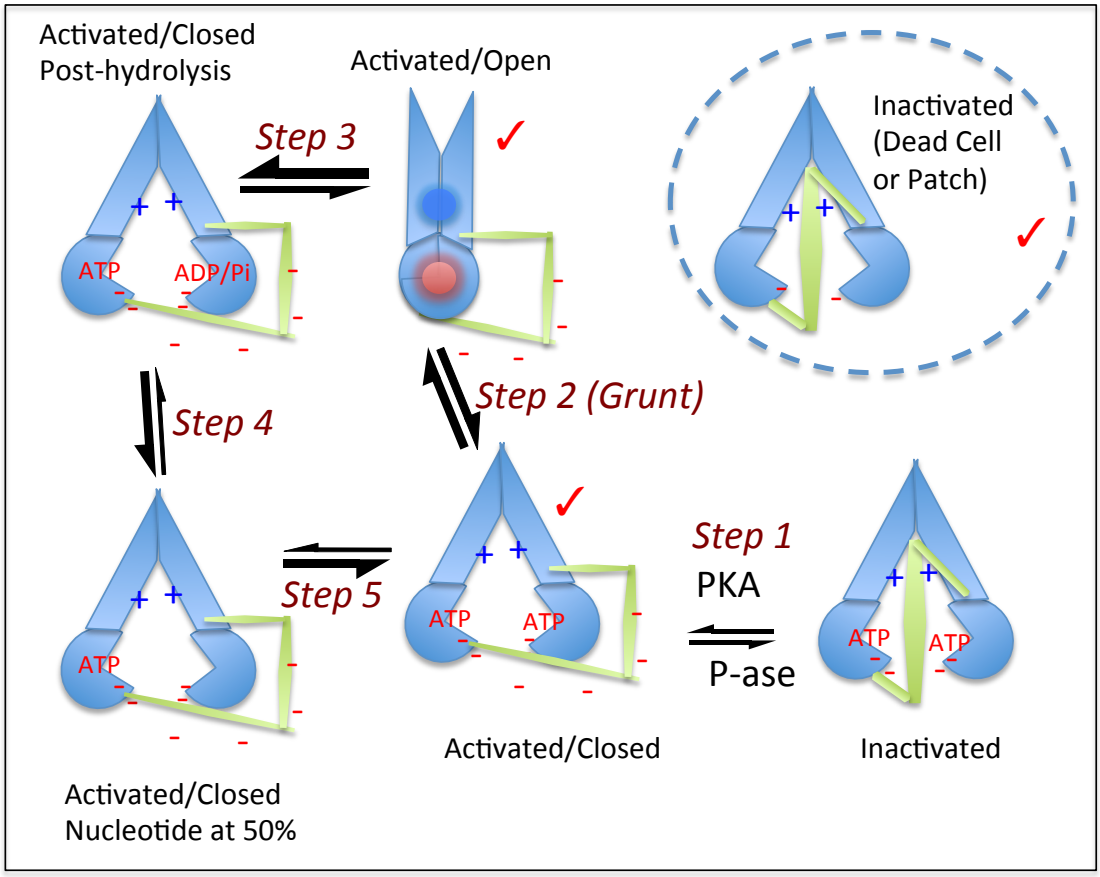

Figure 2: 'Grunt' model for CFTR structure-function relationships. Here nucleotide-free CFTR is considered non-physiological (dashed circle). Inactivated CFTR (bottom right) has R-region (green) impeding NBD dimerisation. Activation by PKA (reversible by protein phosphatase) is via phosphorylation of R-region and removal of the impediment (Step1). NBD dimerisation and production of the open channel (Step 2) is not inevitable because of the need to overcome longer-range charge repulsion as the outward- facing state is approached (red, blue circles, 'Grunt'). Mutations affecting channel open probability are predicted to exert their influence at Step2, along with potentiator compounds such as ivacaftor. Once formed, the outward-facing state is stable due to short-range interactions, but is destabilised in some way by ATP hydrolysis by NBD2 Walker B residues (Step 3). Mutations affecting Step 3 may prolong channel opening. Dissociation of ADP and inorganic phosphate (Step 4) and re-binding of ATP (Step 5) must now occur, and mutations affecting the kinetics of these steps may also affect the overall open probability of the channel. Structural studies by cryo-EM have so far revealed three of these states for CFTR (tick symbols). The relative thickness of the arrows at each step is only indicative of the likely proportions of the participants.

Integration of the biochemical and structural data for CFTR

A model is proposed to explain these observations, which we term the 'Grunt' model (Figure 2). This model assumes that nucleotide will remain bound to CFTR for most of its lifetime in the cell, with a slow rate of ATP hydrolysis. Nucleotide-free CFTR will never exist unless ATP levels drop in the cell due to cell death, but note that this state can be produced and studied experimentally (e.g. in inside out membrane patches (26,33-35)). In order for CFTR activity to be regulated, phosphorylation by PKA and dephosphorylation by protein phosphatase will be needed (step 1). Once phosphorylation of the R-region occurs then this region can dissociate from its interfering position between the NBDs and take up a disordered structure. In this new situation, inward-facing CFTR with no channel activity can alternate with an outward-facing conformation that can form a channel for chloride ions (step 2). Production of the outward-facing state may have a significant energy barrier, possibly because of the long-range influence of electrostatic forces due to the positively-charged residues that cluster in the inward-facing surface of the intracytoplasmic loops as well as the negative charge of the ATP molecules in the NBDs (Figure 1B,C). Once the outward-facing state is formed, short-range interactions (H-bonding, van der Waals) are likely to dominate and stabilize it. Mutations such as G551D that reduce the open probability of the channel are likely to affect the equilibrium at step 2, and we predict that ivacaftor also acts at this step but in this case it will promote the outward-facing state. We expect the drug will be acting in a similar fashion to ABC transporter allocrites (transported substrates) which are known to stimulate ATPase activity when they bind. For exporters in the same family as CFTR, allocrites bind to the inward-facing state with higher affinity and for some transporters, the binding sites have been characterised by mutagenesis and structural studies. For example in P-glycoprotein (ABCB1) which can transport xenobiotics and drugs out of the cell, there are two drug binding sites at the apex of the inner vestibule formed by the two transmembrane domains in the inward-facing conformation(36,37). It is known that ivacaftor is one of the many transported substrates of P-glycoprotein(38).

ATP hydrolysis is likely to occur at step 3 and the model implies that catalysis

requires the NBDs to be dimerised, as they exist in the outward-facing conformation, for this hydrolysis to be efficient. Mutations that affect this step (such as those in the Walker B region) may have some influence on step 2 as well. Indeed, mutation E1371Q in CFTR was used to generate a sufficient proportion of outward-facing CFTR molecules to allow that state to be studied by single-particle cryo-EM (21). Steps 4 and 5 are typical of ABC transporter proteins where one of the ATP binding sites has evolved to be catalytically inactive. There are many ABC transporters that show this feature, including CFTR where the site formed between the NBD1 Walker motifs and the NBD2 signature motif is non-consensus (1). Mutations that affect these steps may also influence the balance at step 2 for the same reasons as above.

Perspectives:

Both inward-facing and outward-facing conformations of CFTR in the presence of ATP have recently been reported for phosphorylated protein (21,23). The inward-facing conformation was also observed in a study of CFTR interacting with NHERF1-PDZ1 domain which is known to bind at the CFTR C-terminus(39). Moreover a detailed study of negatively stained single particles of two purified ABC transporters found a spectrum of conformations in the presence of ATP, with 1-2% in the outward-facing configuration even in the absence of ATP(40). Similarly, structure-based calculations suggest that the free energy changes needed to affect NBD dimerisation may be relatively small (41), and surprisingly, CFTR channel activity can be detected in constructs completely lacking NBD2 (42). Hence there seems to be a remarkable plasticity in ABC protein conformations and structures that are emerging appear to reflect this. The 'Grunt' model seems to be consistent with the (otherwise perplexing) diversity of CFTR structures as well as observations concerning channel-disrupting mutations and potentiators such as Ivacaftor. Future structural studies will highlight the effects of disease-causing mutations and most significant of these will be structures that include information about the binding site(s) of the new therapeutics.

Funding

The authors acknowledge the Cystic Fibrosis Foundation (CFF FORD13XX0) and the Cystic Fibrosis Trust (F508del CFTR SRC) for funding.

Author Contribution

RCF wrote the paper. XM, JC, ADC, ERM discussed and edited the manuscript and contributed to the concepts therein.

Competing interests: RCF consulted for Vertex Inc. in 2016 and 2017.

Acknowledgements: We thank Alessandro Barbieri, Nopnithi Thonghin and Talha Shafi for useful discussions.

References

1. Riordan, J. R. (2008) CFTR function and prospects for therapy. Annu Rev Biochem 77, 701-726

2. Riordan, J. R., Rommens, J. M., Kerem, B., Alon, N., Rozmahel, R., Grzelczak, Z., Zielenski, J., Lok, S., Plavsic, N., Chou, J. L., and et al. (1989) Identification of the cystic fibrosis gene: cloning and characterization of complementary DNA. Science 245, 1066-1073

3. Linton, K. J., and Higgins, C. F. (2007) Structure and function of ABC transporters: the ATP switch provides flexible control. Pflugers Arch 453, 555-567

4. Linton, K. J. (2007) Structure and function of ABC transporters. Physiology (Bethesda) 22, 122-130

5. Jardetzky, O. (1966) Simple allosteric model for membrane pumps. Nature 211, 969-970

6. Gadsby, D. C., Vergani, P., and Csanady, L. (2006) The ABC protein turned chloride channel whose failure causes cystic fibrosis. Nature 440, 477-483

7. Mikhailov, M. V., Campbell, J. D., de Wet, H., Shimomura, K., Zadek, B., Collins, R. F., Sansom, M. S., Ford, R. C., and Ashcroft, F. M. (2005) 3-D structural and functional characterization of the purified KATP channel complex Kir6.2-SUR1. The EMBO journal 24, 4166-4175

8. Bryan, J., and Aguilar-Bryan, L. (1999) Sulfonylurea receptors: ABC transporters that regulate ATP-sensitive K(+) channels. Biochim Biophys Acta 1461, 285-303

9. Lewis, H. A., Buchanan, S. G., Burley, S. K., Conners, K., Dickey, M., Dorwart, M., Fowler, R., Gao, X., Guggino, W. B., Hendrickson, W. A., Hunt, J. F., Kearins, M. C., Lorimer, D., Maloney, P. C., Post, K. W., Rajashankar, K. R., Rutter, M. E., Sauder, J. M., Shriver, S., Thibodeau, P. H., Thomas, P. J., Zhang, M., Zhao, X., and Emtage, S. (2004) Structure of nucleotide-binding domain 1 of the cystic fibrosis transmembrane conductance regulator. Embo J 23, 282-293

10. Lewis, H. A., Zhao, X., Wang, C., Sauder, J. M., Rooney, I., Noland, B. W., Lorimer, D., Kearins, M. C., Conners, K., Condon, B., Maloney, P. C., Guggino, W. B., Hunt, J. F., and Emtage, S. (2005) Impact of the deltaF508 mutation in first nucleotide-binding domain of human cystic fibrosis transmembrane conductance regulator on domain folding and structure. J Biol Chem 280, 1346-1353

11. Cyr, D. M. (2011) Quality Control of Nascent Cftr in the Endoplasmic Reticulum. Pediatr Pulm, 147-148

12. Ren, H. Y., Grove, D. E., De La Rosa, O., Houck, S. A., Sopha, P., Van Goor, F., Hoffman, B. J., and Cyr, D. M. (2013) VX-809 corrects folding defects in cystic fibrosis transmembrane conductance regulator protein through action on membrane-spanning domain 1. Molecular biology of the cell 24, 3016-3024

13. Ward, C. L., Omura, S., and Kopito, R. R. (1995) Degradation of CFTR by the ubiquitin-proteasome pathway. Cell 83, 121-127

14. Kopito, R. R. (1999) Biosynthesis and degradation of CFTR. Physiol Rev 79, S167-173

15. Roxo-Rosa, M., Xu, Z., Schmidt, A., Neto, M., Cai, Z., Soares, C. M., Sheppard, D. N., and Amaral, M. D. (2006) Revertant mutants G550E and 4RK rescue cystic fibrosis mutants in the first nucleotide-binding domain of CFTR by different mechanisms. P Natl Acad Sci USA 103, 17891-17896

16. Kanelis, V., Chong, P. A., and Forman-Kay, J. D. (2011) NMR Spectroscopy to Study the Dynamics and Interactions of CFTR. Cystic Fibrosis: Diagnosis and Protocols, Vol I: Approaches to Study and Correct Cftr Defects 741, 377-403

17. Kanelis, V., Hudson, R. P., Thibodeau, P. H., Thomas, P. J., and Forman-Kay, J. D. (2010) NMR evidence for differential phosphorylation-dependent interactions in WT and Delta F508 CFTR. Embo Journal 29, 263-277

18. Baker, J. M. R., Hudson, R. P., Kanelis, V., Choy, W. Y., Thibodeau, P. H., Thomas, P. J., and Forman-Kay, J. D. (2007) CFTR regulatory region interacts with NBD1 predominantly via multiple transient helices. Nat Struct Mol Biol 14, 738-745

19. Mendoza, J. L., Schmidt, A., Li, Q., Nuvaga, E., Barrett, T., Bridges, R. J., Feranchak, A. P., Brautigam, C. A., and Thomas, P. J. (2012) Requirements for efficient correction of DeltaF508 CFTR revealed by analyses of evolved sequences. Cell 148, 164-174

20. Bozoky, Z., Krzeminski, M., Muhandiram, R., Birtley, J. R., Al-Zahrani, A., Thomas, P. J., Frizzell, R. A., Ford, R. C., and Forman-Kay, J. D. (2013) Regulatory R region of the CFTR chloride channel is a dynamic integrator of phospho-dependent intra- and intermolecular interactions. P Natl Acad Sci USA 110, E4427-4436

21. Baker, J. M., Hudson, R. P., Kanelis, V., Choy, W. Y., Thibodeau, P. H., Thomas, P. J., and Forman-Kay, J. D. (2007) CFTR regulatory region interacts with NBD1 predominantly via multiple transient helices. Nat Struct Mol Biol 14, 738-745

22. Zhang, Z., and Chen, J. (2016) Atomic Structure of the Cystic Fibrosis Transmembrane Conductance Regulator. Cell 167, 1586-1597 e1589

23. Zhang, Z., Liu, F., and Chen, J. (2017) Conformational Changes of CFTR

upon Phosphorylation and ATP Binding. Cell 170, 483-491 e488

24. Liu, F., Zhang, Z., Csanady, L., Gadsby, D. C., and Chen, J. (2017) Molecular Structure of the Human CFTR Ion Channel. Cell 169, 85-95 e88

25. Fay, J. F., Aleksandrov, L., Jensen, T. J., Kousouros, J. N., He, L., Aleksandrov, A. A., Gingerich, D., Riordan, J. R., and Chen, J. (2017) Cryo-Em Visualization of an Active Phosphorylated Cftr Channel. Pediatr Pulm 52, S214-S215

26. Rosenberg, M. F., O'Ryan, L. P., Hughes, G., Zhao, Z., Aleksandrov, L. A., Riordan, J. R., and Ford, R. C. (2012) The cystic fibrosis transmembrane conductance regulator (CFTR): three-dimensional structure and localization of a channel gate. J Biol Chem 286, 42647-42654

27. Hwang, T. C., and Kirk, K. L. (2013) The CFTR ion channel: gating, regulation, and anion permeation. Cold Spring Harb Perspect Med 3, a009498

28. Pollock, N. L., Satriano, L., Zegarra-Moran, O., Ford,R.C. and Moran, O. (2016) Structure of wild type and mutant F508del CFTR: A small-angle X-ray scattering study of the protein–detergent complexes. J. Struct. Biol. 194, 102-111

29. Meng, X., Clews, J., Kargas, V., Wang, X., and Ford, R. C. (2016) The cystic fibrosis transmembrane conductance regulator (CFTR) and its stability. Cell Mol Life Sci 74:23IJ

30. Meng, X., Wang, Y., Wang, X., Wrennall, J. A., Rimington, T. L., Li, H., Cai, Z., Ford, R. C., and Sheppard, D. N. (2017) Two Small Molecules Restore Stability to a Sub-population of the Cystic Fibrosis Transmembrane conductance Regulator with the Predominant Disease-causing Mutation. The Journal of biological chemistry 292, 3706-3719

31. Hopfner, K. P., Karcher, A., Shin, D. S., Craig, L., Arthur, L. M., Carney, J. P., and Tainer, J. A. (2000) Structural biology of Rad50 ATPase: ATP-driven conformational control in DNA double-strand break repair and the ABC-ATPase superfamily. Cell 101, 789-800

32. Higgins, C. F., Haag, P. D., Nikaido, K., Ardeshir, F., Garcia, G., and Ames, G. F. (1982) Complete nucleotide sequence and identification of membrane components of the histidine transport operon of S. typhimurium. Nature 298, 723-727

33. Higgins, C. F. (1992) ABC transporters: from microorganisms to man. Annu Rev Cell Biol 8, 67-113

34. Van Goor, F., Hadida, S., and Grootenhuis, P. (2007) VX-770, a potent, selective, and orally bioavailable potentiator of CFTR gating. Pediatr Pulm, 289-289

35. Hadida, S., Van Goor, F., Dinehart, K., Looker, A. R., Mueller, P., and Grootenhuis, P. D. J. (2014) Case History: Kalydeco (R) (VX-770, Ivacaftor), a CFTR Potentiator for the Treatment of Patients with Cystic Fibrosis and the G551D-CFTR Mutation. Annu Rep Med Chem 49, 383-398

36. Van Goor, F., Yu, H. H., Burton, B., and Hoffman, B. J. (2014) Effect of ivacaftor on CFTR forms with missense mutations associated with defects in protein processing or function. Journal of Cystic Fibrosis 13, 29-36

37. Sheppard, D. N., Gray, M. A., Gong, X., Sohma, Y., Kogan, I., Benos, D. J., Scott-Ward, T. S., Chen, J. H., Li, H., Cai, Z., Gupta, J., Li, C., Ramjeesingh, M., Berdiev, B. K., Ismailov, II, Bear, C. E., Hwang, T. C., Linsdell, P., and Hug, M. J. (2004) The patch-clamp and planar lipid bilayer techniques: powerful and versatile tools to investigate the CFTR Cl- channel. J Cyst Fibros 3 Suppl 2, 101-108

38. Alam, A., Kung, R., Kowal, J., McLeod, R. A., Tremp, N., Broude, E. V., Roninson, I. B., Stahlberg, H., and Locher, K. P. (2018) Structure of a zosuquidar and UIC2-bound human-mouse chimeric ABCB1. P Natl Acad Sci USA 115, E1973-E1982

39. Szewczyk, P., Tao, H., McGrath, A. P., Villaluz, M., Rees, S. D., Lee, S. C., Doshi, R., Urbatsch, I. L., Zhang, Q., and Chang, G. (2015) Snapshots of ligand entry, malleable binding and induced helical movement in P-glycoprotein. Acta Crystallogr D Biol Crystallogr 71, 732-741

40. Lingam, S., Thonghin, N., and Ford, R. C. (2017) Investigation of the effects of the CFTR potentiator ivacaftor on human P-glycoprotein (ABCB1). Sci Rep 7, 17481

41. Al-Zahrani, A., Cant,N., Kargas,V., Rimington, T., Aleksandrov, L., Riordan, J.R. & Ford, R.C. (2015) Structure of the cystic fibrosis transmembrane conductance regulator in the inward-facing conformation revealed by single particle electron microscopy. AIMS Biophys. 2, 131-152

42. Moeller, A., Lee, S. C., Tao, H., Speir, J. A., Chang, G., Urbatsch, I. L., Potter, C. S., Carragher, B., and Zhang, Q. (2015) Distinct conformational spectrum of homologous multidrug ABC transporters. Structure 23, 450-460

43. Kos, V., and Ford, R. C. (2009) The ATP-binding cassette family: a structural perspective. Cell Mol Life Sci 66, 3111-3126

44. Cui, L., Aleksandrov, L., Chang, X. B., Hou, Y. X., He, L., Hegedus, T., Gentzsch, M., Aleksandrov, A., Balch, W. E., and Riordan, J. R. (2007) Domain interdependence in the biosynthetic assembly of CFTR. J Mol Biol 365, 981-994

45. Ikuma, M., and Welsh, M. J. (2000) Regulation of CFTR Cl- channel gating by ATP binding and hydrolysis. Proc Natl Acad Sci U S A 97, 8675-8680

Chapter 5.0

CFTR Structure, Stability, Function & Regulation

Xin Meng[1], Jack Clews[1], Anca Cuita[1,2], Eleanor R. Martin[1] & Robert C. Ford[1,4]

1. School of Biological Sciences, Faculty of Biology Medicine and Health, Michael Smith Building, The University of Manchester, Oxford Road, Manchester M13 9PL, UK.
2. Current address: Institute of Molecular Biology and Biophysics ETH Zurich, HPK G11, Otto-Stern-Weg 5, 8093 Zurich, Switzerland.
3. To whom correspondence should be addressed: bob.ford@manchester.ac.uk

Key words:

ABC transporter, ion channel, CFTR, membrane protein structure, electron microscopy

Abstract

CFTR (Cystic Fibrosis transmembrane conductance regulator) is a unique member of the ATP-binding cassette family of proteins because it has evolved into a channel. Mutations in CFTR cause cystic fibrosis, the most common genetic disease in people of European origins. The F508del mutation is found in about 90% of patients and it causes CFTR instability. Recent cryo-electron microscopy data have shown that CFTR architecture is like other ATP-binding cassette transporters, showing large conformational shifts between cytoplasmic- and extracellular-facing states. Our recent studies into the effects of F508 deletion and various approaches to study its destablising properties are presented here. We also investigate the conformational states of CFTR that exist under various experimental conditions, with the aim of unifying the models that explain structure/stability, structure/function and structure/regulation.

Introduction

Cystic fibrosis transmembrane conductance regulator (CFTR):

CFTR is an ATP-gated chloride channel present in the apical membranes of cells lining the externally-facing surfaces of several organs(Riordan, 2008). Phosphorylation of a highly charged regulatory region (R-region) of CFTR by protein kinase A or C activates the channel, which can then open, allowing chloride ion flux, provided ATP is available(Chappe, Hinkson et al., 2003). Chloride ions pass (passively) through the protein along their concentration gradient. Typically this means that CFTR channel opening is associated with the loss of chloride ions from the cell and their accumulation in the extracellular milieu. The charge imbalance caused by the movement of chloride is corrected by the concomitant flux of sodium ions in the same direction, and the resultant osmotic imbalance is accommodated by the flux of water into the extracellular space. Excess CFTR activity and hence water flux can lead to diarrhea (in the intestinal tract). Sub-normal CFTR activity can lead to constipation in the guts and also stasis of the mucociliary clearance mechanism, vital for maintaining healthy lungs(Donaldson, Bennett et al., 2006). This latter outcome is the most serious symptom for cystic fibrosis (CF) patients who have significantly reduced CFTR activity due to inheritance of two mutated and defective copies of the *cftr* gene(Riordan, Rommens et al., 1989). In CFTR, channel opening is associated with the outward-facing state, where the ATP-binding domains are dimerised(Cai, Sohma et al., 2011, Vergani, Lockless et al., 2005, Yeh, Sohma et al., 2017). CFTR channel function is also activated and controlled by phosphorylation, and here new structural data have provided different models of how phosphorylation could affects CFTR activity(Fay, Aleksandrov et al., 2018, Zhang, Liu et al., 2017).

Mutations in the *cftr* gene are varied, although the predominantly observed mutation in patients of European descent is a deletion of three bases that results in the loss of a phenylalanine residue at position 508 in the protein's amino acid sequence(Riordan et al., 1989, Veit, Avramescu et al., 2016). Interestingly, deletion of this single residue (F508del) leads to a protein that is only a little worse in terms of its intrinsic channel activity(Meng, Wang et al., 2017c).

However, it is noticeably less stable at physiological temperatures(Meng et al., 2017c). The unstable product is recognized and degraded by endoplasmic reticulum (ER) quality control mechanisms, and this occurs so efficiently that little or no F508del CFTR protein reaches the apical membrane(Brodsky, 2001). The high rates of occurrence of the F508del mutation (90% of patients have at least one copy) and disease (~1 in 2000 sufferers, carriage rate ~1 in 25) point to a prior selective advantage of being a carrier in humans with European origins. The exact nature of that advantage is debated(Gabriel, Brigman et al., 1994, Wiuf, 2001), but there is broad agreement that it is is likely to be related to a strong selective pressure imposed by intestinal diseases associated with high rates of infant mortality in the past.

Biochemical and biophysical measurements of CFTR have been crucial in our understanding of the effects of the various CF-causing mutations such as F508del(Meng et al., 2017c, Vernon, Chong et al., 2017, Yang, Hildebrandt et al., 2018). Moreover, the development of fluorescence-based assays for CFTR channel activity has allowed the discovery of small molecules that can potentiate the channel activity and also rescue the instability defect(Galietta, Springsteel et al., 2001). There are now molecules available for the treatment of most patients(Davies, Moskowitz et al., 2018, Keating, Marigowda et al., 2018, Ren, Grove et al., 2013, Yu, Burton et al., 2012) (subject to cost). CFTR is somewhat unusual in that it is clearly a channel that has evolved from a group of proteins that are otherwise active transporters(Dean, Rzhetsky et al., 2001). Our understanding of the CFTR protein is, to a large extent, based on prior studies with these other transporters that couple ATP hydrolysis to substrate transport across a membrane(Higgins, 1992). When compared using sequence homology and phylogenetics, CFTR has been classified into the C sub-family of the eukaryotic ATP-binding cassette transporters(Dean et al., 2001). There are 38 transporter-like proteins belonging to this overall family in humans of which 13 are in the C sub-family. Two other C sub-family members are also non-transporters, and this pair have evolved as switches that control another channel(Mikhailov, Campbell et al., 2005). The remaining 10 members of the C sub-family are transporters and many of them are involved in xenobiotic clearance and hence associated with multi-drug resistance(Higgins, 2007, Rosenberg, Oleschuk et al., 2010).

Comparison of cryo-EM structures for CFTR:

There are now several structures that have been published for CFTR. A summary of the various structures, their overall conformation and the experimental conditions employed to obtain them is proposed in Table I.

Ortholog	EMDB code	PDB code	Experimental conditions	Mutations	Overall State(s)	Ref.
Human CFTR	1966	4a82	Phosphorylation state unknown. No nucleotide. Detergent micelle. Epitaxial 2D crystals. N-linked glycosylation present.	WT with C-term His tag	OF	1
Zebrafish CFTR	8461	5uar	Dephosphorylated. No nucleotide. Detergent micelle. SPA. N-linked glycosylation.	WT	IF	2
Human CFTR	8516	5uak	Dephosphorylated. No nucleotide. Detergent micelle. SPA. N-linked glycosylation.	WT	IF	3
Zebrafish CFTR	8782	5w81	Phosphorylated. ATP present. Detergent micelle. N-linked glycosylation.	E1371Q	OO IF*	4
Chicken CFTR	7793	6d3r	Dephosphorylated. No nucleotide. Detergent micelle. SPA. N-linked glycosylation present.	Stabilising: ΔRI/H1404S/1441X C-term His tag	IF	5
Chicken CFTR	7794	6d3s	Phosphorylated. ATP present. Detergent micelle. N-linked glycosylation.	Stabilising: H1404S/ 1441X/ ΔRI/ C-term His tag	IF	5
Human CFTR	9230	6msm	Phosphorylated. ATP present. Detergent micelle. N-linked glycosylation.	E1371Q	OO	6

Table I. Summary of sub-nanometre resolution cryo-EM structures of full-length CFTR that have been deposited in the EMDB and PDB.
Key: EMDB – Electron Microscopy Databank (density map data). PDB – Protein Databank (atomic model). SPA- single particle averaging. WT – wild type sequence. OF – outward-facing state. IF – inward-facing state. OO – outward/occluded state. IF - evidence for particles in the inward facing state co-existing with the major state. ECL – extracellular loop. C-term – C-terminal. ΔRI - deletion of residues 405–436. 1441X – truncation at this residue. Ref: (1) (Rosenberg, O'Ryan et al., 2012); (2) (Zhang & Chen, 2016); (3) (Liu, Zhang et al., 2017); (4) (Zhang et al., 2017); (5) (Fay, Aleksandrov et al., 2017); (6) (Zhang, Liu et al., 2018)*

An immediate observation based on Table I is that different conformations of the protein can be observed under very similar experimental conditions: For example the fully activated (phosphorylated) state of the protein in the presence of ATP has been reported as being in the outward-occluded conformation in two studies(Zhang et al., 2017, Zhang, Liu et al., 2018), but in another structural study, activated CFTR was found to be in the inward-facing state(Fay et al., 2018). Similarly, the absence of nucleotide was correlated with the inward-facing state in most studies(Fay et al., 2018, Liu et al., 2017, Zhang & Chen, 2016), but in one study the outward-facing state was found instead(Rosenberg, O'Ryan et al., 2011). We would argue that consideration of the plasticity of ABC transporters must be taken into account. There are now several studies where a range of conformations within a population of an ABC transporter under the same conditions has been observed(Moeller, Lee et al., 2015). These studies show that the separation between the NBDs can vary considerably for inward-facing conformations, and that the NBD dimerized state (outward and outward-occluded states) are sampled quite rarely, even in the presence of nucleotide and non-hydrolysable nucleotide analogues. Mutagenesis may also throw some light on these discrepancies (Table I, column 5). Catalytic silencing of ATPase activity alone does not seem to be capable of stabilizing the outward-facing or outward-occluded states, since the H1404S mutation when combined with ATP and phosphorylation was nevertheless associated with the inward-facing state in chicken CFTR(Fay et al., 2018). It seems possible, therefore, that the E1371Q mutation may favour the outward-facing state by changing the charge repulsion at the NBD-NBD interface.

CFTR channel function can be monitored at the single channel level. After activation and the addition of ATP, single CFTR channels can open and 'bursts' of current can be detected(Meng et al., 2017c). The bursts are punctuated by inter-burst intervals of quiescence. In activated human WT CFTR at physiological temperatures and with ATP present, the channels are closed for about 50% of the time(Meng et al., 2017c). Even during the bursts of current, there are rapid 'flickery' closures of extremely short duration. Rationalizing these single channel measurements using the structural data summarized in Table I is not easy and clearly all the cryo-EM structures are not determined under physiological

conditions. One could propose that the outward/occluded state could represent the state of CFTR in the inter-burst duration. Alternatively, although flickery closures are transient at body temperature, low temperature may favour this state, hence the outward-occluded state could be representative of CFTR during a flickery closure.

Epitaxial 2D crystals(Rosenberg et al., 2011) are unlikely to be formed by CFTR molecules with mixed conformational states, hence the crystallization process itself may select for a given conformation, perhaps explaining the observation of the outward-facing state in the absence of nucleotide. Although the phosphorylation state in the 2D crystal study could not be readily controlled, in all the other studies listed in Table I, the phosphorylation state was imposed before structural data were collected. In all the structural studies, full phosphorylation has been associated with the disappearance of a weak sinuous density that was observed for the fully dephosphorylated state between the NBDs and intracytoplasmic loops (ICLs). This weak density was proposed to be part of the 200-residue long disordered regulatory (R) region that links the first NBD to the second TMD(Fay et al., 2018, Zhang & Chen, 2016). Hence models for how phosphorylation of the R-region regulates the channel activity could be proposed: In one model a simple steric blocking of NBD dimerization in the dephosphorylated state would prevent formation of the outward-facing state and hence channel opening(Zhang & Chen, 2016). In the second model the dephosphorylated R-region would not only prevent dimerization but would also insert itself into the cytoplasmic entrance of the channel, blocking it like a plug(Fay et al., 2018). In both these models, phosphorylation of the R-region would cause increased disorder and its dissociation from its position in the dephosphorylated state. Thus from Table I it would appear that a refined model for ABC transporter or CFTR conformation/function relationships is needed. We have proposed that inward-facing, outward-occluded and outward-facing states are always in equilibrium with each other and that the presence of ATP can push the balance in one direction or another(Meng, Clews et al., 2018). Similarly, in CFTR, phosphorylation can influence the equilibrium, especially between the inward-facing and outward-occluded states. Whether a similar phospho-regulation mechanism exists in other ABC transporters remains to be explored.

Further regulation of the activity of CFTR:

Apart from regulation via the linking R-region, CFTR activity may also be influenced via the disordered C-terminal region of the protein. In the structures listed in Table I, no density was observed for the last 40 amino acids, and indeed for the chicken CFTR studies, the C-terminal region was deliberately truncated at residue 1441(Fay et al., 2018). It is known that the CFTR C-terminus displays a PDZ-binding motif, and this allows its interaction with either of the two PDZ domains of NHERF1, a cytoplasmic soluble protein(Moyer, Duhaime et al., 2000). NHERF1 can mediate CFTR-protein interactions with other PDZ binding motif-containing proteins via its two PDZ domains. It can also mediate interaction with the cell cytoskeleton via the Ezrin-binding domain of NHERF1(Moyer, Denton et al., 1999). This has been associated with the formation of a non-mobile pool of CFTR in epithelial cells(Haggie, Stanton et al., 2004, Valentine, Lukacs et al., 2012). Links have also been proposed between CFTR-NHERF1-cytoskeleton interactions and the recycling of CFTR in the cell(Cushing, Fellows et al., 2008). From a structural perspective, the details of the interaction between the NHERF1-PDZ1 domain and the last 5 residues of the CFTR C-terminal region have been well characterized(Karthikeyan, Leung et al., 2001), but the overall effects of NHERF1 binding on CFTR conformation have been studied little. There is some evidence that NHERF1 binding may favour the inward-facing state of the channel(Al-Zahrani, Cant et al., 2015), and it is suspected that the CFTR C-terminus may associate with the R-region when it is phosphorylated(Bozoky, Krzeminski et al., 2013). These data would point to a regulatory system where NHERF1 would bind to the dephosphorylated CFTR protein in its quiescent state.

F508 deletion:

Noticeable by its absence in Table I is a structure for the F508del mutated version of CFTR. Although the effects of this mutation have been examined in the isolated NBD1(Atwell, Brouillette et al., 2010), only minor local changes in the conformation were noted. Furthermore these studies relied on a stabilized, more soluble NBD1 construct that may represent a 'rescued' state. Examination of the available atomic models and the maps from which they are derived suggests that the F508 residue sits at an important interface between NBD1 and TMD2. This location was predicted well before the higher resolution structures of CFTR became available(Dawson & Locher, 2007). Surprisingly, the overall

configuration of this interface remains unchanged throughout the large conformational transitions associated with channel activation(Meng et al., 2018). From an engineering perspective, this implies that F508 is part of a locking-pin component rather than being part of a ball and socket joint. Hence F508 deletion may destabilize the protein by weakening the link between TMD and NBD.

In the studies described below we have tested the effects of the F508del mutation on CFTR using a biophysical and a biochemical assay. The former probes for the native folded state as well as the thermostability of the protein. The latter probes for the native folded state and can also be applied to non-purified CFTR in the membrane it was expressed in. We have also examined the effects of phosphorylation on CFTR conformations using low resolution EM and further explored the link between structure/activity and regulation with the CFTR-interacting protein NHERF1.

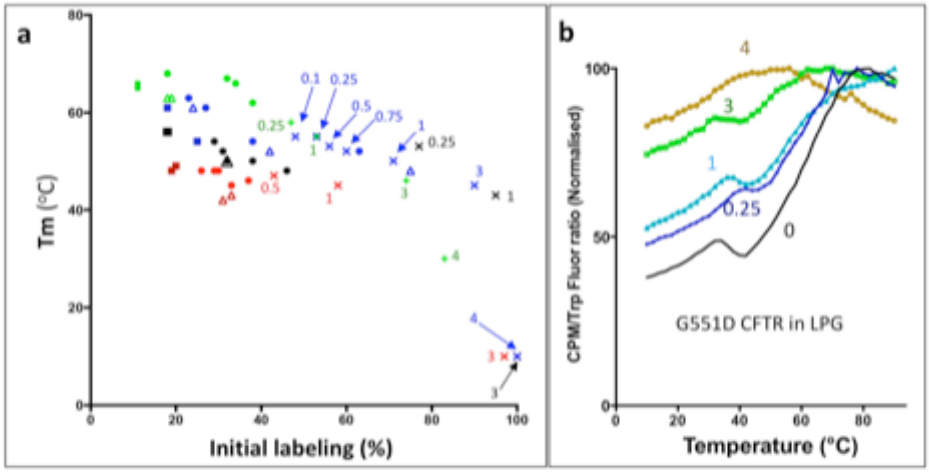

Figure 1: Thermal unfolding of CFTR: (a) Midpoint of thermal unfolding transition (Tm) is plotted against the % of initial labeling at 10oC for several batches of CFTR and under different experimental conditions. Red, black and blue data points represent F508del, WT and G551D CFTR, respectively, purified in DDM detergent. Green points are for G551D CFTR in the presence of LPG14 detergent. Round, square and triangle symbols show the effects of no addition, VX809 (2μM) addition or VX770 (2μM) addition, respectively. Crosses and numbers show the effects of GuHCl addition, with the number indicating the final GuHCl concentration in mol/L. Where no clear thermal unfolding transition was detected (bottom right), the Tm was arbitrarily assigned to the initial labelling temperature (10oC). (b) Exemplar thermal unfolding profiles for CFTR. The data series shown are for CFTR purified in LPG and at different concentrations of GuHCl (numbers indicate molarity).

Results & Discussion

Protein Purification & Characterization.

The expression and purification of full-length CFTR construct with an N-terminal His-SUMOstar tag and a C-terminal GFP-His tag has been described previously (Meng, Wang et al., 2017d, Pollock, Cant et al., 2014b). WT, F508del and G551D versions of this construct were employed for the CFTR stability studies. Generation of a CFTR construct with no GFP-His tag and an authentic C-terminus was carried out for the structural studies and a purification gel is shown in Supplementary Figure 1a. The purified protein was shown to be partly phosphorylated and could be readily dephosphorylated or fully phosphorylated by treatment with the relevant enzymes (Supplementary Figure 1 c,d). Full-length NHERF1, containing two PDZ binding domains and an ezrin binding domain, was expressed in *E.coli*. A gel for the final purification step (size exclusion chromatography) is shown in Supplementary Figure 1b.

CFTR Stability: The CPM Assay

We have employed a fluorescence-based assay for the stability of purified proteins that is based on the labelling of exposed Cys residues by a CPM dye (Alexandrov, Mileni et al., 2008, Meng, Clews et al., 2017a). Figure 1 summarises the data for many experiments with purified CFTR under various conditions. CFTR can be denatured thermally, whereupon more CPM will bind (to previously buried Cys residues)) giving rise to a fluorescence increase from which a mid-point unfolding temperature can be extracted (Tm). Initial labelling of exposed Cys residues at the surface of the folded protein at the start of the experiment is also useful indicator of the native folded state, reporting on batch-to batch quality and can detect the effects of chemical denaturation (e.g. by detergent or chaotropes). For example, increasing concentrations of Guanidium HCl reduce the thermal unfolding transition temperature as well as having a major effect on the native folded state as indicated by the high initial labelling by CPM (Figure 1). Using this assay one can clearly distinguish the lower thermal stability of F508del CFTR (Fig. 1a, red symbols), although there is no clear difference in terms of its initial folded state (within batch-to-batch variability). This supports earlier studies implying that F508del CFTR NBD1 was unaltered in terms of its overall 3D structure(Meng et al., 2017a). Acute addition of the F508del corrector drug (VX809) appears to have an effect on the initial labelling of the protein, with

less exposure of Cys residues implied (square symbols), and there is a small thermostabilisation as reported before(Meng et al., 2017a, Meng et al., 2017d). In contrast, the potentiator compound VX770 appears to have a general destabilizing effect without significantly affecting the initial labelling (triangles, Fig. 1a). Interestingly, the G551D mutation, which induces the closed channel state, has a slight thermostabilising effect on the protein (blue symbols). Although the negatively charged LPG detergent has been shown to be destabilizing for isolated CFTR NBD1(Yang, Hou et al., 2018) (relative to the non-ionic DDM detergent), we find that the thermostability of the G551D full-length CFTR protein is somewhat enhanced in this detergent (Fig.1a, green symbols). However the CPM labelling shows an additional transition prior to the main higher temperature transition (Fig. 1b). This minor transition was not included in the analysis presented in Fig. 1a, but it may indicate some localised low-temperature unfolding by LPG.

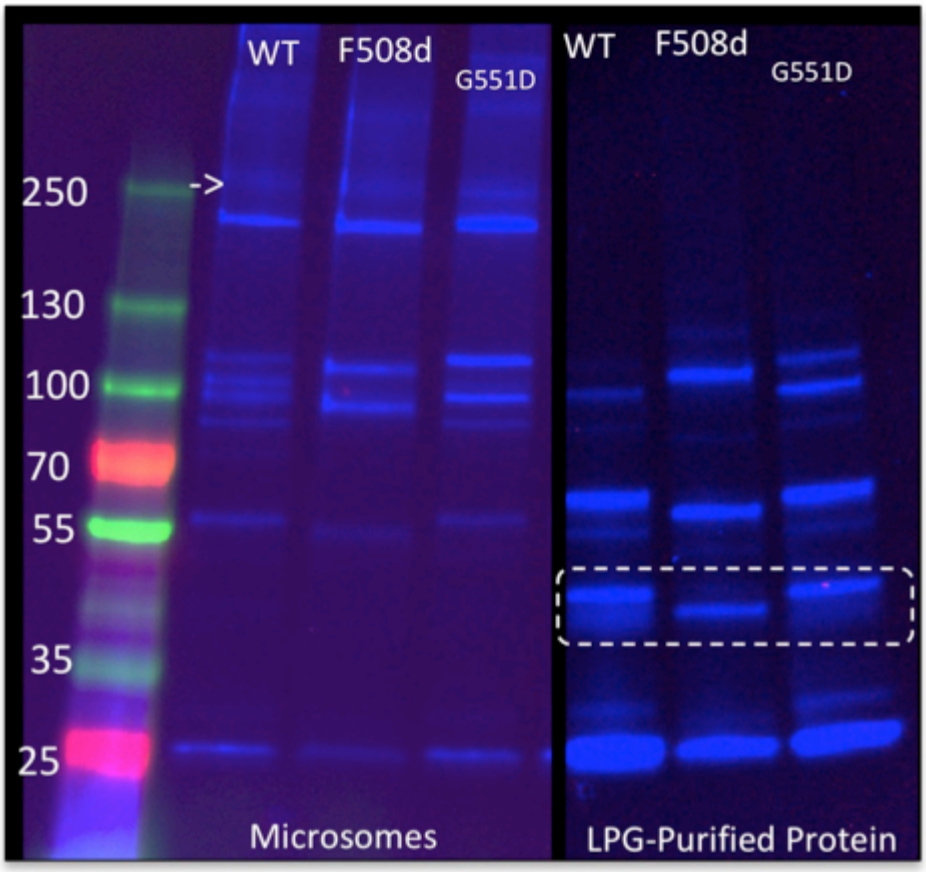

Figure 2: Limited Proteolysis of CFTR variants: Protease was at a ratio of 1:75 (0.3 µg/ml trypsin) with microsomes (left) and purified proteins (right) and detection of C-terminal fragments using the GFP fluorescence. The 25kDa lowest mass fragment is GFP alone (based on excess trypsin experiments and GFP-only controls). GFP is not unfolded by the SDS-PAGE conditions. Full-length protein runs just above the 250kDa marker and is much more protected in microsomes (arrow). The dashed rectangle outlines bands that correspond to GFP with part of NBD2, discussed in the main text.

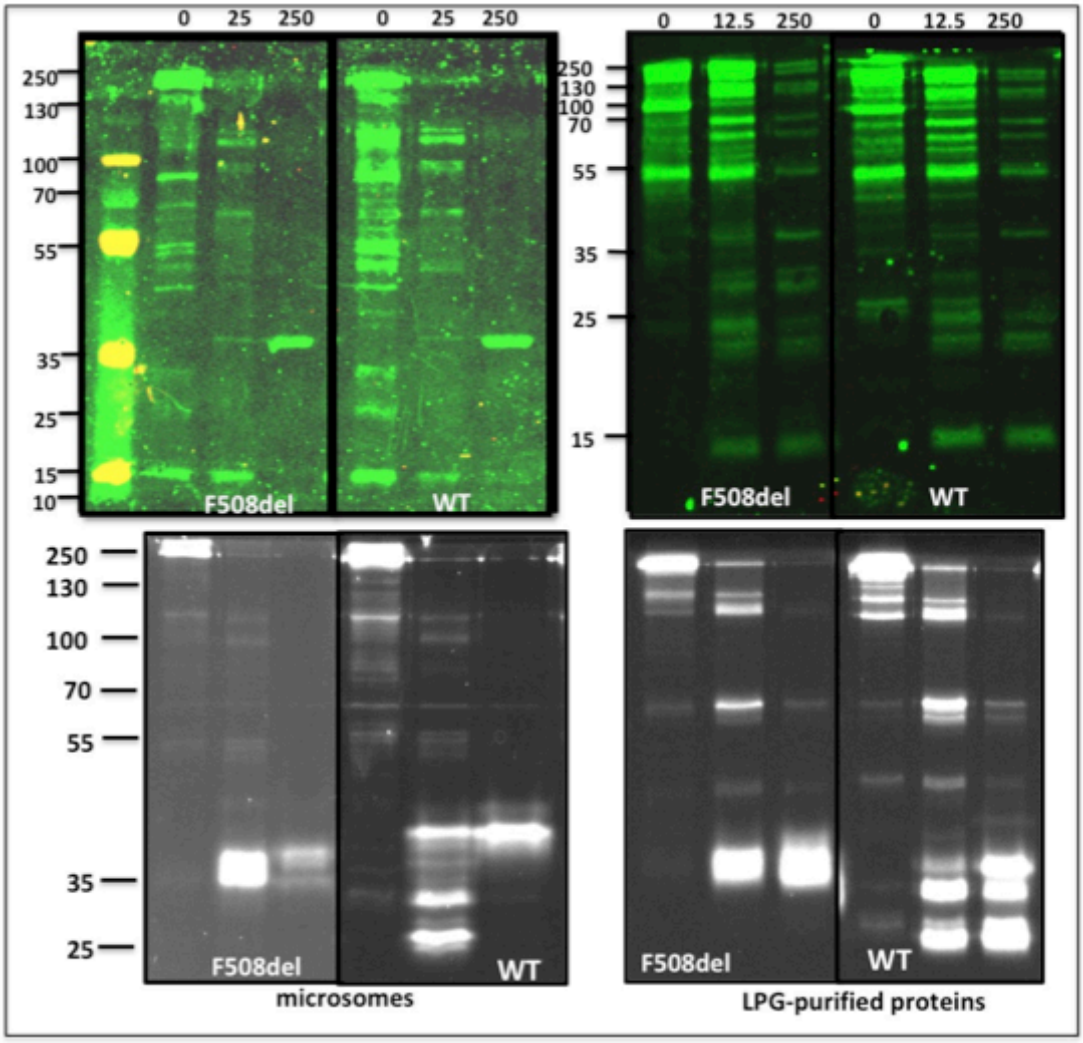

Figure 3: Limited Proteolysis: Digestion with thermolysin at a concentration of 25µg/ml and 250µg/ml with microsomes (left) or LPG-purified proteins (right). The ratio was 1:1 or 10:1 with microsomes or protein. The gel was probed by GFP fluorescence scan (lower panels) or subsequently Western blotted and probed with a SUMO antibody to detect the N-terminal fragments. Note that for microsomes many native yeast SUMO-ylated microsomal proteins are detected in addition to CFTR (left upper panel, no thermolysin). The overall fragmentation patterns with thermolysin are similar although some differences can be observed for the lowest mass C-terminal fragments (lower panels).

CFTR Stability: Limited proteolysis assay

The CPM assay requires purified protein, hence it was useful to compare purified CFTR in LPG with CFTR expressed in membranes. For this we employed limited proteolysis at low temperature followed by SDS-PAGE (Figures 2&3). Proteolytic fragments were visualised using a C-terminal GFP tag as well as an N-terminal SUMO tag (probed with a commercial antibody). Figure 2 shows the effects of limited trypsin concentrations on C-terminal fragments generated from WT, F508del and G551D versions of the protein as described above, with the data for CFTR in microsomes on the left and for purified protein on the right. Figure 3 shows the effects of limited (25 ug/ml) and high (250ug/ml) concentrations of a different protease (thermolysin) and compares WT and F508del versions of the protein in microsomes and after purification. Both the N-terminal fragments (upper panels) and the C-terminal fragments (lower panels) are compared.
The largely unstructured R-region represents a major target for proteolytic enzymes, and hence large fragments around 100kDa, representing TMD2-NBD2-GFP and SUMO-TMD1-NBD1 can be observed at low protease levels for all CFTR variants. Lower mass C-terminal fragments can also be detected at 25 kDa (GFP) and 50-55kDa (NBD2+GFP) with both proteases, implying common protease-sensitive sites at the TMD-NBD linker (55kDa fragment) and at the CFTR C-terminus (25kDa GFP fragment). Despite the presence of F508 in the N-terminal end of CFTR, no obvious differences can be detected in the N-terminal proteolytic cleavage patterns of WT and F508del CFTR (Fig. 3), but the N-terminal patterns are much more complex than the equivalent C-terminal patterns. This applies to both purified CFTR as well as membrane-bound CFTR and implies that the C-terminal end of CFTR may be susceptible to cleavage at a few, particularly sensitive, sites. Some differences in the C-terminal proteolytic cleavage patterns of F508del and WT CFTR were detected when thermolysin was employed, but not with trypsin. The formation of SDS-resistant thermolysin-GFP or thermolysin-SUMO complexes, especially at high thermolysin levels may explain these differences (Supplementary Figure 1). Overall, the conclusions from these limited proteolysis data are that F508del, G551D and WT CFTR display broadly similar sensitivity to proteases at low temperatures and that membrane-bound and detergent-purified CFTR are also similar in terms of their ability to be cleaved by soluble proteases. The discrete nature of the N-terminal and C-terminal bands with masses indicative of cleavage at major domain

interfaces strongly supports the hypothesis that CFTR expressed in yeast microsomes is folded correctly and that after purification it retains a very similar overall conformation, at least at low temperatures. These data also support the hypothesis that F508 deletion mainly affects the thermostability of the protein, rather than affecting the overall fold or topology of the protein(Meng et al., 2017d).

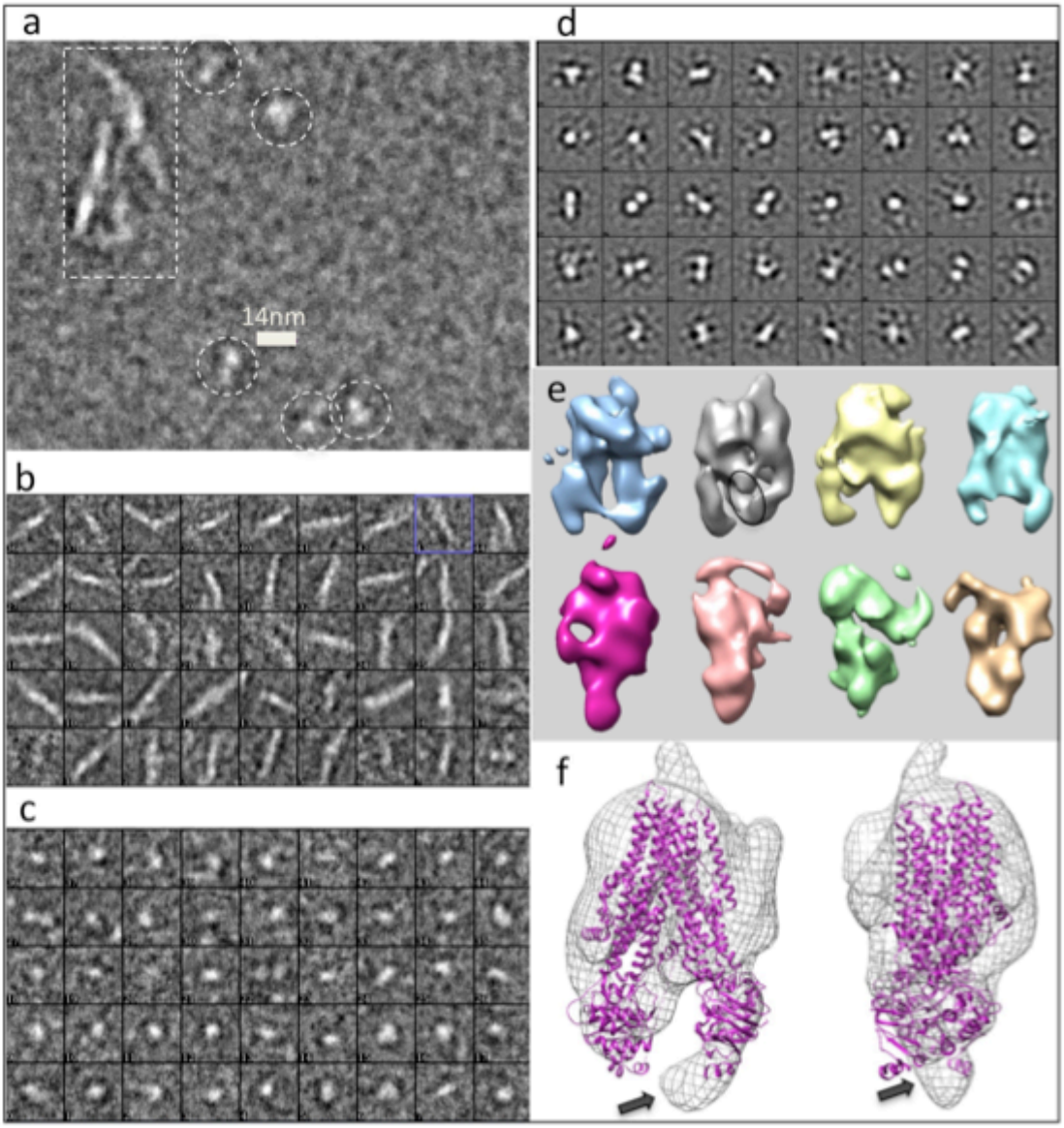

Figure 4: Electron microscopy of phosphorylated and dephosphorylated CFTR. (a) Negatively stained micrograph of LPG-purified dephosphorylated CFTR showing 14nm diameter single particles (circled) and some linear aggregates (rectangle). (b) Examples of linear aggregates. (c) Examples of single particles. (d) 2D class averages for phosphorylated CFTR showing a mixture of inward-facing and outward-facing projection classes. Box size for panels b-c is 29nm. (e) Structures of inward-facing (top) and outward-facing (bottom) 3D classes derived from (l to r): dephosphorylated CFTR; dephosphorylated CFTR + NHERF1; phosphorylated CFTR + NHERF; phosphorylated CFTR. (f) Fitting of the dephosphorylated human CFTR structure (purple ribbon trace) to the dephosphorylated CFTR+NHERF1 map (mesh). Two orthogonal views are displayed. Additional density can be identified close to the NBD2 location after fitting (arrows).

CFTR Structure: Conformational Plasticity & Interaction with NHERF1

Both inward-facing and outward/occluded-facing conformations of CFTR have been reported under similar conditions (+ATP and after phosphorylation, Table I). In order to understand this dichotomy, we have proposed a model(Meng et al., 2018) where CFTR can sample both conformations continuously in the presence or absence of ATP. In this model the equilibrium between inward- and outward-facing states is influenced by the presence of nucleotide and phosphorylated residues in the R-region. In order to explore this further, we studied LPG-purified CFTR single particles by negative-stain EM after phosphorylation and dephosphorylation. We also investigated whether the C-terminal interacting protein, NHERF1 had any effects on the CFTR conformational states. Figure 4a shows an example of data recorded for dephosphorylated CFTR. Single particles can be observed (circled) and these could be selected semi-automatically (Fig. 4c), classified and averaged (Fig. 4d). For dephosphorylated CFTR, but for none of the other conditions, short linear aggregates were also detected in these samples (Fig. 4a, rectangle, Fig. 4b). Similar linear aggregates were previously reported for LPG-purified CFTR where the phosphorylation status was not controlled(Al-Zahrani et al., 2015), and the aggregates may be mediated by intermolecular NBD to R-region interactions which are promoted after dephosphorylation of the R-region(Bozoky et al., 2013). Examination of the projection class averages for all samples implied a mixture of inward- and outward-facing states, as expected, hence a multi-reference refinement was carried out, employing references corresponding to inward-facing and outward/occluded states that had been filtered to low resolution (40Å). Figure 4e shows the resulting 3D representations. No condition resulted in a single conformational state, indeed even dephosphorylated CFTR in the absence of ATP contained particles that gave an outward-facing structure (magenta volume) whilst phosphorylated CFTR in the presence of ATP also had a recognizably inward-facing sub-population of particles with separated NBDs (sky blue volume). Particles corresponding to the inward-facing state of dephosphorylated CFTR with NHERF1 (grey volume) had additional density between the NBDs (ellipse outline, Fig. 4e and arrows, Fig 4f). It seems possible that this could represent the location of NHERF1. No other maps showed a plausible additional density close to the expected position of the C-terminal region. If correct, this would imply that NHERF1 may preferentially bind to the

dephosphorylated state and may take up a discrete location in the inward-facing conformation. This concurs with earlier data showing an association of the C-terminal 40 residues with the R-region of CFTR in the phosphorylated but not dephosphorylated state(Bozoky et al., 2013).

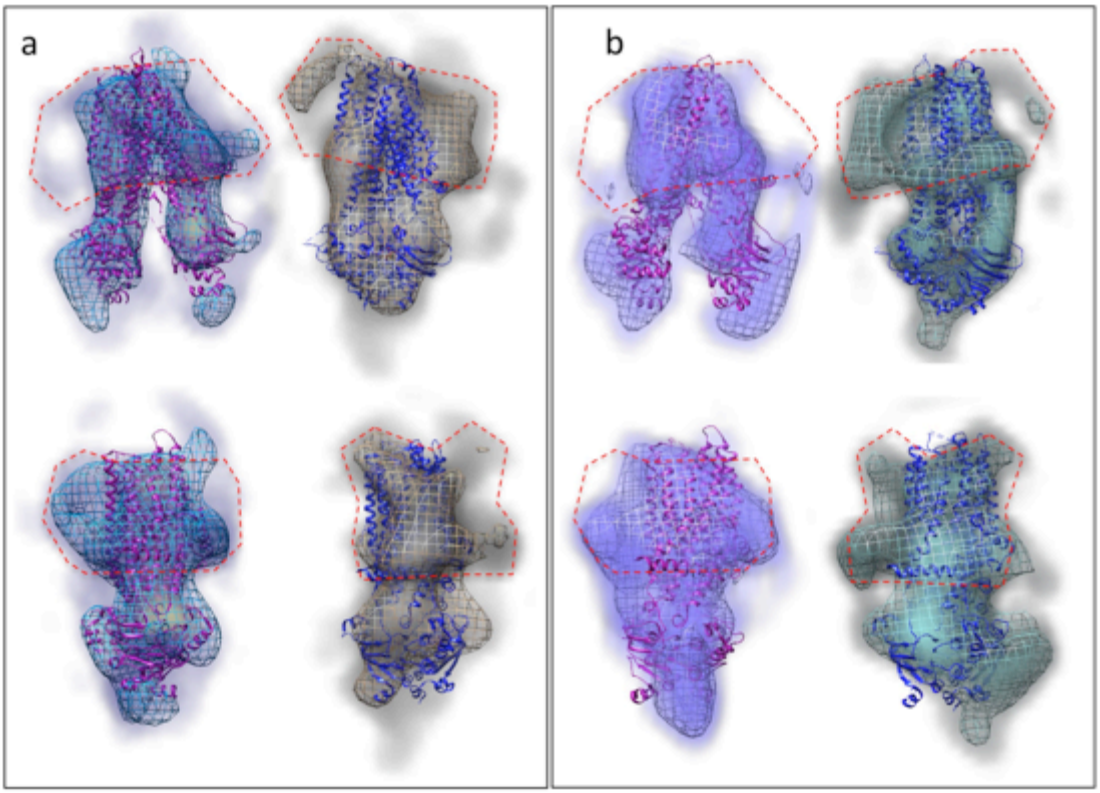

Figure 5: CFTR maps: (a) Fitting of the inward-facing (purple, 5uak) and outward/occluded (blue, 6msm) molecular CFTR models to the equivalent low resolution maps obtained from dephosphorylated CFTR (blue mesh) and phosphorylated CFTR+ATP (brown mesh). The lower panel shows the same models/maps after rotation of each by 90o around the vertical axis. At lower density threshold (shaded regions) the boundaries of the upper LPG micelle can be partially delineated (dashed red outline). (b) As in panel a, but the maps shown are global averages of all particles classified as inward-facing (left) or outward-facing (right).

Figure 5 shows the fitting of the inward-facing human CFTR structure (PDBID 5uak) within the equivalent low resolution map obtained from dephosphorylated CFTR. Despite the low resolution of the negative-stain structure, the overall fit is quite good, with a similar separation distances between the NBDs. The LPG micelle is partly delineated and at lower density thresholds takes on the characterstic toroidal shape (shaded area and dashed red outline). Similarly the outward/occluded CFTR structural model (PDBID 6msm) fits reasonably well within the equivalent map obtained from phosphorylated CFTR in the presence of ATP. Here the detergent micelle appears somewhat smaller and less symmetric (red dashed line).

Global 3D structures representative of all particles across the various experiments were also generated (Figure 5b). These are for significantly larger datasets and show better-defined molecular outlines. The quality of the maps after global averaging suggests that CFTR is not sampling a spectrum of conformations under the varying experimental conditions employed (at least to the low resolution limits obtained here). However the inward-facing global 3D map does show some smearing of one of the NBDs, whilst the other NBD density is well defined. This could reflect some conformational flexing in the inward-facing state, but also could arise from NHERF1 binding to the CFTR C-terminal PDZ binding motif in the dephosphorylated state (Fig. 4f). For the global 3D map of the outward-facing conformation, one would expect very similar conformations as the NBDs should be tightly dimerised.

Conclusions: The studies suggest that the most common CFTR mutation (f508 deletion) mainly affects the stability of the protein rather than its overall 3D conformation. The structural studies suggest that the protein is able to sample inward-facing and outward-facing conformations in both the activated and inactivated states, and that the CFTR-interacting protein, NHERF1 may preferentially associate with the inward-facing, dephosphorylated state. The observation of the outward-facing configuration, even for the inactivated/ dephosphorylated state implies that the R-region may have a loose association between the NBDs and its steric hindrance of the NBD dimer formation observed in some structural studies is not permanent. Similarly, the presence of ATP in phosphorylated CFTR does not appear to result in a uniformly outward-facing

population of molecules. When comparing the various models for CFTR regulation and channel gating, the idea of the R-region acting as a phospho-regulated channel plug appears to be more consistent with the data presented here.(Fay et al., 2018)

Methods:

NHERF1 expression and purification

The cDNA for human NHERF1 was synthesised by Geneart Inc. and cloned into pSY5 vector (Chumnarnsilpa, Lee et al., 2009) using standard ligation independent cloning methods (Aslanidis & de Jong, 1990). Plasmids were transformed into BL21 (DE3) competent *E. coli* (New England Biolabs) according to the manufacturer's instructions. Starter cultures were grown overnight at 37 °C with shaking at 250 rpm in Luria broth (5 g/L yeast extract, 10 g/L peptone, 10 g/L NaCl) supplemented with 100 μg/mL ampicillin. Starter cultures were inoculated at 20 mL/L into auto-induction media (12 g/L tryptone, 24 g/L yeast extract, 9.4 g/L K_2HPO_4, 2.2 g/L KH_2PO_4, 8 mL/L glycerol 50 mM NH_4Cl, 20 mM $MgSO_4$, 5 mM Na_2SO_4, 0.3 % (w/v) α-lactose, 0.015 % (w/v) D-glucose) supplemented with 100 μg/mL ampicillin. Cultures were grown at 37 °C overnight at 15 °C. Cultures were harvested by centrifugation at 4,200xg, 1 hr, 4 °C. Pellets were resuspended in 50 mM Tris.HCl pH 8.0, 500 mM NaCl, 20 mM imidazole and lysed using sonication then centrifuged at 19,000 x g, 1 hr, 4 °C. Filtered (0.45 μm) lysates were loaded onto a 5 mL HisTrap FF Ni-NTA columns (GE healthcare) washed with the same buffer and elution was with 50 mM Tris.HCl pH 8.0, 500 mM NaCl, 250 mM imidazole. The eluted material was de-salted 50 mM Tris.HCl pH 8.0 on a HiPrep 26/10 desalting column (GE healthcare) and loaded onto 1 mL HiTrap Q HP columns (GE healthcare). Following washing, bound NHERF1 was eluted using a gradient of 0-500 mM NaCl. Fractions were collected and further purified by size-exclusion chromatography (SEC) in 50 mM Tris.HCl pH 8.0, 150 mM NaCl using a HiLoad 16/600 Superdex 200 column (GE healthcare). Fractions were combined and concentrated using 30 kDa molecular weight cut-off concentrators and the final NHERF1 concentration was determined using the Pierce Bicinchoninic Acid (BCA) Protein Assay kit (Thermo Scientific) according to the manufacturer's instructions.

CFTR expression and purification

C-terminal eGFP* and StrepII tags were removed from opti-hCFTR within the pTR vector (Rimmington, 2014) using the Site Directed Mutatgenesis Kit (New England Biolabs) according to the manufacturer's instructions. The sequence was confirmed by DNA sequencing and transformed into competent FGY217 *S.*

cerevisiae for expression and purification as previously described (O'Ryan, Rimington et al., 2012, Pollock, Cant et al., 2014a).

Phosphorylation and dephosphorylation

Purified CFTR in 50 mM Tris, pH8, 10% glycerol (v/v), 50 mM NaCl, 1 mM DTT, 0.05% LPG-14 was treated with protein kinase A (PKA) catalytic subunit (New England BioLabs, P6000) as previously described (Zhang and Chen, 2016; Liu et al., 2017). PKA was diluted to 1.6μM and incubated with CFTR at 30 ^{o}C for 1 h with 0.2 mM MgATP. The dephosphorylation reaction was done in presence of Lambda Phosphatase diluted 1:40 (w/w) at 22^{o}C for 1h (Lin et al., 2017). Protein phosphorylation was detected with Pro-Q Diamond stain, as described in the manufacturer's protocol(Steinberg, Rush et al., 2003) and scanned using Trans-UV illumination

CFTR stability assay

The Coumarin maleimide (CPM) assay was adapted from (Alexandrov et al., 2008). DTT, which interferes with the assay, was removed from the protein sample at the SEC purification step. The assay was done either in a conventional fluorimeter connected to a temperature-controlled water bath; or in an Unchained Labs UNCLE instrument using the UV laser(Meng, Clews et al., 2017b). For the latter, emission spectra were scanned every minute at 10 °C for 30min followed by a temperature ramp to 90 °C and spectra were collected at 2 °C increments with a heating rate of approximately 1.5 °C min^{-1}. After subtraction of buffer controls, data were analysed by integrating the Tryptophan (323 nm to 350 nm) and CPM (445 nm to 463 nm) emission peaks. The ratio of the integrals CPM/Trp was employed to compensate for temperature-dependent fluorescence quenching effects and any spikes in the laser output. 1 μg purified CFTR and 0.1 μg CPM were used in each experiment.

Limited proteolysis assay

Limited Proteolysis reactions were carried out at 4°C in a 20μl reaction volume. Thermolysin (G*eobacillus stearothermophilus*) was from *Sigma* CAS # - 9073-78-3. For thermolysin, protein and microsomes were incubated with the enzyme for 15 min at 4°C and then the reaction was halted with 12mM EDTA. Purified

protein was at 25µg/ml and microsomes 50µg/ml while thermolysin was at 12.5µg/ml or 50µg/ml for pure protein reactions, and 25µg/ml or 250µg/ml for microsome reactions. The enzyme was diluted in a calcium-containing thermolysin buffer (50mM Tris, 0.05mM $CaCl_2$). SDS Buffer (50mM Tris, pH7.6, 5% Glycerol, 5mM EDTA, 0.02% Bromophenol Blue, 4% SDS, 50mM DTT) was then added to the reaction 1:1 v:v and left at room temperature for 30 minutes before being run on a 12% polyacrylamide gel for 90 min at 130V. Limited proteolysis experiments with trypsin were conducted at 4°C for 15 minutes and stopped with a protease inhibitor cocktail (5µg/ml E64, 48µg/ml AEBSF, 174µg/ml PMSF, 8.25µg/ml Leupeptin, 8.25µg/ml Pepstatin, 1.75 µg/ml Chymostatin, 2µg/ml Bestatin). Protease was at a ratio of 1:75 (0.3 µg/ml trypsin) with both microsomes and purified proteins.

For Sumo identification, the gel was transferred using the semi-dry method using Anode (Anode I - 30mM Tris, 20% Methanol, Anode II - 300mM Tris, 20% Methanol) and Cathode (40mM 6-amino hexanoic acid, 25mM Tris, 0.01% SDS, 20% Methanol) transfer buffers. Following transfer, the membrane was incubated in 5% w/v BSA in TBST buffer (Tris Buffered Saline – 20mM Tris (pH7.5), 150mM NaCl, 1% Tween20) for 1 hour at room temperature. The membrane was then incubated with an anti-Sumo primary antibody (A*bcam ab176485*) overnight at 4°C. Following incubation, the membrane was washed with TBST buffer 5 times for 5 min each. The membrane was incubated with a secondary antibody (Dnk pAb to Ms IgG (IRD® 800cw A*bcam ab216774*) for an hour at room temperature. Followed by 3 washes with TBST buffer for 5 minutes. The membrane was then viewed on a LiCor Odyssey machine.

Electron Microscopy and structural analysis

Samples were diluted to ~25µg/ml in 50 mM NaCl, 1 mM DTT, 0.05% LPG-14 (Mg-ATP, 2mM, was added for the phosphorylated sample) and then applied to glow-discharged EM grids and negatively-stained as described earlier(Al-Zahrani et al., 2015). Image processing was carried out with the EMAN2 software package(Ludtke, Chen et al., 2004). Single particles were selected using the EMAN2 *interactive particle-picking* tool. Classification of the projection classes allowed the removal of non-CFTR particles (discriminated by size) and

aggregates (discriminated by size and shape). For most specimens this resulted in elimination of about 50% of the automatically-selected particles; about 75% were excluded for the dephosphorylated CFTR sample where linear CFTR aggregates were present. Further reclassification of the included particles identified projection classes consistent with both outward- and inward-facing CFTR particles surrounded by an annular detergent micelle. The particles were therefore further classified using the EMAN2 *multirefine* tool using two 3D reference structures (EMDB_8516 and EMDB_9230 - corresponding to inward-facing and outward-facing conformations respectively filtered to ~50Å resolution). Finally, particles classified with inward-facing or outward-facing references were separately re-refined using the *single map refinement* tool: Here, each dataset was split into two separately-refined subsets to allow the assessment of the resolution of the final map by Fourier shell correlation (FSC). Combination of all the particles classified with the inward-facing reference across all datasets was also carried out and this large dataset (~14,000 particles) was used for a global 3D structure refinement. A similar procedure was performed for all particles associated with the outward-facing state (~13,000 particles).

References

Al-Zahrani A., Cant N., Kargas V., Rimington T., Aleksandrov L., Riordan J.R., Ford R.C. (2015). Structure of the cystic fibrosis transmembrane conductance regulator in the inward-facing conformation revealed by single particle electron microscopy. AIMS Biophysics. 2, 131-152.

Alexandrov A.I., Mileni M., Chien E.Y., Hanson M.A., Stevens R.C. (2008). Microscale fluorescent thermal stability assay for membrane proteins. Structure. 16, 351-359.

Aslanidis C., de Jong P.J. (1990). Ligation-independent cloning of PCR products (LIC-PCR). Nucleic Acids Research. 18, 6069-6074.

Atwell S., Brouillette C.G., Conners K., Emtage S., Gheyi T., Guggino W.B., Hendle J., Hunt J.F., Lewis H.A., Lu F., Protasevich, II, Rodgers L.A., Romero R., Wasserman S.R., Weber P.C., Wetmore D., Zhang F.F., Zhao X. (2010). Structures of a minimal human CFTR first nucleotide-binding domain as a monomer, head-to-tail homodimer, and pathogenic mutant. Protein Eng Des Sel. 23, 375-384.

Bozoky Z., Krzeminski M., Muhandiram R., Birtley J.R., Al-Zahrani A., Thomas P.J., Frizzell R.A., Ford R.C., Forman-Kay J.D. (2013). Regulatory R region of the CFTR chloride channel is a dynamic integrator of phospho-dependent intra- and intermolecular interactions. P Natl Acad Sci USA. 110, E4427-E4436.

Brodsky J.L. (2001). Chaperoning the maturation of the cystic fibrosis transmembrane conductance regulator. Am J Physiol Lung Cell Mol Physiol. 281, L39-42.

Cai Z., Sohma Y., Bompadre S.G., Sheppard D.N., Hwang T.C. (2011). Application of high-resolution single-channel recording to functional studies of cystic fibrosis mutants. Methods Mol Biol. 741, 419-441.

Chappe V., Hinkson D.A., Zhu T., Chang X.B., Riordan J.R., Hanrahan J.W. (2003). Phosphorylation of protein kinase C sites in NBD1 and the R domain control CFTR channel activation by PKA. J Physiol. 548, 39-52.

Chumnarnsilpa S., Lee W.L., Nag S., Kannan B., Larsson M., Burtnick L.D., Robinson R.C. (2009). The crystal structure of the C-terminus of adseverin reveals the actin-binding interface. Proceedings of the National Academy of Sciences of the United States of America. 106, 13719-13724.

Cushing P.R., Fellows A., Villone D., Boisguerin P., Madden D.R. (2008). The relative binding affinities of PDZ partners for CFTR: a biochemical basis for efficient endocytic recycling. Biochemistry. 47, 10084-10098.

Davies J.C., Moskowitz S.M., Brown C., Horsley A., Mall M.A., McKone E.F., Plant B.J., Prais D., Ramsey B.W., Taylor-Cousar J.L., Tullis E., Uluer A., McKee C.M., Robertson S., Shilling R.A., Simard C., Van Goor F., Waltz D., Xuan F., Young T. et al. (2018). VX-659-Tezacaftor-Ivacaftor in Patients with Cystic Fibrosis and One or Two Phe508del Alleles. N Engl J Med. 379, 1599-1611.

Dawson R.J., Locher K.P. (2007). Structure of the multidrug ABC transporter Sav1866 from Staphylococcus aureus in complex with AMP-PNP. FEBS Lett. 581, 935-938.

Dean M., Rzhetsky A., Allikmets R. (2001). The human ATP-binding cassette (ABC) transporter superfamily. Genome Res. 11, 1156-1166.

Donaldson S.H., Bennett W.D., Zeman K.L., Knowles M.R., Tarran R., Boucher R.C. (2006). Mucus clearance and lung function in cystic fibrosis with hypertonic saline. N Engl J Med. 354, 241-250.

Fay J.F., Aleksandrov L., Jensen T.J., Kousouros J.N., He L., Aleksandrov A.A., Gingerich D., Riordan J.R., Chen J. (2017). Cryo-Em Visualization of an Active Phosphorylated Cftr Channel. Pediatric Pulmonology. 52, S214-S215.

Fay J.F., Aleksandrov L.A., Jensen T.J., Cui L.L., Kousouros J.N., He L., Aleksandrov A.A., Gingerich D.S., Riordan J.R., Chen J.Z. (2018). Cryo-EM Visualization of an Active High Open Probability CFTR Anion Channel. Biochemistry. 57, 6234-6246.

Gabriel S.E., Brigman K.N., Koller B.H., Boucher R.C., Stutts M.J. (1994). Cystic fibrosis heterozygote resistance to cholera toxin in the cystic fibrosis mouse model. Science. 266, 107-109.

Galietta L.J., Springsteel M.F., Eda M., Niedzinski E.J., By K., Haddadin M.J., Kurth M.J., Nantz M.H., Verkman A.S. (2001). Novel CFTR chloride channel activators identified by screening of combinatorial libraries based on flavone and benzoquinolizinium lead compounds. J Biol Chem. 276, 19723-19728.

Haggie P.M., Stanton B.A., Verkman A.S. (2004). Increased diffusional mobility of CFTR at the plasma membrane after deletion of its C-terminal PDZ binding motif. J Biol Chem. 279, 5494-5500.

Higgins C.F. (1992). ABC transporters: from microorganisms to man. Annu Rev Cell Biol. 8, 67-113.

Higgins C.F. (2007). Multiple molecular mechanisms for multidrug resistance transporters. Nature. 446, 749-757.

Karthikeyan S., Leung T., Ladias J.A. (2001). Structural basis of the Na+/H+ exchanger regulatory factor PDZ1 interaction with the carboxyl-terminal region of the cystic fibrosis transmembrane conductance regulator. J Biol Chem. 276, 19683-19686.

Keating D., Marigowda G., Burr L., Daines C., Mall M.A., McKone E.F., Ramsey B.W., Rowe S.M., Sass L.A., Tullis E., McKee C.M., Moskowitz S.M., Robertson S., Savage J., Simard C., Van Goor F., Waltz D., Xuan F., Young T., Taylor-Cousar J.L. et al. (2018). VX-445-Tezacaftor-Ivacaftor in Patients with Cystic Fibrosis and One or Two Phe508del Alleles. N Engl J Med. 379, 1612-1620.

Liu F., Zhang Z., Csanady L., Gadsby D.C., Chen J. (2017). Molecular Structure of the Human CFTR Ion Channel. Cell. 169, 85-95 e88.

Ludtke S.J., Chen D.H., Song J.L., Chuang D.T., Chiu W. (2004). Seeing GroEL at 6 A resolution by single particle electron cryomicroscopy. Structure. 12, 1129-1136.

Meng X., Clews J., Kargas V., Wang X., Ford R.C. (2017a). The cystic fibrosis transmembrane conductance regulator (CFTR) and its stability. Cell Mol Life Sci. 74, 23-38.

Meng X., Clews J., Kargas V., Wang X.M., Ford R.C. (2017b). The cystic fibrosis transmembrane conductance regulator (CFTR) and its stability. Cellular and Molecular Life Sciences. 74, 23-38.

Meng X., Clews J., Martin E.R., Ciuta A.D., Ford R.C. (2018). The structural basis of cystic fibrosis. Biochem Soc Trans. 46, 1093-1098.

Meng X., Wang Y., Wang X., Wrennall J.A., Rimington T.L., Li H., Cai Z., Ford R.C., Sheppard D.N. (2017c). Two Small Molecules Restore Stability to a Subpopulation of the Cystic Fibrosis Transmembrane Conductance Regulator with the Predominant Disease-causing Mutation. J Biol Chem. 292, 3706-3719.

Meng X., Wang Y.T., Wang X.M., Wrennall J.A., Rimington T.L., Li H.Y., Cai Z.W., Ford R.C., Sheppard D.N. (2017d). Two Small Molecules Restore Stability to a Subpopulation of the Cystic Fibrosis Transmembrane Conductance Regulator with the Predominant Disease-causing Mutation. Journal of Biological Chemistry. 292, 3706-3719.

Mikhailov M.V., Campbell J.D., de Wet H., Shimomura K., Zadek B., Collins R.F., Sansom M.S., Ford R.C., Ashcroft F.M. (2005). 3-D structural and functional characterization of the purified KATP channel complex Kir6.2-SUR1. Embo J. 24, 4166-4175.

Moeller A., Lee S.C., Tao H., Speir J.A., Chang G., Urbatsch I.L., Potter C.S., Carragher B., Zhang Q. (2015). Distinct conformational spectrum of homologous multidrug ABC transporters. Structure. 23, 450-460.

Moyer B.D., Denton J., Karlson K.H., Reynolds D., Wang S., Mickle J.E., Milewski M., Cutting G.R., Guggino W.B., Li M., Stanton B.A. (1999). A PDZ-interacting domain in CFTR is an apical membrane polarization signal. J Clin Invest. 104, 1353-1361.

Moyer B.D., Duhaime M., Shaw C., Denton J., Reynolds D., Karlson K.H., Pfeiffer J., Wang S., Mickle J.E., Milewski M., Cutting G.R., Guggino W.B., Li M., Stanton B.A. (2000). The PDZ-interacting domain of cystic fibrosis transmembrane conductance regulator is required for functional expression in the apical plasma membrane. J Biol Chem. 275, 27069-27074.

O'Ryan L., Rimington T., Cant N., Ford R.C. (2012). Expression and purification of the cystic fibrosis transmembrane conductance regulator protein in Saccharomyces cerevisiae. J Vis Exp.

Pollock N., Cant N., Rimington T., Ford R.C. (2014a). Purification of the cystic fibrosis transmembrane conductance regulator protein expressed in Saccharomyces cerevisiae. J Vis Exp.

Pollock N., Cant N., Rimington T., Ford R.C. (2014b). Purification of the Cystic Fibrosis Transmembrane Conductance Regulator Protein Expressed in Saccharomyces cerevisiae. Jove-J Vis Exp.

Ren H.Y., Grove D.E., De La Rosa O., Houck S.A., Sopha P., Van Goor F., Hoffman B.J., Cyr D.M. (2013). VX-809 corrects folding defects in cystic fibrosis transmembrane conductance regulator protein through action on membrane-spanning domain 1. Mol Biol Cell. 24, 3016-3024.

Rimmington T.L. (2014) Expression, Purification and Characterisation of the Cystic Fibrosis Transmembrane Conductance Regulator (CFTR) in Saccharomyces cerevisiae. In Faculty of Life Sciences, United Kingdom: University of Manchester

Riordan J.R. (2008). CFTR function and prospects for therapy. Annu Rev Biochem. 77, 701-726.

Riordan J.R., Rommens J.M., Kerem B., Alon N., Rozmahel R., Grzelczak Z., Zielenski J., Lok S., Plavsic N., Chou J.L., et al. (1989). Identification of the cystic fibrosis gene: cloning and characterization of complementary DNA. Science. 245, 1066-1073.

Rosenberg M.F., O'Ryan L.P., Hughes G., Zhao Z., Aleksandrov L.A., Riordan J.R., Ford R.C. (2011). The cystic fibrosis transmembrane conductance regulator (CFTR): three-dimensional structure and localization of a channel gate. J Biol Chem. 286, 42647-42654.

Rosenberg M.F., O'Ryan L.P., Hughes G., Zhao Z., Aleksandrov L.A., Riordan J.R., Ford R.C. (2012). The cystic fibrosis transmembrane conductance regulator (CFTR): three-dimensional structure and localization of a channel gate. J Biol Chem. 286, 42647-42654.

Rosenberg M.F., Oleschuk C.J., Wu P., Mao Q., Deeley R.G., Cole S.P., Ford R.C. (2010). Structure of a human multidrug transporter in an inward-facing conformation. J Struct Biol. 170, 540-547.

Steinberg G.R., Rush J.W., Dyck D.J. (2003). AMPK expression and phosphorylation are increased in rodent muscle after chronic leptin treatment. Am J Physiol Endocrinol Metab. 284, E648-654.

Valentine C.D., Lukacs G.L., Verkman A.S., Haggie P.M. (2012). Reduced PDZ interactions of rescued DeltaF508CFTR increases its cell surface mobility. J Biol Chem. 287, 43630-43638.

Veit G., Avramescu R.G., Chiang A.N., Houck S.A., Cai Z., Peters K.W., Hong J.S., Pollard H.B., Guggino W.B., Balch W.E., Skach W.R., Cutting G.R., Frizzell R.A., Sheppard D.N., Cyr D.M., Sorscher E.J., Brodsky J.L., Lukacs G.L. (2016). From CFTR biology toward combinatorial pharmacotherapy: expanded classification of cystic fibrosis mutations. Mol Biol Cell. 27, 424-433.

Vergani P., Lockless S.W., Nairn A.C., Gadsby D.C. (2005). CFTR channel opening by ATP-driven tight dimerization of its nucleotide-binding domains. Nature. 433, 876-880.

Vernon R.M., Chong P.A., Lin H., Yang Z., Zhou Q., Aleksandrov A.A., Dawson J.E., Riordan J.R., Brouillette C.G., Thibodeau P.H., Forman-Kay J.D. (2017). Stabilization of a nucleotide-binding domain of the cystic fibrosis

transmembrane conductance regulator yields insight into disease-causing mutations. J Biol Chem. 292, 14147-14164.

Wiuf C. (2001). Do delta F508 heterozygotes have a selective advantage? Genet Res. 78, 41-47.

Yang H.B., Hou W.T., Cheng M.T., Jiang Y.L., Chen Y., Zhou C.Z. (2018). Structure of a MacAB-like efflux pump from Streptococcus pneumoniae. Nat Commun. 9, 196.

Yang Z., Hildebrandt E., Jiang F., Aleksandrov A.A., Khazanov N., Zhou Q., An J., Mezzell A.T., Xavier B.M., Ding H., Riordan J.R., Senderowitz H., Kappes J.C., Brouillette C.G., Urbatsch I.L. (2018). Structural stability of purified human CFTR is systematically improved by mutations in nucleotide binding domain 1. Biochim Biophys Acta Biomembr. 1860, 1193-1204.

Yeh H.I., Sohma Y., Conrath K., Hwang T.C. (2017). A common mechanism for CFTR potentiators. J Gen Physiol. 149, 1105-1118.

Yu H., Burton B., Huang C.J., Worley J., Cao D., Johnson J.P., Jr., Urrutia A., Joubran J., Seepersaud S., Sussky K., Hoffman B.J., Van Goor F. (2012). Ivacaftor potentiation of multiple CFTR channels with gating mutations. J Cyst Fibros. 11, 237-245.

Zhang Z., Chen J. (2016). Atomic Structure of the Cystic Fibrosis Transmembrane Conductance Regulator. Cell. 167, 1586-1597 e1589.

Zhang Z., Liu F., Chen J. (2017). Conformational Changes of CFTR upon Phosphorylation and ATP Binding. Cell. 170, 483-491 e488.

Zhang Z., Liu F., Chen J. (2018). Molecular structure of the ATP-bound, phosphorylated human CFTR. Proc Natl Acad Sci U S A.

Supplementary Figures

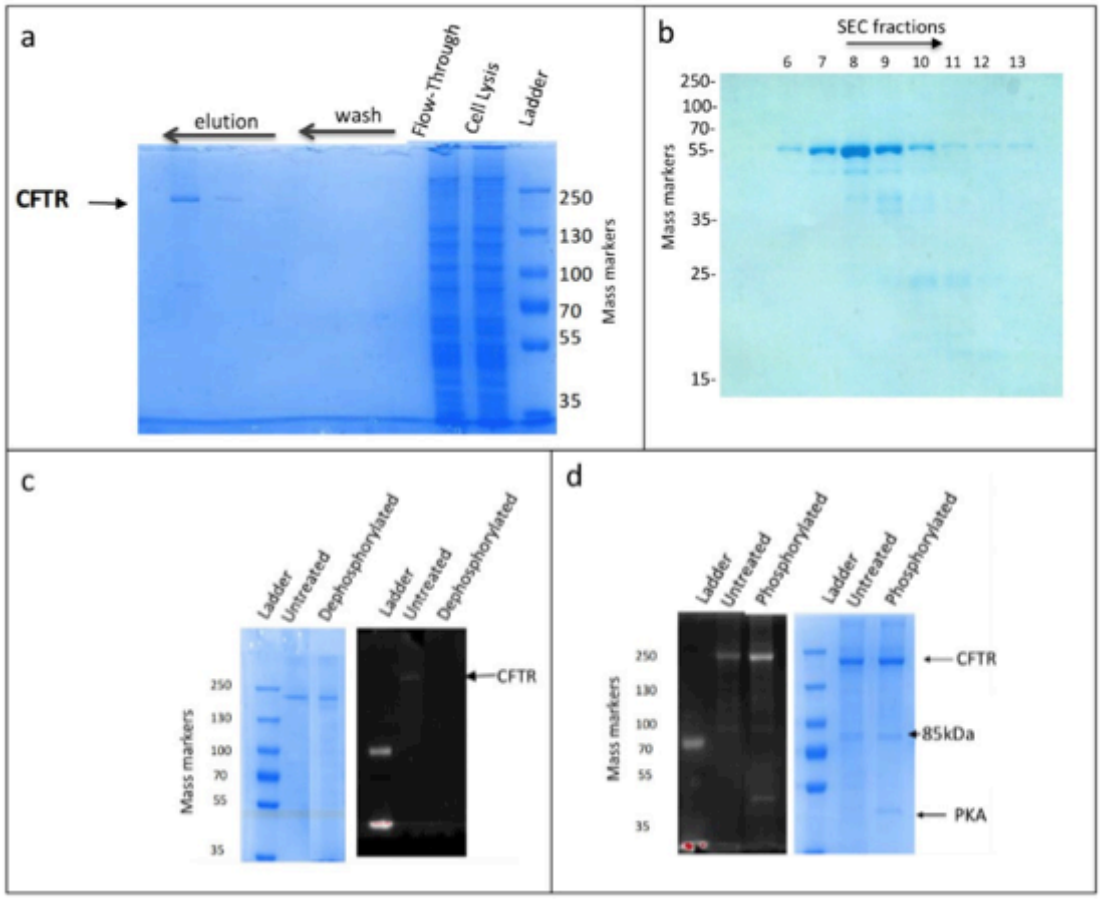

Supplementary Figure 1: Purification and characterisation of proteins: (a) Coomassie stained SDS-PAGE purification gel for CFTR, corresponding to cell lysis extract, flow-through, wash steps and the imidazole elution fractions from the Ni-NTA purification stage, with the major CFTR band eluting at 400mM imidazole. (b) Final purification gel for NHERF1 showing fractions from the 2nd step (size exclusion chromatography – SEC). (c,d) LPG- purified CFTR was treated with (c) lambda phosphatase twice for 1h at 22°C or (d) PKA and 0.2mM ATP for 1h at 30°C. The blue image in each panel represents the Coomassie -stained gel with before and after treatment of CFTR samples. The greyscale image shows the Pro-Q Diamond stained SDS-PAGE counterpart, with phosphorylated protein bands showing up as white. The data shows that purified CFTR retains significant phosphorylation. A weak doublet band around 85kDa may be due to some proteolytic clipping at the R-region at 30°C which is also observed for the control untreated sample at this temperature.

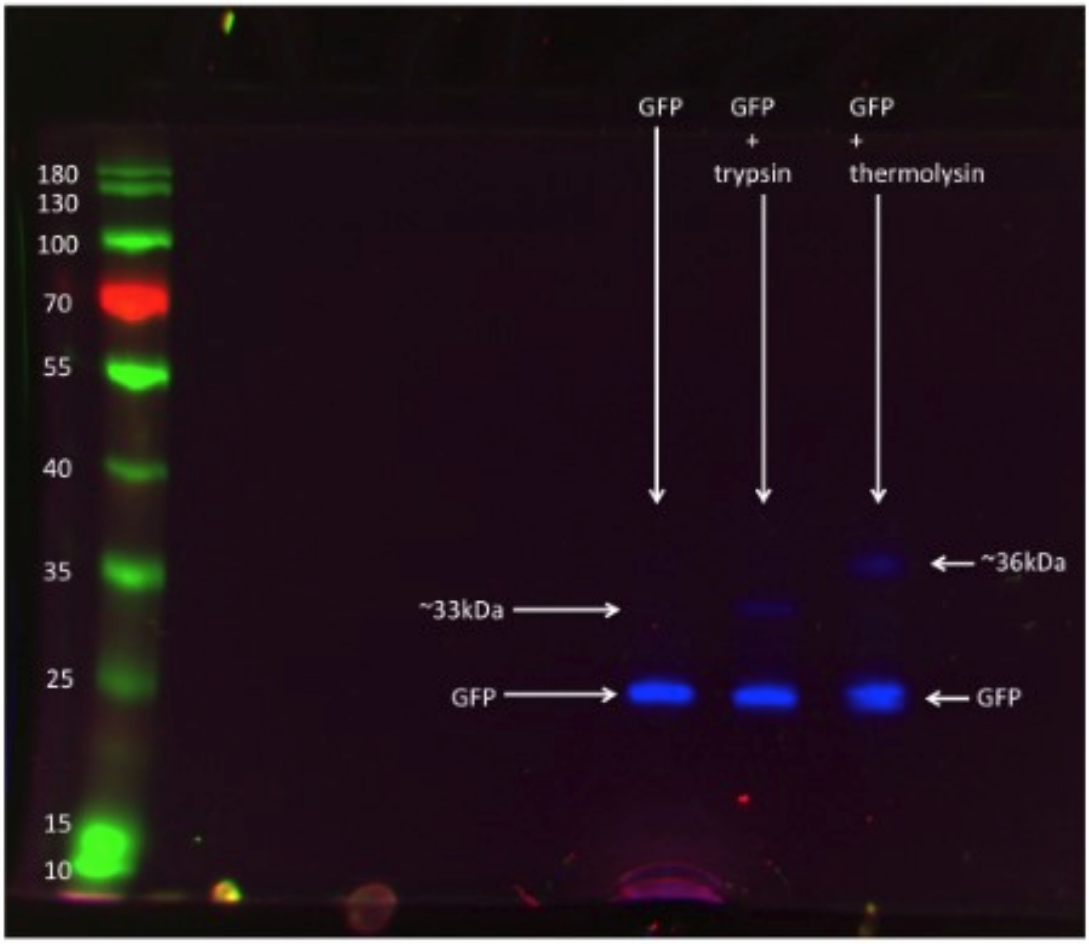

Supplementary Figure 2: GFP-only controls: GFP was treated under limited proteolysis conditions in the same way as CFTR and then run on SDS-PAGE. GFP was resistant to degradation under the limited proteolysis conditions with both thermolysin and trypsin. Higher molecular mass fluorescent bands of ~36kDa and ~34kDa were formed in the presence of thermolysin and trypsin, respectively (indicated). A 36kDa fluorescent band was also detected after treatment of microsomes with high concentrations of thermolysin (Fig.3, main text). The formation of an SDS-stable complex between GFP and protease may be occurring.

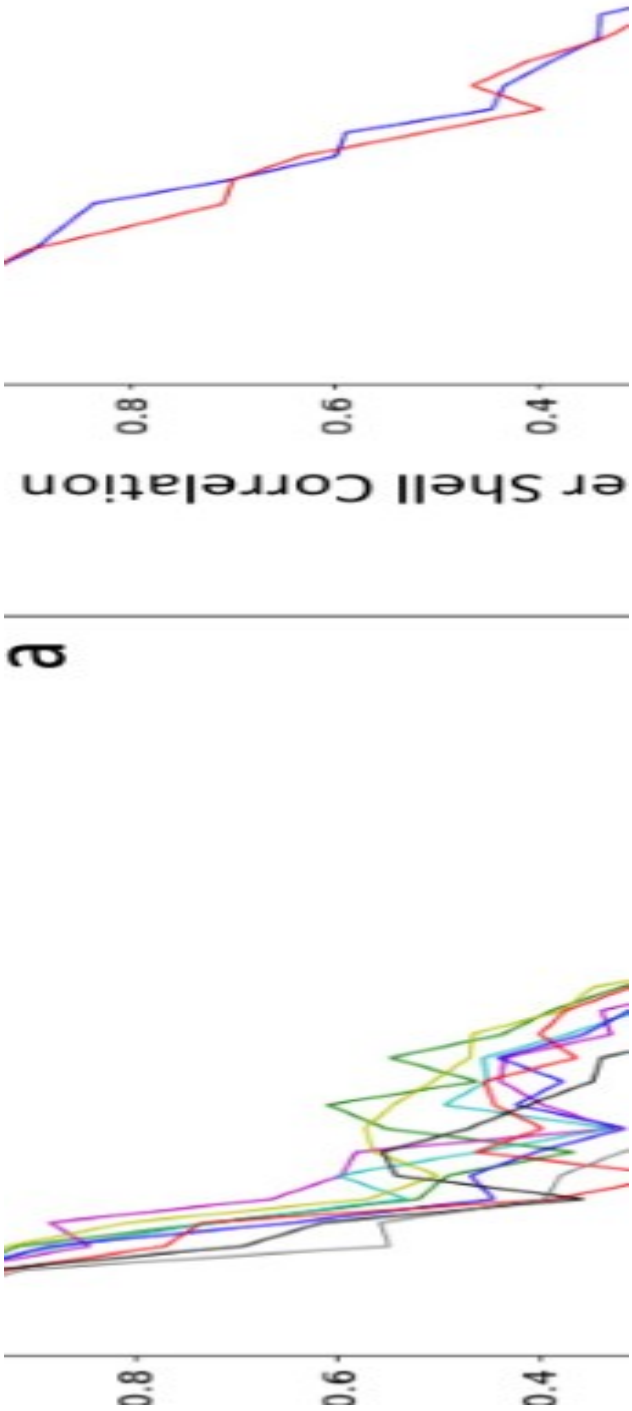

Supplementary Figure 3: Fourier shell correlation plots for CFTR 3D refinements: Black – Dephosphorylated, inward facing state. Grey - Dephosphorylated, outward facing state. Dark blue – Phosphorylated, outward facing state. Red - Phosphorylated, inward facing state. Sky blue – Dehosphorylated + NHERF1, outward facing state. Magenta – Dephosphorylated + NHERF1, inward facing state. Yellow - Phosphorylated + NHERF1, outward facing state. Green - Phosphorylated + NHERF1, inward facing state. The Dephosphorylated, outward facing state (Grey) has the lowest resolution estimate and the fewest contributing particles (635). The highest resolution at FSC=0.5, the more conservative measure, is for the

Dehosphorylated + NHERF1 inward-facing dataset (Magenta) with 2719 particles. (b) Fourier-shell correlation plots for global averages of the inward-facing (blue) and outward-facing (red) states.

Chapter 6.0

CFTR structure and the effects of disease causing mutations probed by limited proteolysis

Jack Clews[1], Xin Meng[1,2], Astynnia Gan[1] and Robert C. Ford[1]

1. Faculty of Biology Medicine and Health, Michael Smith Building, University of Manchester, Oxford Rd, Manchester M13 9PL, UK
2. Current address: MRC Toxicology Unit, Hodgkin Building Lancaster Rd, Leicester LE1 9HN, UK.

Keywords: Membrane protein, structure, cystic fibrosis, protein stability, CFTR, limited proteolysis.

Abstract

Cystic fibrosis is the most common genetic disease in populations of European descent. Mutations in the *cftr* gene lead to loss of CFTR protein and/or loss of its function and cause cystic fibrosis. There are many different disease-associated CFTR mutations, but approximately 90% of patients have at least one copy of the F508del mutation in their *cftr* genes. The deletion of phenylalanine at position 508 in the amino acid chain results in loss of the protein from the plasma membrane due to misfolding/instability. The second most common mutation is G551D where the protein expression is unaffected but causes the channel to remain closed. Here we have studied human CFTR and these two most common disease-causing mutations using a yeast expression system that allows precise timing of the initiation of CFTR expression. CFTR variants express over the same time-course of a few hours in yeast, although polyubiquitination and turnover of F508del CFTR appears to be markedly

more pronounced, resulting in reduced levels of expression. By using limited proteolysis we have probed CFTR in yeast microsomal membranes, as well as after its full purification in detergent micelles. In order to resolve conflicting data derived from cryo-EM studies we test the hypothesis that regulation of the protein by phosphorylation coupled with the presence of ATP has large effects on its overall conformation. We find that phosphorylation has some stabilising effects on the protein but these are not sufficient to stabilise the F508del version of the protein. The stabilising effects of phosphorylation appear to be mainly exerted on the C-terminal half of the protein. The fragmentation patterns of WT CFTR and CFTR variants are similar in phosphorylated and non-phosphorylated CFTR. These data are consistent with a model where CFTR protein is in a state of constant flux, alternating between inward- and outward-facing conformations irrespective of its phosphorylation status and the presence of ATP.

Introduction

CFTR is a member of the ATP binding cassette family of membrane proteins [1]. The function of this protein is to allow the flux of chloride ions [2] and this is different to the rest of the family that are predominantly active transporters. Recent structural data for CFTR has shown that the protein shares a very strong structural homology with other transporter members of the ABC family [3] [4]. The main sequence differentiation between CFTR and other closely related transporters such as ABCC1 (multidrug resistance protein one) and ABCC8 (sulphonylurea receptor one) is the presence of a large internal linker region of approximately 200 residues in length. This structurally disordered region [5] is utilised in CFTR function, and is phosphorylated at multiple sites allowing for the channel function of the protein to operate [6]. Although CFTR is an ATP-gated channel, because of the normally high concentrations of ATP in the cell, the regulation of channel function via the extended linker region is likely to be the most critical [7, 8]. This region of the protein has been termed the regulatory or R-domain. This part of the protein also contains several sites for proteolysis and can be cleaved readily by externally added proteases, yielding N-terminal and C-terminal halves of the protein that are roughly equal in mass. However like many other ABC transporters, CFTR also contains several regions that link the four domains of the protein, i.e. the two transmembrane domains and the two-nucleotide binding domains [9]. CFTR also includes a unique short region of disordered structure inserted at the start of its first nucleotide-binding domain (NBD) [10]. This so-called regulatory insertion also represents a potential site for proteolysis. Removal of the regulatory insertion increases the overall stability of the isolated NBD1 domain [11], and recently it has been shown that it also (by deletion) increases the stability of the full-length protein [12]. However removal of the much larger R- domain does not have this effect and indeed may cause reduction in expression levels. Given the multi domain nature of CFTR as well as the presence of disordered domain-linking regions, the protein can be considered a suitable target for study by limited proteolysis.

In such studies, limiting amounts of protease are added to the protein of interest and then the fragmented protein is run on an SDS-PAGE gel in order to reveal the pattern of proteolysis and the presence of any stable domains, subdomains or major fragments [13, 14]. Such a study can provide information about domain-domain interactions, the overall stability of the protein and its conformation, and may reveal any allosteric changes that influence the exposure of specific linker regions.

In this manuscript, this methodology has been exploited to study the properties of wild type CFTR as well as mutant forms of the protein that occur frequently in humans and which lead to cystic fibrosis. So far, structural data for CFTR has been derived by cryo-EM of the human or chicken WT proteins [3, 4, 15, 16]. In the latter case, stabilizing mutations were included in the chicken protein although its channel activity was enhanced with a very high open probability using the ATPase- limiting H1402S mutation [4]. In the former case, the human protein was also studied with a mutation in the catalytic Walker B glutamate residue (E1371Q) that is essential for ATP hydrolysis and therefore this mutation also greatly enhanced the open probability of the channel[15]. Surprisingly, the structure of chicken CFTR in the presence or absence of ATP and after phosphorylation was relatively unchanged, and in both cases was in the inward-facing state [4]. In contrast the human protein structure showed the inward-facing state in the absence of phosphorylation and nucleotide, but after phosphorylation and when trapped with E1371Q mutation displayed the outward-facing state with ATP bound[15]. Hence one study suggests that CFTR behaves in the typical fashion of an ABC transporter, whilst the other suggests that CFTR is defective in the normal inward-to-outward facing conformational transition that is characteristic of such transporters. In this case, small changes in the local structure of the protein would be proposed to initiate channel opening, whereas in the former case, a large conformational change would be associated with channel opening. Such different mechanistic models should be amenable to testing by limited proteolysis. Recently it has been proposed that CFTR can sample both inward- and outward-facing conformations under a range of experimental conditions [17]. Hence in this model, even fully dephosphorylated CFTR in

the absence of nucleotide can still exist in the outward-facing state for part of the time and similarly the fully phosphorylated protein in the presence of ATP can sample the inward-facing conformation.

The results show that a mutation affecting the maturation of the protein and its ability to reach the plasma membrane have major effects on the limited proteolysis fragmentation results. On the other hand, a mutation that mainly affects the channel function appears to have minimal effects on proteolytic fragmentation pattern. The expressing yeast system was also utilised to look at early stages in the expression of the wild-type and mutated proteins to address the question of whether stability defects in the mutated version of the protein exert their effects at the very earliest stages of expression.

Methods

Time Course – A starter culture containing the constructs from [18] [19] was grown overnight at 30 °C; colonies were taken from a YNB-agar plate. The following morning, the overnight culture was supplemented into a larger culture and this was grown until the culture reached an induction OD of 0.8-1.2. 2% galactose was subsequently added and the monitoring of the time course begun. Samples were taken at relevant time points, span down and broken using a mini Beadbeater. Following further centrifugation, the pellet was re-suspended and the sample taken for SDS-PAGE analysis.

Limited Proteolysis was carried out according to the Limited Proteolysis methods in [17]. The trypsin and thermolysin were used in the same context as written in Figures 2 and 3 of this paper.

Details of the methods used in this paper can be found in Chapter 2 of this thesis, from section 2.5 through to section 2.15.

Results

Figure 1 shows the time-course of CFTR expression in yeast measured using SDS-PAGE and exploiting the GFP tag present at the C-terminus of the polypeptide chain, which is non-denatured under the conditions used for SDS solubilisation [20]. Wild-type CFTR expression can be detected within 1 to 2 hours of induction using galactose as indicated by the observation of a faint single band around the 250kDa marker position. This corresponds to full length CFTR (168 kDa) with the SUMO N-terminal tag (12 kDa) and the C-terminal GFP tag (27 kDa). A similar result was obtained for the G551D version of the protein. These results concur with several other studies that show that the G551D mutation does not significantly affect the maturation of the protein relative to wild-type [21]. Note that additional fluorescent bands can be observed, even at time zero after induction. These bands are likely to be yeast proteins that contain covalently bound FAD which fluoresces in the same region of the spectrum as GFP [18, 19]. The protein observed at around 60 kDa is probably due to succinate dehydrogenase and this abundant mitochondrial protein has been discussed previously [18, 19]. It may be employed as an internal reference when comparing expression levels of proteins in yeast. A higher molecular mass band at approximately 120 kDa has not been previously discussed. This band is clearly present at early stages before full length CFTR becomes apparent on the gel. Interestingly, a search of the yeast flavoproteome reveals no candidate proteins of this molecular mass [22]. However the abundantly expressed fatty acid synthetase beta subunit (product of the fas1 gene) seems a plausible explanation for this band. Examination of the yeast fatty acid synthetase structure reveals a missing, presumably disordered, linker region between the FAD-containing dehydrogenase part of the protein and the dehydratase C- terminal half of the protein. It seems reasonable to propose that the fluorescent band at approximately 120 kDa is due to cleavage of the fatty acid synthetase at the linker position yielding a fragment that is approximately 1109 residues long, equivalent to 123 kDa.

Figure 1

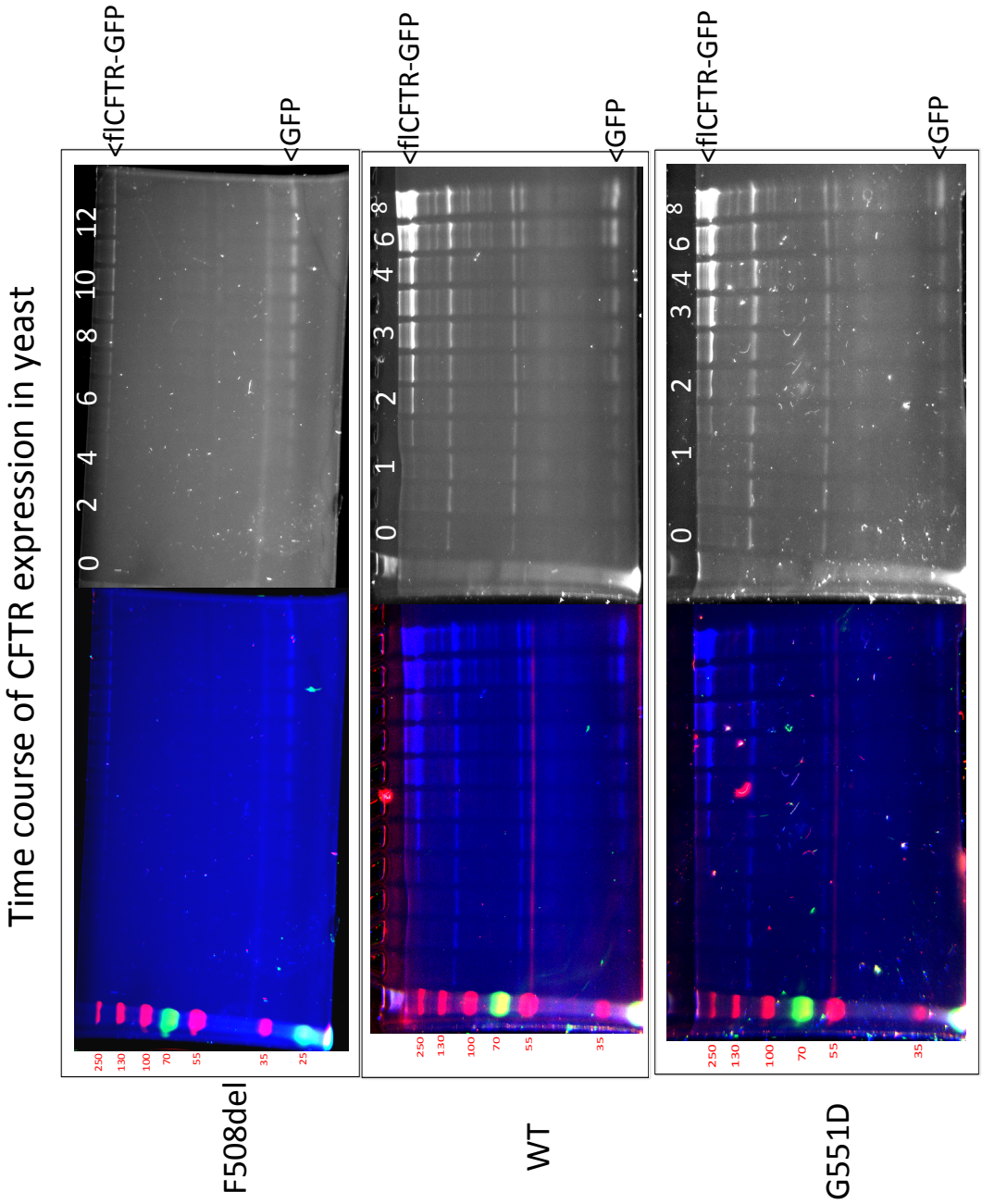
Time course of CFTR expression in yeast
flCFTR-GFP
GFP
F508del
WT
G551D

Figure 1: Time course of CFTR expression in yeast. The left hand panels indicate a multichannel scan of an SDS-PAGE gel containing the cell samples from each time point. The right hand panels indicate an Alexa488 scan of the same gel, visualising the fluorescent signal from the samples in the acrylamide gel. The numbers indicate time (in hr) after induction of expression with 2% galactose. The F508del samples are collected every two hours from 0 hours, that is at the point of induction, up to 12 hours. The WT and G551D samples are collected on the hour from 0 hours, that is at the point of induction, up to 4 hours and then every two hours up to 8 hours. The full-length SUMO-CFTR-GFP band is indicated at the top of each gel, and the cleavage/turnover product of GFP is indicated at the bottom. Each panel is labelled with the construct of CFTR that was used for the experiment

Figure 2

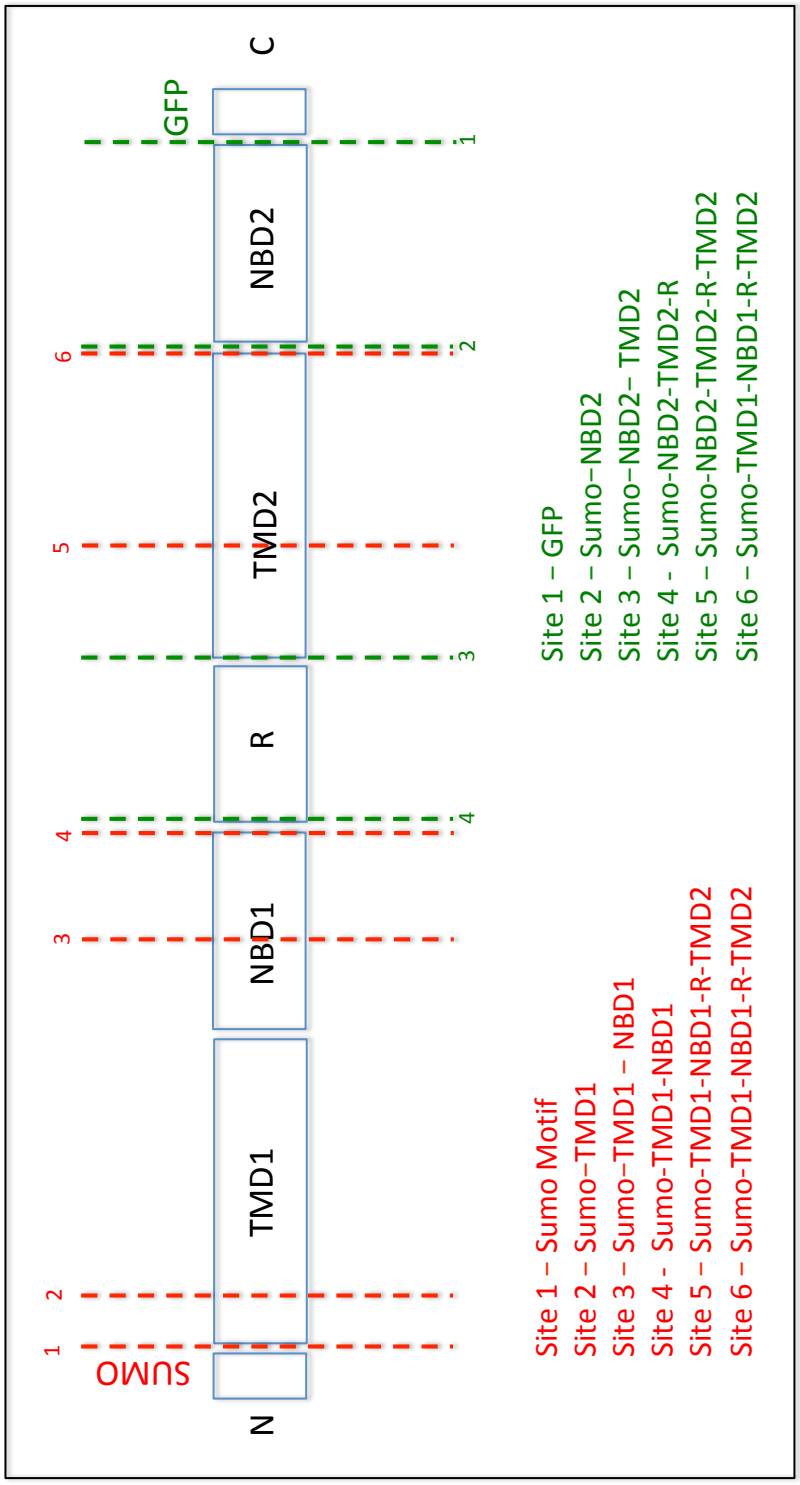

Figure 2: Schematic diagram representing predicted cleavage sites on CFTR. Dotted lines represent cleavage sites of thermolysin. Green indicates fragments that would give a GFP signal while red indicates fragments that would be bound by their SUMO motif and give a signal corresponding to the antibody that would bind there. Below is a list of the fragments and the domains that they would encompass.

Figure 3

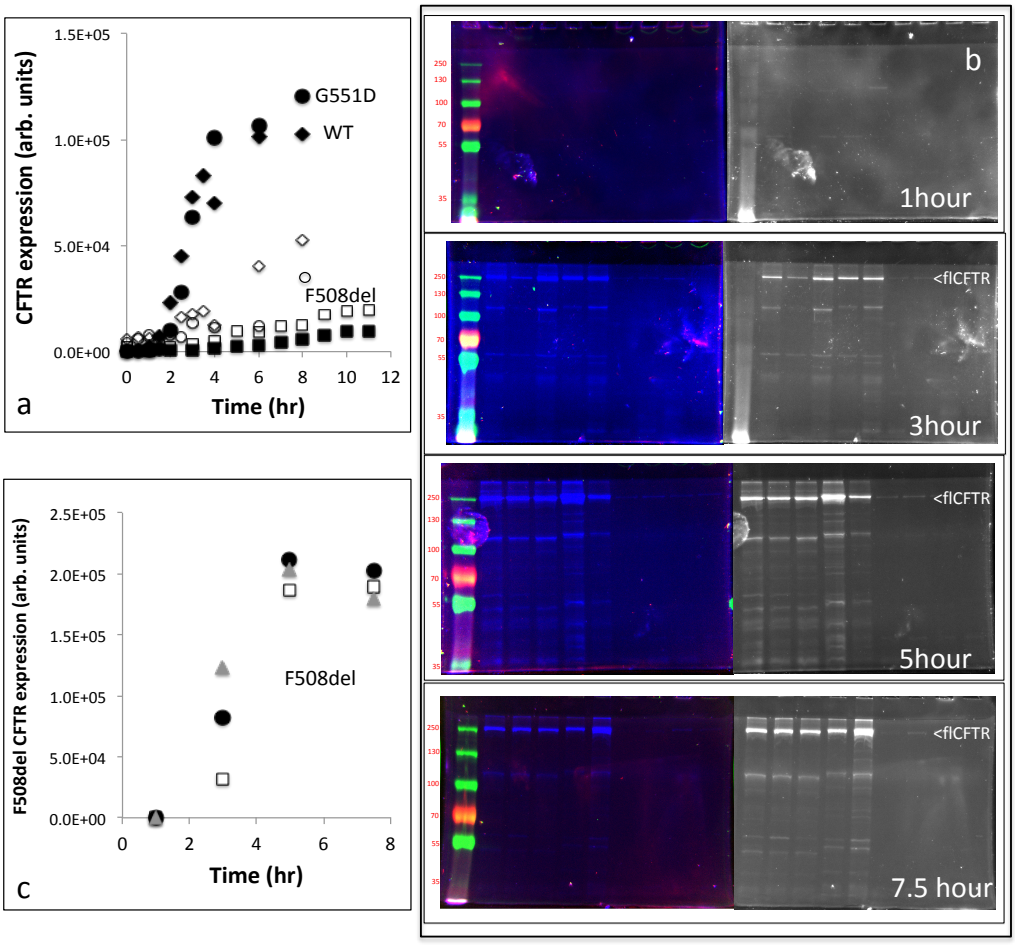
CFTR expression (arb. units)
1.5E+05
1.0E+05
5.0E+04
0.0E+00
G551D
WT
F508del
0 2 4 6 8 10 12
Time (hr)
a
F508del CFTR expression (arb. units)
2.5E+05
2.0E+05
1.5E+05
1.0E+05
5.0E+04
0.0E+00
F508del
0 2 4 6 8
Time (hr)
c
b
1hour
<fICFTR
3hour
<fICFTR
5hour
<fICFTR
7.5 hour

Figure 3: Quantitation of the time-course of expression of CFTR in yeast. Closed symbols represent the quantitation of the full-length protein using SDS-PAGE and the C-terminal GFP tag. Open symbols represent the intensity of the free GFP band, taken as an indication of CFTR turnover/degradation. Squares represent F508del CFTR, diamonds, WT CFTR and circles, G551D CFTR. (b) Larger scale study of F508del CFTR expression in microsomes as a function of time after induction with galactose in yeast. Each gel represents a different time-point. Loading from left to right is: Markers (masses indicated), F508del CFTR, F508del CFTR + VX809, F508del CFTR + VX661. For comparison, the next two tracks correspond to WT CFTR and WT CFTR + VX809. The right hand side of each gel represents controls (unbroken cells). (c) Quantitation of the time course of F508del CFTR expression in yeast in the presence of two corrector drugs (VX809, squares and VX661, circles). Expression in untreated cells is shown with the triangles.

Figure 2 represents a simplified schematic of what would be expected following thermolysin addition to the full length CFTR protein. As the amount of thermolysin increases the ratio of fragments would shift to the left and right for SUMO and GFP respectively, as the larger fragments would themselves be lysed to the smaller fragments. Sites of cleavage were roughly estimated based on signals interpreted from Figure 5 and 6 and predicted sites of thermolysin cleavage based on exposed residues.

The fact that some proteolysis is occurring either before or after harvesting the cells is not surprising and indeed proteolytic fragments of CFTR can also be observed in these gels including free GFP at approximately 27 kDa. What is clear from the figure is the relatively weak expression of the F508del version of the protein. From the signal on the image, the intensity of the full-length CFTR band was quantified relative to the intensity of the liberated GFP band and is shown in Figure 3. The F508del expression is lower than for WT and G551D CFTR and it also shows a relatively higher level of the free GFP band, which may be taken as an indication of greater turnover and degradation of the mutated protein. Turnover and degradation of proteins such as CFTR in yeast is similar to that in mammalian cells, i.e. proteins targeted for degradation become poly-ubiquitinated and then targeted to the proteasome [23] [24]. Therefore, it was investigated whether the yeast system for CFTR expression was employing this mechanism, to preferentially target the F508del version of the protein for degradation. As shown in Supplementary Figure 1, purified CFTR is relatively highly poly-ubiquitinated compared to the wild-type and G551D versions of the protein. As observed in Figure 1 and Figure 3 CFTR often runs as a doublet band around 200 kDa. Although the reason for migrating as a doublet band is not clear it is interesting to observe that the upper band in the doublet appears to be more poly-ubiquitinated relative to the lower band for the F508del version of the protein. Hence from these initial studies it appears that F508del expression in yeast is significantly lower and this is probably due to an increased targeting of the protein to the proteasome.

A more detailed study of the time course of the F508del expression was subsequently undertaken with larger amounts of F508del expressing cells, as shown in Figure 4. F508del CFTR has a half-time for full expression of around 3 to 4 hours and reaches maximum expression levels after 6 to 8 hours. Similar values for the onset of expression of the wild-type and

Figure 4

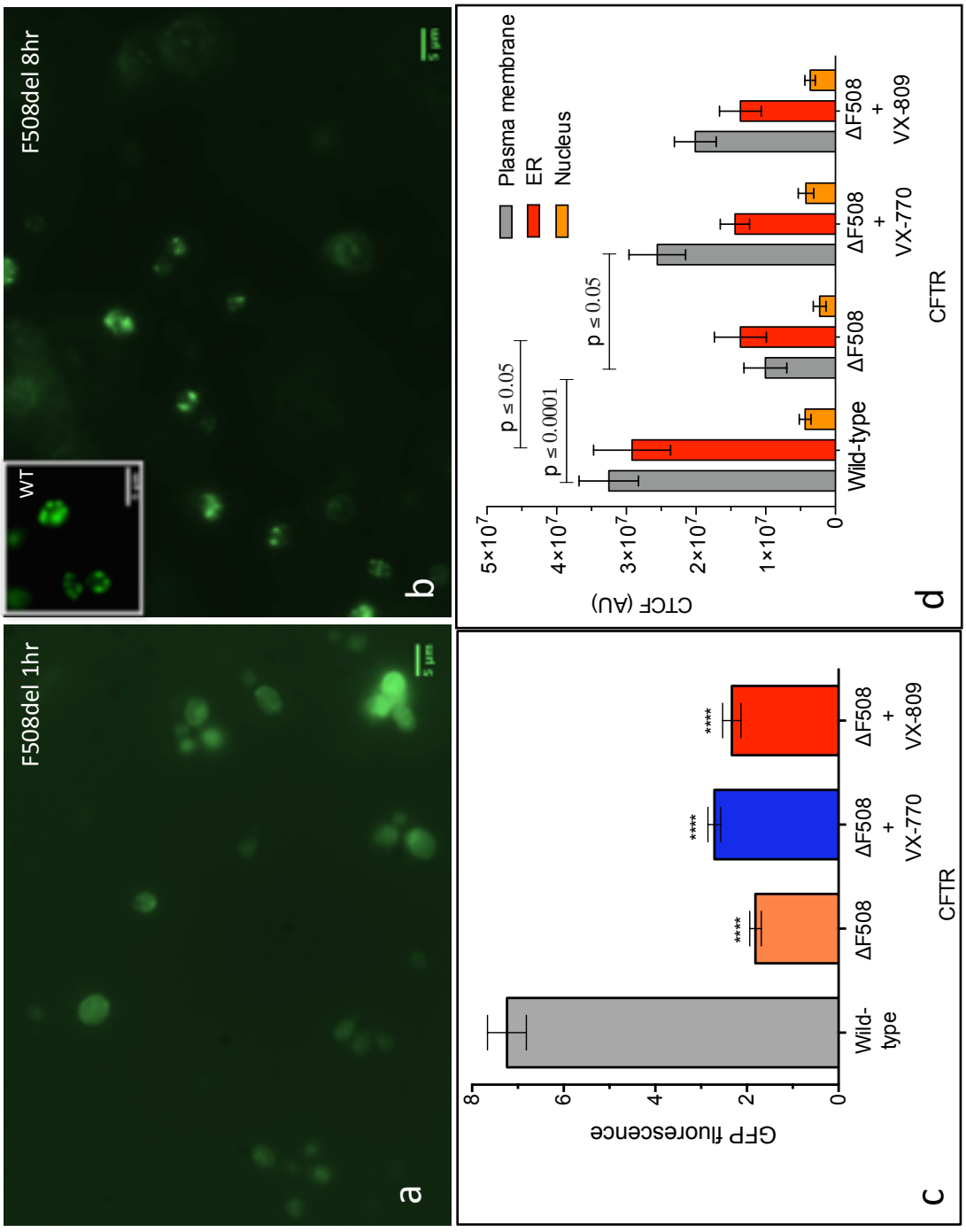
F508del 1hr
a
F508del 8hr
WT
b
GFP fluorescence
Wild-type
ΔF508
ΔF508 + VX-770
ΔF508 + VX-809
CFTR
c
Plasma membrane
ER
Nucleus
p ≤ 0.05
p ≤ 0.0001
p ≤ 0.05
CTCF (AU)
d

Figure 4: CFTR and F508del CFTR in yeast: (a, b) F508del CFTR expression in yeast at 1 hour and 8 hours after induction. Cells show a weak and evenly-distributed GFP fluorescence signal at early time points, whilst at 8 hours the CFTR fluorescence is stronger and localised in internal membranes (fluorescence intensity in panel b is scaled x0.5 relative to in panel a). The inset shows wild-type CFTR for comparison, where fluorescence is strong and localised to punctate regions around the periphery of the cells. Scale bars correspond to 5 μm. (c) Overall cell expression levels at 14 hr post induction determined by quantification of fluorescence (arbitrary units). Level of significance versus the wild-type CFTR expression is indicated with the asterisks. (d) Background-corrected total cellular fluorescence (CTCF) for CFTR is displayed for different regions of the cell with equidistantly spaced rings assigned to nucleus (centre), ER (intermediate) and plasma membrane (outer).

G551D versions of the protein can be observed. Hence F508del expression levels seem to be mainly regulated by the balance between expression and insertion into the ER versus a higher rate of poly-ubiquitination and produce more degradation. As illustrated in Figure (3b), the overall time for expression of F508del does not appear to be affected significantly by the addition of corrector compounds VX-809 and VX-661. In all cases the expression levels reach maximum values around 5 to 7 hours after induction. In summary the production of the F508del version of the protein appears to occur over the same time course as the wild-type protein, that overall expression levels are relatively low due to poly-ubiquitination and targeting to the proteasome and that the corrector compounds that have been shown to rescue at F508del at the plasma membrane [25] [26] [27] do not seem to affect this in any major way in this yeast expression system. Intrinsic yeast proteases associated with the microsomal membranes cause some cleavage of the F508del and wild-type proteins, although the fragmentation patterns appear similar between the two versions of the protein, and similarly are not affected by the presence of VX-809 and VX-661. This was investigated this in greater detail, using externally added proteases at defined concentrations for both microsomally-embedded CFTR as well as for detergent-purified CFTR.

Limited proteolysis with thermolysin was employed to probe the status of CFTR after expression levels had reached maximum (Figure 5). Over a range of protease concentrations from 0 to 250 μg/ml, the microsomal CFTR becomes completely degraded. At the highest thermolysin concentration a single band at approximately 36 kDa can be observed. This band is at a higher molecular mass than isolated GFP and it increases in abundance relative to lower molecular mass bands as a function of the thermolysin concentration. It has been previously shown that commercially available GFP and thermolysin in combination at low temperature form a highly stable complex that resists denaturation by SDS [17]. At lower thermolysin concentrations, C-terminal fragments of CFTR can be

Figure 5

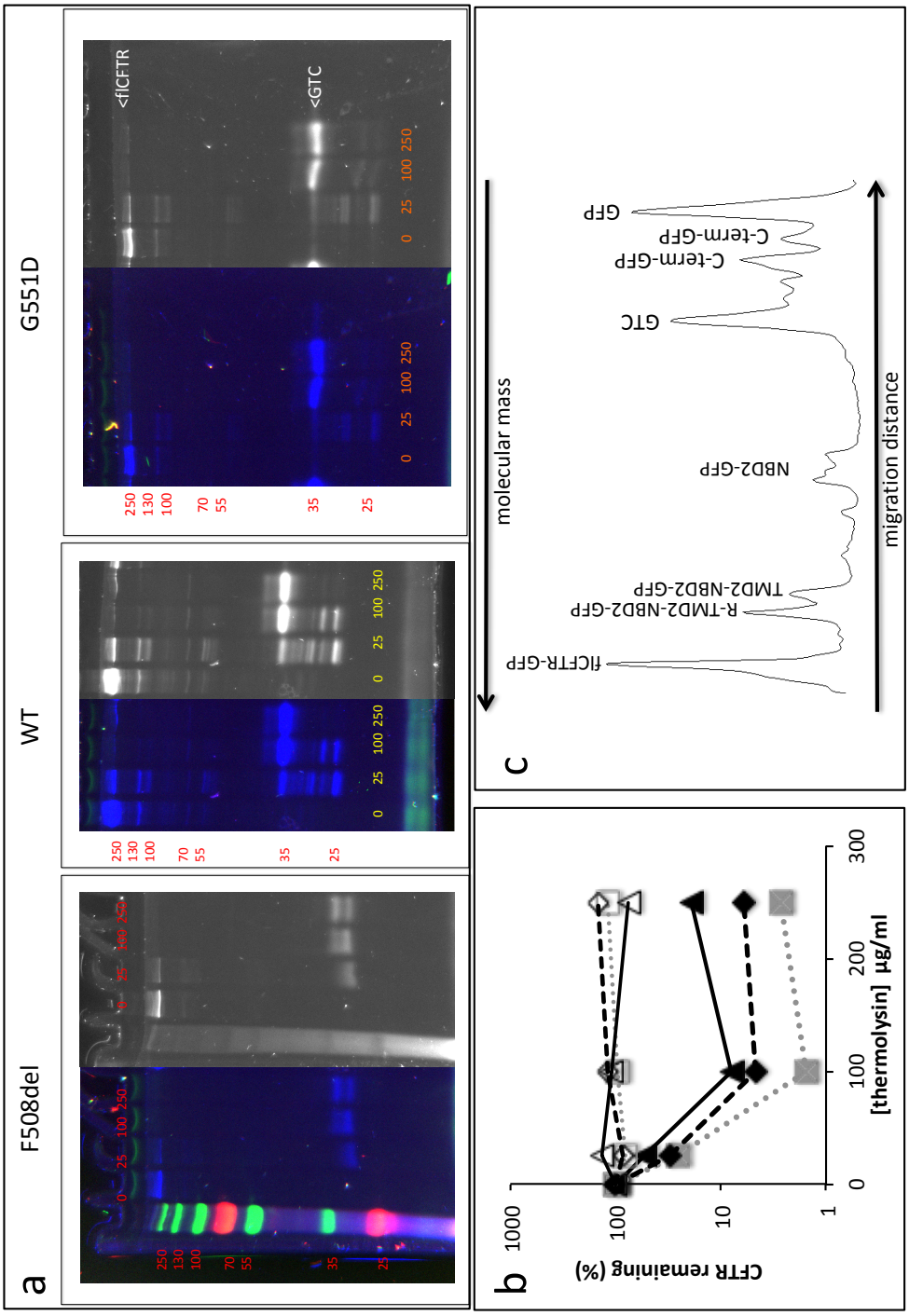
a
F508del
WT
G551D
<fICFTR
<GTC
250
130
100
70
55
35
25
0
25
100
250
b
CFTR remaining (%)
1000
100
10
1
0
100
200
300
[thermolysin] µg/ml
c
molecular mass
migration distance
fICFTR-GFP
R-TMD2-NBD2-GFP
TMD2-NBD2-GFP
NBD2-GFP
GTC
C-term-GFP
C-term-GFP
GFP

Figure 5: (a) Study of membrane-embedded CFTR susceptibility to limited proteolysis with thermolysin and with the concentration of thermolysin (in μg/ml) indicated above or below each track. No attempt was made to regulate the phosphorylation status of CFTR, although its is expected to be largely phosphorylated[17]. WT and G551D limited proteolysis patterns are similar, with a spread of larger and smaller C-terminal fragments. At high concentrations of protease, full-length (fl) CFTR is lost (see next Figure) whilst an SDS-stable complex of cleaved GFP and thermolysin accumulates as a band at ~36kDa- as described earlier [17]. This complex predominates even at lower concentrations of protease in the limited proteolysis pattern of F508del CFTR which also shows relatively less of the larger molecular mass fragments (left panel). (b) Quantitation of the data in (a) showing stability of membrane-embedded CFTR as determined by the amount of full-length CFTR-GFP remaining on SDS-PAGE gels (solid symbols) versus total intensity of all fluorescent bands on the gel (open symbols). WT CFTR is indicated by triangles,, F508del CFTR by squares and G551D CFTR by diamonds. (c) Scan of the track corresponding to WT CFTR treated with 25μg/ml thermolysin with an indication of the likely origins of the fluorescent bands.

observed over a range of masses, for example see wild-type CFTR treated with 25μg per/ml of thermolysin. An interpretation of the composition of these bands is shown in panel C. The fragmentation patterns are consistent with a limited proteolysis condition, i.e. there is no observed smear due to many fragments, but rather discrete bands that are indicative of a discrete number of highly favoured proteolytic cleavage sites (see also Discussion section). Wild type CFTR and G551D CFTR show much more resistance to thermolysin cleavage than F508del CFTR and this difference in stability can be quantified, as shown in panel b. Note that a logarithmic scale is used because of the extremely low amounts of full-length CFTR bands that remain after thermolysin treatment. Subsequent limited proteolysis studies were carried out with purified protein but these results with non-purified CFTR in microsomal membranes are important to demonstrate that the purified protein in detergent is very similar to the protein in microsomal membranes. The main differences that are observed between microsomal CFTR and the detergent purified protein (see later) appears to be in the number of discrete lower molecular mass C-terminal fragments. The existence of more low mass bands for the microsomal CFTR implies that the yeast may have some protective effect on the C-terminal ~40-100 residues of the protein. In mammalian cells, this region of the protein is known to associate with the PDZ-binding domains of NHERF1 [28-30], but in yeast no equivalent membrane-associated protein has so far been identified.

Figure 6

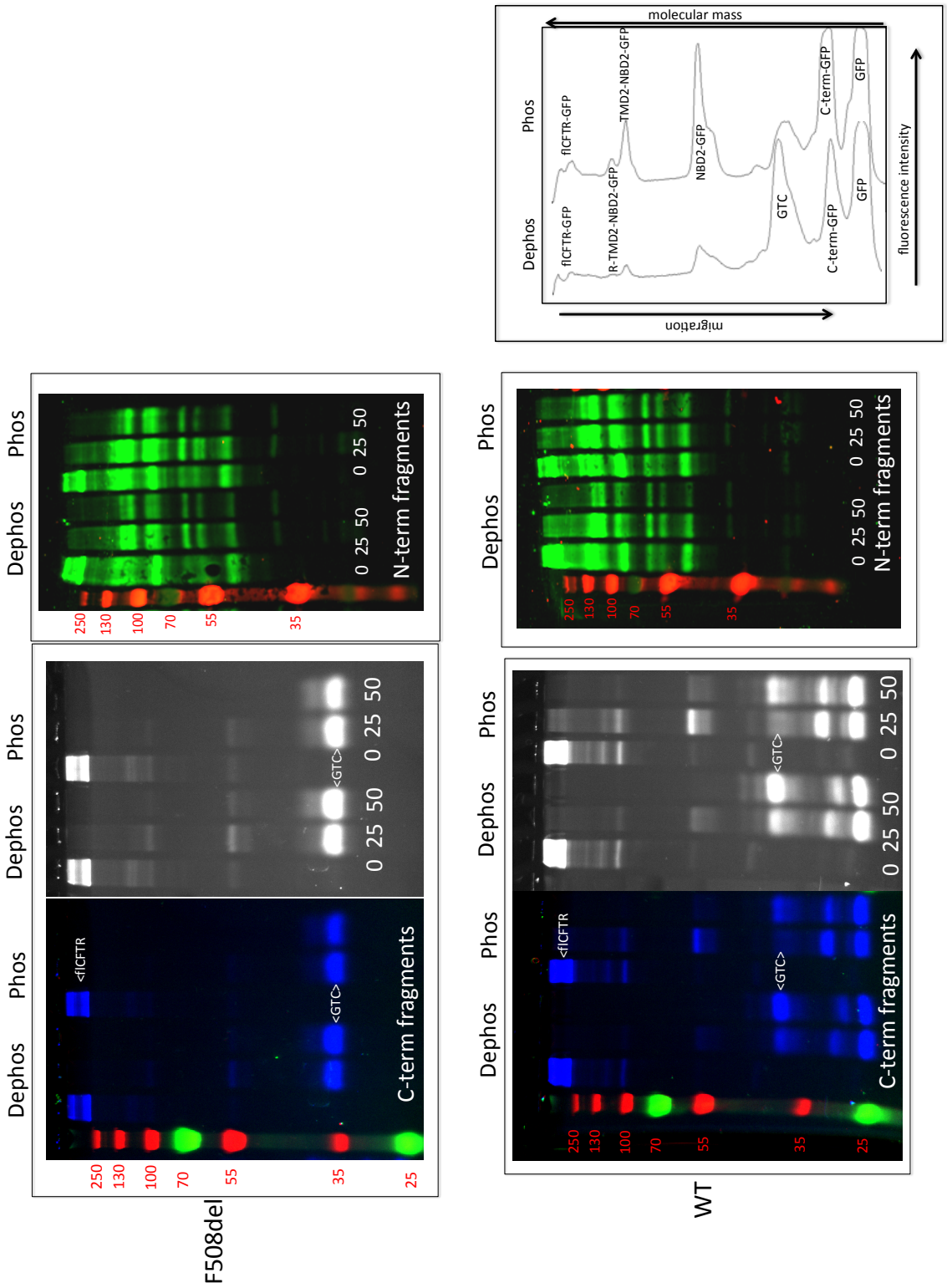
molecular mass
migration
fluorescence intensity
Dephos
Phos
flCFTR-GFP
R-TMD2-NBD2-GFP
TMD2-NBD2-GFP
NBD2-GFP
GTC
C-term-GFP
GFP
N-term fragments
C-term fragments
<flCFTR
<GTC>
0 25 50
250
130
100
70
55
35
25
F508del
WT

Figure 6:

Study of detergent-purified CFTR after full phosphorylation or dephosphorylation using limited proteolysis with thermolysin and detection of the C-terminal fragments using the GFP tag (blue, white bands – left and centre) or detection of the N-terminal fragments using an anti-SUMO antibody (green bands, right). Increasing concentrations of thermolysin used are indicated under each track (in µg/ml). F508 del CFTR (upper panels) appears much more sensitive to thermolysin, with fewer intermediate mass C-term fragments in the proteolysis pattern, and the immediate formation of the GFP-thermolysin complex (GTC) compared to WT CFTR (lower panels). For WT CFTR, phosphorylation in the presence of ATP appears to stabilise it's C-terminal half against proteolysis, as judged by the greater retention of the flCFTR band, the lower predominance of the GTC band as well as the greater abundance of the ~100kDa and 55kDa bands associated with TMD2-NBD2-GFP and NBD2-GFP fragments respectively. In contrast, the phosphorylation status of F508del CFTR appears to have little rescuing effect on the stability. The N-terminal half of CFTR appears to be less sensitive to thermolysin fragmentation, and the stability difference between WT and F508del CFTR appears less pronounced, although still present. Phosphorylation plus ATP again appears to have some stabilising effect, as judged by the increased abundance of 3 bands around ~90, 110,120kDa arising from SUMO-lasso-TMD1-NBD1.

Figure 6 shows the limited proteolysis patterns for purified wild-type and F508del CFTR. Purification allows both C-terminal and N-terminal fragments to be detected. In the case of microsomes this was not possible for the N-terminal fragments, as it relies on an antibody to the SUMO tag at the N- terminus. In yeast there are many sumoylated proteins [31]and hence proteolytic fragments of CFTR could not be distinguished from intrinsic yeast sumoylated proteins (data not shown). When comparing fragmentation patterns for the C-terminal end of CFTR with the N-terminal end, a clear relationship is observed both for wild-type and F508del CFTR. In both cases there is favoured proteolytic cleavage towards the C-terminal half of the protein. This can be appreciated by comparing the spread of fragments in the two situations. For example the C-terminal fragments are in general distributed towards the lower mass end of the range especially at higher thermolysin concentrations whereas the N-terminal fragments are clustered towards the higher mass end of the range. The fragmentation pattern for both F508del and wild-type CFTR is complicated, but using the atomic models and conceptualisation in Fig. 5, one can identify various bands that are present. Scans of the gels and interpretation of the different fragments can be seen in Figure 6.

As also observed for the microsomal membranes, F508del CFTR appears to be considerably more sensitive to thermolysin than wild-type CFTR. This can be particularly appreciated when comparing the C-terminal fragmentation pattern. On the other hand the difference between F508del CFTR and wild-type is not so apparent for the N-terminal fragmentation patterns, although it must be acknowledged that whilst the C-terminal fragments can be reasonably accurately quantitated using the GFP fluorescence, the same cannot be said for Western blotting. For blotting the high sensitivity of the method is advantageous but the linear dynamic range is worse. For both C-terminal and N-terminal fragments there appears to be some stabilisation of wild-type CFTR after phosphorylation of the protein and in the presence of ATP. That these conditions stabilise the wild-type protein can be understood in terms of the likely effects of phosphorylation on the structure. As the outward-facing CFTR model

contains, in general, less structurally disordered residues [3, 4, 15], one may surmise that the phosphorylated form of the protein will be more resistant to proteolysis. In the case of F508del CFTR, effects of phosphorylation are not apparent when comparing the C-terminal fragmentation patterns, however for the N-terminal fragmentation pattern there is some indication that phosphorylation also stabilises the protein against fragmentation by thermolysin. Interpretation of the composition of the N-terminal fragments of CFTR is presented in Supplementary Figure 3. In contrast to the C-terminal fragmentation pattern, this analysis predicts two cleavage points in regions of the structure that are expected to be structured: This is the (structured) linker region between TMD1 and NBD1, at the crossover loop ICL2 that interacts with the C-terminal half of the protein, and at the boundary between the β sheet domain and the α helical domain in NBD1. The latter fragment of ~65 kDa is interesting because this corresponds to the approximate location of F508 in NBD1. Examination of the N-terminal fragmentation pattern for F508del CFTR does not reveal any differences in this region for the dephosphorylated protein, but at intermediate thermolysin concentrations and after phosphorylation, F508del CFTR shows an additional fragment that is a slightly shorter than the 65kDa fragment. Hence there does appear to be some local changes caused by F508 deletion that can be detected by limited proteolysis.

One of the interesting aspects of these results is that regions that are not present in the available cryo-EM structures nevertheless appear to be present to significant extents in some of the fragments. For example the R-region, which one might expect to be cut at several sites does not lead to a smearing of the larger proteolytic fragments (~100kDa), but rather discrete bands were observed. This can be interpreted as implying that the R-region is cleaved preferentially either at its N-terminal end or its C-terminal end but less often towards the middle. These cleavage sites at the ends of the R-region may be preferred due to interactions of the rest of the R-region with other CFTR domains. Similar conclusions may be drawn for the C-terminal end of the protein (the last 40 amino acid residues). One might expect that this part of the protein would be highly susceptible to cleavage, several C-terminal fragments are observed that must contain the

C-terminal region, implying that cleavage must be occurring at other more preferred sites. Again, this may be due to C-terminal interactions with other CFTR domains such as the R-region [32]. In this respect, one of the few differences in fragmentation pattern between phosphorylated and non-phosphorylated CFTR occurs for a CFTR C-terminus/GFP fragment: At 50ug/ml of thermolysin, the first fragment larger than free GFP is at ~28 kDa in dephosphorylated CFTR but at ~30 kDa after phosphorylation. The 2-4 kDa mass additional to GFP would imply these fragments contain all or part of the C-terminal extension. NMR data imply that interaction of the C-terminus with the R-region can occur when the latter is fully phosphorylated [32], hence some protection of the C-terminal region to proteolysis may explain the longer fragment observed after phosphorylation.

Confirmation of the dephosphorylation or phosphorylation of the CFTR constructs was carried out using a pro Q diamond staining of the gels as shown in Supplementary Figure 4. This stain will identify phosphorylated proteins and after fragmentation it is expected that the most abundant fragments present will contain significant portions of the R-region that has several phosphorylation sites. For both wild-type and F508del CFTR dephosphorylated protein shows little staining on the pro Q diamond visualisation and there is almost no signal from dephosphorylated CFTR bands after addition of thermolysin. There is a strong band on all the tracks containing thermolysin at roughly 38 kDa, which probably corresponds to this protease. The fact that the pro Q diamond stain, even under dephosphorylation conditions, detects this protein suggests that this may be an artefact present in the staining. It seems possible that the Zinc bound by the protein may be producing the staining artefact. Despite the additional complexity due to the stain detecting N-terminal, C-terminal and internal fragments of CFTR, there are still discrete bands detectable on the gel. In particular two bands between the 100-130 kDa marker proteins can be detected in both F508del and wild type CFTR. Less well-stained bands can be discerned at approximately 80 kDa and 60 kDa in mass. The lower molecular mass fragments probably represent internal cleavage products of CFTR containing the R-region (e.g. NBD1-R or R-TMD2) whilst the longer

fragments of over 100 kDa probably represent the N and C terminal fragments previously discussed, and where CFTR is being cleaved either at the start or the end of the R region.

Similar experiments on phosphorylated and dephosphorylated CFTR constructs were carried out using an alternative protease, trypsin. The results are shown in Supplementary Figure 5. Overall the results with the trypsin-limited proteolysis are very similar to those using thermolysin. Again the F508del CFTR has a greater sensitivity to the protease than the wild-type protein. As before, the N-terminal half of CFTR appears to be less sensitive to protease action than the C-terminal half. Phosphorylation in the presence of ATP appears to have some stabilising effect on wild-type CFTR when comparing the N-terminal fragments, especially as judged by increased abundance of the bands around 90 to 120 kDa. For wild type and F508del CFTR, phosphorylation in the presence of ATP appears to have minimal impact on the stability at the C-terminal half of the protein to trypsin.

Discussion

This paper aimed to answer the question of CFTR structure and how it changes upon phosphorylation, trying to answer conflicting EM data regarding “in” and “out’ populations of the protein. In light of these conflicting data, the authors of this paper supports the hypothesis that the CFTR protein is in a constant state of flux, with “in” or “out” populations not being entirely distinct from each other. What generates the specific fragmentation patterns observed for CFTR in the presence of proteases? Clearly discrete bands can be observed rather than a smear of fragments (a situation one might expect given the number of potential cleavage sites if the protein was unfolded). The proteolytic fragmentation patterns have been interpreted using models shown in Fig. 5 but also assuming that the process is being controlled principally by the proteolysis kinetics rather than competition (by different sites in CFTR) for the protease. This is because the stoichiometry of protease to target protein is quite high, whereas the low temperature of incubation with CFTR will restrict the

protease activity. Hence fragmentation rates at specific sites will determine the fragmentation pattern on the SDS-PAGE gels, and since the CFTR protein is denatured with SDS after thermolysin treatment, the dissociation rate of the thermolysin-CFTR complex will not be relevant, but rather the on-rate of the substrate and the subsequent rate of conversion to cleaved product. With this conceptualisation in mind it is possible to make some conclusions about the overall structures of wild-type and F508del CFTR under the experimental conditions employed for limited proteolysis including the effects of phosphorylation and the presence of ATP.

Firstly it is assumed that any disordered regions in the protein would be highly preferred sites. The high concentrations of protease, coupled with low incubation temperature ensures that the most dynamic, intrinsically unfolded regions of the protein will be favoured and conversely that any secondary or tertiary structure in the protein would tend to prevent such a region from being cleaved by the protease. Thus, the number of available sites under a given CFTR conformation will determine the C-terminal and N-terminal fragmentation patterns. In contrast the relative abundance of the various fragments will be determined by subtle changes in the rates of proteolysis at different sites, since *a priori* the lower mass fragments will be derived from the higher mass fragments (with the sole exception of the GFP-protease complexes). For example the abundant NBD2-GFP band observed after CFTR phosphorylation could arise either because of greater stability of NBD2 after phosphorylation or because of increased rates of proteolysis at other parts of the protein that would otherwise yield higher mass fragments. For the NBD-GFP band the former explanation (increased stability) seems more reasonable, because in this case the higher mass C-terminal fragments are also more abundant (Figure 6). Based on these considerations, the authors would propose that cleavage at the N- and C-terminal ends of the internal R-region linker are probably the most favoured cleavage sites, followed by the TMD2-NBD2 linker and then the C-terminal extension to NBD2.

Taken as a whole, the limited proteolysis results suggest that the CFTR protein does not show major differences in its fragmentation pattern under

conditions where it is either fully activated or inactivated. This appears to argue against a mechanistic model [16] involving discrete and major conformational shifts: although less fragmentation of the protein is observed after its activation, in terms of the increased abundance of certain fragments, there are no major changes in the pattern *per-se*. When comparing the N-terminal fragments between quiescent and activated states there is an increase in the fragments corresponding to roughly half the CFTR protein after phosphorylation, but no major changes in the fragmentation pattern. Again this implies that conformational shifts due to phosphorylation and ATP may stabilise the protein globally, but these conformational shifts are not sufficient to expose or bury proteolytic cleavage sites. In particular, it would be expected that the R-region would be partly protected in the dephosphorylated state (and indeed segments of the R-region have been observed in cryo-EM structures [4, 15]) however the opposite is observed– i.e. the greater sensitivity of the R-region for cleavage. A model where CFTR displays both inward and outward-facing states continuously and under a range of conditions has also been proposed [33]. This would seem to be in concordance with the limited proteolysis data, i.e. there would be no difference in the fragmentation pattern expected under any selected experimental conditions, but the relative abundance of fragments would be expected to change according to the proportion of each conformational state being sampled.

Figure 7

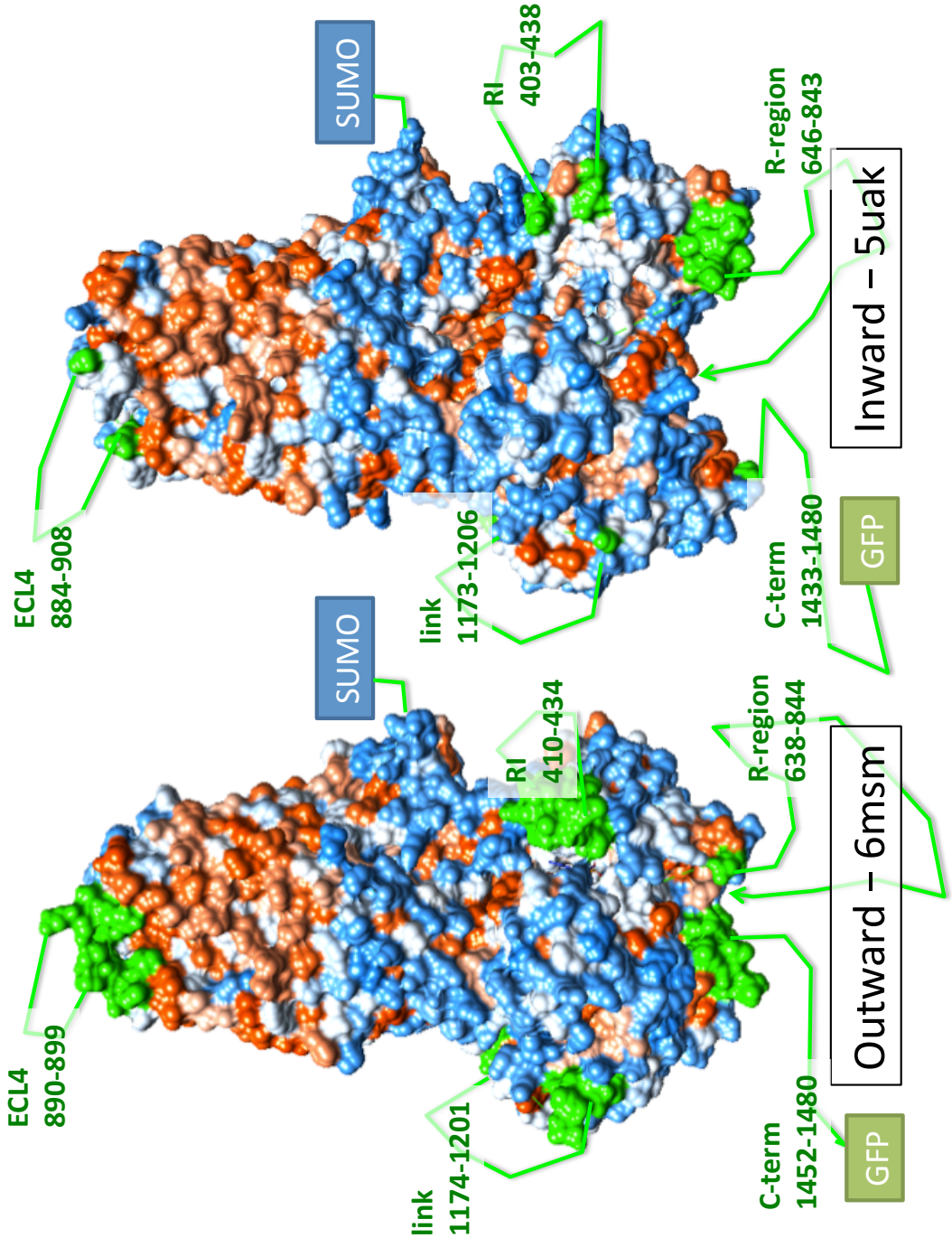
SUMO
RI
403-438
R-region
646-843
Inward – 5uak
ECL4
884-908
link
1173-1206
C-term
1433-1480
GFP
SUMO
RI
410-434
R-region
638-844
Outward – 6msm
ECL4
890-899
link
1174-1201
C-term
1452-1480
GFP

Figure 7: Structures of human CFTR and likely proteolytic cleavage sites (green text and sequence numbers) in unstructured regions. The structures are coloured according to hydrophobicity, with red - hydrophobic, blue - hydrophilic and white –intermediate. The green coloured residues lie at the boundaries of structured regions, and where more than one residue in a boundary is shown it corresponds to a region that is structured in that structure versus the other (also as indicated by comparing the sequence numbering in each structure). The N-terminal SUMO tag and C-terminal GFP tag used in this study are also indicated, but these were not component parts of the two structures shown. In general, the phosphorylated, ATP-bound, outward-facing structure (6msm) has shorter unstructured regions, although the exception to this is the R-region where the inward-facing structure has a helical extension at the end of NBD1 (residues 639-645).

A brief comment can be made about the timescale of the limited proteolysis, as due to the shifting nature of the CFTR protein between states there may be cause that the predicted fragmented states may not be consistently accurate. As the experiments are performed on ice, the fluctuation of the CFTR protein will be at a minimum, and the state with which the individual protein in the experiment will be preserved from when it was purified from its cellular environment. Therefore, accurate predictions about the state of the protein during proteolysis can be made. F508del CFTR has been proposed to be defective because of a mis-folding of the protein [34] and this mis-folded mutant is recognised by the ERAD system and targeted for degradation[9, 35, 36]. However the limited proteolysis experiments with externally added proteases suggest that the overall 3D fold and conformations in the active and quiescent states are all similar to that of wild type and G551D versions of the protein. Similarly, the time course studies, where some intrinsic proteases resulted in the detection of CFTR C-terminal fragments of various lengths do not show any major differences in peptide fragmentation pattern and, by implication, 3D conformation. The major difference that appears to be consistently emerging from these studies is that the F508del CFTR protein is considerably less stable compared to the wild-type protein and G551D proteins. Hence, the need for development of drugs that directly bind to F508del CFTR and help to stabilise the 3D configuration of the protein is strongly indicated by these studies. Drugs that down-regulate the ERAD system [37] would also be favoured provided F508del CFTR can be suitably stabilised at the plasma membrane. Factors associated with determination of the correct folding pathway may be considered as less likely to have therapeutic effects under these considerations, since it can be proposed that F508del CFTR is correctly folded but that its 3D fold is much less stable than normal. Phosphorylation appears to have some stabilising effects on CFTR, but these stabilising effects do not rescue the F508del CFTR instability defect.

A**cknowledgements:** This work was supported by the UK CF Trust via the F508del CFTR strategic research centre grant and a PhD studentship to JC. We acknowledge the contributions of all our fellow members of the strategic research centre and their help in the early stages of analysis and presentation of the data. In particular we acknowledge Professor I. Braakman for scientific insights, introducing us to the limited proteolysis method and for hosting JC in her laboratory. XM was supported by a Cystic Fibrosis Foundation grant (FORD13XX0) as part of the CFTR 3D structure consortium. We acknowledge the members of the consortium for useful contributions and in the design of the original CFTR constructs. We acknowledge the contributions of by Dr X. Wang and Dr T. Rimington who generated the F508del CFTR version of the CFTR construct as part of their MPhil and PhD projects, respectively.

References

[1] Riordan JR, Rommens JM, Kerem B, Alon N, Rozmahel R, Grzelczak Z, et al. Identification of the cystic fibrosis gene: cloning and characterization of complementary DNA. Science (New York, NY). 1989;245:1066-73.
[2] Sheppard DN, Welsh MJ. Structure and function of the CFTR chloride channel. Physiological reviews. 1999;79:S23-45.
[3] Liu F, Zhang Z, Csanady L, Gadsby DC, Chen J. Molecular Structure of the Human CFTR Ion Channel. Cell. 2017;169:85-95.e8.
[4] Fay JF, Aleksandrov LA, Jensen TJ, Cui LL, Kousouros JN, He L, et al. Cryo-EM Visualization of an Active High Open Probability CFTR Anion Channel. Biochemistry. 2018;57:6234-46.
[5] Ostedgaard LS, Baldursson O, Vermeer DW, Welsh MJ, Robertson AD. A functional R domain from cystic fibrosis transmembrane conductance regulator is predominantly unstructured in solution. Proceedings of the National Academy of Sciences of the United States of America. 2000;97:5657-62.
[6] Bozoky Z, Krzeminski M, Chong PA, Forman-Kay JD. Structural changes of CFTR R region upon phosphorylation: a plastic platform for intramolecular and intermolecular interactions. The FEBS journal. 2013;280:4407-16.

[7] Berger HA, Anderson MP, Gregory RJ, Thompson S, Howard PW, Maurer RA, et al. Identification and regulation of the cystic fibrosis transmembrane conductance regulator-generated chloride channel. The Journal of clinical investigation. 1991;88:1422-31.
[8] Picciotto MR, Cohn JA, Bertuzzi G, Greengard P, Nairn AC. Phosphorylation of the cystic fibrosis transmembrane conductance regulator. J Biol Chem. 1992;267:12742-52.
[9] Riordan JR. Assembly of functional CFTR chloride channels. Annual review of physiology. 2005;67:701-18.
[10] Lewis HA, Buchanan SG, Burley SK, Conners K, Dickey M, Dorwart M, et al. Structure of nucleotide-binding domain 1 of the cystic fibrosis transmembrane conductance regulator. The EMBO journal. 2004;23:282-93.
[11] Atwell S, Brouillette CG, Conners K, Emtage S, Gheyi T, Guggino WB, et al. Structures of a minimal human CFTR first nucleotide-binding domain as a monomer, head-to-tail homodimer, and pathogenic mutant. Protein engineering, design & selection : PEDS. 2010;23:375-84.
[12] Aleksandrov AA, Kota P, Aleksandrov LA, He L, Jensen T, Cui L, et al. Regulatory insertion removal restores maturation, stability and function of DeltaF508 CFTR. Journal of molecular biology. 2010;401:194-210.
[13] Kleizen B, van Vlijmen T, de Jonge HR, Braakman I. Folding of CFTR is predominantly cotranslational. Mol Cell. 2005;20:277-87.
[14] Hoelen H, Kleizen B, Schmidt A, Richardson J, Charitou P, Thomas PJ, et al. The primary folding defect and rescue of DeltaF508 CFTR emerge during translation of the mutant domain. PLoS One. 2010;5:e15458.
[15] Zhang Z, Liu F, Chen J. Molecular structure of the ATP-bound, phosphorylated human CFTR. Proceedings of the National Academy of Sciences of the United States of America. 2018;115:12757-62.
[16] Zhang Z, Chen J. Atomic Structure of the Cystic Fibrosis Transmembrane Conductance Regulator. Cell. 2016;167:1586-97.e9.
[17] Meng X, Clews J, Ciuta AD, Martin ER, Ford RC. CFTR structure, stability, function and regulation. Biological chemistry. 2019;400:1359-70.
[18] O'Ryan L, Rimington T, Cant N, Ford RC. Expression and purification of the cystic fibrosis transmembrane conductance regulator protein in Saccharomyces cerevisiae. J Vis Exp. 2012.

[19] Pollock N, Cant N, Rimington T, Ford RC. Purification of the cystic fibrosis transmembrane conductance regulator protein expressed in Saccharomyces cerevisiae. J Vis Exp. 2014.
[20] Mares RE, Melendez-Lopez SG, Ramos MA. Acid-denatured Green Fluorescent Protein (GFP) as model substrate to study the chaperone activity of protein disulfide isomerase. International journal of molecular sciences. 2011;12:4625-36.
[21] Gregory RJ, Rich DP, Cheng SH, Souza DW, Paul S, Manavalan P, et al. Maturation and function of cystic fibrosis transmembrane conductance regulator variants bearing mutations in putative nucleotide-binding domains 1 and 2. Molecular and Cellular Biology. 1991;11:3886-93.
[22] Gudipati V, Koch K, Lienhart WD, Macheroux P. The flavoproteome of the yeast Saccharomyces cerevisiae. Biochimica et biophysica acta. 2014;1844:535-44.
[23] Rodriguez MS, Desterro JM, Lain S, Lane DP, Hay RT. Multiple C-terminal lysine residues target p53 for ubiquitin-proteasome-mediated degradation. Mol Cell Biol. 2000;20:8458-67.
[24] Christiano R, Nagaraj N, Frohlich F, Walther TC. Global proteome turnover analyses of the Yeasts S. cerevisiae and S. pombe. Cell reports. 2014;9:1959-65.
[25] Van Goor F, Hadida S, Grootenhuis PD, Burton B, Stack JH, Straley KS, et al. Correction of the F508del-CFTR protein processing defect in vitro by the investigational drug VX-809. Proceedings of the National Academy of Sciences of the United States of America. 2011;108:18843-8.
[26] Inc. VP. Treatment with VX-661 and Ivacaftor in a Phase 2 Study Resulted in Statistically Significant Improvements in Lung Function in People with Cystic Fibrosis Who Have Two Copies of the F508del Mutation. investors.vrtx.com: Business Wire; 2013. p. 1.
[27] Farinha CM, Sousa M, Canato S, Schmidt A, Uliyakina I, Amaral MD. Increased efficacy of VX-809 in different cellular systems results from an early stabilization effect of F508del-CFTR. Pharmacology research & perspectives. 2015;3:e00152.
[28] Raghuram V, Mak DO, Foskett JK. Regulation of cystic fibrosis transmembrane conductance regulator single-channel gating by bivalent

PDZ-domain-mediated interaction. Proceedings of the National Academy of Sciences of the United States of America. 2001;98:1300-5.
[29] Moyer BD, Duhaime M, Shaw C, Denton J, Reynolds D, Karlson KH, et al. The PDZ-interacting domain of cystic fibrosis transmembrane conductance regulator is required for functional expression in the apical plasma membrane. J Biol Chem. 2000;275:27069-74.
[30] Moyer BD, Denton J, Karlson KH, Reynolds D, Wang S, Mickle JE, et al. A PDZ-interacting domain in CFTR is an apical membrane polarization signal. The Journal of clinical investigation. 1999;104:1353-61.
[31] Esteras M, Liu IC, Snijders AP, Jarmuz A, Aragon L. Identification of SUMO conjugation sites in the budding yeast proteome. Microbial cell (Graz, Austria). 2017;4:331-41.
[32] Bozoky Z, Krzeminski M, Muhandiram R, Birtley JR, Al-Zahrani A, Thomas PJ, et al. Regulatory R region of the CFTR chloride channel is a dynamic integrator of phospho-dependent intra- and intermolecular interactions. Proceedings of the National Academy of Sciences of the United States of America. 2013;110:E4427-36.
[33] Meng X, Clews J, Martin ER, Ciuta AD, Ford RC. The structural basis of cystic fibrosis. Biochemical Society transactions. 2018;46:1093-8.
[34] Du K, Sharma M, Lukacs GL. The DeltaF508 cystic fibrosis mutation impairs domain-domain interactions and arrests post-translational folding of CFTR. Nature structural & molecular biology. 2005;12:17-25.
[35] Ward CL, Omura S, Kopito RR. Degradation of CFTR by the ubiquitin-proteasome pathway. Cell. 1995;83:121-7.
[36] Kopito RR. Biosynthesis and degradation of CFTR. Physiological reviews. 1999;79:S167-73.
[37] Pedemonte N, Galietta LJ. Pharmacological Correctors of Mutant CFTR Mistrafficking. Frontiers in pharmacology. 2012;3:175.

Supplementary Figures

Supplementary Figure 1

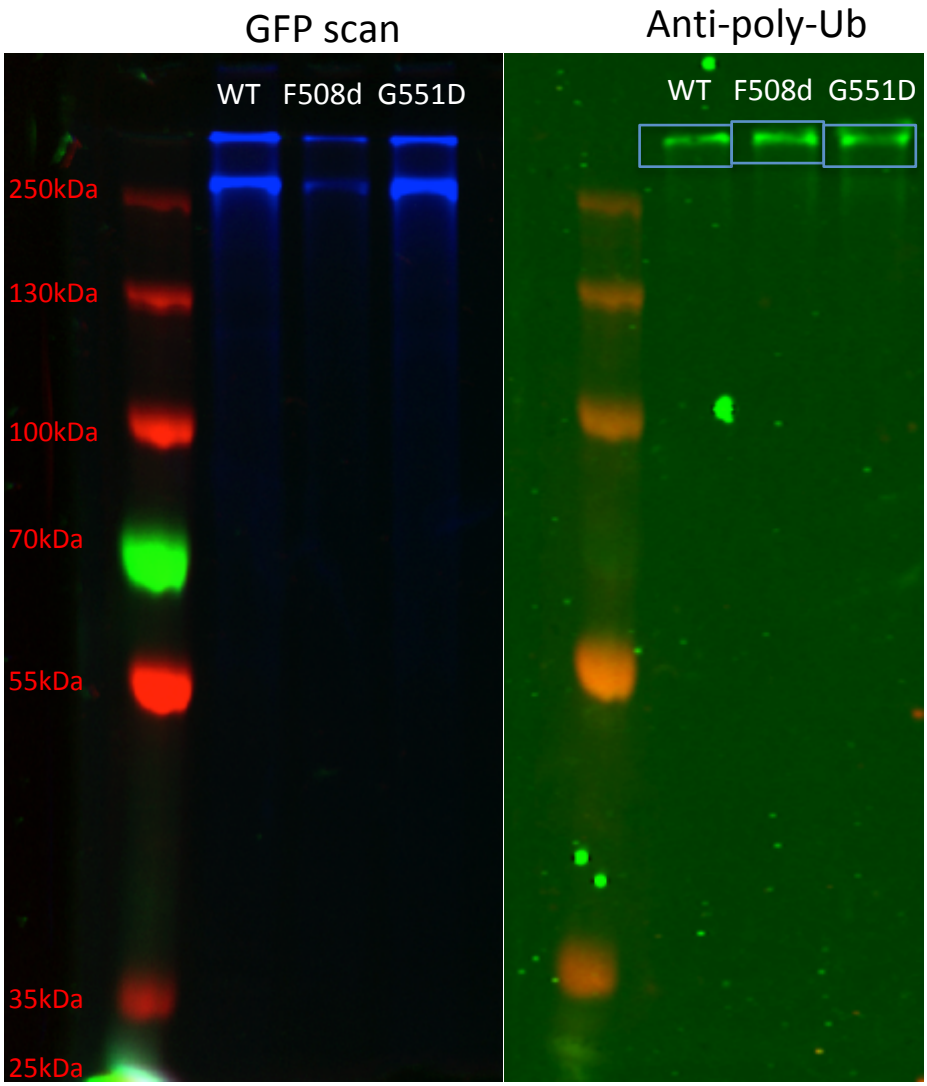

Supplementary Figure 1:

Comparison of wild type, F508del and G551D versions of purified CFTR. The image on the left is recorded with the Alexa488 setting of the imager where the C-terminal tag GFP on the CFTR construct is employed for visualisation and quantitation of the amount of protein. There is less F508del protein than the other two versions on this gel. The protein runs as a doublet. The image on the right is of the same gel after Western blotting and probing with an anti-polyubiquitin antibody. The upper band of the CFTR doublet is much more cross-reactive to the antibody and F508del CFTR shows a greater signal compared to the amount of protein loaded (left panel).

Supplementary Figure 2:

N-terminal fragments of CFTR detected by Western blotting after limited proteolysis with thermolysin as shown in Figure 5, main text. The right hand panel shows a scan of the dephosphorylated and phosphorylated CFTR tracks after treatment with the highest thermolysin concentration. The most plausible composition of the peptide fragments forming the bands is also indicated. Where an apostrophe is shown – e.g. ECL4'- this indicates that cleavage is expected to occur somewhere within this region of the CFTR structure. In contrast to the C-terminal fragmentation pattern, this analysis predicts two cleavage points in structured regions of CFTR: This is in the (structured) linker region between TMD1 and NBD1, at the crossover loop ICL2 that interacts with the C-terminal half of the protein, and at the boundary between the β sheet domain and the α helical domain in NBD1. The latter is interesting because this corresponds to the location of F508 in NBD1

Supplementary Figure 2

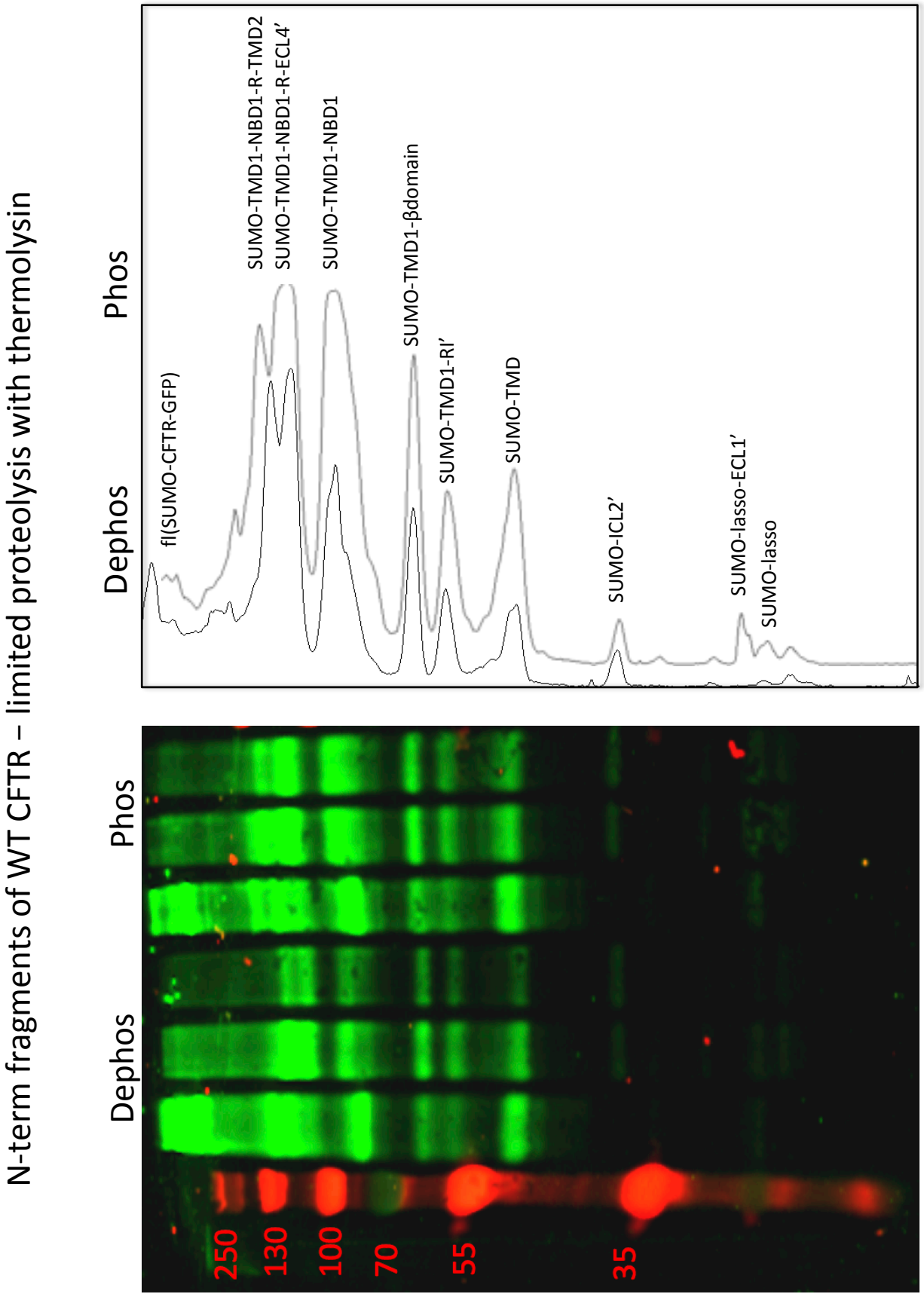

Supplementary Figure 3

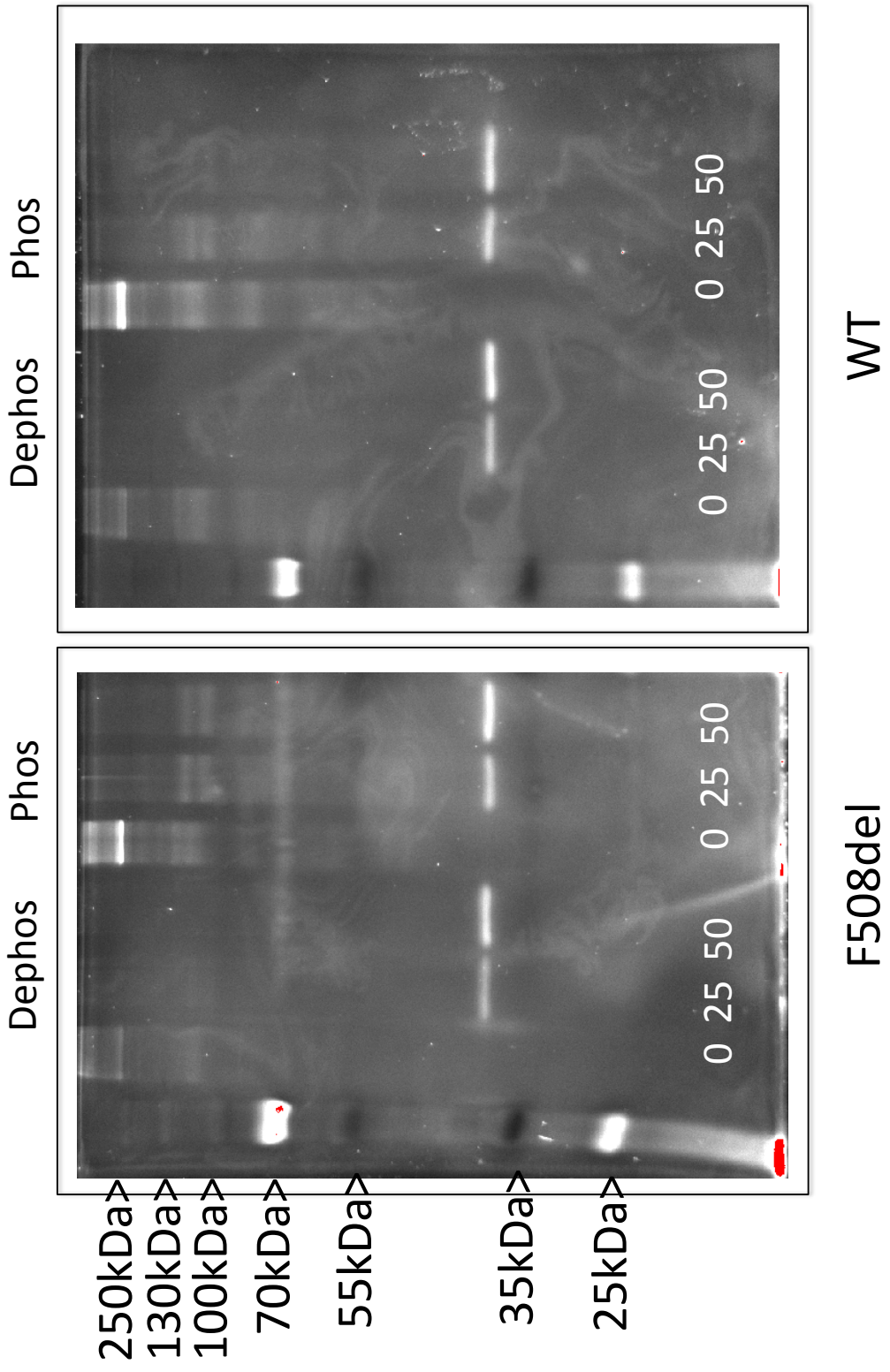

Supplementary Figure 3:
Diamond Q staining for confirmation of the phosphorylation status of purified CFTR after phosphorylation or dephosphorylation and then treatment with different concentrations of thermolysin as described in the main text and Figure 5. Labelling as in Figure 5. 70kDa and 25kDa markers are phosphorylated proteins. A band appearing at ~38kDa appears to be thermolysin. Although the protease is not reported to be phosphorylated, the presence of its Zn ions may result in adventitious phosphate association. Interestingly, the dephosphorylation treatment does not completely remove phosphate groups from the CFTR molecules.

Supplementary Figure 4:
Study of detergent-purified CFTR after full phosphorylation or dephosphorylation and then probed using limited proteolysis with trypsin and detection of the C-terminal fragments using the GFP tag (blue, white bands – left and centre) or detection of the N-terminal fragments using an anti-SUMO antibody (green bands, right). Amounts of trypsin used are indicated under each track (in ng). F508 del CFTR (upper panels) appears more sensitive to trypsin; with less intense intermediate mass C-term fragments in the proteolysis pattern, and the immediate formation of the GFP-trypsin complex (GTrC) compared to WT CFTR (lower panels). For WT and F508del CFTR, phosphorylation in the presence of ATP appears to have minimal impact on the stability of it's C-terminal half to trypsin. The N-terminal half of CFTR appears to be less sensitive to trypsin fragmentation than its C-terminal half, and the stability difference between WT and F508del CFTR is less pronounced. Phosphorylation plus ATP appears to have some stabilising effect on WT CFTR N-terminal end, as judged by the increased abundance of bands around ~90k and ~120Da arising from SUMO-lasso-TMD1-NBD1 and SUMO-lasso-TMD1-NBD1-R respectively.

Supplementary Figure 4

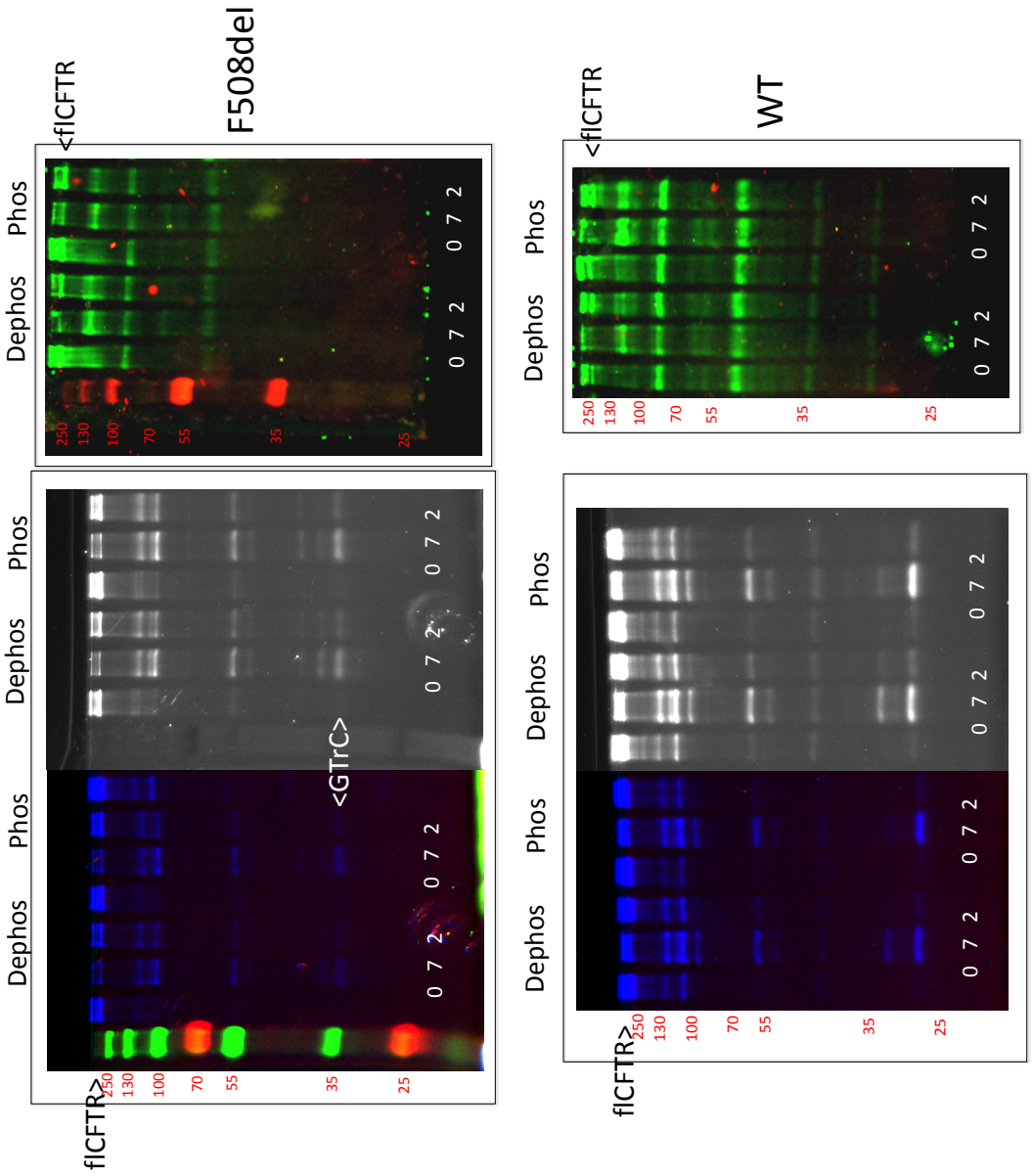

Chapter 7.0

Exploitation of a novel biosensor on the full-length human F508del-CFTR with computational studies, biochemical and biological assays for the characterization of a new Lumacaftor/Tezacaftor analogue

Pasqualina D'Ursi[1§], Matteo Uggeri[1§], Chiara Urbinati[2], Enrico Millo[3,4], Giulia Paiardi[2], Luciano Milanesi[1], Robert C. Ford[5], Jack Clews[5], Xin Meng[5], Paolo Bergese [2], Andrea Ridolfi [6], Nicoletta Pedemonte[7], Paola Fossa[8], Alessandro Orro[1*], and Marco Rusnati[2*]

[1] Institute for Biomedical Technologies, National Research Council (ITB-CNR), Segrate (MI), Italy.
[2] Department of Molecular and Translational Medicine, University of Brescia, Brescia, Italy.
[3] Department of Experimental Medicine, Section of Biochemistry, University of Genoa, Genoa, Italy.
[4] Centre of Excellence for Biomedical Research (CEBR), University of Genova, Viale Benedetto XV 9, 16132 Genova, Italy.
[5] Faculty of Biology, Medicine and Health, University of Manchester, M13PL, United Kingdom.
[6] Consorzio Interuniversitario per lo Sviluppo dei Sistemi a Grande Interfase (CSGI) e Istituto per lo Studio dei Materiali Nanostrutturati (CNR-ISMN), via P. Gobetti 101, 40129 Bologna, Italy.
[7] UOC Genetica Medica, IRCCS Istituto Giannina Gaslini, Genova, Italy.
[8] Department of Pharmacy, Section of Medicinal Chemistry, School of Medical and Pharmaceutical Sciences, University of Genoa, Genoa, Italy.

§ The first two authors contributed equally to this work
* Co-corresponding authors

DECLARATION OF INTEREST

None

ABBREVIATIONS:

Aminoarylthiazole derivatives (AAT); Cholesteryl hemisuccinate (CHS); Cystic fibrosis (CF); cystic fibrosis transmembrane conductance regulator (CFTR); dissipation factor (*D*); dissociation constant (Kd); 1-ethyl-3-(3-diaminopropyl)-carbodiimide hydro-cloride (EDC); Frequency (*f*); molecular dynamics simulation (MDS); N-hydroxysuccinimide (NHS); nucleotide binding domain (NBD); Quartz crystal microbalance with dissipation monitoring (QCM-D); Root mean square fluctuation (RMSF); Root mean square deviation (RMSD); resonance units (RU); solid supported lipid bilayer (SLB); surface plasmon resonance (SPR); transmembrane domains (MSDs).

Abstract

Cystic fibrosis (CF) is mainly caused by the mutation F508del of the cystic fibrosis transmembrane conductance regulator (CFTR) that is thus retained in the endoplasmic reticulum and degraded. New drugs able to rescue F508del-CFTR trafficking to the plasma membrane and its activity are eagerly awaited, a goal that requires the availability of computational and experimental models closely resembling the F508del-CFTR structure and environment *in vivo*.
Here we describe the development of a biosensor based on F508del-CFTR in a lipid environment that proved to be endowed with a wider analytical potential in respect to the previous CFTR-based biosensors. Integrated with a new computational model of the whole human F508del-CFTR in lipid environment and CFTR stability and functional assays, the new biosensor allowed the identification and characterization at the molecular level of the binding mode of some known F508del-CFTR-rescuing drugs and of a new aminoarylthiazole-Lumacaftor/Tezacaftor hybrid derivative endowed with promising F508del-CFTR-binding and rescuing activity.

Keywords: surface plasmon resonance; cystic fibrosis; CFTR; computational chemistry; molecular dynamics.

Introduction

Cystic Fibrosis (CF) is the most common monogenic disorder in Caucasians, caused by different mutations that can occur in different domains of the cystic fibrosis transmembrane conductance regulator (CFTR) [1]. The most frequent mutation is the deletion of phenylalanine 508 (F508del) that causes structural instability of CFTR, its retention in the endoplasmic reticulum and its degradation [2]. The CFTR deficit has a major impact on the respiratory system, with abnormal production of a thick mucus and impairment of innate defence against bacteria. Current therapies, mainly aimed at treating CF symptomatically (e.g. aggressive antibiotic strategies), have significantly pushed forward the mean survival age of patients [3], but the burden of CF care remains very high and life quality/expectancy for most CF patients are still limited.

An ambitious therapeutic alternative is to address CF with drugs that restore membrane expression and activity of mutated CFTR [4]. Despite some success, the development of new CFTR rescuing drugs remains a priority that needs a detailed knowledge of the alterations caused by mutations of F508del-CFTR and of the mechanisms of action of the drugs.

CFTR is a large membrane-integral protein composed of two intracellular nucleotide binding domains (NBDs), one regulatory domain (R), and two transmembrane domains (MSDs) that span the cell membrane six times each [5]. This complexity, along with poor stability and high dynamic fluctuation [6] limited the progress towards appropriate computational and experimental F508del-CFTR models [5, 7].

Surface plasmon resonance (SPR) is an optical technology successfully used to study biomolecular interactions in a variety of biomedical fields [8, 9]. It has been already exploited also for the study of CF but the biosensors used so far has been prepared with isolated domains of CFTR (mainly NBD1, where the F508del mutation occurs [10-17] and R region [18]) or even shorter CFTR peptides [19, 20], thus restricting their analytical potential.

In effect, all the constrains that burden the F508del-CFTR-related biosensor as well as all the other biochemical and computational models limit the reach of the generated results, i.e. by hampering the identification of drugs that bind to F508del-CFTR domains other than NBD1 [21] or by preventing the study of allosteric effects caused by drugs binding to NBD1 but reverberating in other

parts of the protein [22]. In addition, F508del-CFTR *in vivo* is embedded in a lipid membrane, further limiting the significance of results obtained with isolated domains in solution.

Importantly, a model of F508del-CFTR embedded in a lipid environment has been generated [23] and the purification of human intact F508del-CFTR has been reported [24-28]. Starting from this background, here we developed a new biosensor based on the full length human F508del-CFTR and an *ad hoc* computational model, both embedded in a lipid environment. Integrated with well-established biochemical and biological assays, they have been here already exploited to characterize a newly synthesized aminoarylthiazole-Lumacaftor/Tezacaftor hybrid derivative that turned out to be endowed with a promising F508del-CFTR-binding and rescuing activity.

Materials & Methods

Reagents

The compound test set included: a series of four aminoarylthiazole derivatives (AAT, compounds 4, 5, 6 and 7) already analyzed by SPR for their binding to the NBD1 module of F508del-CFTR (see [17] for their chemical structures), Lumacaftor and corrector C4a (here used as controls), Tezacaftor (that has never been subjected to SPR analysis) and the new compound 1-(benzo[d][1,3] dio-xol-5-yl)-N-[5-(4-methoxybenzoyl)-4-(4-methoxyphenyl) thiazol-2-yl] cyclopropane-carboxamide (EN503A), synthesized in our laboratory (see Fig. 1 for the chemical structures of these latter four compounds).

His-tagged human intact F508del-CFTR protein was purified as described by O'Ryan et al., Pollock et al. [24, 26] using LPG14. Murine F508del-NBD1 was obtained from the CFTR Folding Consortium [29]. Lumacaftor and Tezacaftor were from SelleckChem (Houston, TX). C4a from Cystic Fibrosis Foundation Therapeutics (CFFT). Lipids [synthetic phospholipid blend (Dioleoyl) DOPC:DOPS [(7:3 w/w)] from Avanti Polar Lipids (Alabaster, AL). CHAPS and cholesteryl hemisuccinate (CHS) Tris salt from Sigma-Aldrich (St Louis, MO). Carboxy-methyl dextran CM5 sensorchip, anti-His antibody, 1-ethyl-3-(3-diaminopropyl)-carbodiimide hydro-cloride (EDC) and N-hydroxysuccinimide (NHS) from GE-Healthcare (Milwaukee, WI).

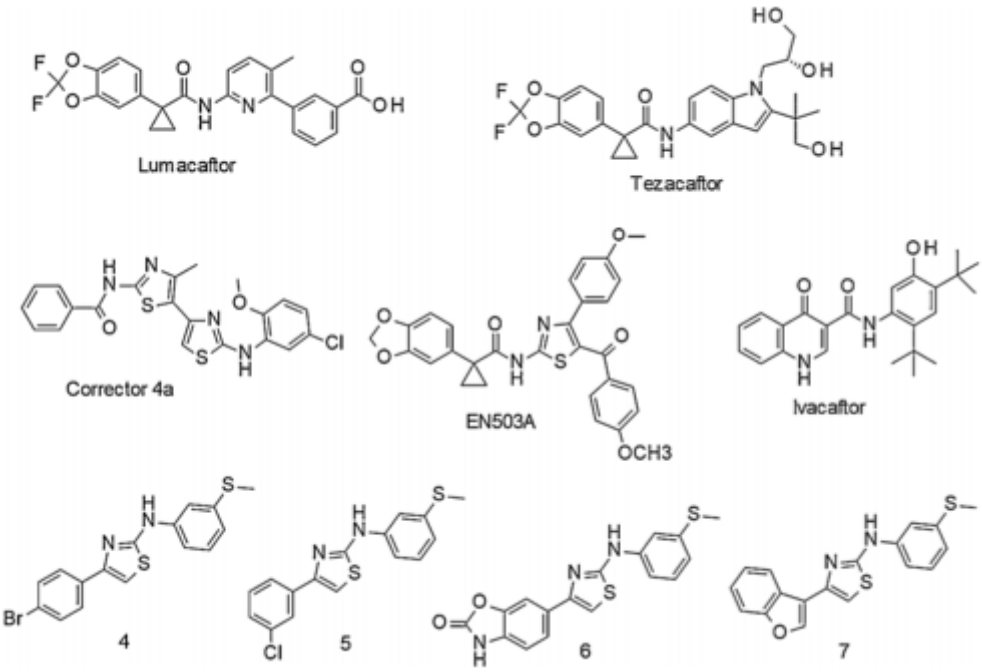

Fig. 1. *Structures of compound test set.*

Quartz Crystal Microbalance with Dissipation monitoring (QCM-D)

In a QCM-D experiment, the piezoelectric quartz crystal oscillates at its own fundamental resonance frequency and the variations in frequency (Δ*f*) and in energy dissipation factor (Δ*D)* are measured. The interaction of the injected solution with the sensor is probed by the change of the sensor *f* and *D* acquired at odd harmonics from 1st to 13th at a constant temperature (25±0.02 °C) and analyzed by the Composite Sauerbrey fit [30] implemented by the software *QSense Dfind* (Biolin Scientific, QSense, Gothenburg, Sweden) that allows the calculation of the sensor-adsorbed mass.

The QCM-D sensor was coated with a thin Au layer, equilibrated in acetone for 30 min and cleaned by UV/ozone plasma (PSD-UVT, Novascan Technologies, Boone, IA) for 30 min. Hepes 50 mM, pH 7 containing NaCl 150 mM (running buffer) was injected in the chamber at 0.1 ml/min until stable *f* and *D* baselines were obtained (drift lower than 2 Hz/h for *f* and 0.2x10^{-6} for *D*). After stabilization, running buffer containing DOPC:DOPS (7:3 W/W) 0.075 mg/ml, 0.02% CHS, 0.1% CHAPS (DOPC:DOPS running buffer), was injected at 0.1 ml/min until both *f* and *D* signals reached a new stabilization. Then, F508del-CFTR (10 mg/ml) in Hepes 50 mM, pH 7 containing NaCl 150 mM DOPC: DOPS (7:3 W/W) 363 mg/ml, 0.06% CHS, 0.3% CHAPS (DOPC:DOPS-F508del-CFTR buffer), that reproduces the composition used for SPR, was injected at 0.05 ml/min until filling up of the chamber, when the flow was stopped for 40 min to allow the system to reach equilibrium, which occurs by spontaneous adsorption of protein-phospholipid structures at the sensor-solution interface. After stabilization, running buffer was injected again at 0.1 ml/min to check the adhesion and stability of the surface-adsorbed structures. Finally, the chamber was washed with ultrapure milliQ water.

CFTR fluorescence-based thermostability assay

Purified wild type CFTR in LPG14 was diluted in the different buffers used for SPR in the absence or in the presence of the various compounds at 4oC and then assessed using the fluorescence-based thermostability assay where (externally-added) CPM and intrinsic tryptophan fluorophores can report on the relative

stability of the protein. CFTR stability was measured using an Unchained Labs UNCLE fluorimeter with the UV laser and as described in [27, 28].

Surface plasmon resonance (SPR)

Preparation of the F508del-CFTR biosensor

A BIAcore X-100 instrument (GE-Healthcare) was used. Anti-His antibody (100 mg/ml in 10 mM sodium acetate pH 4.5) was immobilized on a CM5 sensorchip by standard amine-coupling chemistry [31]. After sensorchip equilibration by injection of DOPC:DOPS running buffer for 1 min at 5 ml/min, human His-tagged intact F508del-CFTR (10 mg/ml, DOPC:DOPS-F508del-CFTR buffer) was injected on the anti-His surface for 3 min at 5 ml/min. A sensorchip coated with anti-His antibody alone was used as negative control for blank subtraction.

Binding analysis

For the evaluation of the capacity of compounds to bind to human intact F508del-CFTR, increasing concentrations of the compounds in PBS, 0.05% surfactant P20 and 5% DMSO, pH 7.4 (PBS-DMSO) were injected over the sensorchip for 90 seconds at 30 ml/min, 25 °C and washed until dissociation. To preserve the immobilized protein and lipid environment on the surface, the single cycle model was adopted [32], where the compounds were injected at increasing concentrations within a single scan without regeneration of the surface between every injection. Dissociation Constant (Kd) values were calculated by steady state analyses performed by fitting the proper form of Scatchard's equation for the plot of the bound resonance units (RU) at equilibrium *versus* the compound concentration in solution. The preparation of the F508del-NBD1 biosensor was performed as described [17].

Cell culture and fluorescence assay for CFTR

CFBE41o-cells stably expressing F508del-CFTR and the halide sensitive (HS)-YFP (YFP-H148Q/I152L) were generated as described [33]. The fluorescence assays of CFTR activity was performed as described [34].

2.6 Computational studies

Modelling of F508del-CFTR in membrane and binding pocket identification

The previously described F508del-CFTR model without R-domain and spanning residue from 646 to 841 [23] was here further developed using the AMBER-14 simulation package. to highlight conformational variations. A lipid bilayer was created using a 140Å x 140Å DOPC model using the webserver CHARMM-GUI Lipid Builder [35], solvated in the TIP3P water model using a force field for lipids LIPID14. A 125ns MDS was performed on the lipid bilayer to stabilize its structure. Stability was evaluated calculating the area per lipid parameter according to the equation:

Area per lipid = (box dimension X)*(box dimension Y)/(number of DOPC in a layer)

where:

area per lipid = (140,00*140,00)/282 = 69,50 Å²/lipid

The F508del-CFTR model was then embedded into the pre-equilibrated DOPC lipid bilayer according to data reported for human CFTR by the "Orientation of Protein in Membrane" database. DOPC residues clashing with F508del-CFTR atoms (< 2,5 Å) were removed to embed the protein. The resulting model was solvated and neutralized with Cl^- ions and subjected to minimizations by AMBER-14 simulation package until the energy minimum value was reached. All systems were simulated at 300 K. Temperature and pressure were kept constant with the Langevin algorithm. Particle-mesh Ewald was used to calculate electrostatic interaction. The simulation was performed by the following steps: heating from 0 to 100K NVT and from 100 to 300K NVT with F508del-CFTR atoms using a 6 Kcal/mol and 4 Kcal/mol restraint, respectively. NPT equilibration of 4ns with F508del-CFTR atoms using a restraint of 2 Kcal/mol and a free-of-restraints production of 25ns. F508del-CFTR stability was assessed by Root Mean Square Deviation (RMSD) analysis of trajectory calculated during the production phase using the respective initial minimized structure as a reference.

Docking simulation and MDS of compound/protein complexes

For each pocket, a local docking was performed to predict the binding of each compound of the test set and to optimize the compound/protein interactions using Autodock Vina [36]. The grid box was centred on the pocket geometric

centre and the search was carried out with the default parameters except for exhaustiveness set at 24. For each compound a screening protocol was carried out selecting all the poses with at most a ΔG of 1 Kcal/mol from the best pose and performing a hierarchical cluster analysis (cluster size of poses and internal RMSD as variables), visual inspection and data integration with the literature.

25ns MDS were performed to evaluate the stability and binding mode of compounds inside each complex and to identify the key residues involved in the interaction. Antechamber was used to parametrize the compounds, adding torsion terms and partial atomic charges. The same MDS protocol described for apo F508del-CFTR was applied, except for a 6 Kcal/mol restraint applied to the compound during the heating and equilibration phases. AMBER 14 and AMBERTools package were used for simulation and post-process of the trajectory. Compounds were built, parameterized (Gasteiger-Hückel method) and minimized with OpenEye Scientific Software (OpenEye Scientific Software, Santa Fe, NM, www.eyesopen.com) using a MMFF94 force field. Regarding Lumacaftor (characterized by a carboxylic moiety) accurate pKa predictions performed with ChemSpider (http://www.chemspider.com) let us reasonably suppose that it maintains its anionic form at physiological pH, so that calculations were performed accordingly.

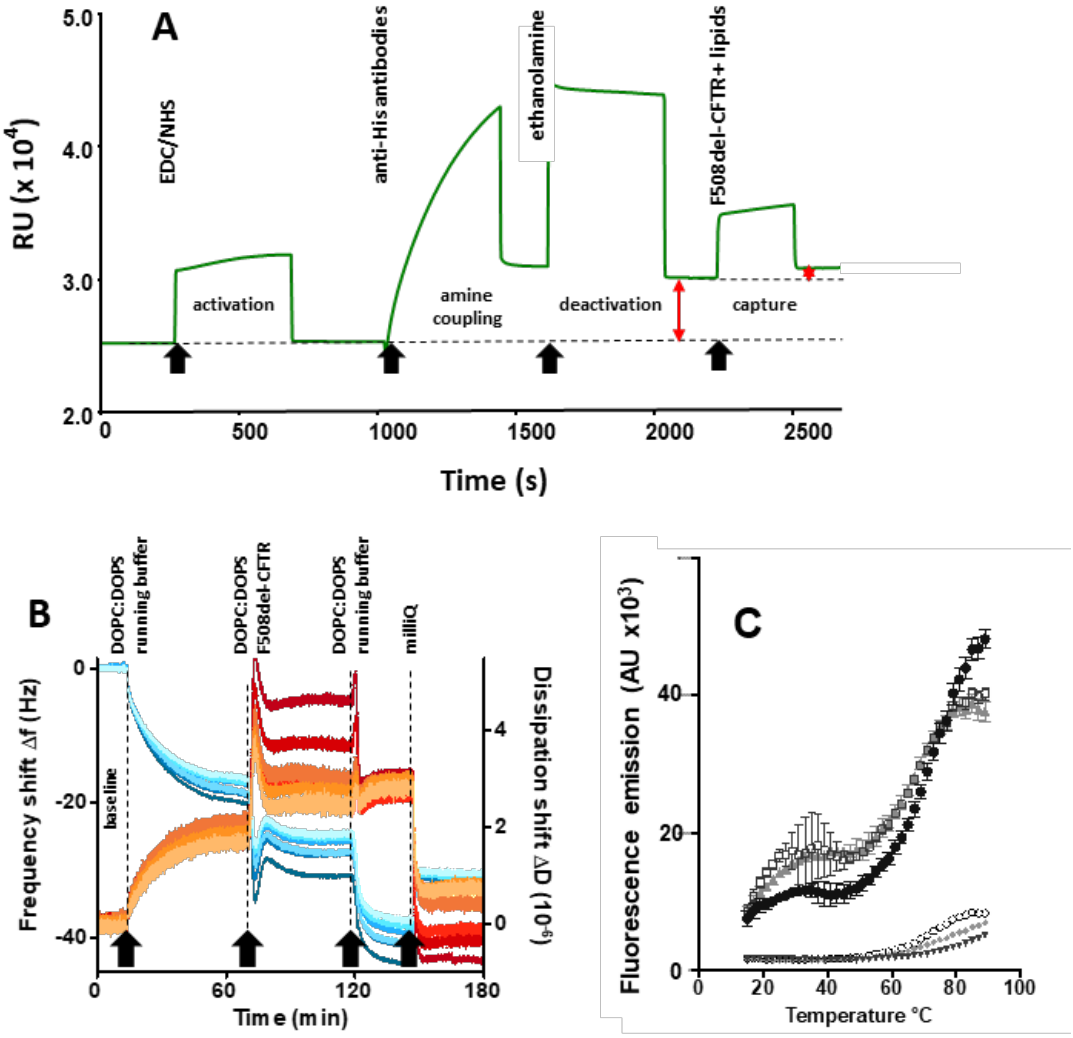

Fig. 2: ***Preparation and characterization of the F508del-CFTR biosensor. A)*** *Representative sensorgram resulting from a procedure of immobilization of anti-His antibody onto a CM5 sensorchip via amine coupling followed by capture of F508del-CFTR. Black arrows: injections. Red arrows: amount of anti-His antibody or F508del-CFTR immobilized to the sensorchip. Dashed lines: baseline at the beginning and at the end of the procedure.* ***B)*** *Organization of DOPC:DOPS and F508del-CFTR at the biosensor solid-liquid interface by QCM-D: Frequency shift (Df, cold colors) and dissipation factor shift (DD, warm colors) odd harmonics (3rd to 13th) versus experimental time coordinate. Black arrows: injection time points of the solutions indicated at the top of the plot.* ***C)*** *Stability of CFTR in the SPR conditions: CFTR was resuspended in the different buffers used for the preparation of the biosensor and evaluated for its stability. Black circles: DOPC:DOPS running buffer; grey triangles: PBS-DMSO; white squares: HBS-EP. The data shown are the result ± s.d. of 3 independent experiments. Buffer/CPM controls were subjected to a single control run (inverted triangles: DOPC:DOPS running buffer; open circles: PBS-DMSO; diamonds: HBS-EP).*

Results

Generation and characterization of the F508del-CFTR biosensor

For F508del-CFTR immobilization, CM5 sensorchip was activated by injecting a mixture of EDC/NHS [31] that gave a transient RU increase (Fig. 2A). Once the trace returned to baseline, anti-His antibody was injected over the sensorchip. Due to the covalent binding of the amine groups of the protein to the carboxy-methyl dextran surface, about 4,100 RU of antibody remained irreversibly attached to the surface (Fig. 2A). The excess of reactive groups were deactivated and F508del-CFTR was finally injected onto the surface allowing the capture of about 350 RU (Fig. 2A).

The F508del-CFTR-DOPC/DOPS configuration at the solid-liquid interface (that constitute the recognition layer of the biosensor) was investigated by QCM-D on a pure Au surface, that fairly mimics the sensorchip hydrophilic surface but features the rigidity and simplicity that allow an accurate determination of mass adsorption and dissipation. The QCM-D quartz crystal sensor responds to adsorbed mass by lowering its frequency (*f)*, while dissipation factor (*D)* changes provide information about the viscosity of the adsorbed layer.

As shown in Fig. 2B, the injection of DOPC/DOPS running buffer and of DOPC:DOPS-F508del-CFTR are both characterized by $\Delta f < 0$ and $\Delta D > 0$, which mirrors the additive mass adsorption at the sensor surface (lipids alone or with the protein, respectively). Dissipation harmonics spread after the injection of DOPC:DOPS-F508del-CFTR, indicating that the adsorbed layer is not tightly bound to the surface, thus generating a large damping effect. The subsequent flushing step with running buffer produces a superposition of the dissipation signals and a further decrease of *f*, indicating that this step stabilizes and promotes uniformity in the adherent layer by further adding phospholipids. The recorded values of Δf *(*$\approx$ -40 Hz) and ΔD *(*$\approx 3 \times 10^{-6}$) indicate the formation of a layer by crowding of nanosized-vesicular structures [37-39].

Finally, the rinsing with milliQ water, which provides an osmotic shock, causes a further sharpening and stabilization of the layer, as indicated by the Δf harmonics that tightly line up at ≈ - 30Hz. Overall, the layer remains not tightly bound to the surface, as indicated by the fact that the ΔD harmonics get back to 0, but largely and uniformly spread around it. Application of the Composite Sauerbrey fit [30] to the data gives a value of the final adsorbed mass on the surface equal to 884 ng/cm^2, which is about 75% higher than the value expected

for a solid supported lipid bilayer (SLB) only made of phospholipids (about 500 ng/cm^2) [38, 39]. The presence of F508del-CTFR cannot account for this mass difference, since it would imply a F508del-CFTR/phospholipid ratio in the layer equal to about 1/340, against a F508del-CFTR/phospholipid ratio in solution equal to 1/10,000.

These results indicate that the formation of a SLB in the SPR experiments (which does not even feature the milliQ control rinsing) is very unlikely. However, they confirm the formation of a continuous viscous layer of vesicular nanostructures bearing a high density of protein embedded in their membrane, a topology that ensures a good amount of F508del-CFTR maintained in a proper membrane-like environment.

We also checked for any non-specific denaturation effect of the buffers used in the biosensor experiments. As shown in Fig. 2C, all the buffers tested displays similar initial labelling of surface-exposed Cys residues of CFTR at the temperature employed for the SPR assay, indicating that none of them has any significant effects on the 3D fold of the protein. Similarly, no major differences are observed in subsequent thermal unfolding of the protein, although the protein appears to be slightly stabilized in the CHAPS/CHS/lipid-containing buffer, with a thermal unfolding transition T_m = 69 °C with respect to PBS-DMSO or HBS-EP buffers (T_m = 67 °C for both), as also manifested in a lower initial labeling of CFTR by CPM at 15 ^{o}C. In comparison, CFTR in its usual purification buffer shows a T_m in the range 62-67 °C [28]. Buffer/CPM controls show low CPM fluorescence (Fig. 2C). These results demonstrate that DMSO (used for SPR, see Section 2.4), is unlikely to destabilize CFTR and that the protein may instead be slightly stabilized by the membrane-like environment.

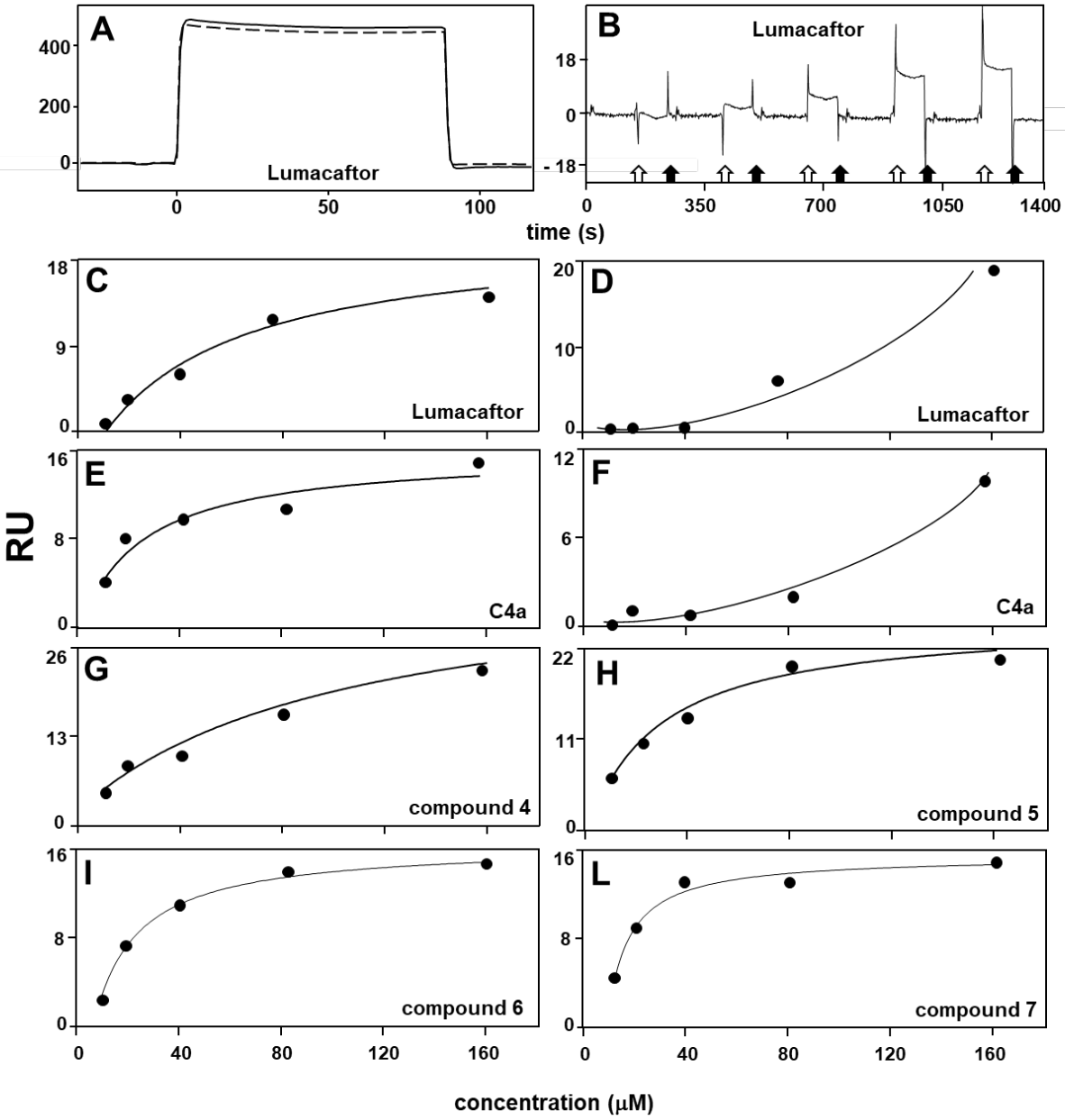

Fig. 3: ***Validation of the analytical performances of the F508del-CFTR biosensor. A)*** *Sensorgrams showing the binding of Lumacaftor (160 mM) to the F508del-CFTR- or to the control anti-his antibody-coated surfaces with lipids (straight and dashed lanes, respectively).* ***B)*** *Representative blank-subtracted sensorgrams derived from a single cycle analysis of Lumacaftor (10, 20, 40, 80, 160 mM) injected on the F508del-CFTR biosensor with lipids. White and black arrows: start and end of the injections, respectively.* ***C-L)*** *Representative steady-state analysis of the indicated compounds injected (at 10, 20, 40, 80, 160 mM) onto the F508del-CFTR biosensor in the presence* ***(C-E, G-L)*** *or in the absence (****D, F****) of lipids.* ***H)*** *Binding of the indicated compounds (at 7.5 mM) to a biosensor containing F508del-NBD1. The data shown are the result ± s.d. of 5 independent experiments.*

Validation of the analytical performances of the F508del-CFTR biosensor

Once demonstrated the stability of F508del-CFTR and of the lipid environment, and their proper organization on the sensorchip surface, we evaluated the effective binding capacity of the mutated protein on the biosensor. To this aim, we used the control compounds Lumacaftor and C4a and a series of ATT already characterized for their capacity to bind to the mouse F508Δ-NBD1 [17]. As shown in Fig. 3A, the injection of Lumacaftor on the sensorchip causes a relevant increase of RU on both the F508del-CFTR and on the control surface (anti-Hys antibody alone) that however does not hamper the determination of a specific binding when the sensorgram is black-subtracted (Fig. 3B). Similar results were obtained for all the other compounds tested (data not shown). Beside Lumacaftor, also all the other compounds tested bound to the F508Δ-NBD1 biosensor in a saturable and dose-dependent manner (Fig. 3C, E, G-L). Relevant is the binding of C4a, that we demonstrated to be unable to bind to F508Δ-NBD1 [17]. Similarly, compound 7 that was predicted (by computational analysis) and demonstrated (by SPR) to be devoid of NBD1 binding capacity [17], binds to immobilized F508del-CFTR with the highest affinity (Tab. 1).

The lipid environment is required for the binding capacity of F508del-CFTR, as demonstrated by the fact that F508del-CFTR immobilized in the absence of lipids binds Lumacaftor and C4a in an unsaturable way (Fig. 3D, F), evidence of a very low affinity, non-specific interaction. Similar results were obtained for the other compounds tested (Tab. 1).

In conclusion, the capacity to detect those compounds that bind F508del-CFTR in domains other than NBD1, points to the F508del-CFTR biosensor as an improved tool with a greater potential in respect to the previous CFTR-based biosensors used so far.

Practical exploitation of the F508del-CFTR biosensor for the identification of novel rescuing small molecules

In an effort to develop hybrid small molecules endowed with an increased F508del-CFTR rescuing activity, compound EN503A was produced in our laboratory and was subjected to binding analysis with the novel F508del-CFTR biosensor. Tezacaftor, a compound with the common scaffold benzo [1,3] dioxol-5-yl-cyclopro-panecarboxylic moiety of EN503A, approved for CF treatment [40]

but that has never been subjected to SPR analysis, was also added to this study to gain new insights into its binding mode. As shown in Fig. 4A-C, the two compounds bind to immobilized F508del-CFTR in a dose-dependent, saturable way. The affinity of Tezacaftor/F508del-CFTR interaction is about three times lower than that of Lumacaftor, while the affinity of EN503A/F508del-CFTR interaction is higher than that of both Tezacaftor and Lumacaftor (Table 1). The compounds were also subjected to SPR analysis with an F508del-NBD1 biosensor. To allow a direct comparison of their NBD1-binding capacity, a single subsaturating concentration equal to15 mM (that is around the Kd of Lumacaftor/F508del-NBD1 interaction [17]) was tested. As shown in Fig. 4D, Lumacaftor, but not C4a, bind to NBD1, in agreement with our previous report [17]. In the same experimental conditions, EN503A binds NBD1, while Tezacaftor showed a very limited NBD1-binding capacity.

These results confirm the increased screening potential of the F508del-CFTR biosensor with respect to the biosensors containing the isolated NBD1 [10-20] and demonstrate its effective capacity to identify new binders to be subjected to further analysis to validate their effective rescuing capacity.

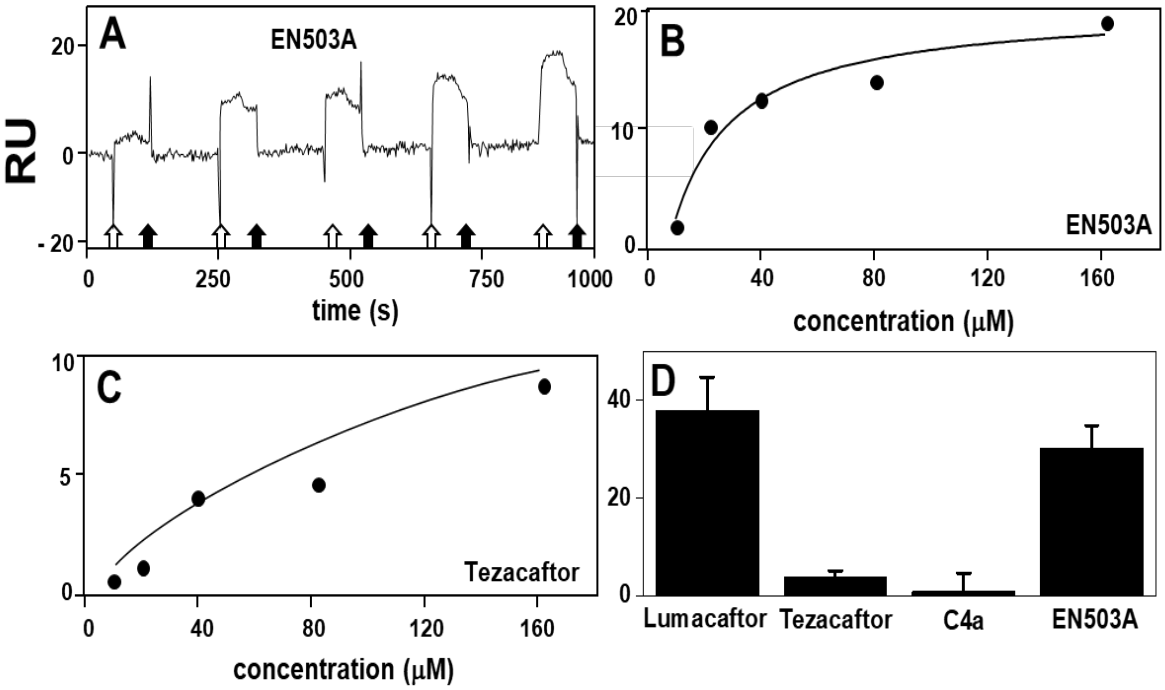

Fig. 4: Practical exploitation of the F508del-CFTR biosensor for the identification of novel rescuing small molecules. A) *Representative blank-subtracted sensorgrams derived from a single cycle analysis of EN503A (10, 20, 40, 80, 160 mM) injected on the F508del-CFTR biosensor with lipids. White and black arrows: start and end of the injections, respectively.* ***B, C)*** *Representative steady-state analysis of the indicated compounds injected (at 10, 20, 40, 80, 160 mM) onto the F508del-CFTR biosensor in the presence of lipids.* ***D)*** *Binding of the indicated compounds (at 7.5 mM) to a biosensor containing F508del-NBD1. The data shown are the result ± s.d. of 5 independent experiments.*

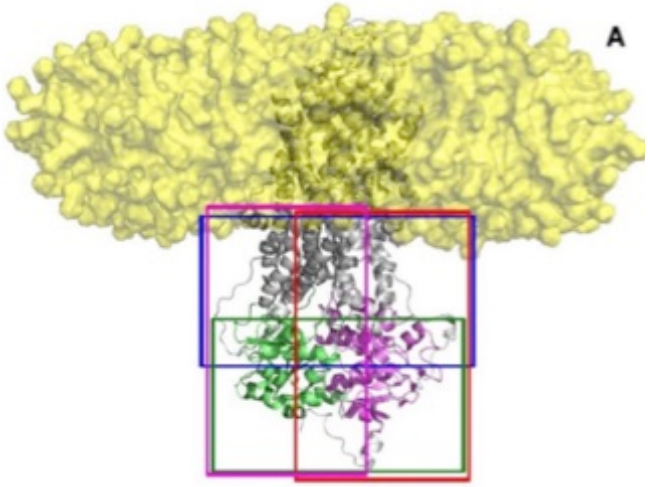
A

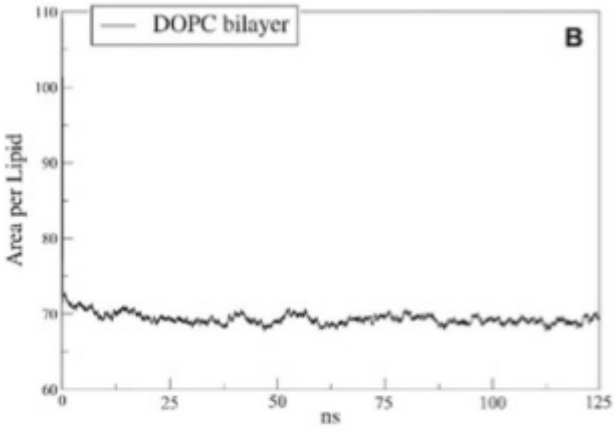
DOPC bilayer
B
Area per Lipid
ns

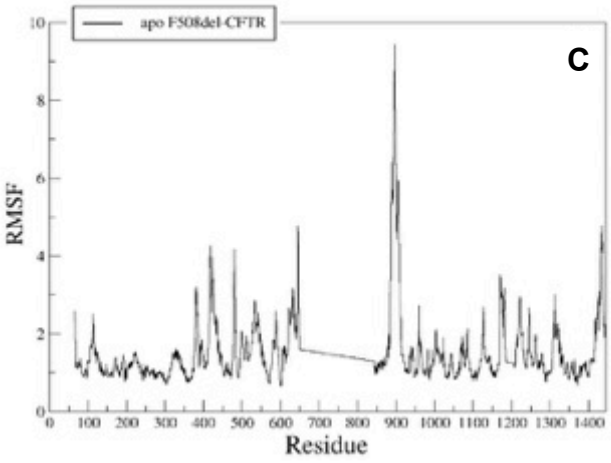
apo F508del-CFTR
C
RMSF
Residue

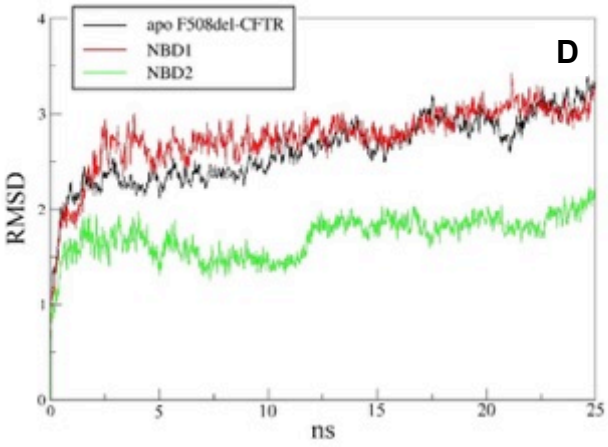
apo F508del-CFTR
NBD1
NBD2
D
RMSD
ns

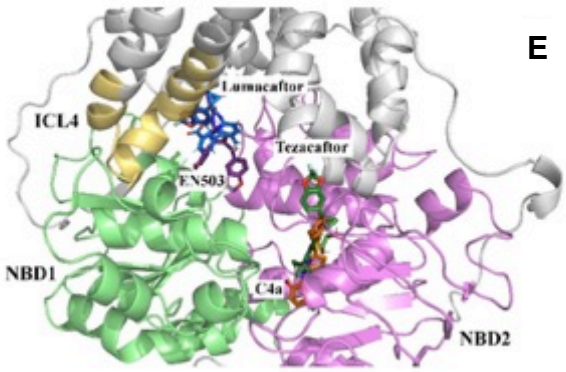
E
Lumacaftor
ICL4
Tezacaftor
F/N503
NBD1
C4a
NBD2

Fig. 5: Apo F508del-CFTR cluster, MDS trajectory analysis and docking poses of data-set. ***A)*** *F508del-CFTR is shown as cartoon, transmembrane domains in grey, NBD1 and NBD2 in green and violet, respectively. The lipids are in yellow. Red box delimits the NBD1-MSDs region partially overlapping NBD2-MSDs, purple box the NBD2-MSDs region partially overlapping NBD1-MSDs, green box the NBD1-NBD2 region and blue box the MSDs, NBD1 and NBD2 region.* ***B)*** *Area per lipid along the trajectory.* ***C)*** *RMSF of F508del-CFTR apo.* ***D****) RMSD of F508del-CFTR apo, NBD1 and NBD2.* ***E)*** *Docking Poses of compounds into apo F508del-CFTR. Lumacaftor (blue), Tezacaftor (dark green), C4a (orange) and EN503A (purple) are shown as stick, NBD1 (green), NBD2 (violet), ICL4 (gold) as cartoon.*

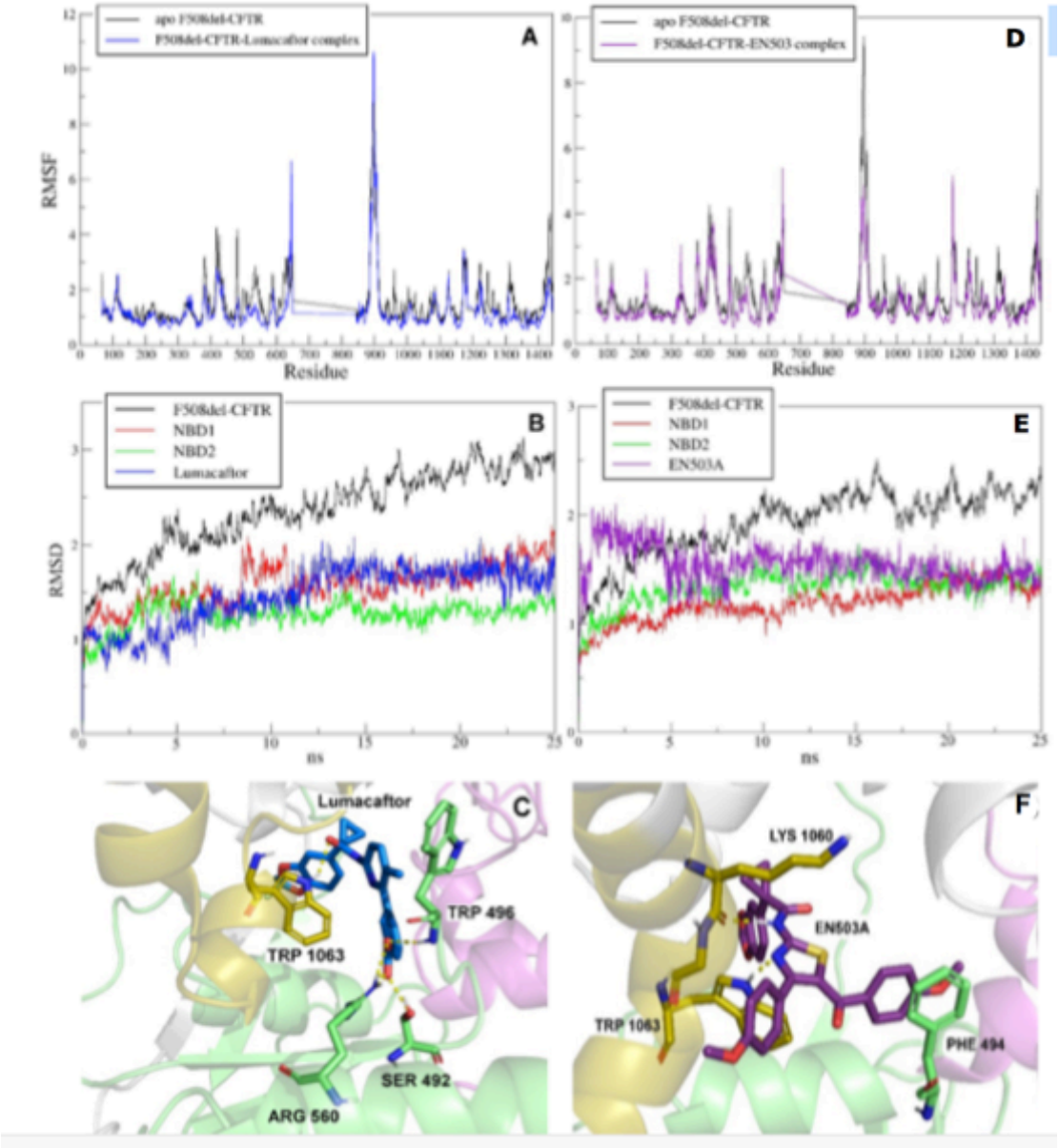

Fig. 6: MDS trajectory analysis of F508del-CFTR/Lumacaftor (A-C) and F508del-CFTR/EN503A ***(D-F) complexes. A)*** *RMSF of F508del-CFTR apo and F508del-CFTR/Lumacaftor complex.* ***B)*** *RMSD of complexed F508del-CFTR, NBD1, NBD2 and Lumacaftor****. C)*** *MDS interactions of Lumacaftor (blue) with the indicated residues of NBD1 (green) and ICL4 (gold).* ***D)*** *RMSF of F508del-CFTR apo and F508del-CFTR/EN503A complex.* ***E)*** *RMSD of complexed F508del-CFTR, NBD1, NBD2 and EN503A.* ***F)*** *Interactions of EN503A (purple) with the indicated residues of ICL4 (gold) and NBD1 (green). In* ***C*** *and* ***F****, compounds and residues are shown as stick, H-bonds as dot lines.*

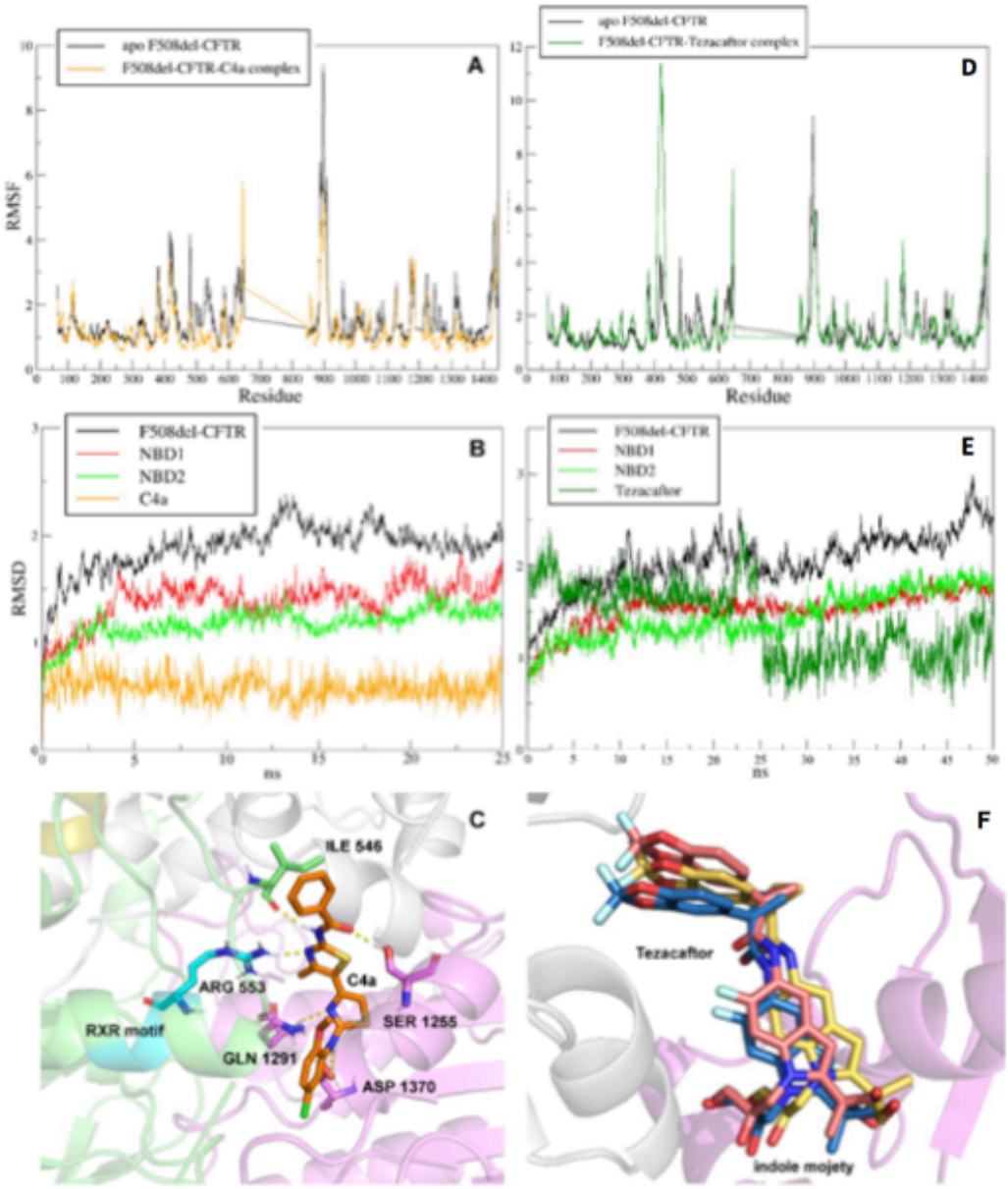

Fig. 7: MDS trajectory analysis of F508del-CFTR/C4a (A-C) and F508del-CFTR/Tezacaftor (D-F) complexes. ***A)*** *RMSF of F508del-CFTR apo and F508del-CFTR/C4a complex.* ***B)*** *RMSD of complexed F508del-CFTR, NBD1, NBD2 and C4a.* ***C)*** *Interactions of C4a (orange) with the indicated residues of NBD2 (purple), NBD1 (green) and RXR motif (aqua).* ***D)*** *RMSF of F508del-CFTR apo and F508del-CFTR/C4a complex.* ***E)*** *RMSD of complexed F508del-CFTR, NBD1, NBD2 and Tezacaftor.* ***F)*** *Tezacaftor binding poses (teal, yellow and coral) are shown in NBD2 binding pocket (violet). The poses obtained by cluster analysis highlight the indole moiety swinging. In* ***C*** *and* ***F****, compounds and residues are shown as stick, H-bonds as dot lines.*

compound	human intact D508-CFTR		mouse D508-NBD1
	with lipids	without lipids*	**
Lumacaftor	72.8 ± 19.5 (7)	>25,000 (2)	24.2 ± 6.2
C4a	18.6 ± 8,6 (3)	>25,000 (2)	no binding
4	146.6 ± 61 (5)	> 1,000 (2)	99.3 ± 14.5
5	19.7 ± 3.3 (4)	> 1,000 (2)	40.3 ± 2.5
6	44.1 ± 10.2 (9)	> 1,000 (2)	197.9 ± 4.5
7	4.5 ± 2.1 (6)	>1,000 (2)	no binding
Tezacaftor	206,1 ± 11,3 (3)	not determined	no binding
EN503A	9.2 ± 2.8 (3)	not determined	not determined

*Tab. 1. Binding of the compounds to F508del-CFTR immobilized in the presence or in the absence of lipids. Kd values are reported in mM. The number of repeated independent calculations (performed on two-three distinct sensorchips) are indicated in brackets. * Values of Kd predicted by the BIAEVALUATION software. ** As a comparison, the Kd values of the binding of the compounds to mouse D508-NBD1 published in [17] are reported.*

Computational studies

SPR-generated binding data can greatly profit from computational studies and vice versa [41]. In the field of CF, we have found a good consensus between computational predictions and SPR binding data based on F508del-NBD1 [17]. On these bases, we decided to develop a new *ad-hoc* computational model of the whole human F508del-CFTR in a lipid environment, to perform virtual docking and MDS with the compound data-set and to compare the predictions with the results generated by SPR with the F508del-CFTR biosensor.

The previously described F508del-CFTR model without R-domain and spanning residue from 646 to 841 [23] was here further developed (Fig. 5A). A lipid bilayer was created and its stability evaluated calculating the area per lipid parameter, obtaining an average value of 69,43 $Å^2$/lipid (Fig. 5B). F508del-CFTR embedded in the stabilized DOPC environment was subjected to a 25ns MDS to obtain a stable starting simulation system. The stability of the protein was evaluated through trajectory analysis Root Mean Square Fluctuation (RMSF) and RMSD.

RMSF of F508del-CFTR apo shows that the most flexible residues span from 885 to 912, corresponding to an extracellular loop distinct from the intracellular portion of our interest. NBD1 (residues 423-646) shows a higher average fluctuation than NBD2 (residues 1210-1443), while the MSDs are well embedded in the lipids, showing a low fluctuation (Fig. 5C).

RMSD was carried out from the first frame of the simulation using the backbone atoms (Cα, C, N) of the protein except for regions 404-437 (H1b and H1c, with highly flexibility [42]), 623-646 (NBD1 C-terminus), 885-912 (solvent-exposed extracellular loop), 1166-1186 (extended loop between TM12 and NBD2) and 1414-1445 (C-terminus). Taking into account the complexity of F508del-CFTR, the protein remains stable during the simulation, while NBD1 and NBD2 stability is reached after 12ns (Fig. 5D).

Based on RMSD results, cluster analysis was performed using the frames between 12.5 and 22.5ns. CFTR being a multi-domain protein, this analysis was performed considering functional domains described in Fig. 5A. A visual inspection of all collected clusters produced a total of 17 conformations on which the CASTp web server [43] was executed to identify those binding pockets included in the intracellular space of the protein. Compounds volume was evaluated through the web server Molecular Volume Calculator [44] obtaining:

341.396 Å^3 for Lumacaftor, 395.021 Å^3 for Tezacaftor and 412.128 Å^3 for EN503A. All pockets with a volume smaller that 200 Å^3 were thus discarded along with those not in the region of interest (i.e. the lipid bilayer or the extracellular portion). 75 pockets were eventually selected and subjected to Autodock Vina docking studies with the compounds. A total of 7,370 poses were obtained, that were ranked and filtered to reduce their number, progressively to 254 by ΔG, 78 by cluster analysis, 47 by visual inspection, and finally to 12 by data integration with literature. These were then subjected to 25ns MDS with the compounds to evaluate their stability and binding mode with F508del-CFTR, considering only the stable complexes. As shown in Fig. 5E, Lumacaftor and EN503A dock in a pocket at the NBD1-ICL4 interface, while C4a and Tezacaftor dock in NBD2.

Trajectory analysis shows a RMSF of the Lumacaftor-bound protein with an average fluctuation value that is lower than that of the apo form, indicating that F508del-CFTR gains stability when complexed (Fig. 6A). RMSD of the F508del-CFTR/Lumacaftor complex (Fig. 6B) shows that it reaches stability at 12ns (see Fig. 5C), with deviations for the whole protein, its NBD modules and Lumacaftor reported in Tab. 2.

Interaction studies highlight three strong H-bonds between Lumacaftor and S_{492}, W_{496}, R_{560} of NBD1 (Fig. 6C) with 88%, 81.5 % and 78% of time persistence, respectively, and one H-bond with W_{1063} of ICL4 with a lower persistence (53%). Lumacaftor is strongly anchored by a salt bridge between its carboxylic group and R_{560} plus additional H-bonds with the S_{492} side chain and W_{496} nitrogen backbone. A further H-bond is formed by the amidic carbonyl oxygen and W_{1063} nitrogen. Lipophilic interactions involve W_{401}, F_{490}, F_{494}, K_{1060} ,W_{1063} and aromatic and heteroaromatic rings of Lumacaftor, in particular pi-pi interactions (data not shown). These prediction are supported by recent experimental data suggesting a binding pocket for Lumacaftor between NBD1 and ICL4 [22].

RMSF demonstrates a higher stability of the F508del-CFTR also when complexed with EN503A (Fig. 6D). Accordingly, RMSD shows that the complex reaches its stability at 10ns, with values similar to those displayed by Lumacaftor (Tab. 2 and Fig. 6E). EN503A fully overlaps the common portion of the scaffold with Lumacaftor and shares the same H-bond interaction with W_{1063} (66% persistence). EN503A shows H-bonds also with K_{1060} (75% persistence), plus a by pi-pi interaction with F_{494} from 4 to 4,5 Å (Fig. 6F). Further hydrophobic

contacts involve S_{169}, W_{401}, V_{1345} residues and the dioxolphenyl portion of EN503A. W_{496}, G_{1061}, F_{1294} residues are involved instead with methoxyphenyl and methoxybenzoil rings of the ligand. The H-bonds between EN503A and the protein involve K_{1060} carbonyl oxygen and the amidic nitrogen of the compound, while the nitrogen of W_{1063} indole nucleus is engaged in an H-bond with the nitrogen of the tiazolic ring of the compound. The W_{1063} interaction is formed after 10ns and it is retained along all MDS.

For the F508del-CFTR/C4a complex, RMSF shows a lower fluctuation value than the apo form (Fig. 7A) and, again, RMSD indicates that the complex reaches its stability at 4ns (Tab. 2 and Fig. 7B). Trajectory analysis of the complex shows that C4a creates five H-bonds with I_{546} and R_{553} of NBD1 and S_{1255}, Q_{1291} and D_{1370} of NBD2 (Fig. 7C) with persistence equal to 96%, 81%, 94%, 80% and 92%, respectively. C4a makes also hydrophobic interactions with P_{1290} and the first aminoarylthiazole ring of the ligand plus Y_{1219} and L_{1261} with C4a benzylic ring. Other H-bonds are N_{1370} side chain with the aminic nitrogen, Q_{1291} side chain and the heterocyclic nitrogen of the first thyazolic ring, R_{553} side chain and the heterocyclic nitrogen of the sub-sequent thyazolic ring, I_{546} backbone and the amidic nitrogen and S_{1255} side chain with the carbonyl oxygen of the amidic group.

At variance with the other compounds, Tezacaftor/F508del-CFTR complex shows a RMSF comparable to the apo form (Fig. 7D). RSMD shows that the whole protein and the two NBDs reach their stability only at 10ns, before the ligand, which retains a first stable pose from 5 to 20ns by means of an H-bond with R_{553}. This pose is however subsequently lost, becoming unstable (Fig. 7E). After 25ns, Tezacaftor gains again a partial stable pose, but with the substituted indole moiety of the molecule still swinging inside the binding pocket (Fig. 7F). For this reason MDS of Tezacaftor complex were extended until 50ns. Additional H-bonds were not determined but the ligand makes hydrophobic interactions with M_{691}, I_{546} and the substituted dioxolphenyl portion, while the indole moiety interacts with L_{1254} and L_{1260}.

Effects of the compounds on CFTR stability and trafficking defects

As already mentioned, once identified by SPR and further characterized by computational studies, a putative CF drug needs to be assayed for its effective capacity to stabilize the mutated CFTR and to rescue its activity. To this aim, in a

first series of experiments, we used the fluorescence-based thermostability assay already exploited to study Lumacaftor [27]. As shown in Fig. 8A, both compounds show some stabilizing effect on the protein at low concentrations and low temperature with a lower overall labelling of surface-exposed Cys residues at moderate temperatures indicated by the reduced CPM fluorescence. At the high temperature unfolding transitions, both compounds show a concentration-dependent broadening of the transition which appears to be of greater magnitude for Tezacaftor. A similar unfolding behaviour, with a low temperature pre-transition followed by a large broad higher temperature unfolding transition, has been already detected for a related protein (ABCB1/P-glycoprotein) [45, 46]. Hence, the binding of Tezacaftor and EN503A can be detected by the CPM assay, but their effects on the stability of CFTR are complex and temperature-dependent. However, at temperatures similar to physiological, both compounds exert a slight stabilising effect.

To correlate the CFTR binding and stabilizing capacity of the compounds to their rescuing activity, we exploited the YFP functional assay in F508del-CFTR CFBE41o-cells [34]. As shown in Fig. 8B, Lumacaftor exerts a rescuing activity with slightly higher potency than that of Tezacaftor (ED_{50} = 160 and 220 nM, respectively). Interestingly, the new hybrid compound EN503A shows the most potent F508del-CFTR-rescuing activity (ED_{50} = 80 nM).

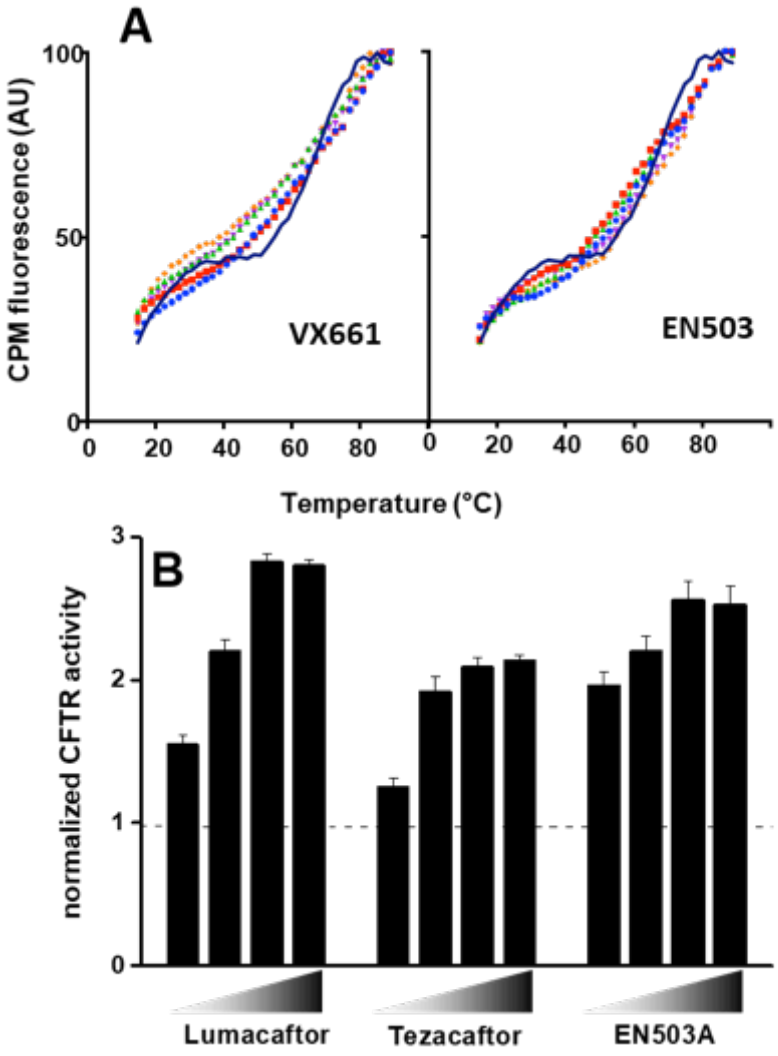

Fig. 8: A) Effect of Tezacaftor and EN503A on CFTR stability. *Increasing concentrations of the two compounds were evaluated. Blue circles: 10 μM; red squares 40 μM; green triangles: 80 μM; purple inverted triangles: 120 μM; orange diamonds: 180 μM.* ***B) Activity of compounds as correctors.*** *The bar graphs report F508del-CFTR activity in CFBE41o-cells after treatment with the indicated compounds for 24 h at 0.08, 0.4, 2.0 and 10 mM. The dashed line indicates the level of activity in cells treated with vehicle alone. The data shown are the result ± s.d. of 3 independent experiments.*

	whole protein	NBD1	NBD2	compound
F508del-CFTR apo	2.0-3.0	2.5-3.0	1.5-2.0	//
F508del-CFTR/Lumacaftor	2.0-3.0	1.5-2.0	1.0-1.5	1.5-2.0
F508del-CFTR/C4a	~ 2.0	1.0-1.5	1.0-1.5	~ 0.5
F508del-CFTR/Tezacaftor	2.0-3.0	~ 1.5	~ 1.5	1.0-2.0
F508del-CFTR/EN503A	2.0-2.5	1.0-1.5	1.0-1.5	1.0-1.5

Tab. 2. RMSD of F508del-CFTR in its apo form or complexed with the compounds. *The values (in Å) of deviation of F508del-CFTR, NBD1, NBD2 and correctors during MD simulation are reported.*

Discussion

The development of drugs targeting F508del-CFTR can be considered still in its infancy, with plenty of work to do to identify new active compounds. Also, for each new drug, and even for some old ones, a detailed characterization of their binding mode and molecular mechanisms of action is required. To achieve these goals, new computational and biochemical models are essential to reproduce closely the physiological conditions.

Biosensors are widely exploited in biomedical research. Unfortunately, surface-immobilization of a protein can cause the loss of its correct fold or can mask binding domains [47, 48], this being more probable for proteins as large as CFTR, whose 3D structure also depend on its association to cell membranes. Because of this complexity, the CFTR-related biosensors developed previously have been prepared only with isolated domains of the protein (mainly NBD1) [10-20], limiting the validity of such analyses.

It has been shown to be possible to immobilize seven-spanning membrane receptors on a SPR sensorchip in an oriented way, to reconstitute a membrane environment and to perform valuable binding analyses [49-51]. In parallel, a recombinant form of the human intact F508del-CFTR has been made available [24-27]. Taking advantage of this knowledge, here we generated a biosensor containing the F508del-CFTR in a membrane-like environment.

QCM-D suggests that, on the hydrophilic carboxy-methyl dextran surface, the lipids organize a layer of vesicular nanostructures/patches that, bearing a high density of F508del-CFTR in a proper membrane-like environment, allows the characterization of its binding to our compound test set. Lipids are required for saturable binding of drugs to F508del-CFTR. Indeed, when immobilized in their absence, F508del-CFTR binds to Lumacaftor in a non-specific, non-saturable manner, suggesting that, without the stabilizing membrane-like environment, the protein loses its 3D structure and hence its specific binding pockets. Lumacaftor has been however shown to bind in a saturable manner to isolated F508del-NBD1 immobilized by simple amine coupling [17], implying that the isolated module does not require the lipids to retain its correct 3D.

The antibody-mediated capture here adopted leads to the immobilization of a limited amount of F508del-CFTR (350 RU) that is about 30 times lower than that obtained by amine coupling immobilization of NBD1 (11,000 RU) [17]. Despite this, the new biosensor with F508del-CFTR in lipid environment provides

meaningful and reproducible binding data, further indicating that the (relatively) low amount of protein is present on the surface in a properly oriented way, available for binding with putative drugs. It is also worth to note that, as expected, the lipids present on the sensorchip surface aspecifically sequester a big amount of the lipophilic compounds (as shown for Lumacaftor in Fig. 3A) without however hampering the unmasking of the specific binding to immobilized F508del-CFTR.

Due to compounds hydrophobicity, DMSO is required in the buffer used in the SPR analysis. Despite its complex architecture and the presence of lipids, the F508del-CFTR biosensor can be used in the presence of DMSO. This is in agreement with the observation that the DMSO-containing buffer used for SPR does not destabilize CFTR (Fig. 2C) and with similar rhodopsin biosensor [50]. The compatibility with DMSO, and thus the possibility to study small water-insoluble chemical compounds, is mandatory for the first steps of any drug discovery process, including that for a CF drug.

Here, the F508del-CFTR biosensor has been exploited to characterize a large compound test set (see section 2.1 and Fig. 1). All the compounds bound to the F508del-CFTR biosensor, including C4a, compound 7 and Tezacaftor, that do not bind to a biosensor containing the isolated NBD1 module, indicating that the F508del-CFTR biosensor represents a new tool endowed with a broader screening capacity with respect to the previous ones.

Compound 6 binds to the human intact F508del-CFTR with an affinity that is 5 times higher than that measured for the isolated NBD1. It is tentative to hypothesize that, beside its binding to NBD1, in the complex structure of the intact protein, compound 6 finds additional points of contact that stabilize the interaction increasing its affinity. Further computational studies are required to substantiate this hypothesis.

Surprisingly instead, Lumacaftor and compound 4 bind to the human intact F508del-CFTR with affinities that are slightly lower than those measured for the isolated NBD1. This can be due to structural differences existing between the two proteins (that are of human and murine origin, respectively) or to the exposure of artefactual binding surface on the isolated NBD1 that are instead absent in the intact protein.

Beside the comparison between the binding data generated by biosensors containing NBD1 alone or the intact F508del-CFTR, it is equally important to

compare the binding data with virtual predictions: Computational studies predicted Lumacaftor and EN503A to share the same binding pocket, interacting with residues of NBD1 and ICL4 through a similar network. Important to note however, only EN503A sets up pi-pi interactions with residue F_{494} of the NBD1 Q-loop, a residue that is crucial for NBD1-NBD2 dimerization [52]. This can be tentatively related to the higher F508del-CFTR rescuing capacity of EN503A with respect to Lumacaftor and, more in general, to the other compounds here tested. In agreement previous reports [53] and with SPR data, our computational studies predicted C4a to bind to NBD2, with a stable H-bond network and involving R_{553} of the RXR motif, a residue that plays an important role in the correct folding and stability of F508del-CFTR [54]. Similar binding features were observed for Tezacaftor, which displays however only a partially stable pose during the MDS. This can be related to the high Kd values calculated by SPR for Tezacaftor/F508del-CFTR interaction. Relevant to this point, it has been proposed that a low affinity binding can effectively generate an unstable pose during MDS [55]. Also, the inability of Tezacaftor to decrease F508del-CFTR fluctuation and its swinging binding mode could be associated to its behaviour in the thermostability assay, where it exerts a negative effect when assayed at high doses. Importantly, this is the first experimental characterization of Tezacaftor binding to F508del-CFTR, despite extensive study for its F508del-CFTR-rescuing effect.

Beside computational prediction, the binding data generated with the F508del-CFTR biosensor are in agreement also with the results from the biological assay. Indeed, the F508del-CFTR-rescuing activity of EN503A is significantly higher than those of control compounds, being thus correlated to its F508del-CFTR binding affinity, that is 7 and 20 times higher than that of Lumacaftor and Tezacaftor, respectively. Thus, EN503A emerges as a new F508del-CFTR corrector endowed with both a high affinity and F508del-CFTR-rescuing activity, thus representing an interesting compound to be further developed as a CF drug.

Conclusions

Novel CF drugs are eagerly awaited, a goal that requires appropriate computational and experimental models closely resembling the physiological conditions. Here, we have developed a new biosensor containing the human intact F508del-CFTR in a membrane-like environment that turned out to be

endowed with a broad screening capacity, allowing the identification of binders that would have been otherwise lost with previous biosensors prepared with isolated module(s) of the protein. The F508del-CFTR has been then integrated in a pipeline of analyses made up of well-established biochemical and biological assay flanked to an *ad hoc* computational model. A good consensus was found among the results obtained within the pipeline suggesting the F508del-CFTR biosensor as an "ideal bridge" between computational studies and biochemical/biological modelst functional to the identification and understanding of the mechanism of action of novel putative CF drugs.

Acknowdgements

This work was supported by: Fondazione Italiana Fibrosi Cistica (FFC, Delegation of Turin) FFC#11/2018 to MR, PF and AO; FFC #6/2017 (Delegation of Verona Valpolicella) to EM; Italian Ministry of Health "Cinque per mille" and Ricerca Corrente (Linea1) to NP; MIUR PON ELIXIR "CNR-BiOmics and PB05", "InterOmics" to AO; Cystic Fibrosis Trust (F508del SRC) and Cystic Fibrosis Foundation (FORD13XX0) to RCF.
MU is recipient of a fellowship by FFC.
We wish to thank for her technical assistance Dr. Michela Corsini (University of Brescia), recipient of a fellowship for technicians by FFC and Prof. Eugenio Monti (University of Brescia) for helpful discussion.

References

[1] X. Meng, J. Clews, E.R. Martin, A.D. Ciuta, R.C. Ford, The structural basis of cystic fibrosis, Biochemical Society transactions (2018).
[2] C.M. Farinha, E. Miller, N. McCarty, Protein and lipid interactions - Modulating CFTR trafficking and rescue, Journal of cystic fibrosis : official journal of the European Cystic Fibrosis Society 17(2S) (2018) S9-S13.
[3] J.S. Elborn, Cystic fibrosis, Lancet 388(10059) (2016) 2519-2531.
[4] M.C. Dechecchi, A. Tamanini, G. Cabrini, Molecular basis of cystic fibrosis: from bench to bedside, Annals of translational medicine 6(17) (2018) 334.

[5] I. Callebaut, P.A. Chong, J.D. Forman-Kay, CFTR structure, Journal of cystic fibrosis : official journal of the European Cystic Fibrosis Society 17(2S) (2018) S5-S8.
[6] T.C. Hwang, J.T. Yeh, J. Zhang, Y.C. Yu, H.I. Yeh, S. Destefano, Structural mechanisms of CFTR function and dysfunction, The Journal of general physiology 150(4) (2018) 539-570.
[7] H.A. Lewis, X. Zhao, C. Wang, J.M. Sauder, I. Rooney, B.W. Noland, D. Lorimer, M.C. Kearins, K. Conners, B. Condon, P.C. Maloney, W.B. Guggino, J.F. Hunt, S. Emtage, Impact of the deltaF508 mutation in first nucleotide-binding domain of human cystic fibrosis transmembrane conductance regulator on domain folding and structure, The Journal of biological chemistry 280(2) (2005) 1346-53.
[8] M. Rusnati, P. Chiodelli, A. Bugatti, C. Urbinati, Bridging the past and the future of virology: surface plasmon resonance as a powerful tool to investigate virus/host interactions, Critical reviews in microbiology 41(2) (2015) 238-60.
[9] M. Rusnati, M. Presta, Angiogenic growth factors interactome and drug discovery: The contribution of surface plasmon resonance, Cytokine & growth factor reviews 26(3) (2015) 293-310.
[10] P. Trouve, M.A. Le Drevo, M. Kerbiriou, G. Friocourt, Y. Fichou, D. Gillet, C. Ferec, Annexin V is directly involved in cystic fibrosis transmembrane conductance regulator's chloride channel function, Biochimica et biophysica acta 1772(10) (2007) 1121-33.
[11] T.S. Scott-Ward, M.D. Amaral, Deletion of Phe508 in the first nucleotide-binding domain of the cystic fibrosis transmembrane conductance regulator increases its affinity for the heat shock cognate 70 chaperone, The FEBS journal 276(23) (2009) 7097-109.
[12] A. Premchandar, A. Kupniewska, A. Bonna, G. Faure, T. Fraczyk, A. Roldan, B. Hoffmann, M. Faria da Cunha, H. Herrmann, G.L. Lukacs, A. Edelman, M. Dadlez, New insights into interactions between the nucleotide-binding domain of CFTR and keratin 8, Protein science : a publication of the Protein Society 26(2) (2017) 343-354.
[13] G. Faure, N. Bakouh, S. Lourdel, N. Odolczyk, A. Premchandar, N. Servel, A. Hatton, M.K. Ostrowski, H. Xu, F.A. Saul, C. Moquereau, S. Bitam, I. Pranke, G. Planelles, J. Teulon, H. Herrmann, A. Roldan, P. Zielenkiewicz, M. Dadlez, G.L. Lukacs, I. Sermet-Gaudelus, M. Ollero, P.J. Corringer, A. Edelman, Rattlesnake Phospholipase A2 Increases CFTR-Chloride Channel Current and Corrects

F508CFTR Dysfunction: Impact in Cystic Fibrosis, Journal of molecular biology 428(14) (2016) 2898-915.
[14] J. Colas, G. Faure, E. Saussereau, S. Trudel, W.M. Rabeh, S. Bitam, I.C. Guerrera, J. Fritsch, I. Sermet-Gaudelus, N. Davezac, F. Brouillard, G.L. Lukacs, H. Herrmann, M. Ollero, A. Edelman, Disruption of cytokeratin-8 interaction with F508del-CFTR corrects its functional defect, Human molecular genetics 21(3) (2012) 623-34.
[15] L.A. Borthwick, M. Kerbiriou, C.J. Taylor, G. Cozza, I. Lascu, E.H. Postel, D. Cassidy, P. Trouve, A. Mehta, L. Robson, R. Muimo, Role of Interaction and Nucleoside Diphosphate Kinase B in Regulation of the Cystic Fibrosis Transmembrane Conductance Regulator Function by cAMP-Dependent Protein Kinase A, PloS one 11(3) (2016) e0149097.
[16] F. Borot, D.L. Vieu, G. Faure, J. Fritsch, J. Colas, S. Moriceau, M. Baudouin-Legros, F. Brouillard, J. Ayala-Sanmartin, L. Touqui, M. Chanson, A. Edelman, M. Ollero, Eicosanoid release is increased by membrane destabilization and CFTR inhibition in Calu-3 cells, PloS one 4(10) (2009) e7116.
[17] M. Rusnati, D. Sala, A. Orro, A. Bugatti, G. Trombetti, E. Cichero, C. Urbinati, M. Di Somma, E. Millo, L.J.V. Galietta, L. Milanesi, P. Fossa, P. D'Ursi, Speeding Up the Identification of Cystic Fibrosis Transmembrane Conductance Regulator-Targeted Drugs: An Approach Based on Bioinformatics Strategies and Surface Plasmon Resonance, Molecules 23(1) (2018).
[18] A.K. Gakhal, T.J. Jensen, Z. Bozoky, A. Roldan, G.L. Lukacs, J. Forman-Kay, J.R. Riordan, S.S. Sidhu, Development and characterization of synthetic antibodies binding to the cystic fibrosis conductance regulator, mAbs 8(6) (2016) 1167-76.
[19] K.M. Weixel, N.A. Bradbury, Mu 2 binding directs the cystic fibrosis transmembrane conductance regulator to the clathrin-mediated endocytic pathway, The Journal of biological chemistry 276(49) (2001) 46251-9.
[20] J.H. Lee, W. Richter, W. Namkung, K.H. Kim, E. Kim, M. Conti, M.G. Lee, Dynamic regulation of cystic fibrosis transmembrane conductance regulator by competitive interactions of molecular adaptors, The Journal of biological chemistry 282(14) (2007) 10414-22.
[21] O. Laselva, S. Molinski, V. Casavola, C.E. Bear, Correctors of the Major Cystic Fibrosis Mutant Interact through Membrane-Spanning Domains, Molecular pharmacology 93(6) (2018) 612-618.

[22] R.P. Hudson, J.E. Dawson, P.A. Chong, Z. Yang, L. Millen, P.J. Thomas, C.G. Brouillette, J.D. Forman-Kay, Direct Binding of the Corrector VX-809 to Human CFTR NBD1: Evidence of an Allosteric Coupling between the Binding Site and the NBD1:CL4 Interface, Molecular pharmacology 92(2) (2017) 124-135.
[23] L. Belmonte, O. Moran, On the interactions between nucleotide binding domains and membrane spanning domains in cystic fibrosis transmembrane regulator: A molecular dynamic study, Biochimie 111 (2015) 19-29.
[24] N. Pollock, N. Cant, T. Rimington, R.C. Ford, Purification of the cystic fibrosis transmembrane conductance regulator protein expressed in Saccharomyces cerevisiae, Journal of visualized experiments : JoVE (87) (2014).
[25] E. Hildebrandt, Q. Zhang, N. Cant, H. Ding, Q. Dai, L. Peng, Y. Fu, L.J. DeLucas, R. Ford, J.C. Kappes, I.L. Urbatsch, A survey of detergents for the purification of stable, active human cystic fibrosis transmembrane conductance regulator (CFTR), Biochimica et biophysica acta 1838(11) (2014) 2825-37.
[26] L. O'Ryan, T. Rimington, N. Cant, R.C. Ford, Expression and purification of the cystic fibrosis transmembrane conductance regulator protein in Saccharomyces cerevisiae, Journal of visualized experiments : JoVE (61) (2012).
[27] X. Meng, Y. Wang, X. Wang, J.A. Wrennall, T.L. Rimington, H. Li, Z. Cai, R.C. Ford, D.N. Sheppard, Two Small Molecules Restore Stability to a Subpopulation of the Cystic Fibrosis Transmembrane Conductance Regulator with the Predominant Disease-causing Mutation, The Journal of biological chemistry 292(9) (2017) 3706-3719.
[28] X. Meng, J. Clews, A.D. Cuitaa, E.R. Martin, R.C. Ford, CFTR structure, stability, function and regulation, Biological chemistry (2018).
[29] K.W. Peters, T. Okiyoneda, W.E. Balch, I. Braakman, J.L. Brodsky, W.B. Guggino, C.M. Penland, H.B. Pollard, E.J. Sorscher, W.R. Skach, P.J. Thomas, G.L. Lukacs, R.A. Frizzell, CFTR Folding Consortium: methods available for studies of CFTR folding and correction, Methods in molecular biology 742 (2011) 335-53.
[30] G. Sauerbrey, Verwendung von Schwingquarzen zur Wägung dünner Schichten und zur Mikrowägung., *Zeitschrift für Phys.* 222 (1959) 206-222.
[31] C. Urbinati, A. Bugatti, P. Oreste, G. Zoppetti, J. Waltenberger, S. Mitola, D. Ribatti, M. Presta, M. Rusnati, Chemically sulfated Escherichia coli K5 polysaccharide derivatives as extracellular HIV-1 Tat protein antagonists, FEBS letters 568(1-3) (2004) 171-7.

[32] H.H. Trutnau, New multi-step kinetics using common affinity biosensors saves time and sample at full access to kinetics and concentration, Journal of biotechnology 124(1) (2006) 191-5.
[33] V. Tomati, E. Pesce, E. Caci, E. Sondo, P. Scudieri, M. Marini, F. Amato, G. Castaldo, R. Ravazzolo, L.J.V. Galietta, N. Pedemonte, High-throughput screening identifies FAU protein as a regulator of mutant cystic fibrosis transmembrane conductance regulator channel, The Journal of biological chemistry 293(4) (2018) 1203-1217.
[34] E. Pesce, M. Bellotti, N. Liessi, S. Guariento, G. Damonte, E. Cichero, A. Galatini, A. Salis, A. Gianotti, N. Pedemonte, O. Zegarra-Moran, P. Fossa, L.J. Galietta, E. Millo, Synthesis and structure-activity relationship of aminoarylthiazole derivatives as correctors of the chloride transport defect in cystic fibrosis, European journal of medicinal chemistry 99 (2015) 14-35.
[35] S. Jo, T. Kim, V.G. Iyer, W. Im, CHARMM-GUI: a web-based graphical user interface for CHARMM, Journal of computational chemistry 29(11) (2008) 1859-65.
[36] O. Trott, A.J. Olson, AutoDock Vina: improving the speed and accuracy of docking with a new scoring function, efficient optimization, and multithreading, Journal of computational chemistry 31(2) (2010) 455-61.
[37] R.P. Richter, R. Berat, A.R. Brisson, Formation of solid-supported lipid bilayers: an integrated view, Langmuir : the ACS journal of surfaces and colloids 22(8) (2006) 3497-505.
[38] R. Richter, A. Mukhopadhyay, A. Brisson, Pathways of lipid vesicle deposition on solid surfaces: a combined QCM-D and AFM study, Biophysical journal 85(5) (2003) 3035-47.
[39] C. Montis, S. Busatto, F. valle, A. Zendrini, A. Salvatore, Y. Gerelli, D. Berti, P. bergese, Biogenic Supported Lipid Bilayers from Nanosized Extracellular Vesicles, Advanced Biosystems 2 (2018) 1700200.
[40] H.X. Wu, M. Zhu, X.F. Xiong, J. Wei, K.Q. Zhuo, D.Y. Cheng, Efficacy and Safety of CFTR Corrector and Potentiator Combination Therapy in Patients with Cystic Fibrosis for the F508del-CFTR Homozygous Mutation: A Systematic Review and Meta-analysis, Advances in therapy 36(2) (2019) 451-461.
[41] X. Du, Y. Li, Y.L. Xia, S.M. Ai, J. Liang, P. Sang, X.L. Ji, S.Q. Liu, Insights into Protein-Ligand Interactions: Mechanisms, Models, and Methods, International journal of molecular sciences 17(2) (2016).

[42] H.A. Lewis, S.G. Buchanan, S.K. Burley, K. Conners, M. Dickey, M. Dorwart, R. Fowler, X. Gao, W.B. Guggino, W.A. Hendrickson, J.F. Hunt, M.C. Kearins, D. Lorimer, P.C. Maloney, K.W. Post, K.R. Rajashankar, M.E. Rutter, J.M. Sauder, S. Shriver, P.H. Thibodeau, P.J. Thomas, M. Zhang, X. Zhao, S. Emtage, Structure of nucleotide-binding domain 1 of the cystic fibrosis transmembrane conductance regulator, The EMBO journal 23(2) (2004) 282-93.
[43] W. Tian, C. Chen, X. Lei, J. Zhao, J. Liang, CASTp 3.0: computed atlas of surface topography of proteins, Nucleic acids research 46(W1) (2018) W363-W367.
[44] B. Jayaram, T. Singh, G. Mukherjee, A. Mathur, S. Shekhar, V. Shekhar, Sanjeevini: a freely accessible web-server for target directed lead molecule discovery, BMC bioinformatics 13 Suppl 17 (2012) S7.
[45] Z. Yang, Q. Zhou, L. Mok, A. Singh, D.J. Swartz, I.L. Urbatsch, C.G. Brouillette, Interactions and cooperativity between P-glycoprotein structural domains determined by thermal unfolding provides insights into its solution structure and function, Biochimica et biophysica acta. Biomembranes 1859(1) (2017) 48-60.
[46] A.T. Clay, P. Lu, F.J. Sharom, Interaction of the P-Glycoprotein Multidrug Transporter with Sterols, Biochemistry 54(43) (2015) 6586-97.
[47] C. You, J. Piehler, Functional protein micropatterning for drug design and discovery, Expert opinion on drug discovery 11(1) (2016) 105-19.
[48] G. Faccio, From Protein Features to Sensing Surfaces, Sensors 18(4) (2018).
[49] O.P. Karlsson, S. Lofas, Flow-mediated on-surface reconstitution of G-protein coupled receptors for applications in surface plasmon resonance biosensors, Analytical biochemistry 300(2) (2002) 132-8.
[50] I. Navratilova, M. Dioszegi, D.G. Myszka, Analyzing ligand and small molecule binding activity of solubilized GPCRs using biosensor technology, Analytical biochemistry 355(1) (2006) 132-9.
[51] C. Giagulli, A.K. Magiera, A. Bugatti, F. Caccuri, S. Marsico, M. Rusnati, W. Vermi, S. Fiorentini, A. Caruso, HIV-1 matrix protein p17 binds to the IL-8 receptor CXCR1 and shows IL-8-like chemokine activity on monocytes through Rho/ROCK activation, Blood 119(10) (2012) 2274-83.
[52] W.M. Rabeh, F. Bossard, H. Xu, T. Okiyoneda, M. Bagdany, C.M. Mulvihill, K. Du, S. di Bernardo, Y. Liu, L. Konermann, A. Roldan, G.L. Lukacs, Correction of both NBD1 energetics and domain interface is required to restore DeltaF508 CFTR folding and function, Cell 148(1-2) (2012) 150-63.

[53] T. Okiyoneda, G. Veit, J.F. Dekkers, M. Bagdany, N. Soya, H. Xu, A. Roldan, A.S. Verkman, M. Kurth, A. Simon, T. Hegedus, J.M. Beekman, G.L. Lukacs, Mechanism-based corrector combination restores DeltaF508-CFTR folding and function, Nature chemical biology 9(7) (2013) 444-54.
[54] P.A. Chong, P.J. Farber, R.M. Vernon, R.P. Hudson, A.K. Mittermaier, J.D. Forman-Kay, Deletion of Phenylalanine 508 in the First Nucleotide-binding Domain of the Cystic Fibrosis Transmembrane Conductance Regulator Increases Conformational Exchange and Inhibits Dimerization, The Journal of biological chemistry 290(38) (2015) 22862-78.
[55] K. Liu, H. Kokubo, Exploring the Stability of Ligand Binding Modes to Proteins by Molecular Dynamics Simulations: A Cross-docking Study, Journal of chemical information and modeling 57(10) (2017) 2514-2522.

Chapter 8.0

Assessment of fluorescent assays for F508del CFTR stability and the screening of FDA-approved and natural product compound libraries

Jack Clews[1,3], Xin Meng[1,2,3] and Robert C. Ford[1]

3. Faculty of Biology Medicine and Health, Michael Smith Building, University of Manchester, Oxford Rd, Manchester M13 9PL, UK
4. Current address: MRC Toxicology Unit, Hodgkin Building Lancaster Rd, Leicester LE1 9HN, UK.
5. These authors contributed equally to the work.

Keywords: Fluorescence, drug screening, cystic fibrosis, protein thermostability, F508del CFTR.

Abstract

The cystic fibrosis transmembrane conductance regulator (CFTR) is a membrane protein in the ABC transporter family that operates as an ATP-regulated chloride channel. Loss of CFTR function leads to cystic fibrosis, the most common inherited disease in humans of European origins. By far the most common disease-causing mutation is the deletion of phenylalanine at position 508 in the CFTR sequence (F508del). F508 deletion causes instability and the mutated protein is recognised by the ER quality control system and targeted for degradation. This study describes the use of fluorescence assays to probe the stability of the purified F508del CFTR protein. Two different assays were developed and employed to screen drug libraries for potential stabilisers and destabilisers of the

protein. This paper describes the benefits of the two assays and their potential drawbacks. Results are presented for the screening of two libraries of compounds: an FDA-approved drug library (1300 compounds) and a natural product library (130 compounds). The efficiency of the two screens are discussed and false positive and negative hits are identified and explained.

Introduction

The screening of drug libraries for discovery of compounds for the treatment of diseases is a major part of the activity of the pharmaceutical industry [1]. For example, an effective screen for the function of the CFTR protein has led to the development of new drugs that have proven efficacious for the treatment of cystic fibrosis (CF) [2-5]. The drugs that were discovered using this screen fall into different categories which are together important in the therapeutic strategy. The first type of drug to be developed was a potentiator that increased the likelihood of channel opening and was primarily targeted at patients with missense mutations such as G551D that had effects on the channel properties of the protein [6]. In the case of G551D the channel remains predominantly closed even after activation with protein kinase A (PKA) and the addition of ATP [7]. The second type of drug to be developed was a corrector that in some way stabilised defective forms of the protein and allowed such mutant forms to successfully reach the plasma membrane [2, 5, 6]. The most common CF-causing mutation (F508del), which is present in about 90% of patients, falls into this category [8]. Having reached the plasma membrane the activity of such mutant forms of the protein can be further enhanced by the addition of the potentiator compound [9].

More efficient corrector compounds have recently been developed such that it now appears likely that about 90% of the cystic fibrosis patients in the world could be treated with such pharmacotherapy [10-14]. However there are currently barriers to this strategy, primarily associated with the cost of the currently available drugs[15]. Moreover the patients are not cured but rather the condition is managed in this therapeutic strategy.

Hence at the moment it appears as though the patients will require the existing costly pharmacotherapy for their entire lives [16]. The F508del CFTR protein in patients that was previously present in minute amounts may now reach significant levels in the plasma membrane of cells in patients treated with the corrector compounds [17]. It is therefore important to understand the effects of routine medicinal and pharmaceutical compounds on mutant CFTR protein such as F508del CFTR, as well as the effects of FDA-approved drugs that may be used to treat CF patients for other diseases during their lives.

Indeed it is expected that any compounds will in fact more likely have a therapeutic, manageable effect. Largely because of the nature of F508del-CFTR, correction that not only rescues from the cell quality control machinery is needed, but potentiation and amplification of the rescued protein is required due to the increased turnover of the protein at the membrane. Therefore, the likelihood of a compound having restorative effects on the protein solving these three issues is unlikely. Indeed it is desired in the CFTR-pharmacological industry that a novel drug may have an increased correction affect allowing for greater synergistic, combination therapy than already exists. This paper desires to find a corrector that will fulfil the rescue of protein from the cell quality control machinery. Compounds that may fulfil the other two roles can be taken for further testing based on their predicted effect extrapolated from their stabilising or destabilising of the protein.

In order to allow such studies, production and purification of the F508del CFTR protein is required [18, 19] as well as the development of assays [20, 21] to study the effects of such compounds directly on the purified protein. Such studies would hopefully allow the identification of compounds that could act as destabilisers [22, 23] or stabilisers of the mutant protein. Two such assays based on the Cys-reactive compound CPM are described here. This compound is normally non-fluorescent or has low fluorescence in aqueous systems, but becomes intensely fluorescent upon formation of a covalent linkage with exposed Cys residues on the surface of proteins. Upon protein unfolding and denaturation, exposure of previously buried Cys residues allows further CPM binding to the protein and an increase of fluorescence that is a useful indicator of the stability of the protein. The

initial labelling with CPM (at low temperature used for CFTR purification) gives an idea of the initial folded status of the protein and this initial labelling value can be greatly increased by the addition of chaotropes such as guanidium HCl and urea [24]. The subsequent denaturation of the protein can be followed by monitoring the increase in CPM fluorescence as more previously buried Cys residues become exposed, and this allows the intrinsic thermostability of the protein to be assessed [25]. However the CPM fluorescence in a system containing F508del CFTR at a physiological temperature can also provide information about the long term stability of the protein at 37^{o}C, a temperature where F508del CFTR is known to lose function rapidly [25].

This paper describes the development of the CPM assay for screening small compound libraries in a 96-well or 48-capillary format for F508del CFTR-stabilising or destabilising compounds.

Methods

Protein

Protein purified according to Method section 2.9-11 (in this thesis) was used at a concentration of 200-1000ng according to Methods section 2.12. Due to batch to batch variability during the purification process, the concentration and stability of the protein would vary between batch and therefore separate runs of each assay are compared together.

CPM Dye

A cpm dye was used in both assays for measuring the stability of the protein. For reference, see Methods section 2.15 in this thesis.

48 Well Assay

The 48-capillary format assay was conducted using an “UNcle “ from UnChained labs. For each assay, the maximum number of wells for testing was 48 wells. Data in this paper includes batch formations with less than 48 data points due to some wells not being utilised for samples. Instead

these wells would be used for run validating negative controls (data points without protein and dye confirming that the fluorescence is not a false positive signal), or indeed the capillaries may not always be viable for use due to dust build up, presence of air bubbles in the sample or residue from a previous sample. In these cases, the data sets are included for each 'batch' - that is the number of samples tested in one run of the UNcle machine, due to variability between protein aliquots, therefore a dataset from this assay will have a maximum of 48 samples but may indeed be less.

CFTR protein would be incubated with the relevant compound for 15 minutes at 4°C prior to loading. CPM dye would be added during the loading process and each well would contain a different sample set.

The 48-capillary format assay was conducted in the same way as Methods 2.3 from [26] and the CFTR stability assay methods described in [27].

96 Well Assay

The 96-well assay was conducted using a BioTek Synergy H1 Multi-Mode Reader; purified hCFTR was exposed to the CPM dye at concentrations specified in Methods section 2.12 of this thesis and relevant compound in the plate reader with constant recording from the instrument.

Drug library

Both assays tested compounds from an FDA approved compound library provided by Apex BioTechnology. This library consisted of FDA approved compounds with a wide variety of pharmacological properties and targets including cystic fibrosis compounds developed by Vertex, VX-809, 661 and 770. Due to the blind nature of the testing process, these compounds from the library were not used as positive or negative controls.

The 96 well assay, due to its higher throughput nature, tested all compounds sequentially from that library. Whereas, the 48 well assay tested select compounds at random in a blind format. Both of the assays tested the compounds in singular repeats in order to maximise the throughput efficiency of the assays.

Results

Figure 1 shows a schematic description of the two different assays employed in this work. Panel a shows the expected features of the isothermal CFTR stability assay using CPM. At 37°C the F508del CFTR protein has Cysteine (Cys) residues in its structure that are exposed to the soluble environment and can therefore bind to the CPM dye and this leads to an initial rapid increase in CPM fluorescence followed by a slower increase due to the instability of the protein at the physiological temperature. In this assay the protein is finally denatured by a 1 hour incubation at 55°C and then the CPM fluorescence is measured. Any Cys residues not exposed at 37°C will become exposed and the fluorescence now reaches 100% of the maximum value. In the presence of a destabilising compound the fluorescence from CPM will rise more rapidly and may reach 100% of the maximum value indicating that the CFTR protein is completely denatured at 37°C. In this case, the CPM fluorescence actually decreases at 55°C due to thermal quenching. Thermal quenching occurs when the high temperatures cause complete unfolding of the protein leading to aggregation as the abundance of unfolded protein reacts into each other. This prevents the fluorescent signal from being accurately recorded via the machine leading to the phenomenon of thermal quenching. In the presence of a stabilising compound, indicated by the blue line in Figure 1, a slower increase in fluorescence at 37°C will be observed and proportionately larger shift to 100% labelling at 55°C.

The second assay as illustrated in Figure 1b is able to measure the thermostability of the CFTR protein. In this case the protein and CPM are heated in 10µL volume capillaries and the instrument is capable of

measuring the initial labelling of protein at low temperature as well as the midpoint temperature for thermal unfolding. For this assay the de-stabiliser may cause greater initial labelling as well as shift in the midpoint thermal unfolding temperature to lower values. Conversely a stabilising compound may reduce the amount of initial labelling and may shift to high temperatures the midpoint for thermal and folding. Note that in this assay there is also a phase in the fluorescence profile where it decreases, and again this is due to the thermal quenching of the CPM fluorescence.

The assay illustrated in Figure 1a is from a 96 well format and utilises every single compound from the library. Figure 1b uses a 48 well format and is used for a select amount of compounds chosen at random to reduce bias.

Figure 1

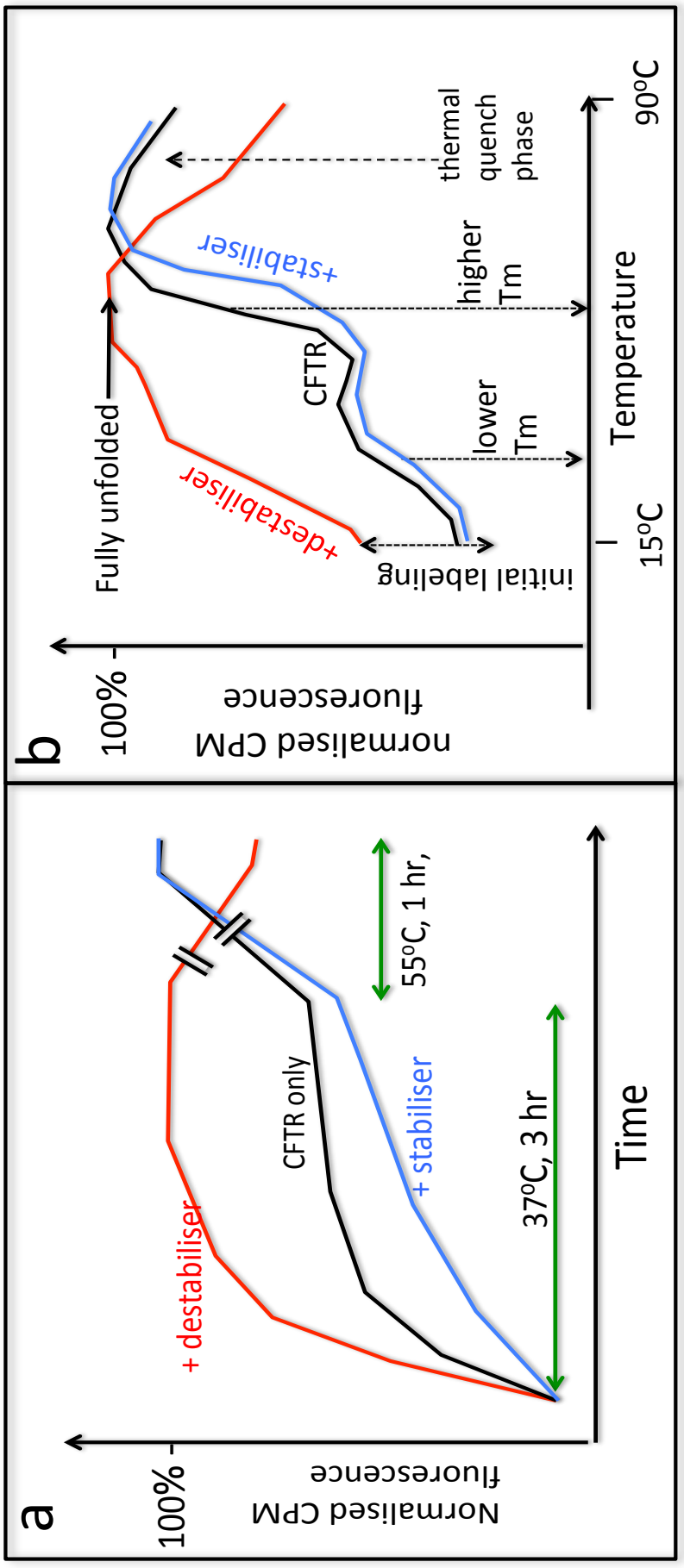
a
Normalised CPM fluorescence
100%
Time
37°C, 3 hr
55°C, 1 hr,
CFTR only
+ stabiliser
+ destabiliser
b
normalised CPM fluorescence
100%
Temperature
15°C
90°C
initial labeling
Fully unfolded
CFTR
lower Tm
higher Tm
thermal quench phase
+stabiliser
+destabiliser

Figure 1:

Schematic description of the two assays employed to assess CFTR stability: (a) CFTR stability at physiological temperature is assessed by binding of CPM to surface-exposed Cys residues which causes a large increase in the CPM fluorescence yield. After 3 hours, the protein is fully denatured by heating at 55^{o}C for an hour, whereupon all Cys residues become exposed and labeled by CPM. Where protein is fully denatured at 37^{o}C, then thermal quenching of fluorescence at 55^{o}C will be observed (red line). The black line shows the expected profile for CFTR and the red and blue lines indicate the expected effects of destabiliser and stabiliser compounds, respectively. (b) CFTR thermostability is assessed by heating the protein (at roughly 1.5^{o}C/min) in a 48-well capillary format after an initial CPM labeling at 4^{o}C for 1 hour. The extent of initial labeling reports on the preservation of the native conformation of the protein, whilst the midpoints of the two thermal unfolding events (Tm) show any stabilising (blue line) or destabilising (red line) effects of added compounds.

Figure 2:

F508del CFTR stability: (a) Data for a single 96-well plate, using the first assay (stability at physiological temperature). Potential destabiliser traces can be observed at the top of the plot, and these show thermal quenching at 55^{o}C rather than an increase in CPM fluorescence. The red line indicates the profile for the CFTR control. The traces can be adequately analysed using a single exponential increase, corresponding to an unfolding half-time at 37°C. (b) Global analysis of over 1000 different compounds all tested at a concentration of 10 μM using the 96-well assay. Different colours and symbols correspond to different purified protein batches and 96-well plates. The red line encloses the main cluster of experiments, with the spread of initial labeling mainly accounted for by batch-to-batch variability in purification and a mean unfolding half time of about 1hr at 37°C. The black dashed line indicates a portion of the graph of interest for destabilising compounds, whilst stabiliser compounds are expected to be found in the top left portion of the graph.

Figure 2

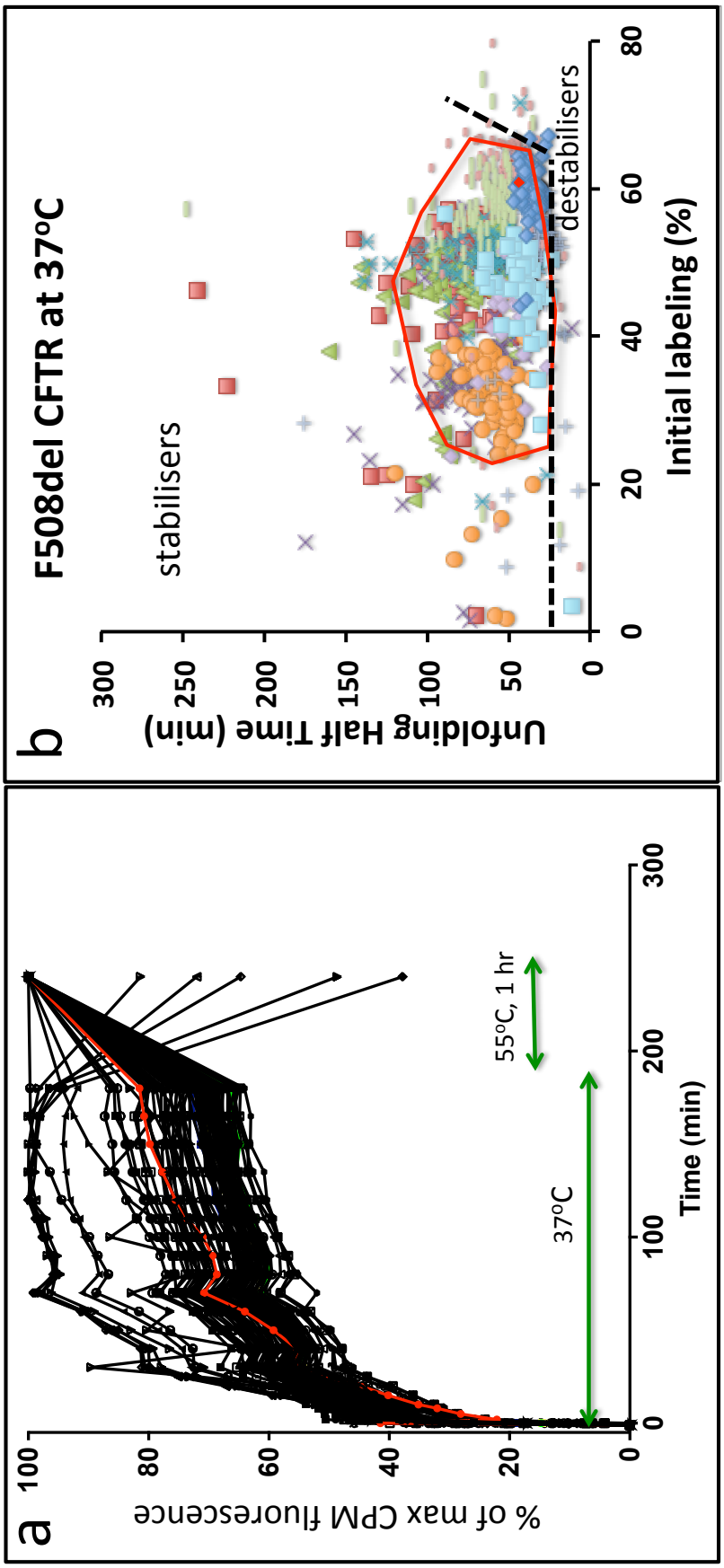
a
% of max CPM fluorescence
100
80
60
40
20
0
0
100
200
300
Time (min)
37°C
55°C, 1 hr
b
F508del CFTR at 37°C
Unfolding Half Time (min)
300
250
200
150
100
50
0
stabilisers
destabilisers
0
20
40
60
80
Initial labeling (%)

Figure 2 shows the actual CPM labelling data for the isothermal stability assay. In panel A, 96 profiles are superimposed with the control F508del CFTR sample indicated by the red line. The increase in CPM fluorescence can be fitted as single exponential for the data at 37°C. The fitting of the exponential rise is done between 20 minutes and 180 minutes to allow for the initial labelling event to be accounted for. From the exponential fits the initial labelling and unfolding half-time at 37°C can be estimated. These two parameters are plotted in Figure 2b. The data cluster in a region of the graph corresponding to initial labelling values between about 30 and 60% which has previously been found to be a range determined by batch to batch variability [8]. Similarly most of the experiments cluster around folding half times at 37°C of between 40 and 80 minutes. These half times for unfolding are roughly equivalent to measurements of loss of structure or function at this temperature [25]. Of interest are the experimental points that lie outside the main cluster indicated by the red ring. These are experiments where F508del CFTR is incubated with compounds that increase the unfolding half-time at 37°C and/or reduce the initial labelling of the protein. At this stage, a manual appraisal of the stabilising hits needs to be undertaken in order to eliminate false positives (see later).

The destabilising compounds will lie to the bottom and right-hand side of the plot since they will cause either a reduction in unfolding half-time and/or an increase in the initial labelling of the protein. Although this part of the graph is rather compressed using a linear axis for the unfolding half-time at 37°C, it is possible to plot the data using a logarithmic scale for the y-axis, and this allows a better visual identification of potential destabilising compounds. Again at this point manual checking of the identities of the destabilising hits should be carried out in order to eliminate false negatives.

Figure 3

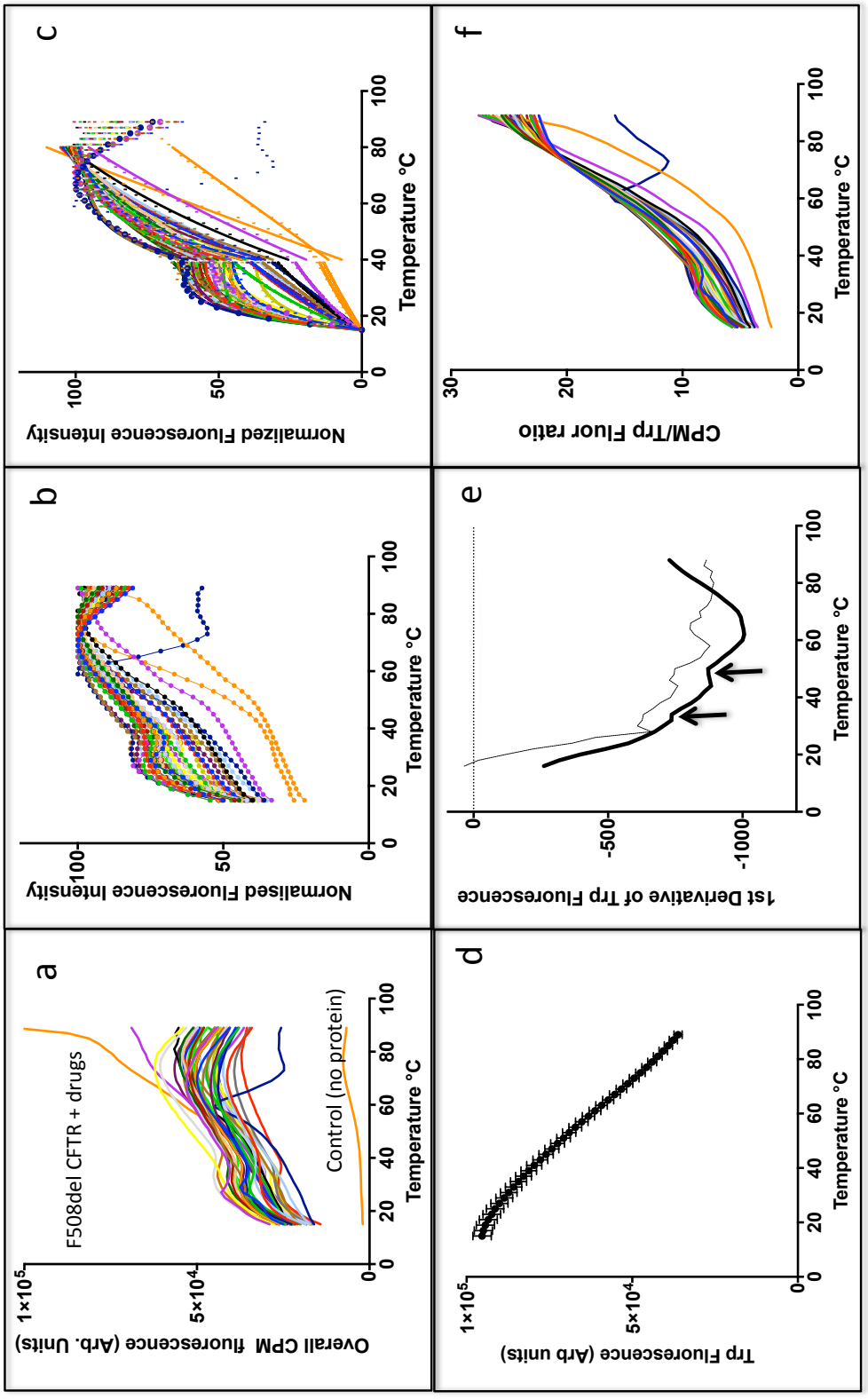
a
Overall CPM fluorescence (Arb. Units)
1×10^5
5×10^4
0
F508del CFTR + drugs
Control (no protein)
0 20 40 60 80 100
Temperature °C
b
Normalised Fluorescence Intensity
100
50
0
0 20 40 60 80 100
Temperature °C
c
Normalized Fluorescence Intensity
100
50
0
0 20 40 60 80 100
Temperature °C
d
Trp Fluorescence (Arb units)
1×10^5
5×10^4
0
0 20 40 60 80 100
Temperature °C
e
1st Derivative of Trp Fluorescence
0
-500
-1000
0 20 40 60 80 100
Temperature °C
f
CPM/Trp Fluor ratio
30
20
10
0
0 20 40 60 80 100
Temperature °C

Figure 3: F508del CFTR thermostability: (a) Raw data for CPM fluorescence increase as a function of temperature for F508del samples with 46 different FDA-approved drugs (indicated by different colours). ***(****b) as in (a) but with CPM fluorescence normalised to maximum fluorescence and zero fluorescence for each sample. Note that in one experiment (blue trace) the unfolding curve is anomalous, likely due to migration of a bubble in the capillary. (c) As in (b) but with normalisation to maximum and minimum fluorescence values (symbols), and with the data fit using two exponential functions to account for the two phases in the CFTR unfolding profile (solid lines). (d) Tryptophan fluorescence averaged for the 45 samples showing normal CPM fluorescence profiled. Thermal quenching of Trp fluorescence occurs with no obvious unfolding transition. Error bars indicate SEM. (e) First derivative of the averaged Trp fluorescence (black line) shows two inflexions around 33 and 47°C (arrows). Grey line shows the relatively noisy trace for one run (control protein with no drug). (f) as in (b), but CPM fluorescence was scaled using the intrinsic Trp fluorescence (panel d) to account for the background thermal quenching of fluorescence. This plot implies that the higher-temperature thermal unfolding event at 45-60°C exposes more Cys residues than the lower-temperature unfolding event around 30-35°C. Figure 3e shows two inflexions in the curve. These represent unfolding events of the protein, the initial unfolding representing unfolding of the less stable nucleotide binding domains, the second inflexion representing unfolding of the more thermally stable transmembrane domains.*

Figure 3 summarises the CPM stability assay data for the thermal unfolding of F508del CFTR. Panel (a) shows the unprocessed CPM fluorescence data for 46 compound containing capillaries (This assay holds a maximum of 48 capillaries, 46 is the number included from this batch of testing, the other two wells would be accounted for with negative controls (absence of protein and dye respectively). In order to allow better visualisation of each experiment with a different drug (or with no protein control) they are discriminated with different coloured lines. The majority of the fluorescence profiles cluster together in terms of overall intensity as well as their general shape. A feature of the CFTR unfolding profile that has previously been described [8, 25] is the two-phase nature of the unfolding, with a low temperature unfolding event between 20 and 40°C and a higher temperature unfolding event between 45 and 65°C. These two events may be related to unfolding of different domains within the protein. A similar multiple event and folding profile has been described for other membrane proteins with multiple subunits or domains [28]. The F508del CFTR data also shows the initial labelling at 15°C, and this parameter can be easily read at this stage from the digital record of the fluorescence profile. More typically however, the data can be first normalised with the minimum value set to 0 and the maximum value set to 100%, and this allows a value for the initial labelling that will not be significantly affected by any loading errors or small differences in the optical path length of the capillaries. Nevertheless, some profiles now appear as outliers from the main cluster of traces, this can be understood in terms of potential false positives (see later). One profile (blue coloured trace) shows a normal initial profile up to 60°C and then deviate markedly with a decrease in fluorescence. This anomalous behaviour may be caused by the formation or migration of an air bubble within the capillaries, and such behaviour may be observed in roughly every 50 experiments.

Panel C shows the same data but now normalised with the minimum value set to 0 and the maximum value to 100%. This plot allows the assessment of just the thermal unfolding phases of the profiles and their analysis using non-linear regression analysis and curve fitting. This allows the estimation

of mid-point thermal unfolding values for the lower temperature and higher temperature transitions. This rough fitting allows an assessment of the individual effects of compounds tested in a semi-automated fashion.

The instrument employed for this assay provides a very rich collection of data, and it measures fluorescence over a large range of wavelengths. Since the excitation source is at 266 nm, it is possible to measure intrinsic protein fluorescence arising predominantly from tryptophan residues in the protein. The tryptophan fluorescence profiles as a function of temperature for F508del CFTR are very similar and an average of 45 different experiments is shown in Figure 3d with error bars indicating the degree of variation from one experiment to another. Note that there is no obvious inflection in the fluorescence profile due to protein unfolding, but rather the profile is dominated by thermal quenching. In order to detect effects on the tryptophan fluorescence profile that are a result of protein unfolding a first derivative plot was used, as shown in Figure 3e. The first derivative plot of the averaged tryptophan fluorescence shows two inflection points that probably correspond to the low temperature and high temperature unfolding events observed for the CPM fluorescence traces. However, the signal to noise ratio for individual experiments was not sufficient to allow such precision. For example the first derivative plot of the tryptophan fluorescence profile for a single experiment (control protein alone) is shown (grey trace), and whilst some features of the averaged profile may be present, the overall signal is indistinct and hard to interpret. It has previously been shown that it is possible to compensate for the thermal quenching of the CPM fluorescence using the tryptophan fluorescence profile as a guide. When this is applied, as illustrated in Figure 1f, It is clear that the high temperature unfolding transition is significantly larger than the low temperature unfolding transition, implying that more Cys residues become exposed during the latter unfolding event. For the purposes of the screening assay, however the uncompensated CPM fluorescence data was employed, as shown in panels a-c.

Figure 4

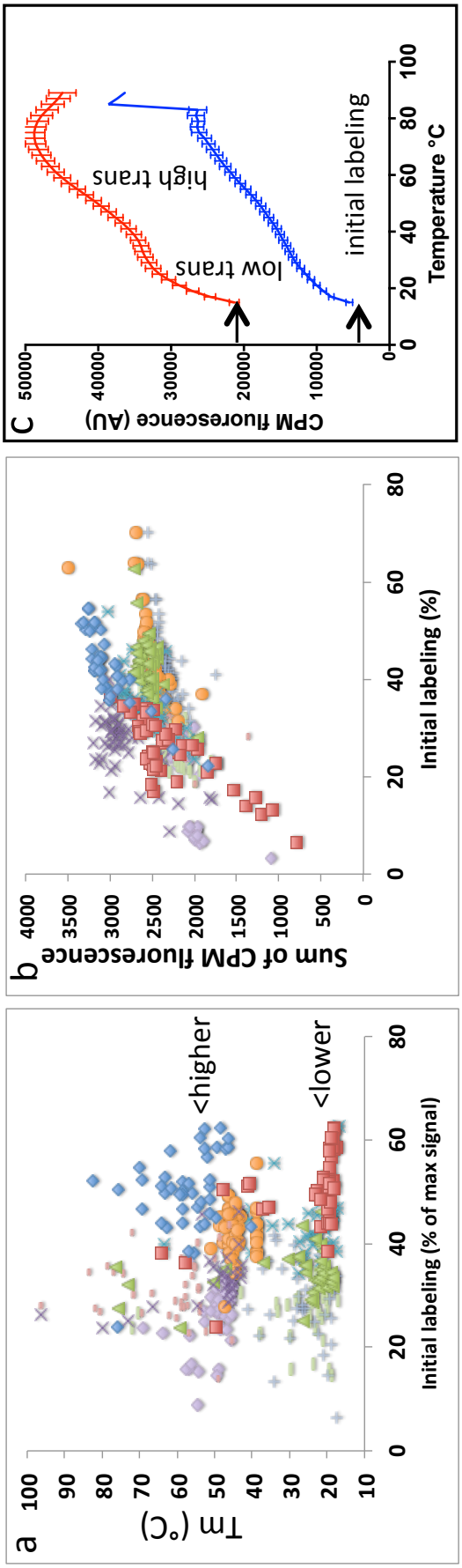
a
Tm (°C)
Initial labeling (% of max signal)
<higher
<lower
b
Sum of CPM fluorescence
Initial labeling (%)
c
CPM fluorescence (AU)
Temperature °C
high trans
low trans
initial labeling

Figure 4: Plots of parameters extracted by curve-fitting to the thermal unfolding profiles of F508del CFTR tested in the presence of FDA-approved drugs. (a) Plot of the fitted Tm values for a double unfolding event against the degree of initial labeling. The lower temperature transition clusters around 20-30 °C. The higher temperature thermal unfolding event appears to show a greater spread of estimated mid-points than the lower event. Experiments of interest lie towards the top left (stabiliser candidates) and bottom right (destabiliser candidates) of each cluster. (b) An alternative representation that does not rely on curve fitting: Here the sum of the CPM fluorescence values after normalisation is plotted against the initial labeling. In this case potential destabilising hits will be found in the top right region of the plot whilst stabiliser hits will deviate from their clusters to the bottom left of the plot. In both panels, colours and symbols are used to differentiate different experimental runs and protein batches with each point representing a single thermal unfolding experiment for a single drug or natural product. (c) Average of 35 thermal unfolding runs for two different F508del CFTR protein batches with different compounds. The raw CPM fluorescence data is shown, with error bars indicating the standard error of the mean value. One batch of protein shows a generally higher fluorescence overall, but this will be compensated for by normalisation of the fluorescence. This batch also demonstrates a higher initial labeling value (arrows).

The data for the thermal unfolding assay is more complex than for the isothermal stability assay. Therefore several different ways of plotting the data can be considered in order to identify potential stabilising or destabilising compounds. Figure 4 shows some different ways of plotting the data, although in each case the initial labelling of the protein is used for the x-axis. This is important because it provides an internal control of any batch-to-batch variability in the overall sample that should be considered as well as the stability-moderating effects of compounds. Again, potential hits that shift the midpoint thermal unfolding temperatures of the lower or higher transitions can be identified using these plots. As before, manual intervention at this stage is needed in order to isolate any false hits.

Figure 5

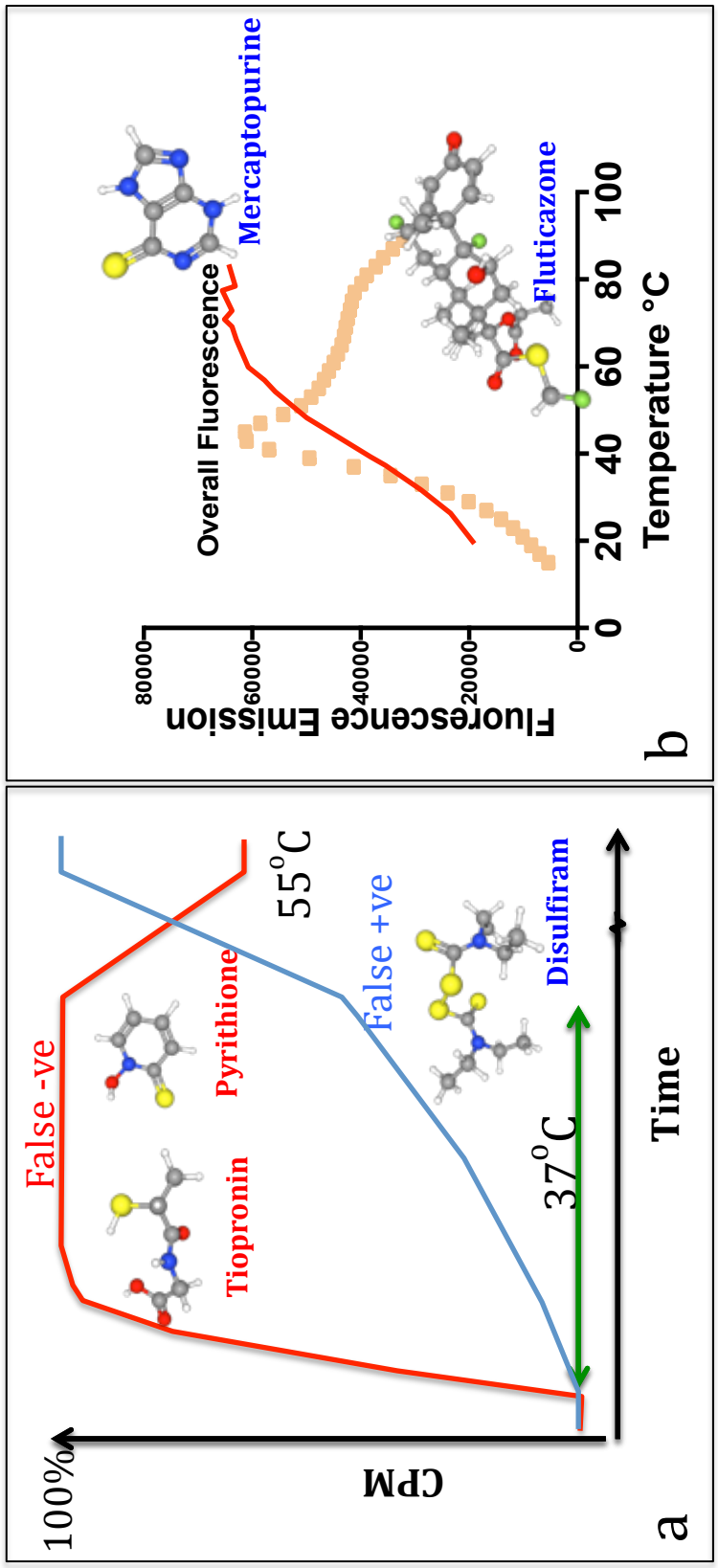
a
CPM
100%
Time
False -ve
Pyrithione
Tiopronin
55°C
False +ve
Disulfiram
37°C
b
Fluorescence Emission
80000
60000
40000
20000
0
Overall Fluorescence
Mercaptopurine
Fluticazone
0
20
40
60
80
100
Temperature °C

Figure 5: Examples of false hits: (a) The assay at physiological temperatures yields false stabilisers and false destabilsers. These are predominantly sulphur-containing compounds that can form adducts with CPM. False positives form the adduct slowly whilst false negatives have fast reaction kinetics. Such anomalies can be identified in the higher intensity of the fluorescence prior to normalisation as these drug-CPM adducts have much higher concentrations than the CPM-labeled protein. (b) Examples of false hits from the thermal unfolding assay. An apparent destabiliser (fluticazone, square symbols)) reacts rapidly with CPM and then fluorescence is quenched beyond 40°C. Some fluorescence derived from CPM labeling of protein between 40 and 90 degrees can be inferred. Another sulphur-containing compound (mercaptopurine) reacts more slowly with CPM Compound structures are coloured according to their elements and were obtained from PubChem [31].

Discussion

No single assay for the screening of compounds and their effects on the biophysical properties and activity of a given protein will be perfect, and hence it is important to assess the strengths and weaknesses of the two assays that we have described in this manuscript. The use of tryptophan fluorescence for thermal stability has been described in several papers [29] [30] but, as illustrated in Figure 3, the quantities of protein required to achieve a sufficient signal to noise ratio to allow the determination of thermal unfolding events is high. The use of a Cys-reactive probe such as CPM allows a more sensitive assay to be employed that can distinguish relatively small shifts in thermal stability. Moreover the high fluorescence output of the probe allows the minimisation of the amount of protein required for each drug to be screened. For example in the 48 well capillary format a few tens of nanograms of protein are sufficient to achieve good signal to noise. However such assays that involve the external addition of fluorescent reporter molecules, even when such a molecule is very small, inevitably lead to an increased likelihood of misleading results (false positives and negatives). In the case of CPM, for both the isothermal and thermal unfolding assays, the main type of misleading result occurs with drugs or natural products that also contain a sulphur atom that is capable of forming a covalent bond with CPM. Figure 5A illustrates this type of behaviour for the isothermal stability assay, with the expected traces for a false negative in red and false positive in blue. In these cases (e.g. tiopronin and pyrithione) it seems likely that the false negative compounds form a covalent bond with CPM with fast kinetics, hence the initial labelling and fluorescence increase at 37°C is very rapid, and then following heating to 55°C some thermal quenching will be observed. In contrast false positives such as the compound disulfiram appear to label quite slowly and show a slow fluorescence increase at 37°C, followed by a large increase in fluorescence after heating to 55°C where the reaction's kinetics will be greater. In both these cases, the false hits can be identified in the raw fluorescence data (e.g. Figure 1a) since these compound-CPM adducts will have significantly higher fluorescence at the ~10μM concentrations

present than for the CFTR-CPM adducts which will be in the ~50-100 nM range.

For the thermal unfolding assay, as illustrated in Figure 3, the sulphur containing drugs and natural products also give rise to several false positives and false negatives. However for this assay the use of the 266 nm laser excitation source also gives rise to other types of false hits. For example strongly fluorescent compounds or drugs and natural products with large delocalised electrons systems frequently appear as hits. In some cases this may be because these compounds can also lead to absorption of the 266 nm light and anomalous behaviour. This defect in the assay also means that ATP can only be employed at relatively low concentrations (e.g. at or below 1mM) because nucleotides also strongly absorb 266nm light. Some false hits also appear to arise due to the intrinsic fluorescence of the drug or natural product, which can compete with the CPM signal. Future work would ideally use a dedicated instrument with a laser source closer to the CPM excitation maximum around 384nm.

Acknowledgements: This work was supported by the UK CF Trust via the F508del CFTR strategic research centre grant via a PhD studentship to JC. We acknowledge the contributions of all our fellow members of the strategic research centre and their help in the early stages of analysis and presentation of the data. In particular we acknowledge Professors D. Sheppard and F. Becq for their scientific insights. XM was supported by a Cystic Fibrosis Foundation grant (FORD13XX0) as part of the CFTR 3D structure consortium. We acknowledge the members of the consortium for useful contributions and in the design of the original CFTR constructs. We acknowledge the contributions of by Dr X. Wang and Dr T. Rimington who generated the F508del CFTR version of the CFTR construct as part of their MPhil and PhD projects, respectively.

References:

[1] Dandapani S, Rosse G, Southall N, Salvino JM, Thomas CJ. Selecting, Acquiring, and Using Small Molecule Libraries for High-Throughput Screening. Current protocols in chemical biology. 2012;4:177-91.

[2] Van Goor F, Hadida S, Grootenhuis PD, Burton B, Stack JH, Straley KS, et al. Correction of the F508del-CFTR protein processing defect in vitro by the investigational drug VX-809. Proceedings of the National Academy of Sciences of the United States of America. 2011;108:18843-8.

[3] Verkman AS, Lukacs GL, Galietta LJ. CFTR chloride channel drug discovery--inhibitors as antidiarrheals and activators for therapy of cystic fibrosis. Current pharmaceutical design. 2006;12:2235-47.

[4] Galietta LV, Jayaraman S, Verkman AS. Cell-based assay for high-throughput quantitative screening of CFTR chloride transport agonists. American journal of physiology Cell physiology. 2001;281:C1734-42.

[5] Van Goor F, Straley KS, Cao D, Gonzalez J, Hadida S, Hazlewood A, et al. Rescue of DeltaF508-CFTR trafficking and gating in human cystic fibrosis airway primary cultures by small molecules. American journal of physiology Lung cellular and molecular physiology. 2006;290:L1117-30.

[6] Van Goor F, Hadida S, Grootenhuis PD, Burton B, Cao D, Neuberger T, et al. Rescue of CF airway epithelial cell function in vitro by a CFTR

potentiator, VX-770. Proceedings of the National Academy of Sciences of the United States of America. 2009;106:18825-30.
[7] Cai Z, Taddei A, Sheppard DN. Differential sensitivity of the cystic fibrosis (CF)-associated mutants G551D and G1349D to potentiators of the cystic fibrosis transmembrane conductance regulator (CFTR) Cl- channel. J Biol Chem. 2006;281:1970-7.
[8] Meng X, Clews J, Kargas V, Wang X, Ford RC. The cystic fibrosis transmembrane conductance regulator (CFTR) and its stability. Cellular and Molecular Life Sciences. 2017;74:23-38.
[9] Gees M, Musch S, Van der Plas S, Wesse AS, Vandevelde A, Verdonck K, et al. Identification and Characterization of Novel CFTR Potentiators. Frontiers in pharmacology. 2018;9:1221.
[10] Inc. VP. Treatment with VX-661 and Ivacaftor in a Phase 2 Study Resulted in Statistically Significant Improvements in Lung Function in People with Cystic Fibrosis Who Have Two Copies of the F508del Mutation. investors.vrtx.com: Business Wire; 2013. p. 1.
[11] McNamara JJ, McColley SA, Marigowda G, Liu F, Tian S, Owen CA, et al. Safety, pharmacokinetics, and pharmacodynamics of lumacaftor and ivacaftor combination therapy in children aged 2-5 years with cystic fibrosis homozygous for F508del-CFTR: an open-label phase 3 study. Lancet Respir Med. 2019;7:325-35.
[12] Davies JC, Moskowitz SM, Brown C, Horsley A, Mall MA, McKone EF, et al. VX-659-Tezacaftor-Ivacaftor in Patients with Cystic Fibrosis and One or Two Phe508del Alleles. The New England journal of medicine. 2018;379:1599-611.
[13] Taylor-Cousar JL, Munck A, McKone EF, van der Ent CK, Moeller A, Simard C, et al. Tezacaftor-Ivacaftor in Patients with Cystic Fibrosis Homozygous for Phe508del. The New England journal of medicine. 2017;377:2013-23.
[14] Incorporated VP. FDA Approves SYMDEKO® (tezacaftor/ivacaftor and ivacaftor) to Treat the Underlying Cause of CF in Children Ages 6-11 Years with Certain Mutations in the CFTR Gene. Business Wire; 2019.
[15] Wise J. NHS and Vertex remain deadlocked over price of cystic fibrosis drug. BMJ (Clinical research ed). 2019;364:l1094.

[16] Schneider EK, Reyes-Ortega F, Li J, Velkov T. Can Cystic Fibrosis Patients Finally Catch a Breath With Lumacaftor/Ivacaftor? Clinical pharmacology and therapeutics. 2017;101:130-41.
[17] Farinha CM, Sousa M, Canato S, Schmidt A, Uliyakina I, Amaral MD. Increased efficacy of VX-809 in different cellular systems results from an early stabilization effect of F508del-CFTR. Pharmacology research & perspectives. 2015;3:e00152.
[18] O'Ryan L, Rimington T, Cant N, Ford RC. Expression and purification of the cystic fibrosis transmembrane conductance regulator protein in Saccharomyces cerevisiae. J Vis Exp. 2012.
[19] Pollock N, Cant N, Rimington T, Ford RC. Purification of the cystic fibrosis transmembrane conductance regulator protein expressed in Saccharomyces cerevisiae. J Vis Exp. 2014.
[20] de Wilde G, Gees M, Musch S, Verdonck K, Jans M, Wesse A-S, et al. Identification of GLPG/ABBV-2737, a Novel Class of Corrector, Which Exerts Functional Synergy With Other CFTR Modulators. Frontiers in pharmacology. 2019;10.
[21] Phuan PW, Yang B, Knapp JM, Wood AB, Lukacs GL, Kurth MJ, et al. Cyanoquinolines with independent corrector and potentiator activities restore ΔPhe508-cystic fibrosis transmembrane conductance regulator chloride channel function in cystic fibrosis. Molecular pharmacology. 2011;80:683-93.
[22] Veit G, Avramescu RG, Perdomo D, Phuan PW, Bagdany M, Apaja PM, et al. Some gating potentiators, including VX-770, diminish DeltaF508-CFTR functional expression. Science translational medicine. 2014;6:246ra97.
[23] Cholon DM, Quinney NL, Fulcher ML, Esther CR, Jr., Das J, Dokholyan NV, et al. Potentiator ivacaftor abrogates pharmacological correction of DeltaF508 CFTR in cystic fibrosis. Science translational medicine. 2014;6:246ra96.
[24] Alexandrov AI, Mileni M, Chien EY, Hanson MA, Stevens RC. Microscale fluorescent thermal stability assay for membrane proteins. Structure (London, England : 1993). 2008;16:351-9.
[25] Meng X, Wang Y, Wang X, Wrennall JA, Rimington TL, Li H, et al. Two Small Molecules Restore Stability to a Subpopulation of the Cystic Fibrosis

Transmembrane Conductance Regulator with the Predominant Disease-causing Mutation. J Biol Chem. 2017;292:3706-19.
[26] D'Ursi P, Uggeri M, Urbinati C, Millo E, Paiardi G, Milanesi L, et al. Exploitation of a novel biosensor based on the full-length human F508del-CFTR with computational studies, biochemical and biological assays for the characterization of a new Lumacaftor/Tezacaftor analogue. Sensors and Actuators B: Chemical. 2019;301:127131.
[27] Meng X, Clews J, Ciuta AD, Martin ER, Ford RC. CFTR structure, stability, function and regulation. Biological chemistry. 2019;400:1359-70.
[28] Kohlstaedt M, von der Hocht I, Hilbers F, Thielmann Y, Michel H. Development of a Thermofluor assay for stability determination of membrane proteins using the Na(+)/H(+) antiporter NhaA and cytochrome c oxidase. Acta crystallographica Section D, Biological crystallography. 2015;71:1112-22.
[29] Malik A, Khan JM, Alamery SF, Fouad D, Labrou NE, Daoud MS, et al. Monomeric Camelus dromedarius GSTM1 at low pH is structurally more thermostable than its native dimeric form. PLoS One. 2018;13:e0205274.
[30] Ingham KC, Brew SA, Broekelmann TJ, McDonald JA. Thermal stability of human plasma fibronectin and its constituent domains. J Biol Chem. 1984;259:11901-7.
[31] https://pubchem.ncbi.nlm.nih.gov/.

Chapter 9.0 Conclusion

9.1 Furthering the drug screen

The original aim of the PhD project was to promote the identification and development of novel modulators that can correct the F508del mutation. Previous drug screens for CFTR have been carried out in cell-based assays, where potential hits would have a higher chance of being proteostasis regulators rather than pharmacological modulators [22-24]. The rationale here is that by working on purified protein any positive hits identified from these screens will be compounds binding to the CFTR protein. Having identified some initial hits that appear to stabilise F508del CFTR and that have some effects on CFTR function, as demonstrated in the Becq laboratory (unpublished results), future studies may be considered as described below:

(i) Following on from the primary drug screen described in Chapter 8, a further cell-based, *in vivo* assay would be required in order to investigate the effect of any hits on the actual rescue of the mutated CFTR. Such a switch from high-throughput to high content assays would be typical for a drug discovery effort. This further testing would ideally first be with a CFTR-expressing epithelial cell line, and then an epithelial lung cell line, and then with patient-derived cells. Ideally it would be using an assay already developed by a laboratory that has experience in in such assays such as the Sheppard laboratory [25], the Becq laboratory [26] or a similar assay such as the YFP assay seen by Galietta. [22] as described above, some testing has already been done in the Becq laboratory.

(ii) A further extension of the stability assay using the current positive hits would be first to carry out extensive dose-response experiments to determine the optimum concentrations at which they stabilise F508del CFTR. Following this, one would probably utilise the structures of the most potent hits to identify commercially available and structurally homologous compounds that would then be tested for F508del CFTR stabilisation. An idea of the structure-activity relationship would then be built up and with the aim of producing a pharmacophore for F508del CFTR stabilisation.

Such information could be fed into a separate effort using computer-aided methods such as drug-docking and in-silico screening of virtual compounds against available CFTR structures. [6, 7, 14, 15, 27]

9.2 Elucidating the conformational state of CFTR

A separate foundation of the work was to investigate the biogenesis of F508del CFTR at early time points and its structure relative to the wild-type protein. Although some low-resolution data is available via small angle X-ray scattering (SAXS) for F508del CFTR [28], in the absence of a high-resolution structure, limited proteolysis work was performed. This method also had the advantage of being applicable to membrane-embedded F508del CFTR. The work was able to benefit from having specific antibodies and a GFP tag that can report on the individual domains present in the proteolysis profiles. Work like this has been carried out previously in Utrecht. [16, 17] Work by Bertrand and colleagues allowed them to identify components of the proteolysis profile that belong to individual domains and therefore gave a more accurate view of how the protein is folded and the effects of certain mutations and conditions on the conformation of the overall protein. The novelty of the research presented here was the ability to compare membrane-embedded and isolated purified protein such that CFTR conformation can be monitored under a range of conditions such as when phosphorylated or dephosphorylated or when drugs are present. As the structures of the protein are elucidated more information can be identified and conferred from the data that is presented here. In particular, a high-resolution structure for the F508del CFTR protein would be particularly important for interpretation of the limited proteolysis data presented in this thesis.

Similarly, an area of research that would require more work would be the finer dissection of when and where the F508del mutation affects the biogenesis of CFTR. Specifically, the cystic fibrosis research field would be interested in what part of the conformation of the mutated protein leads to degradation by the cell quality control machinery. This has already been partially answered by Bertrand and colleagues [16, 17] and the work here also suggests that proteases appear to distinguish F508del CFTR at a few

specific sites, but it would require further elucidation with chaperones to allow more insights into the ER quality control of F508del CFTR. The thesis' time course data shows a model by which this data could be sought. The time course experiment could be scaled up to a point by which purified protein could be collected for many time points between 0 and 4 hours. Undergoing the experiment at a fermenter scale would aid the process as enough material could be collected for each time point to carry out multiple experiments. The time course data showed very weak signal for the earlier time points for F508del CFTR, however it was carried out on a small scale. If enough material could be collected there should be enough signal in order to start gathering information regarding the early time points, and if sufficient amounts of protein can be purified, then structural analyses by cryo-EM or SAXS can be attempted. Limited proteolysis experiments, as previously described could be carried out in order to distinguish at which point folded domains become present in the early time points, and if there are minute differences between F508del, WT and the G551D mutant once both TMD1 and most of NBD1 have been translated. At the early time points, the N-terminal domains may be more sensitive to the proteases and therefore would show a distinct pattern compared to later time points (after 8 hours). These experiments would rely on the SUMO tag at the N-terminus and the anti-SUMO antibodies, although the experiments described in chapter 5 show proof of principle for this. Optimising the amount of protease and the different proteases to use would allow us to experiment with the visualisation of the proteolytic profile. Using other domain specific antibodies, as previously suggested, would allow us to experiment between the different constructs and see in greater detail which domains are affected as the protein is generated. It would be interesting to attempt structural studies of protein being expressed at early time points if enough material were acquired. Comparison by negative stain electron microscopy (EM) would be likely to be most useful in identifying the changes in conformation seen as the protein is generated because it can be done with relatively small amounts of protein and is not sensitive to high concentrations of salt and glycerol that may be needed to stabilise immature forms of the protein. Previous negative stain electron microscopy work has been carried out in this lab with a scale of ng

quantities of protein; therefore generating similar quantities of material from different induction time points should be feasible.

Chapter 7 of this thesis details work carried out developing a novel biosensor. Due to the candidate's small contribution the paper, discussion of the work is included here so as not to change the text of the final paper that has already been published.
During the work undertaken for this paper, the studies involved use of WT protein as a comparison. The data is not published in this current paper. The WT protein behaves similarly in that binds to the scaffold in the same way F508del does. WT has been used in surface plasmon resonance before.

A criticism of this approach may be that no negative controls in the regard of compounds that are known to not bind to CFTR were used, however samples including just buffer and lipids were used showing the validity of the assay.
Previous correctors have been shown to bind to the nucleotide-binding domain [29] Indeed this is the part of the protein, which is desired to be corrected, as this is where F508del first affects the protein [30] leading to whole protein instability [31]. Therefore it is useful to extrapolate that rescue of NBD1 can lead to whole protein rescue.

Due to the expense and high material demand of this approach, the position of this experimental procedure in the drug development/testing process should be considered. The nature of the experiment and the machinery leads the process to be a low/medium throughput approach. Therefore, significant arguments could be made for this approach to be defended as a characterisation approach – appearing after a medium/high-throughput approach such as that described in chapter 8 of this thesis. Indeed the method described in chapter 8 may provide less exact data but it's ability to test a much higher quantity of compounds with less amount of purified material allows for it to appear earlier on in the drug development process. Therefore, this thesis provides a series of pharmacological experiments, which would aim to effectively find new compounds by investigating the effect on the purified CFTR protein. Chapter 8 details the CPM assays as a

high throughput means to ascertain compounds that are interacting with the protein, while chapter 7 indicates a means to more closely investigate the binding efficacy and stability effect of the compound on the protein.

EN503A should be further tested with cellular based assays to assess toxicology/ dosage/ affect on different cell types. As detailed in chapter 8, ideally the compounds would undergo testing in a robust, mammalian cell line capable of expressing epithelial membrane proteins, such as that of BHK cells, following on this testing would be undertaken on a bronchial epithelial cell line, as effective treatment for the patient will primarily show rescue in this area for the patient, as seen by current treatments measure of lung capacity [19]. Indeed it is lung recovery by which existing compounds have been measured due to the debilitating nature of the affect of the disease on this part of the body. Following positive data from bronchial epithelial cell lines, testing should be undertaken on cystic fibrosis patient derived cells to show effective delivery and healthy dosage that may used for patient treatment..

Overall the work in this thesis provides insight into the structural and pharmacological gaps still present in the field and makes attempt at providing the foundational means to fill in these gaps and provide correction of the disease. Indeed, more direct pharmacological therapy is needed that addresses the base function of the F508del defect. The screening assays aim to present a solution to this issue, allowing for a finer approach to finding a corrector. Further elucidation of when and where the mutation affects the protein in its biogenesis is also needed in order to ascertain what effective 'correction' looks like.
The means by which the effect on the biogenesis of the protein is measured can provide a platform to which potential drugs could be measured for their effective correction. Comparison of the WT and the mutated protein at the early time points will provide a spectrum of structural correction in which the mutated protein in combination with an effective corrector treatment will more closely resemble that of the WT protein.

The work in this thesis provides a foundation for these gaps present in the field and future studies may be carried out on extrapolation of the foundations and principles provided by this thesis.

10.0 References

[1] Boyle MP, Bell SC, Konstan MW, McColley SA, Rowe SM, Rietschel E, et al. A CFTR corrector (lumacaftor) and a CFTR potentiator (ivacaftor) for treatment of patients with cystic fibrosis who have a phe508del CFTR mutation: a phase 2 randomised controlled trial. Lancet Respir Med. 2014;2:527-38.

[2] Cholon DM, Quinney NL, Fulcher ML, Esther CR, Jr., Das J, Dokholyan NV, et al. Potentiator ivacaftor abrogates pharmacological correction of DeltaF508 CFTR in cystic fibrosis. Science translational medicine. 2014;6:246ra96.

[3] Veit G, Avramescu RG, Perdomo D, Phuan PW, Bagdany M, Apaja PM, et al. Some gating potentiators, including VX-770, diminish DeltaF508-CFTR functional expression. Science translational medicine. 2014;6:246ra97.

[4] Pedemonte N, Galietta LJ. Pharmacological Correctors of Mutant CFTR Mistrafficking. Frontiers in pharmacology. 2012;3:175.

[5] Riordan JR, Rommens JM, Kerem B, Alon N, Rozmahel R, Grzelczak Z, et al. Identification of the cystic fibrosis gene: cloning and characterization of complementary DNA. Science (New York, NY). 1989;245:1066-73.

[6] Zhang Z, Chen J. Atomic Structure of the Cystic Fibrosis Transmembrane Conductance Regulator. Cell. 2016;167:1586-97.e9.

[7] Liu F, Zhang Z, Csanady L, Gadsby DC, Chen J. Molecular Structure of the Human CFTR Ion Channel. Cell. 2017;169:85-95.e8.

[8] Drew D, Newstead S, Sonoda Y, Kim H, von Heijne G, Iwata S. GFP-based optimization scheme for the overexpression and purification of eukaryotic membrane proteins in Saccharomyces cerevisiae. Nat Protoc. 2008;3:784-98.

[9] Woolford CA, Daniels LB, Park FJ, Jones EW, Van Arsdell JN, Innis MA. The PEP4 gene encodes an aspartyl protease implicated in the posttranslational regulation of Saccharomyces cerevisiae vacuolar hydrolases. Mol Cell Biol. 1986;6:2500-10.

[10] Newstead S, Kim H, von Heijne G, Iwata S, Drew D. High-throughput fluorescent-based optimization of eukaryotic membrane protein overexpression and purification in Saccharomyces cerevisiae. Proceedings of the National Academy of Sciences of the United States of America. 2007;104:13936-41.

[11] Kim H, Yoo SJ, Kang HA. Yeast synthetic biology for the production of recombinant therapeutic proteins. FEMS Yeast Res. 2015;15:1-16.

[12] Bozoky Z, Krzeminski M, Muhandiram R, Birtley JR, Al-Zahrani A, Thomas PJ, et al. Regulatory R region of the CFTR chloride channel is a dynamic integrator of

phospho-dependent intra- and intermolecular interactions. Proceedings of the National Academy of Sciences of the United States of America. 2013;110:E4427-36.
[13] Bozoky Z, Krzeminski M, Chong PA, Forman-Kay JD. Structural changes of CFTR R region upon phosphorylation: a plastic platform for intramolecular and intermolecular interactions. The FEBS journal. 2013;280:4407-16.
[14] Zhang Z, Liu F, Chen J. Molecular structure of the ATP-bound, phosphorylated human CFTR. Proceedings of the National Academy of Sciences of the United States of America. 2018;115:12757-62.
[15] Fay JF, Aleksandrov LA, Jensen TJ, Cui LL, Kousouros JN, He L, et al. Cryo-EM Visualization of an Active High Open Probability CFTR Anion Channel. Biochemistry. 2018;57:6234-46.
[16] Kleizen B, van Vlijmen T, de Jonge HR, Braakman I. Folding of CFTR is predominantly cotranslational. Mol Cell. 2005;20:277-87.
[17] Hoelen H, Kleizen B, Schmidt A, Richardson J, Charitou P, Thomas PJ, et al. The primary folding defect and rescue of DeltaF508 CFTR emerge during translation of the mutant domain. PLoS One. 2010;5:e15458.
[18] Meng X, Clews J, Ciuta AD, Martin ER, Ford RC. CFTR structure, stability, function and regulation. Biological chemistry. 2019;400:1359-70.
[19] Inc. VP. Treatment with VX-661 and Ivacaftor in a Phase 2 Study Resulted in Statistically Significant Improvements in Lung Function in People with Cystic Fibrosis Who Have Two Copies of the F508del Mutation. investors.vrtx.com: Business Wire; 2013. p. 1.
[20] Cha Y, Erez T, Reynolds IJ, Kumar D, Ross J, Koytiger G, et al. Drug repurposing from the perspective of pharmaceutical companies. British journal of pharmacology. 2018;175:168-80.
[21] Lingam S, Thonghin N, Ford RC. Investigation of the effects of the CFTR potentiator ivacaftor on human P-glycoprotein (ABCB1). Scientific reports. 2017;7:17481.
[22] Galietta LV, Jayaraman S, Verkman AS. Cell-based assay for high-throughput quantitative screening of CFTR chloride transport agonists. American journal of physiology Cell physiology. 2001;281:C1734-42.
[23] Pedemonte N, Lukacs GL, Du K, Caci E, Zegarra-Moran O, Galietta LJ, et al. Small-molecule correctors of defective DeltaF508-CFTR cellular processing

identified by high-throughput screening. The Journal of clinical investigation. 2005;115:2564-71.
[24] Verkman AS, Lukacs GL, Galietta LJ. CFTR chloride channel drug discovery--inhibitors as antidiarrheals and activators for therapy of cystic fibrosis. Current pharmaceutical design. 2006;12:2235-47.
[25] Cai Z, Taddei A, Sheppard DN. Differential sensitivity of the cystic fibrosis (CF)-associated mutants G551D and G1349D to potentiators of the cystic fibrosis transmembrane conductance regulator (CFTR) Cl- channel. J Biol Chem. 2006;281:1970-7.
[26] Becq F, Mettey Y, Gray MA, Galietta LJ, Dormer RL, Merten M, et al. Development of substituted Benzo[c]quinolizinium compounds as novel activators of the cystic fibrosis chloride channel. J Biol Chem. 1999;274:27415-25.
[27] Kaur T, Madgulkar A, Bhalekar M, Asgaonkar K. Molecular Docking in Formulation and Development. Current drug discovery technologies. 2019;16:30-9.
[28] Pollock NL, Satriano L, Zegarra-Moran O, Ford RC, Moran O. Structure of wild type and mutant F508del CFTR: A small-angle X-ray scattering study of the protein-detergent complexes. Journal of structural biology. 2016;194:102-11.
[29] Hudson RP, Dawson JE, Chong PA, Yang Z, Millen L, Thomas PJ, et al. Direct Binding of the Corrector VX-809 to Human CFTR NBD1: Evidence of an Allosteric Coupling between the Binding Site and the NBD1:CL4 Interface. Molecular pharmacology. 2017;92:124-35.
[30] Thomas PJ, Pedersen PL. Effects of the delta F508 mutation on the structure, function, and folding of the first nucleotide-binding domain of CFTR. J Bioenerg Biomembr. 1993;25:11-9.
[31] Du K, Sharma M, Lukacs GL. The DeltaF508 cystic fibrosis mutation impairs domain-domain interactions and arrests post-translational folding of CFTR. Nature structural & molecular biology. 2005;12:17-25.